CAPACI OCCASIO
FOUNDED 1894

SAIMM

JOURNAL OF THE SOUTHERN AFRICAN INSTITUTE OF MINING AND METALLURGY

VOLUME 117 NO. 6 JUNE 2017

New Concept Mining

Support for the World's Deepest Mines

Integrated systems of safety and support

MP1 Bolt®

The MP1 Bolting system is an end-anchored yielding bolt for fully mechanised installation. MP1's end anchor provides immediate support upon installation and tensioning. After full encapsulation with pumpable resin or grout, two pairs of double paddles act as additional anchors to secure the unit. The encapsulation can be performed either mechanically or manually.

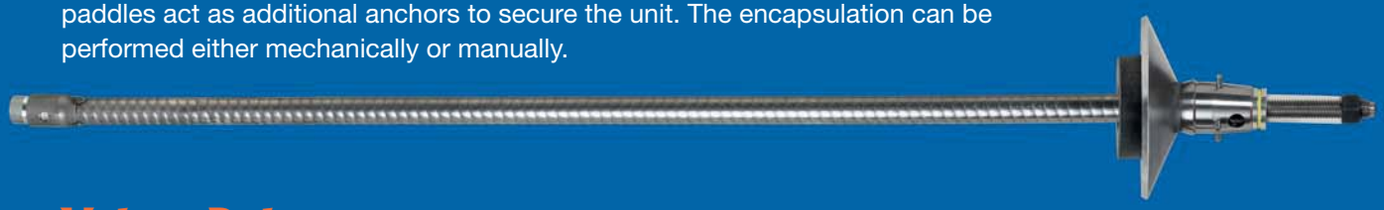

Vulcan Bolt®

The Vulcan Bolt is an integrated primary and secondary support system, that offers immediate support, with full load and yielding capacity on installation. The unique design creates an active support system with a full column frictional bond without the use of resin or grout and also gives excellent resistance to shear. This system provides a consistent load performance over a range of hole sizes, with the ability to accommodate an irregular rock face.

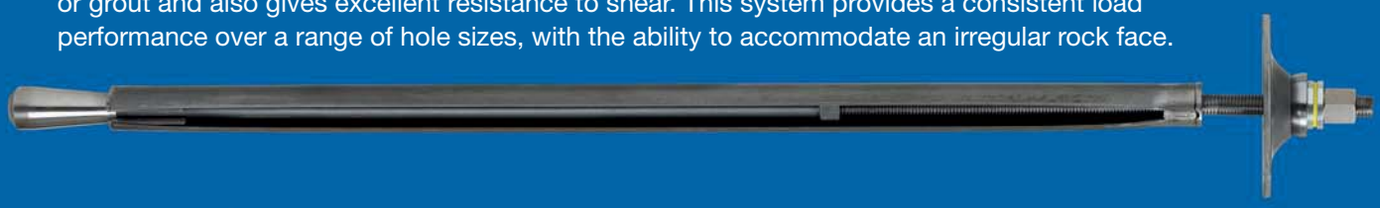

Par1 Resin Bolt®

The Par1 Resin Bolt is a single pass, spin-to-stall resin-anchored, yielding bolt and can be supplied with attachment points for meshing and lacing if required. The spin-to-stall resin provides the bolt with immediate support upon installation for tensioning. The bolt has a set of paddles which assist in the mixing of the resin and act as additional anchors when the resin is set.

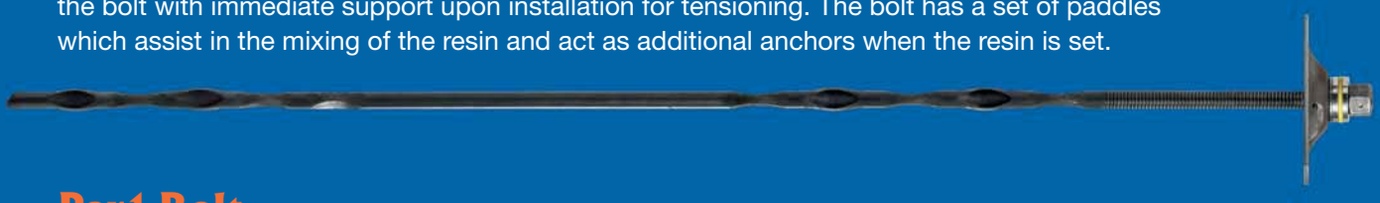

Par1 Bolt®

The Par1 Bolting system is an end-anchored yielding bolt that is grout or resin encapsulated post-installation. It can be provided with attachment points to incorporate areal coverage to provide an integrated dynamic support system if required.

+27 11 494 6000
www.ncm.co.za

THERE'S ONLY ONE SPARE PART FOR A WARMAN®

A GENUINE WARMAN® SPARE PART

Only Warman® spare parts provide the superior performance and longer wear life that Warman® is renowned for. That's because Warman® spare parts are made from superior materials and are backed by technical knowledge and expert services. So to ensure your Warman® pump continues to work like a Warman® pump, use genuine Warman® spare parts.

Now you can buy your Warman® slurry spares 24/7 online at **www.weirafricastore.com.**

For more information contact us on +27 (0)11 9292600.

Get more from your mine with Warman®.
Visit www.warman.weir today.

WEIR

WARMAN®

Minerals
www.minerals.weir
www.weirafricastore.com

The Southern African Institute of Mining and Metallurgy

OFFICE BEARERS AND COUNCIL FOR THE 2016/2017 SESSION

Honorary President
Mike Teke
President, Chamber of Mines of South Africa

Honorary Vice-Presidents
Mosebenzi Zwane
Minister of Mineral Resources, South Africa

Rob Davies
Minister of Trade and Industry, South Africa

Naledi Pandor
Minister of Science and Technology, South Africa

President
C. Musingwini

President Elect
S. Ndlovu

Senior Vice-President
A.S. Macfarlane

Junior Vice-President
M. Mthenjane

Immediate Past President
R.T. Jones

Honorary Treasurer
J. Porter

Co-opted Member
Z. Botha

Ordinary Members on Council

V.G. Duke
I.J. Geldenhuys
M.F. Handley
W.C. Joughin
M. Motuku
D.D. Munro
G. Njowa
A.G. Smith
M.H. Solomon
M.R. Tlala
D. Tudor
D.J. van Niekerk
A.T. van Zyl

Past Presidents Serving on Council

N.A. Barcza
R.D. Beck
J.R. Dixon
M. Dworzanowski
H.E. James
G.V.R. Landman
J.C. Ngoma
S.J. Ramokgopa
M.H. Rogers
D.A.J. Ross-Watt
G.L. Smith
W.H. van Niekerk
R.P.H. Willis

Branch Chairpersons

Botswana	L.E. Dimbungu
DRC	S. Maleba
Johannesburg	J.A. Luckmann
Namibia	N.M. Namate
Northern Cape	C.A. van Wyk
Pretoria	P. Bredell
Western Cape	C.G. Sweet
Zambia	D. Muma
Zimbabwe	S. Matutu
Zululand	C.W. Mienie

Corresponding Members of Council

Australia:	I.J. Corrans, R.J. Dippenaar, A. Croll, C. Workman-Davies
Austria:	H. Wagner
Botswana:	S.D. Williams
United Kingdom:	J.J.L. Cilliers, N.A. Barcza
USA:	J-M.M. Rendu, P.C. Pistorius

PAST PRESIDENTS

*Deceased

* W. Bettel (1894–1895)
* A.F. Crosse (1895–1896)
* W.R. Feldtmann (1896–1897)
* C. Butters (1897–1898)
* J. Loevy (1898–1899)
* J.R. Williams (1899–1903)
* S.H. Pearce (1903–1904)
* W.A. Caldecott (1904–1905)
* W. Cullen (1905–1906)
* E.H. Johnson (1906–1907)
* J. Yates (1907–1908)
* R.G. Bevington (1908–1909)
* A. McA. Johnston (1909–1910)
* J. Moir (1910–1911)
* C.B. Saner (1911–1912)
* W.R. Dowling (1912–1913)
* A. Richardson (1913–1914)
* G.H. Stanley (1914–1915)
* J.E. Thomas (1915–1916)
* J.A. Wilkinson (1916–1917)
* G. Hildick-Smith (1917–1918)
* H.S. Meyer (1918–1919)
* J. Gray (1919–1920)
* J. Chilton (1920–1921)
* F. Wartenweiler (1921–1922)
* G.A. Watermeyer (1922–1923)
* F.W. Watson (1923–1924)
* C.J. Gray (1924–1925)
* H.A. White (1925–1926)
* H.R. Adam (1926–1927)
* Sir Robert Kotze (1927–1928)
* J.A. Woodburn (1928–1929)
* H. Pirow (1929–1930)
* J. Henderson (1930–1931)
* A. King (1931–1932)
* V. Nimmo-Dewar (1932–1933)
* P.N. Lategan (1933–1934)
* E.C. Ranson (1934–1935)
* R.A. Flugge-De-Smidt (1935–1936)
* T.K. Prentice (1936–1937)
* R.S.G. Stokes (1937–1938)
* P.E. Hall (1938–1939)
* E.H.A. Joseph (1939–1940)
* J.H. Dobson (1940–1941)
* Theo Meyer (1941–1942)
* John V. Muller (1942–1943)
* C. Biccard Jeppe (1943–1944)
* P.J. Louis Bok (1944–1945)
* J.T. McIntyre (1945–1946)
* M. Falcon (1946–1947)
* A. Clemens (1947–1948)
* F.G. Hill (1948–1949)
* O.A.E. Jackson (1949–1950)
* W.E. Gooday (1950–1951)
* C.J. Irving (1951–1952)
* D.D. Stitt (1952–1953)
* M.C.G. Meyer (1953–1954)
* L.A. Bushell (1954–1955)
* H. Britten (1955–1956)
* Wm. Bleloch (1956–1957)
* H. Simon (1957–1958)
* M. Barcza (1958–1959)
* R.J. Adamson (1959–1960)
* W.S. Findlay (1960–1961)
  D.G. Maxwell (1961–1962)
* J. de V. Lambrechts (1962–1963)
* J.F. Reid (1963–1964)
* D.M. Jamieson (1964–1965)
* H.E. Cross (1965–1966)
* D. Gordon Jones (1966–1967)
* P. Lambooy (1967–1968)
* R.C.J. Goode (1968–1969)
* J.K.E. Douglas (1969–1970)
* V.C. Robinson (1970–1971)
* D.D. Howat (1971–1972)
  J.P. Hugo (1972–1973)
* P.W.J. van Rensburg (1973–1974)
* R.P. Plewman (1974–1975)
* R.E. Robinson (1975–1976)
* M.D.G. Salamon (1976–1977)
* P.A. Von Wielligh (1977–1978)
* M.G. Atmore (1978–1979)
* D.A. Viljoen (1979–1980)
* P.R. Jochens (1980–1981)
  G.Y. Nisbet (1981–1982)
  A.N. Brown (1982–1983)
* R.P. King (1983–1984)
  J.D. Austin (1984–1985)
  H.E. James (1985–1986)
  H. Wagner (1986–1987)
* B.C. Alberts (1987–1988)
  C.E. Fivaz (1988–1989)
  O.K.H. Steffen (1989–1990)
* H.G. Mosenthal (1990–1991)
  R.D. Beck (1991–1992)
* J.P. Hoffman (1992–1993)
* H. Scott-Russell (1993–1994)
  J.A. Cruise (1994–1995)
  D.A.J. Ross-Watt (1995–1996)
  N.A. Barcza (1996–1997)
* R.P. Mohring (1997–1998)
  J.R. Dixon (1998–1999)
  M.H. Rogers (1999–2000)
  L.A. Cramer (2000–2001)
* A.A.B. Douglas (2001–2002)
  S.J. Ramokgopa (2002-2003)
  T.R. Stacey (2003–2004)
  F.M.G. Egerton (2004–2005)
  W.H. van Niekerk (2005–2006)
  R.P.H. Willis (2006–2007)
  R.G.B. Pickering (2007–2008)
  A.M. Garbers-Craig (2008–2009)
  J.C. Ngoma (2009–2010)
  G.V.R. Landman (2010–2011)
  J.N. van der Merwe (2011–2012)
  G.L. Smith (2012–2013)
  M. Dworzanowski (2013–2014)
  J.L. Porter (2014–2015)
  R.T. Jones (2015–2016)

Honorary Legal Advisers
Scop Incorporated

Auditors
Messrs R.H. Kitching

Secretaries
The Southern African Institute of Mining and Metallurgy
Fifth Floor, Chamber of Mines Building
5 Hollard Street, Johannesburg 2001 • P.O. Box 61127, Marshalltown 2107
Telephone (011) 834-1273/7 • Fax (011) 838-5923 or (011) 833-8156
E-mail: journal@saimm.co.za

Typeset and Published by

The Southern African Institute of Mining and Metallurgy
P.O. Box 61127
Marshalltown 2107
Telephone (011) 834-1273/7
Fax (011) 838-5923
E-mail: journal@saimm.co.za

Printed by

Camera Press, Johannesburg

Advertising Representative

Barbara Spence
Avenue Advertising
Telephone (011) 463-7940
E-mail: barbara@avenue.co.za

The Secretariat
The Southern African Institute of Mining and Metallurgy

ISSN 2225-6253 (print)
ISSN 2411-9717 (online)

SAIMM
JOURNAL OF THE SOUTHERN AFRICAN INSTITUTE OF MINING AND METALLURGY

VOLUME 117 NO. 6 JUNE 2017

Contents

PAPERS OF GENERAL INTEREST

Journal Comment

We have a Problem?

I start my Journal Comment with the iconic phrase: 'Houston, we have a problem'. Those with good memories might just recall that these were the words spoken by astronaut Jack Swigert during the aborted Apollo 13 moon mission, when he reported to ground control an under-voltage on the capsule buss. At least that's what I recall he said.

Something in the back of my mind suggested that it might just be prudent to check the correctness of the quotation. The words were actually spoken by Kevin Bacon who starred as Jack Swigert in the movie 'Apollo 13'. What Swigert actually said was: 'OK, Houston, we've had a problem here'. Close enough – I prefer the movie version!

And why exactly is this relevant? It's because we have a serious problem in South Africa, to which I expect the obvious retort: 'which one in particular are you referring to?' Now, now, this really is serious!

Those who read my Journal Comment will have noticed that I always start in a light-hearted way, but then move on to a serious matter. This particular topic came to my attention when I read the abstracts of the upcoming papers to be published in the *Journal* – and this Comment is no different. The paper that pricked my consciousness is 'The geoscience education pipeline in South Africa: issues of skills development, equity, and gender' by Ann Cameron of the University of the Witwatersrand, and the problem is the state of education in South Africa.

The problems of our education system are manifold, starting at the very bottom with access to books, overcrowded classrooms, schools without flushing toilets, and rising to high-level questions around the value and appropriateness of outcomes-based education when most students do not have access to libraries and computers, and the poor standard of science and mathematics teaching at secondary level. At tertiary level, do I have to say anything more than #FeesMustFall?

In the run-up to the World Economic Forum Africa 2017 in Durban the former president of Tanzania said that 'the education crisis on the continent was today's civil rights struggle', and that education standards in middle-income countries lagged high-income countries by as much as 70 years.

'Inclusive Growth' of the South African economy (to use a catch-phase of the WEF meeting) will not be achieved by nationalizing the banks and mines, nor by threatening to shut down mining operations because they do not meet unreasonable and unattainable targets set by the 2016 Mining Charter, upon which there was little or no consultation with the industry. I fully understand that the mining industry must transform, and requiring an ever-increasing percentage of procurement spend with BEE-compliant companies is both necessary and praiseworthy.

But let's not kid ourselves – issuing shares to a minute percentage of the population who happen to be employed by the company, or live in the surrounding community, or who are someone's favourite entrepreneurs, might assist in transforming the industry (providing, of course, they do not sell their shares), but will hardly create inclusive growth of the economy. And the plea at the WEF for increased fixed investment in SA will continue to fall on deaf ears when regulatory uncertainty in the MPRDA and Mining Charter drops our ranking ever further in the Fraser Institute Survey of desirable countries for mining investment.

What will assist in creating an inclusive and growing economy is improving and levelling, to however small a degree, the unequal educational system so that every school leaver has a chance to sell his/her skills and ability into the marketplace. I have no doubt that there are many dedicated and selfless educationalists who are doing their utmost to improve the standard of teaching of our children. However, it surprises me that we only hear about education at year-end with the Matric results, or when the on-line registration of new learners crashes (it didn't on the second of May this year!), or when there is some scandal over cyber-bullying, or misappropriation of money, or sexual abuse of children. Why is the quality of education not high in the public discourse – continually? And why does it require the former president of Tanzania to bring to our attention the obvious crisis in our education system?

We have seen, over and over again, that when they invest effectively in the education of their children, counties without natural resources invariably outperform those that are well-endowed. I use the word 'effectively' with deliberation, because that is where we, as a nation, fail.

And so we come back to the interesting paper on skills development in geoscience education, highlighting the critical need for managerial skills, not just technical knowledge, and the call for curriculum adjustment to meet these changing needs. I can't wait to read the full paper! I give my apologies to the authors of the other papers in the June edition of the *Journal* in that I do not have the space to discuss the implications of their excellent research. For the mining engineers there are five papers that deal with seismic activity, rock fracture and stress, and electronic safety equipment. For the metallurgists, there are five papers covering solvent extraction, flotation, coal characterization, resource estimation, and (my personal focus) geoscience education.

I started with Apollo 13, and I end with Hidden Figures – go figure! Enjoy reading the papers in this month's *Journal*.

R. Paul

The modern mining professional – a mining CEO's perspective

I had the opportunity of attending the Annual General Meeting of the Association of Mine Managers of South Africa (AMMSA) on 31 March 2017. Mr Steve Phiri, the Chief Executive Officer of Royal Bafokeng Platinum (RBPlat) delivered the keynote address, which he titled 'Towards a lasting legacy: the modern mine manager'. This insightful address resonated with my President's Corner in the May edition of the *Journal*, in which I wrote about 'the Mine of the Future'. Although his address spoke directly to mine managers, I sensed that it was also aimed at mining professionals within the ranks of the SAIMM. I will now draw some parallels between his message to modern mine managers and its implications for modern professionals in the SAIMM.

Mining has, still is and will continue to play a significant role through backward, forward, and lateral linkages into other sectors of the South African economy, as indicated by the often-quoted approximate 8% direct and 18% indirect contribution to the country's gross domestic product (GDP). Accordingly, and as noted by Mr Phiri, the role of the mine manager remains vital, and when the challenges facing the industry are considered, this role is a formidable one. The mine manager relies on technical input from mining professionals in order to deliver on his or her mandate. This makes the role of the mining professional equally vital and formidable if we are to strategically steer the industry forward into the future.

Whatever we do as managers or professionals in carefully navigating the future, Mr Phiri challenged us all to ensure that we leave behind a positive legacy for future generations. This includes going beyond compliance for our social licences to operate, and integrating sustainability into the very fibre of our business strategy in order to leave a positive legacy. Are we advocating this view as professionals in the mining industry?

Lower commodity prices compounded by low productivity continue to be challenges that severely affect the global competiveness of the country's mining industry. These challenges require us as an industry to continuously explore effective cost-containing strategies. It is therefore imperative that we regularly optimize and build flexibility into our business systems, respond to these challenges, and leverage the role of new technology and mechanization into our production processes so that we can mine more safely and productively. The modern mine manager (and by extension the modern mining professional) is one who works smarter, adapts to new technologies, is responsive to the changing business environment, allows for flexibility in their business model, and innovates to transform the mining business model. Does this vision by a mining CEO resonate with your vision as a mining professional?

Mr Phiri also argued that the modern mine manager would become irrelevant if he or she cannot combine their technical skills with people skills in order to navigate an increasingly complex and combative labour and industrial relations and stakeholder landscape. He therefore proposed that an organization such as AMMSA (and by extension the SAIMM) should be pushing for training at our educational institutions that emphasizes these skills in the curricula to adequately prepare mine managers (and mining professionals) for the environment in which they will operate. How much attention do we as mining professionals pay to training in integrating technical and soft skills? Have you ever attended an SAIMM conference on this subject?

In his concluding remarks, Mr Phiri emphasised that it is not always possible to predict with certainty what the world and the mining industry will look like in the future, as there is no 'crystal ball' for this kind of thing. Therefore, we each have our own vision of the future of our companies, but we can collectively work towards a common purpose and broader vision of mining, that of leaving a positive legacy for future generations.

The papers in this edition of the Journal address some of the pertinent issues alluded to by Mr Phiri. For example, one paper presents a systems approach to achieving a relative balance between safety and productivity; another presents findings on the value of steel cabling and mesh wrapped around pillars to improve stability and safety; and another paper calls for curriculum adjustments to address changing skills needs as demanded by the evolving mining landscape. The overall message is simple and clear – whatever we do in our personal capacities or as a professional organization, we need to continually pause, reflect, and ask ourselves if we really are creating a positive legacy for future generations.

C. Musingwini
President, SAIMM

Global Mining Standards and Guidelines Group

The SAIMM is a member of the Global Mining Standards and Guidelines Group (GMSG), who facilitate global mining collaborations on solutions to common industry problems, needs and technology through standards, guidelines, and best practices. GMSG operates on the five principles of inclusivity, collaboration, innovation, optimization, and technology.

Underground Communications Infrastructure Guideline Parts 1 and 2

GMSG has successfully published the first two parts of its Underground Mine Communications Infrastructure Guideline: Positioning and Needs Analysis, and Scenarios and Applications. The guideline is being developed by the Underground Mining Working Group's Communications Infrastructure subcommittee. It will provide a high-level view of the processes needed by mine owners and operators to meet planning and design requirements when creating or replacing underground mine communications infrastructure.

Battery Electric Vehicles Underground Guideline

GMSG and the Canadian Mining Innovation Council (CMIC) are pleased to announce the publication of the Recommended Practices for Battery Electric Vehicles in Underground Mining Guideline. This document is meant to serve as a blueprint for original equipment manufacturers (OEMs) to move forward in research and development, and references existing standards and guidelines related to battery electric vehicles (BEVs). Before this publication, there were no documents specifically related to BEVs in an underground mining environment.

The Underground Communications Infrastructure Guideline Parts 1 and 2 and the Recommended Practices for Battery Electric Vehicles in Underground Mining Guideline are available for download in the GMSG library: http://www.globalminingstandards.org/gmsg-library/

For more info on GMSG's guidelines work, please visit www.globalminingstandards.org

H. Ednie

PAPERS IN THIS EDITION

These papers have been refereed and edited according to internationally accepted standards and are accredited for rating purposes by the South African Department of Higher Education and Training

Papers of General Interest

These papers will be available on the SAIMM website
http://www.saimm.co.za

PAPERS IN THIS EDITION

These papers have been refereed and edited according to internationally accepted standards and are accredited for rating purposes by the South African Department of Higher Education and Training

These papers will be available on the SAIMM website
http://www.saimm.co.za

http://dx.doi.org/10.17159/2411-9717/2017/v117n6a1

Near-surface wave attenuation (kappa) of Far West Rand micro-events

by M.B.C. Brandt

Synopsis

The near-surface wave attenuation factor k (kappa), which describes the attenuation of seismic waves with distance in the upper 1–3 km of the Earth, was determined for the Far West Rand gold mining area using seismic data recorded by station Parys (PRYS) of the South African National Seismograph Network. Twenty micro-events in the magnitude range $0.7 \leq M_L \leq 1.8$ for the period 1 July to 15 November 2015 were analysed. For the analysis a 10-second window for the S phase portion of the vertical component seismogram was selected. The result was an average $k = 0.048 \pm 0.014$ s, which is much higher than for a stable continental region where $k \approx 0.006$ s. This is because the assumed Brune source model is inappropriate for describing mining-related events that often have moment tensors with a volumetric (implosive) component. The average k was calculated to be 0.098 ± 0.038 s for explosions of a similar magnitude. This higher value derived for mining-related k may be employed as a means of correcting the Brune source spectrum to calculate seismic moment as well as corner frequency for events in the mining areas of South Africa.

Keywords

Kappa, near-surface attenuation, mining-related seismic event, spectral analysis.

Introduction

Brandt (2015) and Birch, Cichowicz, and Grobbelaar (2015) recently undertook studies to determine the quality factor Q and attenuation parameter α, which describe the attenuation of seismic waves with distance, for South African earthquakes and mining-related seismic events, respectively. Brandt (2015) derived an attenuation relation of $Q(f) \approx 400f^{0.7}$, whereas Birch, Cichowicz, and Grobbelaar (2015) estimated the relation $Q(f) = 327f^{0.81}$ for the Kaapvaal Craton. However, both these studies determined Q without knowledge of the near-surface attenuation, which is quantified by the factor k (kappa). The general decrease in amplitude of seismic waves caused by attenuation may be described by using the quality factor Q, as was proposed over 50 years ago (*e.g.* Havskov and Ottemöller, 2010b):

$$A(f,t) = A_0 e^{\frac{-\pi f t}{Q(f)}} \quad [1]$$

where A_0 is the initial amplitude, $A(t)$ the amplitude after the waves have travelled for time t, f represents the frequency, and $Q(f)$ is the general frequency-dependent quality factor. Q has been observed to have strong regional variations in the crust and a frequency dependence of the form

$$Q(f) = Q_0 f^{\alpha} \quad [2]$$

(*e.g.* Kvamme and Havskov, 1989; Kvamme, Hansen, and Bungum, 1995; Malagnini, Herrmann, and Koch, 2000) when $f > 1$ Hz and $Q(f)$ is nearly constant for 0.1 Hz $< f <$ 1.0 Hz (*e.g.* Stein and Wysession, 2003). The frequency dependence is often found to be stronger with increasing tectonic activity and is thought to be related to the decrease in homogeneity within the crust (*e.g.* Kvamme and Havskov, 1989; Birch, Cichowicz, and Grobbelaar, 2015). Q is also thought to be mostly constant along the ray path for local seismology observations, with the exception of the near-surface layers (1–3 km), which generally have a much lower Q than the rest of the path and tend to filter out high-frequency energy between 5–25 Hz (*e.g.* Havskov and Ottemöller, 2010b). The attenuation term in Equation [1] may be separated into surface and deeper crust effects:

$$A(f,t) = A_0 e^{-\pi f \kappa} e^{\frac{-\pi f t}{Q(f)}} \quad [3]$$

with k representing the near-surface attenuation. The parameter k describes the asymptotic high-frequency slope of the spectrum of a seismogram. A low value for k corresponds to a seismogram with abundant high-frequency energy, whereas a high value corresponds to a minimal amount of high-frequency energy (Kilb *et al.*, 2012). Kappa varies with region (stable continental area *vs.* active tectonic region) and surface geology (very hard rock *vs.* softer rock) (Douglas *et al.*,

* *Council for Geoscience, Geophysics Competency, South Africa.*

 ISSN 2225-6253. Paper received Dec. 2015; revised paper received Mar. 2017.

2010). In this study, to determine k, the quality factor $Q(f)$ in Equation [3] was fixed at a predetermined value of Q = 400 and α = 0.7, which is suitable for the regional distances monitored by the National Seismograph Network (Brandt, 2015).

Two routine methods are available to determine k (Kilb *et al.*, 2012).

- In the original definition given by Anderson and Hough (1984), k is estimated for frequencies larger than the source spectrum corner frequency, f_0, from the linear range of the acceleration spectral amplitude decay where the signal is above the noise floor. At first only applied to large earthquakes ($M_L \geq 5$), this method was later modified to include events of smaller magnitudes ($M_L \geq 3.4$) where the signal has an adequate signal-to-noise ratio (Douglas *et al.*, 2010)
- A modified definition applicable to micro-events with magnitude M < 1 assumes that the low-frequency displacement source spectrum is flat below the corner frequency, f_0, and that any slope is attributable only to the attenuation (Havskov and Ottemöller, 2010b). An advanced definition extends the frequency range to where k affects the corner frequency (typical for magnitudes $1.0 < M_L \leq 3.4$ in the frequency range 5–25 Hz) and assumes an earthquake source model and/or a spectral shape to solve for k, the seismic moment, stress drop, and source dimension simultaneously (García, Romacho, and Jiménes, 2004).

In this study, k was calculated using a data-set of micro-events of $M_L \leq 1.8$ located mostly in the Far West Rand gold mining area. The SEISAN earthquake analysis software (Havskov and Ottemöller, 2010a) was used to determine k with a spectral analysis of the seismic signals recorded by a nearby, suitably calibrated seismograph station, properly installed on bedrock. The analysis closely follows the routine data processing techniques prescribed by Havskov and Ottemöller (2010b), who determined seismic moments on vertical-component seismograms. The advantage of this approach is that the spectral analysis will be backward-compatible to the 1990s, when waveform recording by the National Network was on vertical-component seismographs only (Saunders *et al.*, 2008). For comparison, k was also calculated for a data-set of explosions of similar-sized magnitudes that had occurred in the Sasolburg coal mining area with similar epicentral distances. It was envisaged that the resultant k would be useful for the attenuation relation required by spectral analysis of mining-related events when calculating moment magnitude, M_w, for S-waves with the seismograms recorded by the National Seismograph Network (Saunders *et al.*, 2008; Brandt, 2015). However, owing to the limited frequency range of 4–9 Hz of the analysis, this derived k should not be extrapolated for strong ground motion engineering applications.

Method

Determining k with signals originating from micro-events is the preferred method, given that larger earthquakes of $M_L \geq 3.4$ occur infrequently in the Far West Rand. Figure 1 is a map showing the data-set of 20 micro-events (19 in the Far West Rand and one in the Central Rand) for the magnitude range $0.7 \leq M_L \leq 1.8$ over the period 1 July to 15 November 2015. The typical epicentre uncertainty of events located with the National Network is ±5 km for the Far West Rand (Brandt, 2014), although micro-events are only detected by a small number of nearby stations where the P- and S-phases usually have low signal-to-noise ratios. Hence the location uncertainty may be as large as ±10 km. The analysis was performed using the signals recorded by the seismograph station at Parys (PRYS) with epicentral distances of 51–83 km for the Far West Rand events and 109 km for the Central Rand event. Station PRYS is suitably calibrated up to a maximum frequency of 9 Hz, beyond which the anti-alias filters influence the signal, making it difficult to calibrate. The station is also properly installed on bedrock, which ensures that no unwanted signal distortions or amplifications occur at the site.

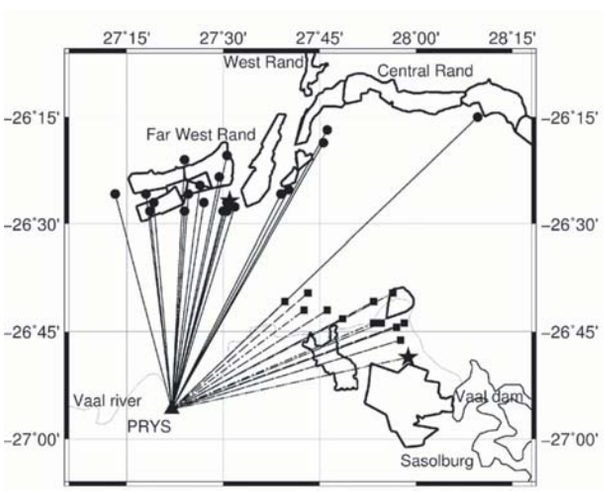

Figure 1—Map of epicentres in the Far West Rand and Central Rand gold mining areas and the seismograph station at Parys (PRYS). The analysis was carried out on waves recorded by the station (triangle with station code) that travelled along ray paths (thin lines) originating from 20 events (dots) in the gold mining areas (delineated by thick lines). The star depicts the event investigated in Figure 3. The explosions analysed for comparison (squares) travelled along ray paths (thin dash-dot lines) from the Sasolburg coal mining area (delineated by thick lines) to PRYS. The explosion investigated in Figure 5 is depicted by a star. The Vaal River is displayed as a spatial reference

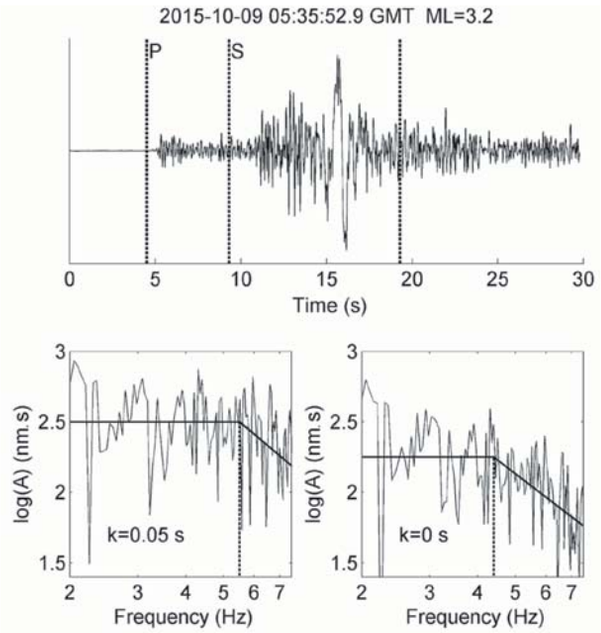

Figure 2—Example to show how κ shapes the source spectrum of the small event that occurred on 9 October 2015 at 05:35:52.9 GMT with an epicentral distance of 56 km and magnitude M_L = 3.2. The top trace shows the seismogram with the 10-second long S-phase window (between the dashed lines) selected for spectral analysis. The bottom left panel shows the respective source spectrum for the signal with κ = 0.05 s (determined in this study) and the bottom right panel shows the same with κ = 0 s. Attenuation parameters are set at Q = 400 and α = 0.7 (Brandt, 2015) for both source spectra. Flat levels and high-frequency roll-offs of the spectra are indicated by means of solid lines, and corner frequencies by dashed lines. Note that both spectra at the bottom are displayed on a log-log scale

For the analysis it was assumed that signals are generated following the Brune source model (Brune, 1970, 1971):

$$S(f) = \frac{M_0}{\left(1+\left(\frac{f}{f_0}\right)^2\right)4\pi\rho v^3} \quad [4]$$

where M_0 (Nm) is the seismic moment, ρ is the density (kg/m^3), v is the velocity (m/s) at the source, and f_0 is the corner frequency. Therefore the log-log shape of the displacement source spectrum is flat at low frequencies below f_0 with a level proportional to the seismic moment. At high frequencies above f_0 the spectrum rolls off at a slope of -2 (Havskov and Ottemöller, 2010b). Figure 2 shows how k shapes the source spectrum of a small earthquake with a magnitude of M_L = 3.2 (with the uncorrected f_0 between 5 and 25 Hz) at an epicentral distance of 56 km. If the attenuation parameters are fixed at Q = 400 and α = 0.7 (Brandt, 2015) an increase in k from 0 s to 0.05 s leads to an increase in the spectral level (*i.e.* M_0) and an increase for f_0 from approximately 4.3 Hz to 5.5 Hz. If the quality factor is fixed, k should not affect the corner frequency of a medium-sized earthquake with $M_L \geq 3.4$ or a micro-event of $M_L < 1$.

Anderson and Hough's (1984) definition of k is based on the premise that the corner frequency, f_0, of an earthquake of magnitude $M_L \geq 5$ is below 5 Hz and hence the shape of the source spectrum roll-off in the frequency range 5–25 Hz is influenced only by the attenuation (Kilb *et al.*, 2012). The actual analysis was performed using an acceleration Fourier spectrum which allowed the analyst to identify the frequency, f_E, where the downward trend towards higher frequencies starts. If f_E is larger than the corner frequency it is possible to analyse smaller-magnitude earthquakes, provided that the signal-to-noise ratio is adequate. The smallest-magnitude earthquake suitable for analysis may be as low as M=3.4 (Douglas *et al.*, 2010). The modified definition is based on the premise that f_0 of micro-events with $M_L < 1$ is above 25 Hz and, hence, the spectral level will depend on only M_0 and the attenuation. This is the micro-event analogue for determining k for larger earthquakes over the frequency range 5–25 Hz (Havskov and Ottemöller, 2010b; Kilb *et al.*, 2012). Taking the natural logarithm of Equation [3] gives:

$$ln\left(A(f,t)\right) = \ln(A_0) - \pi f\kappa - \frac{tf\pi}{Q(f)} \quad [5]$$

When plotting $ln(A(f,t))$ as a function of f on a lin-log scale, Equation [5] will give a straight line with slope $\lambda = \pi(k + t/Q)$ if Q is frequency-independent. If $Q = Q_0 f$, the slope simply becomes $\lambda = -\pi k$. If $Q(f)$ is known, as was the case for this study, the spectrum is first corrected for $Q(f)$ and then k is determined directly.

The first step in the signal analysis was to select suitable events for further processing. Figure 3 shows an example of the semi-automatic selection procedure. The S-phase portion of the vertical-component seismogram was identified and the applicable displacement source spectrum calculated. The signal spectrum and the noise spectrum for a 10 s window preceding the P phase were plotted together to identify signals with a signal-to-noise ratio of at least 2. Next, the spectrum was lightly smoothed, corrected for $Q(f)$, and plotted on a lin-log graph. A line was semi-automatically fitted over the high-frequency linear trend between 4–9 Hz. A preliminary value for κ was derived from the slope of the line and checked for consistency ($0.001 < k < 0.1$) for those results where the correlation between the fitted line and the

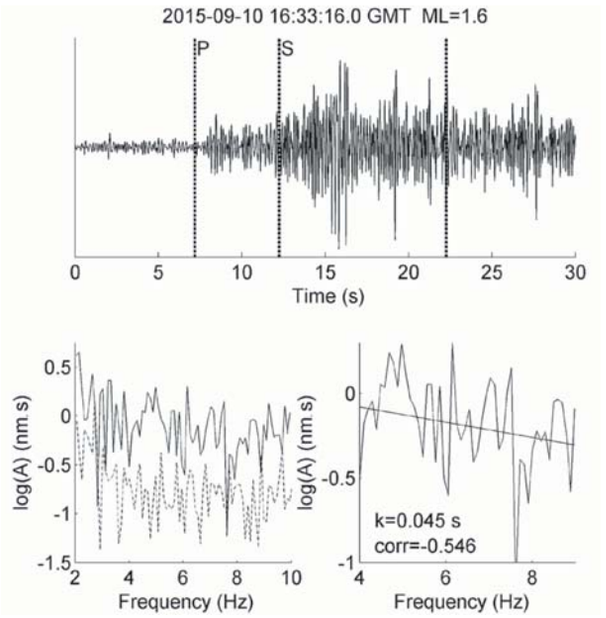

Figure 3— Example of an analysis to select the event that occurred on 10 September 2015 at 16:33:16.0 GMT with an epicentral distance of 64 km and magnitude M_L = 1.6 for further processing. The top trace shows the seismogram with the 10-second long S-phase window (between the dashed lines) selected for spectral analysis. The bottom left panel shows the respective displacement spectra for the signal (solid line) and noise (dashed line): signals selected for further processing required a minimum signal-to-noise ratio of 2. The bottom right panel shows the respective signal spectrum, smoothed once, that has a high-frequency linear trend between 4 Hz and 9 Hz: signals for further processing required a negative correlation of at least 0.5. For a positive correlation coefficient, the amplitudes increase with increasing frequency. Spectra were first corrected for quality factor parameters Q = 400 and α = 0.7 (Brandt, 2015). A standard least-squares regression fits the displacement spectrum with a line from whose slope κ is given by κ = -λ/π. Note that both spectra at the bottom are displayed on a lin-log scale

signal was acceptable (absolute corr. < 0.5). No mining logs were available to identify explosions, hence this test should eliminate blasts as well as events caused by slip fractures from further processing. (Also see k determined for explosions, below.) Since station PRYS is suitably calibrated only up to a maximum frequency of 9 Hz, the derived values for κ are valid only for low-frequency near-surface attenuation. But since the data-set contained only one suitable event of $M_L < 1$, the 4–9 Hz frequency range allowed this analysis to be extended to include larger-magnitude events up to $M_L < 1.8$ with corner frequencies $f_0 > 9$ Hz (*i.e.* less than 25 Hz).

The procedure to calculate k for micro-events is as follows (Havskov and Ottemöller, 2010b):

- Select small events with a high corner frequency
- Next, select events with an adequate signal-to-noise ratio
- Calculate and draw the instrument-corrected S-phase displacement source spectrum (corrected for Q and α)
- Fit a straight line over the linear trend of the flat part of the lightly smoothed lin-log spectrum where $f < f_0$
- Obtain the slope and calculate a preliminary consistent k for the line that fits the spectrum with an acceptable correlation
- Determine the average κ from all the selected heavily smoothed spectra.

All 20 heavily smoothed spectra selected for further analysis in view of deriving the average k = 0.048 ± 0.017 s are shown in Figure 4. Heavy smoothing suppresses frequency subranges between 4 and 9 Hz that deviate substantially from the linear trend and cause the linear fit to yield spurious results. The averaging procedure takes the different spectral levels attributable to the magnitude range $0.7 \le M_L \le 1.8$ of the events (and hence different seismic moments) into account.

Values of k were also calculated for a data-set of explosions of similar magnitudes that occurred in the Sasolburg coal mining area over the period 20 January to 2 July 2015, with similar epicentral distances (between 37 km and 64 km) for comparison (Figure 1). The same procedure as before was followed, except that the consistency check was relaxed to $0.001 < k < 0.15$. Figure 5 shows an example of such a selection analysis, as well as the analysis, to derive average k = 0.098 ± 0.038 s for 13 explosions in the magnitude range $1.3 \le M_L \le 1.8$.

Discussion and conclusion

Determining average k from micro-events provided a viable alternative to analysing larger earthquakes, which occur infrequently in the Far West Rand area. The result of this analysis yielded a k = 0.048 s, in line with the typical expected value of 0.05 s (Havskov and Ottemöller, 2010b) but which is higher than for other stable continental regions. Various investigations have found that in western North America (an active tectonic region where the surface rock is predominantly soft), rock sites have a k of about 0.04 s, whereas rock sites in eastern North America (a stable continental region where the surface rock is predominantly very hard) have $k \approx 0.006$ s (Atkinson, 1996; Douglas *et al.*, 2010). The values of mean k obtained for areas in mainland France vary between those obtained in North America and hard-rock sites in the Alps, where values as low as 0.0254 s

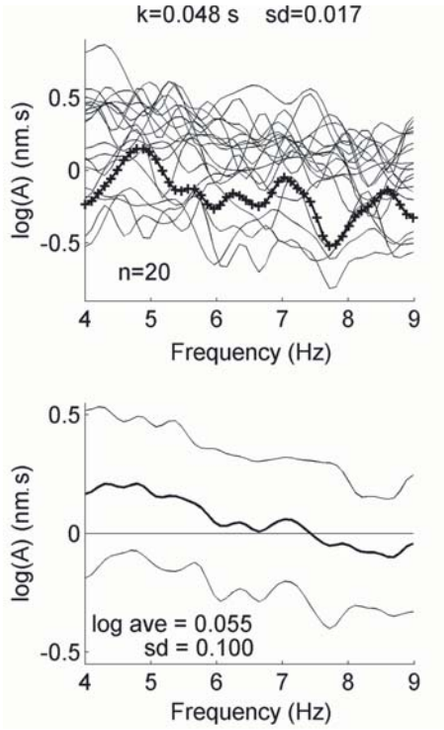

Figure 4—Analysis to determine average κ with standard deviation. The top panel shows all 20 signal spectra, smoothed five times, that had been selected before for further processing. The spectrum selected in Figure 3 is indicated by means of a thick line marked with +. The bottom panel shows the average of the log spectra with standard deviation. Since the events have different seismic moments, the dB values are averaged for each frequency and the average log value of $1/\kappa$ with standard deviation is calculated from which $\kappa = 0.048 \pm 0.017$ s is derived

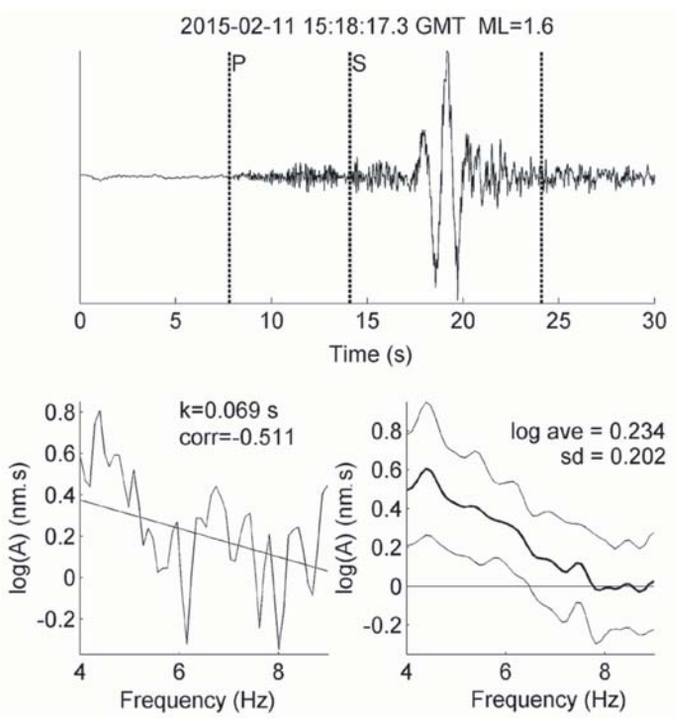

Figure 5—Example of an analysis to select the explosion that occurred on 11 February 2015 at 15:18:17.3 GMT with an epicentral distance of 62 km and magnitude $M_L = 1.6$ for further processing. The top trace shows the seismogram with the 10-second long S-phase window (between the dashed lines) selected for spectral analysis. The bottom left panel shows the respective signal spectrum, smoothed once, that has a high-frequency linear trend between 4 Hz and 9 Hz. Spectra were first corrected for quality factor parameters $Q = 400$ and $\alpha = 0.7$ (Brandt, 2015). A standard least-squares regression fits the displacement spectrum with a line from whose slope κ is given by $\kappa = -\lambda/\pi$. The bottom right panel shows the average of all 13 heavily smoothed log spectra with standard deviation (only one lightly smoothed example spectrum is shown in the left panel). Since the explosions have different seismic moments, the dB values are averaged for each frequency and the average log value of $1/\kappa$ with standard deviation is calculated, from which $\kappa = 0.098 \pm 0.038$ s is derived. Note that both spectra at the bottom are displayed on a lin-log scale

have been recorded (Douglas *et al.*, 2010). García, Romacho, and Jiménes (2004) determined values from 0.01 s to 0.04 s for southern Spain, and the result presented in this paper is even higher than the average k of 0.04 s calculated for northeastern Sonora, Mexico, which is a tectonically active region (Fernández, Castro, and Huerta, 2010).

The result presented here is similar to the value of 0.05 s obtained by Malagnini, Herrmann, and Koch (2000) for central European earthquakes, but lower than the 0.08 s determined for explosions in the same area. Malagnini, Herrmann, and Koch (2000) note that almost doubling of k is needed to fit the source spectra of the explosions, because they are located on the surface causing seismic waves to travel twice through the highly attenuating near-surface layers. These authors further state that, while the Brune source model (Brune, 1970, 1971) is inappropriate for describing an explosive source, it is nevertheless used to avoid the problem of relating corner frequencies to explosive yields. Events related to deep mining activities in the Far West Rand have focal depths of 1–4 km, in comparison to tectonic earthquakes that occur at depths greater than 4 km (Brandt, 2014). Mining-related events also often have moment tensors with a volumetric component (implosive) comparable in magnitude to their shear components (McGarr, 2002). The high value obtained for average k may be the result of additional near-surface attenuation at the focus and the effect of the implosive component not accounted for in the Brune source model.

To test this hypothesis, k was calculated for explosions in the Sasolburg coal mining area. The result of $k \approx 0.1$ s is slightly higher than for central European explosions with k = 0.08 s (Malagnini, Herrmann, and Koch, 2000) but, as expected, is double the value of k calculated for the Far West Rand mining-related events. The higher value for k could indicate that the magnitude of the volumetric component (explosion) is much larger than that of the shear component and that the waves have travelled twice through the highly attenuating near-surface layers. The higher standard deviation of ± 0.038 for k may be ascribed to inhomogeneous near-surface attenuation where rock properties may change abruptly in the upper 1–3 km of the crust.

The purpose of this investigation was to derive a value for mining-related k that will be useful for the attenuation relation required by spectral analysis when calculating moment magnitude, M_w, for S-waves using the seismograms recorded by the National Seismograph Network. The higher value derived for k from mining-related events may be employed as a way to correct the source spectrum for additional attenuation at the focus and for the implosive component. If this procedure is sound, it will be possible to develop the method into a standard procedure to calculate seismic moment (and hence moment magnitude) as well as corner frequency (and, as a result, stress drop) for events related to the mining areas of South Africa. Ultimately, seismic moments calculated with this technique must be validated against those determined by international agencies such as the National Earthquake Information Centre in the USA (NEIC). This presents a future challenge for South Africa as the level of seismicity is low and the country is surrounded on three sides by ocean with only a few seismographs installed on remote islands. Hardly any seismic events are assigned surface wave and/or body wave magnitudes by NEIC. Even fewer, if any, events are reported with seismic moments.

Owing to the limited frequency range of 4–9 Hz of the foregoing analysis, k should not be extrapolated in the context of strong ground motion engineering applications to frequencies beyond 9 Hz.

Acknowledgements

This research was funded as part of the operation and data analysis of the South African National Seismograph Network. I wish to thank the Council for Geoscience for permission to publish the results. Zahn Nel undertook the language editing.

References

Andersen, J.G. and Hough, S.E. 1984. A model for the shape of the Fourier amplitude spectrum of acceleration at high frequencies. *Bulletin of the Seismological Society of America*, vol. 74. pp. 1969–1993.

Atkinson, G.M. 1996. The high-frequency shape of the source spectrum for earthquakes in eastern and western Canada. *Bulletin of the Seismological Society of America*, vol. 86. pp. 106–112.

Birch, D.J., Cichowicz, A., and Grobbelaar, D. 2015. Q-coda estimation in the Kaapvaal craton. *Journal of the Southern African Institute of Mining and Metallurgy*, vol. 115. pp. 541–548.

Brandt, M.B.C. 2014. Focal depths of South African earthquakes and mine events. *Journal of the Southern African Institute of Mining and Metallurgy*, vol. 114. pp. 1–8.

Brandt, M.B.C. 2015. Qc and Qs wave attenuation of South African earthquakes. *Journal of Seismology*. doi 10.1007/s10950-015-9536-6

Brune, J.N. 1970. Tectonic stress and the spectra of seismic shear waves from earthquakes. *Journal of Geophysical Research*, vol. 75. pp. 4997–5009.

Brune, J.N. 1971. Correction. *Journal of Geophysical Research*, vol. 76. p. 5002.

Douglas, J., Gehl, P., Bonilla, L.F., and Gélis, C. 2010. A kappa model for mainland France. *Pure and Applied Geophysics*, vol. 167. pp. 1303–1315. doi: 10.1007/s00024-010-0146-5

Fernández, A.I., Castro, R.R., and Huerta, C.I. 2010. The spectral decay parameter kappa in northeasten Sonora, Mexico. 2010. *Bulletin of the Seismological Society of America*, vol. 100. pp. 196–206.

García, J.M., Romacho, M.D., and Jiménes, A. 2004. Determination of near-surface attenuation, with k parameter, to obtain the seismic moment, stress drop, source dimension and seismic energy for microearthquakes in the Granada basin (Southern Spain). *Physics of the Earth and Planetary Interiors,* vol. 141. pp. 9–26.

Havskov, J. and Ottemöller, L. 2010a. SEISAN earthquake analysis software for Windows, Solaris, Linux and Macosx. Ver. 8.3. University of Bergen, Norway.

Havskov, J. and Ottemöller, L. 2010b. Routine data processing in earthquake seismology. Springer Science + Business Media. 347 pp. doi: 10.1007/978-90-481-8697-6

Kilb, D., Biasi, G., Anderson, J., Brune, J., Peng, Z., and Vernon, F.L. 2012. A comparison of spectral parameter kappa from small and moderate earthquakes using Southern California ANZA seismic network data. *Bulletin of the Seismological Society of America*, vol. 102. pp. 284–300.

Kvamme, L.B. and Havskov, J. 1989. Q in southern Norway. *Bulletin of the Seismological Society of America*, vol. 79. pp. 1575–1588.

Kvamme, L.B., Hansen, R.A., and Bungum, H. 1995. Seismic-source and wave-propagation effects of Lg waves in Scandinavia. *Geophysical Journal International,* vol. 120. pp. 525–536.

Malagnini, L., Herrmann, R.B., and Koch, K. 2000. Regional ground-motion scaling in Central Europe. *Bulletin of the Seismological Society of America,* vol. 90. pp. 1052–1061.

McGarr, A. 2002. Control of strong ground motion of mining-induced earthquakes by the strength of seismic rock mass. *Journal of the South African Institute of Mining and Metallurgy,* vol. 102. pp. 225–229.

Saunders, I., Brandt, M.B.C., Steyn, J., Roblin, D.L., and Kijko, A. 2008. The South African National Seismograph Network. *Seismological Research Letters,* vol. 79. pp. 203–210. doi: 10.1785/gssrl.79.2.203

Stein, S. and Wysession, M. 2003. Introduction to Seismology, Earthquakes and Earth Structure. Blackwell. 498 pp. ◆

http://dx.doi.org/10.17159/2411-9717/2017/v117n6a2

Activity-based risk management for the acquisition of electronic mine safety equipment

by G.P.R. van der Merwe*, J.E.W. Holm†, and A.J. Hofmann†

Synopsis

A new approach is proposed to perform relativistic comparisons between alternative operational risk management solutions by taking into account the impact of each operational activity on overall system performance. A specific case study, to which this new approach is applied, involves the deployment of safety systems in underground mining operations. Conflicting objectives to be satisfied are the minimization of risk to human lives and the minimization of production losses. As the focus in this case is primarily on the mitigation of risk, the approach that was applied is referred to as activity-based risk (ABR) analysis. Existing development process and risk management methods used in the South African mining environment were analysed by means of observations, a case study, technical documentation, and literature review. It was evident from this analysis that a discontinuity existed between the acquisition and operational phases in terms of the management of safety risk in the acquisition of electronic safety equipment when viewed from a full life-cycle perspective. This discontinuity could be addressed by defining a risk perspective in the system development phase by employing ABR in the preliminary design phase of a system's engineering life-cycle. The focus of the ABR system development process is to find the functional definition and configuration of safety equipment that addresses both safety and productivity when taking into account human performance variability. In doing so, a balance between productivity and safety is found in a relativistic sense.

Keywords
activity-based risk, risk, modelling, acquisition, electronic safety equipment.

Introduction

In any system life-cycle, two major phases exist, namely system acquisition and operation (including maintenance). A distinction is made between acquisition and procurement, where acquisition includes system development and integration as specific engineering activities. In the development phase of a new system, conceptual design, preliminary design, and detail design phases follow in this order to define a complete system, after which the system is put into production and implemented in an operational environment—these activities chronologically define system acquisition in the context of this paper. It is not uncommon that differences exist between the risk management perspective during acquisition of a system and risk management perspective during operation, where non-technical aspects are often ignored during acquisition, but are then encountered and found to be problematic during operation (Leveson, 2012). These differences also exist in the mining industry.

This research was initiated when a discontinuity was observed between engineering (mainly responsible for acquisition) and mining operations dependent on electronic equipment for safe operations. It was thus necessary to investigate and reduce the magnitude of this discontinuity as it could lead to loss of human lives. The two cultures within these two sections of the same organization can never be fully harmonized, as an acquisition culture usually focuses on the management of projects with clear start and end dates, while an operations culture is essentially focused on the management of events that are cyclic in nature.

A generic framework for the assessment and management of risk, which we will call activity-based risk (ABR), was developed to provide an abstract view of equipment and its relation to operational risk with a distinctly pragmatic focus. The aim of the ABR acquisition process model is to assist risk analysts, engineers, and operations managers by providing a full life-cycle view of risk during acquisition when the most important system and operational design decisions must be made.

There are different ways to demonstrate the value of risk modelling. The ABR approach provides decision support information in the form of relativistic risk comparisons to enable well-informed trade-off studies. A relativistic approach allows the engineer to decide on functionality and resource definitions in the development phase (a function-focused approach), and allows the manager to understand the impact of resource selection (a resource-focused approach) on the risk of a system in operation.

* *Jericho Systems Pty Ltd, South Africa.*
† *North-West University, University in Potchefstroom, South Africa.*

 ISSN 2225-6253. Paper received Mar. 2016; revised paper received Apr. 2016.

ABR, as such, provides a view of risks associated with specific activities forming part of a larger operation, with the aim of defining an equipment configuration (including a 'function set') that is optimally designed to support specific operations. The end result of ABR analysis is an equipment functional configuration that has been optimized based on the analysis of its expected behaviour in actual operations, as opposed to a configuration that has been defined in disregard of its interaction with the operational domain.

The following sections define challenges of existing acquisition processes, provide a solution to these challenges in the form of an ABR process, and demonstrate by means of simulation the advantages of using ABR management.

Challenges of existing processes for acquisition of mine safety equipment

Shortfalls in existing acquisition processes were determined from an analysis of available literature, observations from practical projects, and a specific case study (van der Merwe, 2014)

- *Product / system requirements:* From observations it was found that, when acquiring new equipment for mines, the preliminary design phase that follows the concept phase was neglected in many instances due to project time constraints and limited project resource capability. The preliminary design phase should include system behavioural analysis, architectural design, requirements allocation, and system synthesis and evaluation. Omission of any of these steps will result in major problems during the subsequent development, deployment and operational phases
- *Sub-optimal safety technology:* Through observations, it was established that sub-optimal safety technology could be deployed in operations due to limited effort in the preliminary design phase. It was found that either end-products did not fully address the initial problem or that the end-product reduced productivity—that is, initial requirements had not been properly validated. When safety systems have a negative impact on production they often tend not to be accepted by end-users and are often vandalized or bypassed. The result is that more than one development iteration may be required to determine a suitable solution, with budget, time, resource, and legal implications
- *Focus on hazard exposure and expert input:* Traditionally, risk analyses relied heavily on hazard analyses without taking into account the complexities of safety systems (Leveson, 2012). This was supported by observations. The result is that hazards to humans are identified, but the effects of production and technology risk are not always fully evaluated with regard to functionality, usability, and reliability in complex systems. While hazard analyses remain critical and must be performed for all products and systems, form should follow function, and not the other way round. It would normally be assumed that the integrity of such a risk assessment result is determined by the experience of the risk assessment team. Thus, regardless the level of experience of the assessment team, the lack of a systems engineering (SE) approach to system safety can still lead to invalid or suboptimal results (Aven, 2009; Leveson, 2012)
- *Impact of technology:* Due to the lack of independent assessment, risk assessment quality varies between different safety equipment suppliers, since suppliers are sometimes required to perform assessments on their own equipment. This makes it very hard to identify a safety product or system with the lowest risk score as a uniform measurement standard is not used across assessments (Backlund and Hannu, 2002). The technology supplier is, in many cases, not aware of the exact operating conditions under which a product will operate and often does not take productivity into account
- *Human integration:* Observations showed that consideration of human performance variability was not evident in risk analysis processes as a particular focus. The focus in a risk analysis is based on what the impact will be on the human, while the impact of humans on technology and the environment is often not considered formally. To arrive at valid results, human behaviour must be integrated in the evaluation of risk in an operational environment as variability in human operator performance has been shown to have the highest impact on risk (Oberholzer and Thorpe, 1995; Leveson, 2012; Dekker, 2001, Hallbert, 2006; Badenhorst and van Tonder, 2004).

Activity-based risk

An acquisition process based on ABR can address the shortfalls identified above, since ABR has the following characteristics:

- It is a relativistic approach for comparison of different technologies in an integrated operational environment
- It addresses risk and cost reduction by following an iterative design, simulation, and evaluation approach using a functional framework
- It incorporates the impact of human error using risk scores and profiles that define human performance (from which probability distributions are derived)
- It translates risk to understandable operational response measures determined from consistent, realistic simulations
- It provides a balanced solution that takes into account the abilities of technology (in terms of functional requirements) and human resources (in terms of risk performance)
- It provides a body of reference knowledge that is reusable and adaptable to accommodate system improvement over time
- It provides visual results from simulations for decision support
- As ABR follows an SE process, it brings together stakeholders from engineering and mining through a requirements management process
- The ABR acquisition process specifically addresses a discontinuity between acquisition and operations by focusing on a functional analysis performed in the preliminary design phase of the product life-cycle.

Figure 1 provides a process flow view of ABR as described in the sections to follow.

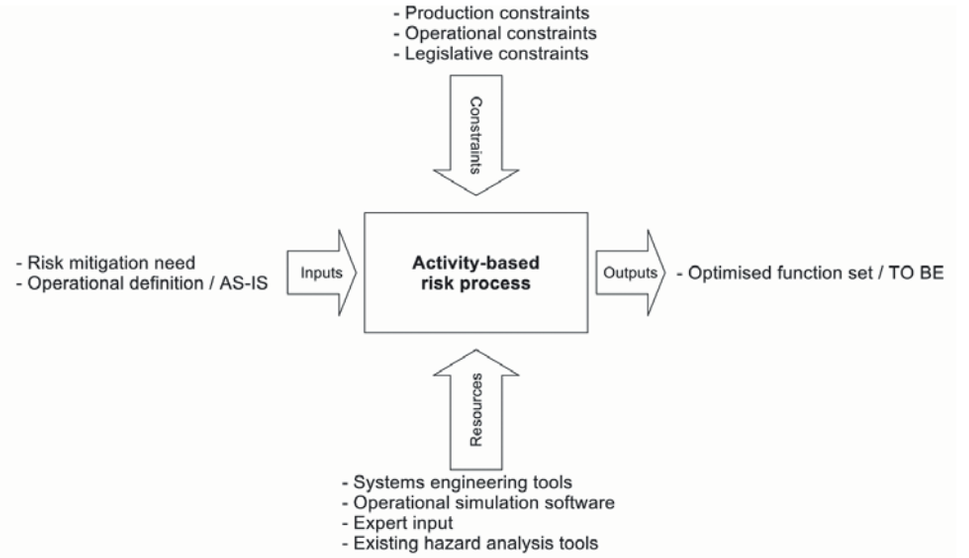

Figure 1—Process flow view of ABR method

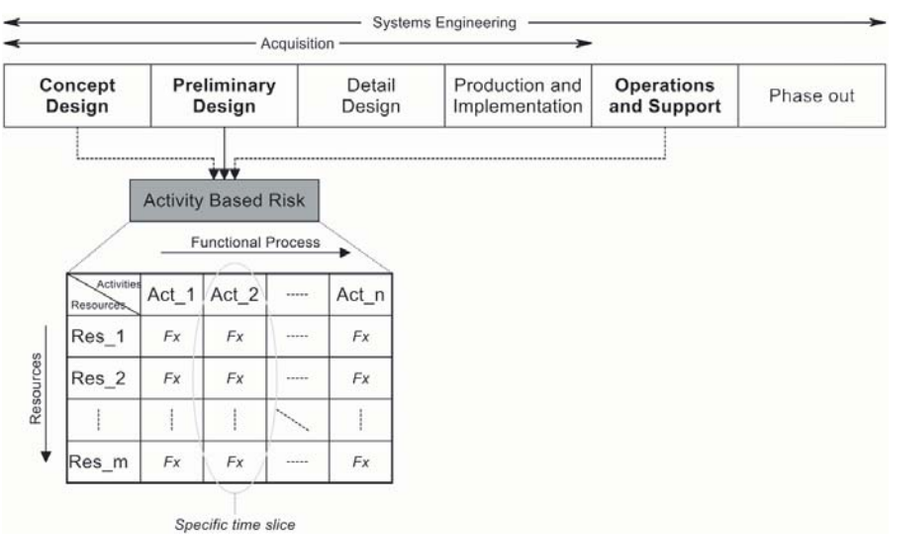

Figure 2—Activity-based risk within the SE process

The most important objective of ABR is to provide a *function set,* selected by a scientifically sound evaluation process, where this resulting function set clearly defines the safety system's behaviour and architecture—that is, the resulting function set is an unambiguous functional specification.

The ABR method thus makes use of a SE process with specific focus on preliminary design. Functional analysis forms an important part of this design activity. In the ABR process, system activities in the diagram in Figure 2 (indicated as Act_*n*) are identified as subsets of a full function set. This is done to allow focused analysis of individual activities and identification of high-risk activities and critical resources. Each system activity is a logical grouping of functions that draws together resources (Res_*n*) so that an *integrated analysis* is done when analysing *individual activities*. That is, smaller groupings of functions are analysed in such a way that all participating resources are taken into account, as opposed to considering failures of individual resources in isolation.

All system functions and resource operational states must be mapped to all system activities for modelling purposes in a form similar to a swim lane analysis as found in business process engineering literature (Jeyaraj and Sauter 2014). This is shown in Figure 2, with resource functions and states represented by '*Fx*'. In the diagram, '*Fx*' represents more than one function of a resource. The resource allocation table allows the designer to determine risks related to failures of resources and related system functions from the table. This approach enables 'optimization' of a system in terms of functional requirements and allows definition of desired characteristics of operators (and other human resources) that interact with the system.

ABR is thus a logical extension of the concept of baseline hazard identification. Baseline hazard assessment defines relative risk of high-level activities (for example, stoping) in terms of its baseline risk profile, which in turn is based on environmental factors and activities conducted in such hazardous environments (Boshoff, 2014; Paithankar, 2011). High-level activities can be broken down into smaller activity groupings that combine tasks in a logical way. This classifies ABR analysis—in this context—as a *middle-out* approach, as opposed to a *top-down* or *bottom-up* approach.

ABR relies heavily on the simulation of a system in operation in order to deal with complexity issues. A simulation is done instead of a pure mathematical analysis as it has the following advantages:

- A solid understanding of core operational activities (from a functional flow and architecture) is gained by engineering and operations when drawing up an understandable operational model. An understandable model is more pragmatic than purely mathematical and statistical models that require specialist knowledge and are difficult to understand
- Process blocks are defined (from a functional analysis) and used in simulations to implement complex functions, which assist with the understanding and modelling of a large number of resource functions, resources states, and interdependencies between resources and their states. This aligns well with the advantages of functional resonance accident modelling (FRAM) (Herrera, 2012)
- An integrated view of all relevant resources is obtained in the simulation model as the simulation does not focus on a single resource (as is usually the case in human factor analysis), but on the complete set of integrated resources that take part in that system activity
- A relativistic comparison can be made between candidate systems or products because a simulation model is drawn up for each candidate system. Variations between candidate systems are implemented fairly easily, as a basic simulation framework is constructed for the first model and then adapted for alternative models
- Information is preserved in the model for future adaptation to a selected system. This prevents reinvention of solutions and provides a body of knowledge for business continuity.

Implementation of ABR is shown in Figure 3. The sequence of steps is as follows.

Step 1: Define AS-IS design

The AS-IS design defines safety equipment currently in use. If no specific safety equipment exists and new technology is introduced, the AS-IS environment and operational functions are defined by a comprehensive operational analysis.

Step 2: Do concept design for the TO-BE system

The conceptual design of a safety system is typically defined by the mine in consultation with subject matter experts. This defines all required characteristics for the TO-BE system. From this conceptual design, operational requirements are used as inputs to the preliminary design step.

The feedback loop in Figure 3 allows a designer to improve the concept design iteratively by comparing simulated candidate systems, as opposed to physically implementing each system. It is imperative to consider more than one solution, or variations of a solution, as the focus of ABR is to provide a relativistic comparison of candidate systems.

Step 3: Perform functional analysis on candidate systems

The system AS-IS functional analyses (from the preliminary design) is adapted to address requirements of the TO-BE candidate systems. An adapted functional analysis is provided for each candidate system. Commonly, candidate systems are altered versions of the AS-IS or new concept system.

Step 3.1: Define system functional architecture

A functional architecture is drawn up for each candidate system to define a configuration of functional units for all candidate models, including performance and allocated non-functional characteristics. All physical resources linked to functional units of the system architecture must be identified.

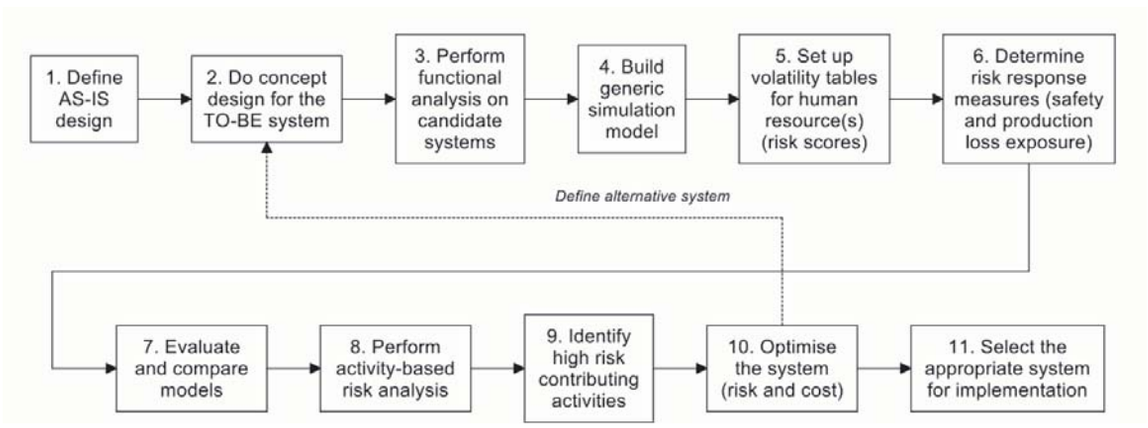

Figure 3—The ABR-based acquisition process

Step 3.2: Define system interfaces

System interface definitions form part of the system architecture and define all interdependencies between architectural components. Interfaces between resources (humans/equipment/environment) must be clearly indicated and defined. These interfaces must include:

- Functional interfaces in the abstracted model, showing interdependencies that will affect functional flow for modelling purposes
- Physical interfaces, such as mechanical, electrical, IT-related, and user/ergonomic interfaces.

Step 3.3: Define functional flows/states for resources

All resource states and functions are defined, where resources typically include operators and other end-users of the system, as well as core operational equipment and safety system equipment operating within a specific environment.

Functional flows (from the preliminary design) are augmented by event trees to account for human resource variability and human-equipment interaction. An event tree exists for every candidate system, thus taking into account variability in technology. The flows include functions of all acting human resources. In an event tree, all possible routes are established by evaluating all possible decisions and actions taken by a human resource, given the operational flow and environment.

It is important to note that for the implementation of the ABR approach the outcomes of interactions between human functions, equipment, and the environment are presented as states in an event tree. This allows a designer to define system state diagrams that represent the interaction of all candidate safety systems with human operators, operational equipment, and the operational environments.

The definition and clear documentation of functional flows and states are critical to the ABR process, as these will directly assist with the implementation of a system model when a simulation model is constructed. State modelling requires specialist knowledge about the states that safety equipment can assume – therefore, safety equipment designers must be part of the functional modelling process.

Step 3.4: Define activities

A set of required system activities is defined for all candidate systems. System activities are subsets of the overall function set and are logical activities that form part of the operation of a system; for example, phases of a functional flow over time. A system activity is a logical grouping that draws together all participating resources in a subset of the overall functional flow.

A common set of activities must be used for all candidate systems for relativistic comparison, even though some activities may not be present in all candidate systems.

It is critical to identify transitions between activities, as risk conditions usually change during such transitions. For example, changing from a safe to an unsafe state requires coordination between resources; if this is not correctly implemented it may lead to transient effects.

Step 3.5: Allocate resources

A resource allocation is performed in a tabular format with system activities along columns and resources along rows. The predefined states for each resource and the functions that may be performed within these states are also linked to each activity using this table. Resources that contribute to activities must be presented as primary or secondary: primary resources perform core functions, while all remaining resources perform secondary functions.

A resource allocation is the first step towards identification of resource risks of a system. This table allows identification of critical resources and the impact on system activities when resources fail. This is also a first step towards risk mitigation by identifying alternative functions and resources. A more detailed risk analysis is performed in the following steps.

Step 4: Build generic simulation model

A detailed comparison between the alternative safety systems requires an analysis of all processes and resource states for a representative set of scenarios. As manual analysis alone cannot deal with this level of complexity a simulation model is implemented for each candidate system within the defined operational environment. A simulation platform such as SIMIO® is employed to implement all candidate systems as a set of interconnected process blocks. Outputs from such simulations will be used to identify risks during later steps of the process.

Functional flows (translated to event trees) include human resource decisions and actions that can be implemented as process flows in simulation software, while states of equipment are used to model interactions between resources according to the functional flow. This approach simplifies the analysis of operationally complex models significantly. Visual representation of system elements and their interactions is also available to support design decisions.

Validation of operational performance parameters is important when constructing an operational model. Performance parameters define activities in functional flows and must be defined and allocated to represent real-world scenarios accurately. In many instances system performance is dependent on risk profiles / scores of human resources.

A design team defines candidate system models with their parameters and operational performance measures so that parameters and performance measures agree and align across different models. This is done to allow a relativistic comparison between candidate models.

Step 5: Set up volatility tables for human resources

Volatility tables introduce human error in a multidimensional operational context. Volatility tables are therefore set up for activities where humans may deviate or fail. Decisions and/or alternative actions at branches in the event tree are identified in the functional analysis where all possible branches in the system's functional flow are defined.

In order to draw up such tables, the design team must define risk scores for system operators. It is possible to use psychometric modelling for this purpose (Dekker, 2001, 2006; Embrey and Zaed, 2010), particularly for operators that work in high-risk environments.

A risk rating of a human resource is used in the simulation model to define the required parameters of a probability density distribution for failures at specific tasks in

an operational workflow. These probability distributions will be implemented by the simulation software in order to generate realistic distributions of system outcomes that take into account the variability of human operator actions.

The operational model thus combines the realistically expected behaviour of humans and technology through operational workflows, event trees, and resource allocations for each activity. This is done in a multidimensional operational environment, taking into account all system resource states and interdependencies.

Although the estimation of human performance parameters introduces an element of uncertainty, the relativistic approach followed in the ABR method largely alleviates this issue. It must be taken into account that the ultimate aim is to identify the most appropriate safety equipment based on a realistic comparison of alternatives. As all candidate systems make use of the same human resources with the same estimated characteristics, the estimated accuracy of human performance parameters is important but not overly critical.

Step 6: Determine risk response measures/factors

Appropriate risk response measures must be identified for use in the simulation model to represent risk in an operational sense. These risk response measures are dependent on the type of risk being analysed and are selected to be semantically appropriate in an operational environment; they can typically be time of exposure to unsafe conditions and number of equipment or human failures.

Safety and production are juxtaposed and must be balanced in a production environment. For this reason two separate measures are required that relate directly to safety and production. Measures aligned with safety and production risk are hazardous exposure (time) and production loss (time), respectively. Hazardous exposure is the time a human operator spends in a hazardous environment when the system is in an unsafe state. Production loss time is production time lost due to suspension of operations for safety and other reasons.

One may argue that hazardous exposure does not always lead to an accident, and that time lost for production does not imply production would have taken place. However, the probability of an injury or fatality occurring when the system is in an unsafe state is proportional to the time operators spend in hazardous environments, and production time lost could have been used for production in a productive organization. Moreover, a safety culture may increase or decrease the probability of injuries and fatalities, and a production culture affects the probability of production in a similar fashion. As long as a realistic and consistent risk allocation method is followed, the result of the ABR process is a relativistic comparison between candidate systems as the same set of conditions apply to all candidate systems.

Step 7: Evaluate and compare models

In essence, candidate systems are compared by taking into consideration system sensitivity with respect to human variability in a predefined operational environment. Simulation response measures are evaluated for each candidate system to minimize the selected risk response measures, that is, to obtain the minimum hazardous exposure and minimum loss in production time.

Multiple simulation runs are executed for each alternative option in order to generate representative statistics for performance measures, due to the stochastic nature of human activity in process models. The number of simulation runs is selected to provide statistics within acceptable confidence intervals. From the response measures of simulations, trends and worst-case scenarios are determined.

Step 8: Perform detailed risk analysis

A detailed risk analysis is imperative in the ABR process, as this is where risks associated with activities are identified. In this step, a table is constructed indicating the impact when deviations or failures are introduced into a specific activity. This allows identification of high-risk activities that are sensitive to human variation in the system. These activities are addressed when performing system optimization.

The process for performing a detailed risk analysis is shown in Figure 4.

All identified activities are analysed sequentially. Primary resources must be analysed specifically, but all activities are taken into account during simulation. When a candidate system's technology (equipment) does not act as a primary resource for an activity, the candidate system does not constitute a primary contributor to risk for that activity.

When the candidate system acts as a primary resource, all possible human variations/deviations for this activity are analysed. Typical deviations include time to execute a task or failure to execute a task. In many activities, failures result in activities not being performed. Once possible deviations have been determined, each deviation is implemented and simulations are run for the complete system, including all variations. Response measures from simulations are compared with response measures of the candidate system model without deviations. This comparison shows the impact of deviations on activities. Impacts are updated in an activity risk table. Once all activities have been analysed and the activity risk table has been completed, high-risk activities are identified for adaptation, replacement, or removal.

Step 9: Select high-risk activities

High-risk activities are summarized in an activity risk table. Activities that are sensitive to failure and performance deviation will show up in the table and are identified as critical. These activities are used in the optimization step.

Step 10: Optimize the system

A system can be optimized with respect to risk by addressing high-risk activities first. This is achieved by evaluating candidate system models where high-risk activities (or technologies) can be altered to reduce risk, or where risk controls can be added. Each candidate system is analysed to determine the impact on activities for all systems, until an optimized system is obtained either in terms of risk or cost, depending on the risk appetite of the mine.

The winning system is further optimized for cost by adapting or removing high-cost functions and activities. In the evaluation of a system, focus is maintained on the cost of the actual system hardware and its supporting elements only, excluding the cost of injuries or fatalities. This is achieved by reducing the functionality of the successful system by using

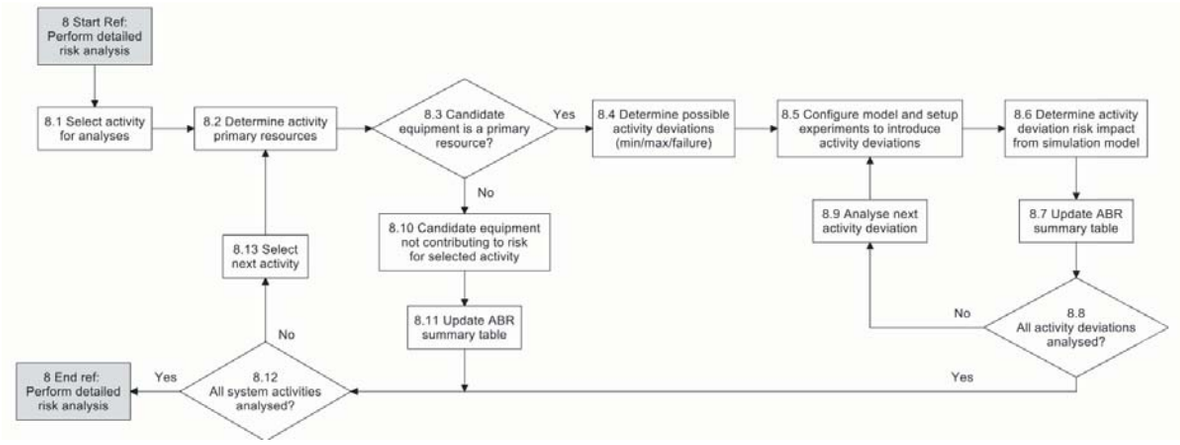

Figure 4—Process for step 8: performing an ABR analysis

results from the analysis. Throughout, inclusion of critical features and exclusion of redundant features are ensured. With every change, however small, the complete system must be re-evaluated.

This optimization cycle allows for risk reduction by adjusting or removing high-risk functions, but also provides valuable information on the sensitivity of the system with respect to human performance variation. A system can be optimized up to a point by altering technology, after which residual risk must be reduced by addressing human factors specifically. Human factors are changed by changing organizational policy and culture, which results in changes in support processes (training, safety awareness, etc.), operational measurement, and control processes and procedures.

When optimizing a system for cost, the design team and other stakeholders must perform a trade-off analysis between modifying system functions and modifying human procedures to reach a point that is regarded as optimal. This may include cases where it is more cost-effective to use a more affordable system with reduced functionality, and to address residual risk by modifying human procedures instead of investing in further technology. ABR analysis shows where the point of diminishing returns lies.

Step 11: Select the appropriate system for implementation

Once the system has been optimized for functionality and cost, specific system characteristics are used as inputs to the detail requirements for the detail design phase of the SE life-cycle, after which the system is implemented and evaluated in operation.

Results

The ABR process was validated by means of a real-world case study, in which the ABR process was applied to a winch signalling safety system for scraping operations in stopes. Four candidate systems were analysed and evaluated using the ABR process. The first system was a conventional air-whistle system (AWS) that represented the AS-IS system. The TO-BE system was an electronic signalling system (ESS), a concept proposed by a local mine (ESS1). The ABR analysis of these two systems identified high-cost and high-risk functions associated with ESS1, resulting in the identification of two further candidate systems, namely a risk-reduced system (ESS2) and a cost-reduced system (ESS3). The risk-reduced system focuses purely on reducing risk (that is, reducing hazardous exposure, for example), while the cost-reduced system focuses on a balance between risk and cost by considering both hazardous exposure and production loss.

In the ABR analysis of the winch signalling system, five risk levels for the human resources were defined, with 1 being low risk and 5 being high risk. In order to understand the effect of operator risk, a system designer has to adjust the risk level of an operator, followed by an analysis of the complete system (that is, including all system elements). The complete system analysis may then show an increase or decrease in production and, similarly, an increase or decrease in risk. This form of sensitivity analysis allows the designer to find an optimal risk level for an operator, or identify a point of diminishing returns where a decrease in risk level no longer yields dividends. The operator risk levels were incorporated into an operational simulation model developed and implemented in SIMIO®, an object-oriented software modelling tool (Pegden and Sturrock, 2013). Interesting results relating to hazardous exposure and production loss are presented in Figure 5 and Figure 6.

Figure 5 and Figure 6 show results for scenarios where the risk levels of miner crossing a gully (MCRL) varied between 1 and 5, coupled with a risk level of a winch driver (WDRL) at level 3 on the same risk scale—these risk values translated directly to decisions and actions at key points in the validated simulation model's work flow. An average risk of level 3 was assigned to the winch driver as the impact of the winch driver on risk was small compared to that of miners.

To compare the candidate systems in a relativistic sense, normalized risk-related factors were defined (not risk in strict definition, but rather a normalized score that fits the ontology of the mining environment). The production loss factor (PLF) represented possible production loss time on a scale of 1 to 10. For example, a PLF value of 3 implied that 30% of maximum possible production time was lost. A hazardous exposure factor (HEF) represented time during which a gully was used by miners while in an unsafe state. For example, an HEF value of 2 implied that a miner was in an unsafe gully 20% of the time.

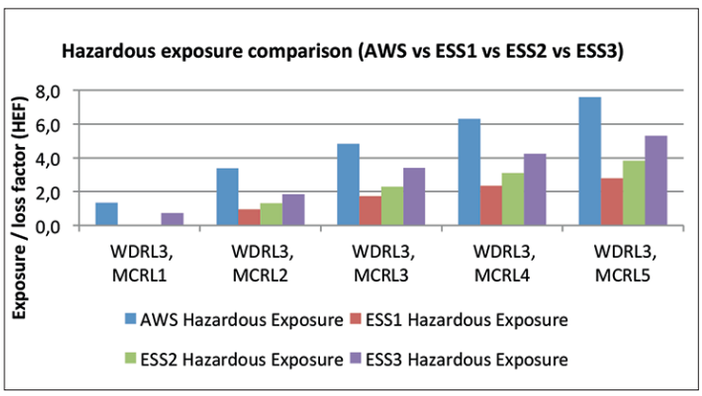

Figure 5—ABR analysis – hazardous exposure comparison

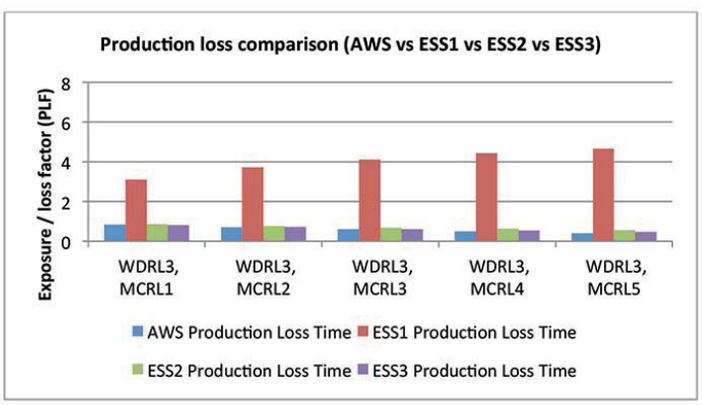

Figure 6—ABR analysis – production loss comparison

A sufficient number of simulations runs were performed to obtain statistically significant, normalized results. Results for different scenarios (Figure 5 and Figure 6) show high hazardous exposure for the AWS and low production loss – this was also observed in practice. The ESS1 system directly addressed hazardous exposure by lowering this level, but showed a significant increase (as observed) in production loss. The results from the risk-reduced system (ESS2) show that production losses were significantly reduced, but with a slight increase in hazardous exposure. The ESS3 system with cost-reduced functionality showed a further increase in hazardous exposure while the production loss remained at a low level. Interestingly, both the AWS and ESS1 systems were rejected by the mines, while the ESS2 and ESS3 systems were retained. The decision to select the ESS2 and ESS3 systems was based on physical evaluation of all systems in controlled environments.

From Figure 5 it is noted that hazardous exposure increases significantly as the risk level (MCRLn) of the miner crossing the gully increases for an average-risk winch driver (WDRL3), which demonstrates the system's sensitivity with respect to the risk level of a miner crossing. The system was found to be significantly less sensitive with respect to the risk level of a winch driver when electronic winch signalling equipment was used to control the overall system states and state transitions (not shown, but determined from ABR analysis). It was also seen from ABR analysis that with the AWS system, the hazardous exposure increased significantly when the winch driver risk level increased; this is due to limited system state control when using an AWS system.

Figures 7 to 10 show the sensitivity of the change in risk level of the resources with respect to hazardous exposure and production loss. The analysis shows that hazardous exposure increases significantly as the risk level of the miner crossing the gully increases (Figure 7) while the system (except for the AWS) is less sensitive to a change in the risk level of a winch driver operating the signalling system (Figure 8). The main reason for the decrease in sensitivity of the electronic signalling systems with respect to the winch driver (ESS 1 – 3) is that the system can be tripped from a gully and is not entirely dependent on a winch operator.

Production loss sensitivity with respect to resources as displayed in Figures 9 and 10 is fairly low (less than 1, on a scale of 1 to 10) for all systems except ESS1, since ESS1 requires a winch driver to perform gully inspection after every voluntary trip condition—clearly a time-consuming task. In contrast it can be seen that for the AWS, ESS2, and ESS3 production loss decreases slightly with an increase in resource risk level. This is because a more risky winch driver will ignore more signals from the gully, thus using the

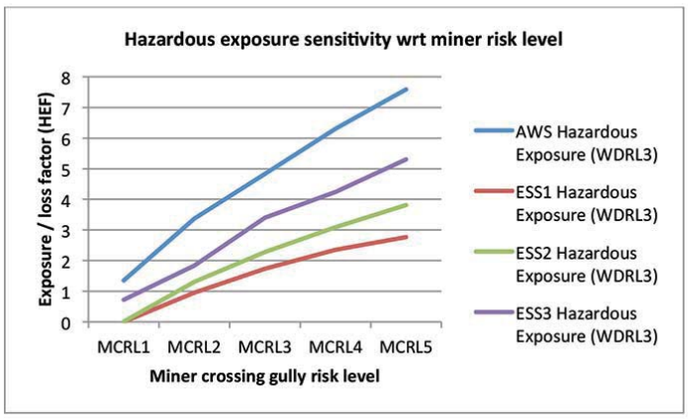

Figure 7—ABR analysis – hazardous exposure sensitivity with respect to miner risk level

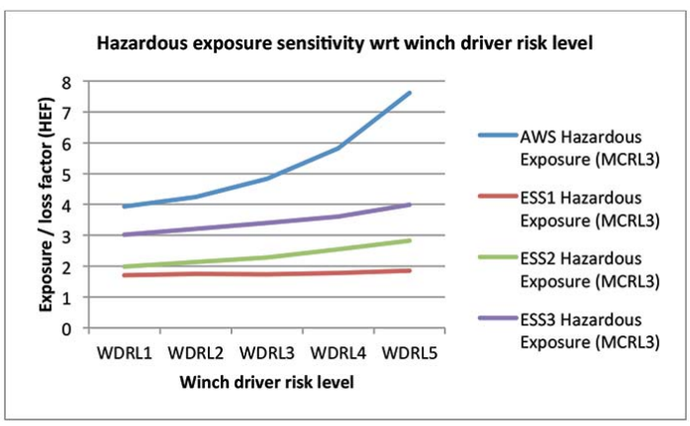

Figure 8—ABR analysis – hazardous exposure sensitivity with respect to winch driver risk level

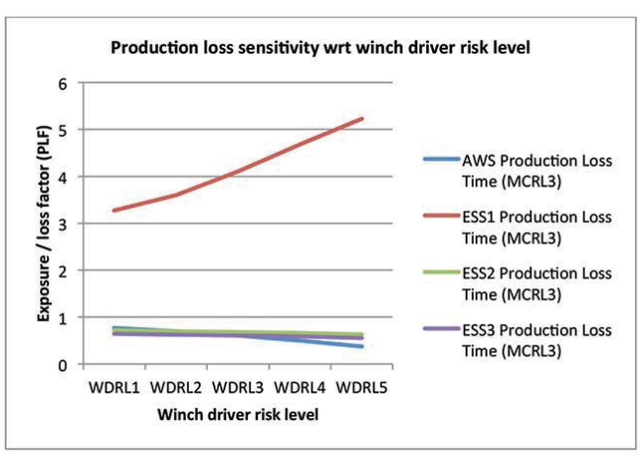

Figure 9—ABR analysis – production loss sensitivity with respect to winch driver risk level

system in an unsafe state. The same happens with miners crossing a gully: more risky miners will ignore (or fail to determine) gully states and will cross gullies in unsafe states.

A balance between production loss and hazardous exposure must be obtained, both of which are provided by ESS2 (risk-reduced) and ESS3 (cost-reduced), with ESS3 being slightly less costly but more risky than ESS2. From the results, it is clear that the function sets of ESS2 and ESS3 represent solutions that are more suitable than the AWS or ESS1 alternatives, as long as winch drivers' and (mostly) miners' risk levels are properly managed.

Conclusion

An activity-based risk (ABR) method was developed to address shortfalls in the acquisition of electronic safety

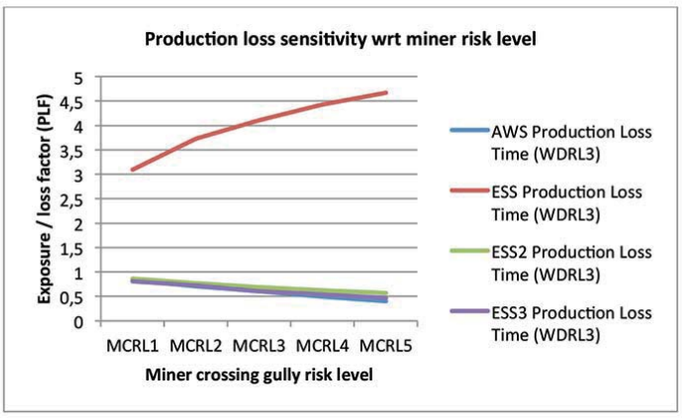

Figure 10—ABR analysis – production loss sensitivity with respect to miner crossing risk level

equipment in mines. Most notably, ABR supports the selection of an optimal function set with respect to risk-related factors and cost while also addressing operational requirements. ABR is most effective when used during the preliminary design phase of a systems engineering process, and provides a framework for drawing comparisons between candidate systems. Constructing and simulating a state-space representation of the operational environment allows the modelling of human behaviour in a complex operational environment and forms a critical element of ABR.

In a real-world case study, an electronic winch signalling system was analysed to address safety risks in winch scraping activities. The ABR method was employed to determine high-risk activities for three candidate systems, resulting in the definition of a risk-reduced system where a balance was found between production risk and hazardous exposure. A cost-reduced system was also evaluated, and showed a slight increase in hazardous exposure with respect to the risk-reduced system, but allowing equipment cost to be significantly reduced. Feedback obtained from mines correlated with the ABR model results and validated findings in the winch signalling case study.

Results from this research show that human behaviour can be modelled in complex systems by following a structured process of modelling and analysis. Operational models should be used to determine function sets for equipment by considering risk and production losses and allowing variation in equipment functionality and human behaviour.

The results provide conclusive evidence that in order to accurately compare alternative solutions to operational problems it is essential to perform a detailed analysis that quantifies the impact of each process activity on each of the operational performance criteria. It was furthermore shown that the impact of both technology and human resources, and the interaction between these, on operational performance must be clearly described for each alternative solution. Evidence was presented to demonstrate how a simulation approach can be used to implement a relativistic comparison between alternatives that can support accurate and reliable decision-making about the acquisition of safety systems before such systems are deployed, in the process saving significant costs in terms of unsuccessful system deployments, loss in production, and risk to human lives.

Future work will include a comparison between the results produced by the simulators developed as part of this research and actual operational activities in mines that employ different safety concepts. This will allow the proposed approach to be refined and the simulators to be calibrated to real-world results.

References

Aven, T. 2009. Trends in quantitative risk assessments. *International Journal of Performability Engineering*, vol. 5, no. 5. p. 447.

Backlund, F. and Hannu J. 2002.Can we make maintenance decisions on risk analysis results? *Journal of Quality in Maintenance Engineering*, vol. 8, no. 1. pp. 77–91.

Badenhorst, F., and van Tonder, J. 2004. Determining the factors causing human error deficiencies at a public utility company. *South African Journal of Human Resource Management,* vol. 2, no. 3. pp. 62–69.

Boshoff, T. Not dated. Different risk assessment types. http://www.labourguide.co.za [Accessed 18 October 2014].

Dekker, S.W.A. 2001. The re-invention of human error. *Human Factors and Aerospace Safety*, vol. 1, no. 3. pp. 247–265.

Dekker, S.W.A. 2006.The Field Guide to Human Error. Cranfield University Press, Bedford, UK.

Embrey, D. and Zaed, S. 2010. A set of computer based tools identifying and preventing human error in plant operations. *Proceedings of the 6th Global Conference on Safety*. AIChE, San Antonio, TX. pp. 1–11.

Hallbert, B., Boring, R., Gertman, D., Dudenhoeffer, D., Whaley, A., Marble, J., and Joe, J. 2006. Human event repository and analysis (HERA) system, overview. Division of Risk Assessment and Special Projects, Office of Nuclear Regulatory Research, US Nuclear Regulatory Commission.

Herrera, I.A., and Woltjer, R. 2010. Comparing a multi-linear (STEP) and systemic (FRAM) method for accident analysis. *Reliability Engineering & System Safety*, vol. 95, no. 12. pp. 1269–1275.

Jeyaraj, A. and Sauter, V.L. 2014. Validation of business process models using swimlane diagrams. *Journal of Information Technology Management*, vol. XXV, no. 4. pp. 27–37.

Leveson, N.G. 2012. Engineering a Safer World: Systems Thinking Applied to Safety. MIT Press, Cambridge, MA.

Oberholzer, J. and Thorpe, L. 1995. An assessment of the most significant causes of transportation and machinery accidents on collieries. Safety in Mines Research Advisory Committee, COL 203, August 1995. Johannesburg, South Africa. pp. 1–64.

Paithankar, A. 2011. Hazard identification and risk analysis in mining industry. Department of Mining Engineering, National Institute of Technololgy, Rourkela, India.

Pegden, C. and Sturrock, D. 2013. Rapid modeling solutions: introduction to simulation and Simio. Simio LLC, Pittsburgh, PA

Van der Merwe, G.P.R. 2014. A risk-based approach to the acquisition of electronic safety equipment for mines. PhD thesis, North-West University, Potchefstroom, South Africa. ◆

http://dx.doi.org/10.17159/2411-9717/2017/v117n6a3

Strapping of pillars with cables to enhance pillar stability

by L.R. Alejano*§, J. Arzúa†, U. Castro-Filgueira* and F. Malan‡

Synopsis

Pillar design for underground mining is typically done using empirical formulae or numerical modelling. Practical experience and recent literature, nevertheless, illustrate the shortcomings of these design approaches. Ongoing monitoring of pillars is therefore recommended to minimize the risk associated with these designs.

In a mine where a large number of pillars are cut, different pillar strengths can be expected owing to variations in rock mass strength from area to area. This problem is compounded by the fact that in mining environments the pillars are not always cut according to the prescribed dimensions. Although the original design using either empirical methods or modelling may predict stable pillars, unstable pillars will be encountered in reality. Very conservative designs with large factors of safety may circumvent this problem, but this approach is uneconomical.

A possible solution to localized stability problems may be to enhance the strength of a few unstable pillars. It may even be hypothesized that reinforcing a few critical pillars may prevent 'pillar runs' on a much larger scale. Rockbolting, strapping of pillars, and pillar shotcreting have occasionally been used in the past as possible solutions. It appears that these have not been successful in all cases and large collapses have occurred in spite of the pillar remedial work.

The authors investigated the strapping of pillars by conducting laboratory tests on cabled rock specimens. The results were qualitatively compared to actual attempts of pillar reinforcement available in the literature, as well as additional observations in an old haematite room-and- pillar mine in Spain. Based on these results, the value of steel cabling and mesh wrapped around pillars to improve stability is demonstrated. Some cases where this approach will not be successful are also discussed.

Keywords
room and pillar mining, pillar stability, support, strapping, cables.

Introduction

Although the extraction ratios in room and pillar mining can be low in some cases, it is still a widely used mining method for coal, base metals, industrial minerals (quartz, magnesite, rock salt), and ornamental stone (marble, slate). A major reason is that it tends to be cheaper than fill methods and is more environmentally friendly compared to caving methods (Alejano *et al.*, 2012).

Classic empirical pillar strength formulae are typically used as a first approximation for the design of pillars in coal (Salamon and Munro, 1967; Hustrulid, 1976; Bieniawski, 1992), hard rock (Hedley and Grant, 1972), and metal mines (Lunder and Pakalnis, 1997). This, in combination with stress estimates derived from the tributary area, can be used to calculate the factor of safety for the pillars (Brady and Brown, 2006). Alternatively, some authors have based their designs on numerical modelling studies (Martin and Maybee, 2000; Murali Mohan, Sheorey, and Kushwaha, 2001; Jaiswal and Shrivastva, 2009; Esterhuizen, Dolinar, and Ellenberger, 2011).

Recent reviews of pillar design methods and studies on typical problems encountered in room and pillar mines have nevertheless indicated that neither classic empirical formulae nor numerical methods will always guarantee stable designs (Malan and Napier, 2011; Hedley, Roxburgh, and Muppalaneni, 1984; Dismuke, Forsyth, and Stewart, 1994; van der Merwe, 2006). The variable strength of the rock mass may lead to local instabilities, or massive collapses may even be encountered (Malan and Napier, 2011). Very conservative designs, on the other hand, are also not satisfactory as they result in poor mineral extraction.

An evaluation of the strength of slender pillars based on a number of pillar failures in mines was conducted by Esterhuizen (2006). This indicated that for pillars having a width to height ratio in the range of 0.6 to 0.7, failure has been observed for pillar stresses varying between 20% and 65% of the laboratory rock strength. This is a wide range and illustrates that care should be exercised when choosing conservative designs to ensure safety *versus* higher extraction ratios to ensure more profitable operations.

* *Department of Natural Resources & Environmental Engineering, University of Vigo, Spain.*

† *Department of Metallurgical and Mining Engineering, Universidad Católica del Norte, Antofagasta, Chile.*

‡ *Department of Mining Engineering, University of Pretoria, Pretoria, South Africa.*

§ *Corresponding Author.*

 ISSN 2225-6253. Paper received May 2016; revised paper received Aug. 2016.

Strapping of pillars with cables to enhance pillar stability

Khair and Peng (1985), Chase, Zipf, and Mark (1994), and Zipf (2001) describe collapses of room and pillar mines in the USA. Malan and Napier (2011), van der Merwe (2006), and Madden, Canbulat, and York (1998) reviewed a number of similar collapses in South Africa. Similar studies have been conducted in Brazil, China, and Kazakhstan (Zingano, Koppe, and Costa, 2004; Wang, Shang, and Ma, 2008; Mansurov and German, 2009). The term 'catastrophic pillar failure' describes the mechanism whereby one or a few pillars fail initially; their load is then transferred to adjacent pillars, which also fail. This may result in a 'pillar run' and hundreds of pillars may fail in the process. It is hypothesized that if the initial pillars remain stable, catastrophic pillar failure can be prevented.

Based on this information and hypothesis, it would be useful for the mining industry to have an inexpensive technique available that can be easily applied to stabilize pillars after the initial signs of failure are observed. Such a technique, based on a laboratory study and tested in one mine, is presented in this paper. After the unstable pillars have been identified, the proposal is to wrap mesh around these pillars and then attach a number of pre-stressed steel cables around the pillar. This technique can also be applied to pillars that initially appear stable but are subjected to smaller factors of safety caused by poor blasting or poor excavation control.

The application and studies of similar techniques have very seldom been reported in the literature. In South Africa, a few cases exist of hard rock pillar failure where attempts were made to strengthen the pillars. Malan and Napier (2011) describe the reinforcement of pillars traversed by thick clay layers (up to 300 mm thick in some cases) using mesh and lacing (cabling) at the Wonderkop mine. The reinforcement of the pillars in this case was unfortunately not successful and the mine collapsed. This failure was attributed to the drilling process, which introduced additional water into the clay and this probably weakened the pillars further. The same authors reported a further failed attempt to increase the pillar confinement using fibre-reinforced shotcrete in a platinum mine in the Bushveld Complex. Siwak (1984) reported a similar failure in pillars in underground chalk quarries in northern France. The pillars were supported with a 6 mm thick layer of glass fibre reinforced resin, but the additional confinement only delayed, and did not prevent, the eventual failure. In contrast, Esterhuizen *et al.* (2011) reported the apparently successful use of rib pillar support, such as chain link mesh and bolts, to prevent further deterioration of large pillars in underground stone mines in the USA.

Collapses have occurred in Lorraine (France) during the last 50 years above abandoned room- and- pillar iron ore mines (Grgic, Hommand, and Hoxha, 2003). Wojtkoviak, Rai, and Bonvallet (1985) presented an interesting study of the effectiveness of various approaches to pillar reinforcement based on laboratory test samples. These included mine fill, rockbolting, shotcrete or resin spraying, and steel banding (pillar strapping). The tests demonstrated an increase in pillar strength using all these techniques, but unfortunately the study did not investigate the post-failure behaviour of pillars. An interesting statement in the paper is that the stability of the pillars will not ensure the stability of the entire excavation.

To demonstrate the value of pillar reinforcement, a rock engineering study of the testing of cable-reinforced rock specimens in the laboratory is presented in this paper. A case study is also described where this technique was successfully applied to control pillar failure in a small haematite mine.

Based on the information obtained, some guidelines are given on the applicability of the technique, as the success of this will be dependent on the type of pillars, geometry, and behaviour of the rock mass. The objective of the paper is not to change current methods used to design room and pillar mines, but to provide mining companies with a possible solution to localized stability problems in room and pillar operations. It is important to note that this technique will not be useful if there are serious design flaws in the regional layouts of room and pillar operations, such as the omission of regional barrier pillar support or if the assumed strength of the rock mass is completely wrong.

Behaviour of cable-reinforced pillars based on laboratory tests

Initial tests studying the effect of cable reinforcement

For the initial study, four uniaxial compressive strength tests were conducted in the laboratory on intact specimens of Indiana limestone 54 mm in diameter and 108 mm high. For these tests, the axial and radial strains were controlled and the load was increased to achieve a radial strain of 5% (if possible).

As shown in Figure 1, the first test was a standard uniaxial compression test, while in the other three tests the samples were surrounded by four straps. The strapping consisted of polyamide tie wraps and 2 mm and 3 mm steel cables. The cable strapping consisted of steel wire ropes clamped using U-shaped bolts. In order to keep the cables positioned correctly on the samples, pieces of cardboard were inserted between the cables and the sample before testing.

Figure 1 illustrates the stress-strain curves for the tests. The pre-peak behaviour of the sample was essentially unaffected by the presence of the strapping.The post-failure behaviour, in contrast, was significantly affected. The post-failure behaviour occured in a more controlled manner, which is particularly noticeable in the radial strain branch (σ_1, ε_3). Secondly, the strapped samples did not dilate as much as in the standard test (ε_v, ε_1). Additionally, whereas the standard test illustrates no residual sample strength (at ε_1 = 1% the strength decreased to almost zero), the samples still had a residual strength for strains ε_1 > 5%. It is also noteworthy that the control of dilation, as well as the residual strength, seems to be more pronounced for the stiffer and more robust strapping.

As a first conclusion, these initial tests indicated that strapping affects the post-failure behaviour by controlling the lateral strain, reducing the dilation, and ensuring that the specimens retain some residual strength. These effects are more pronounced when the strapping elements are stiffer and more robust. The peak strength of the specimens seems to be unaffected by the strapping, and this is probably due to the lack of initial tension in the cables.

Estimating the effect of cabling for large-scale specimens

A previous study (Arzúa and Alejano, 2013) investigated the

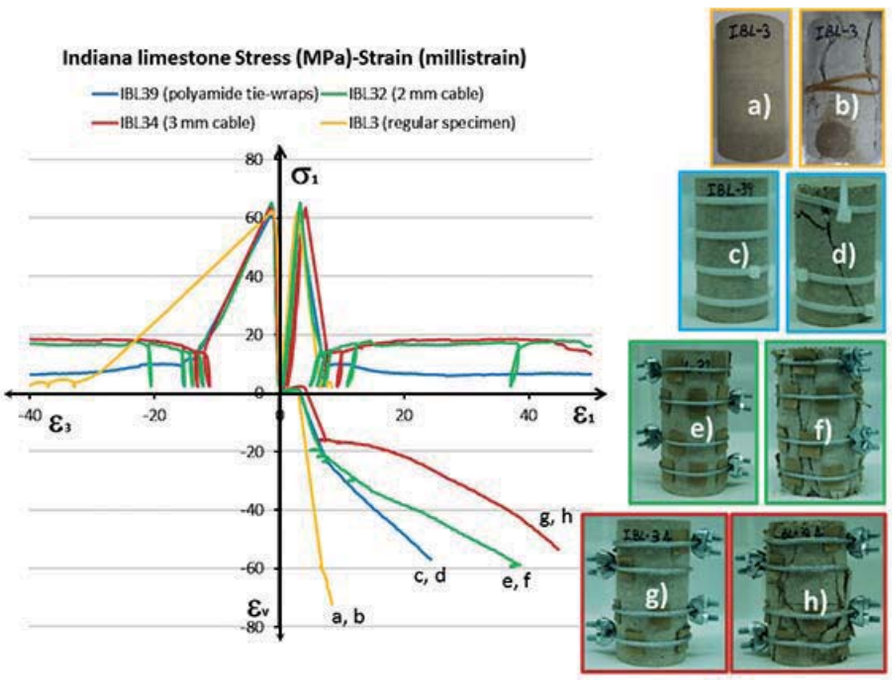

Figure 1—The complete stress-strain curves for four samples of Indiana limestone tested under uniaxial compression loading conditions. The photographs show the samples before and after testing. (a) and (b) untied, (c) and (d) polyamide tie straps, (e) and (f) 2 mm wire, (g) and (h) 3 mm cable)

complete stress-strain response of intact granitic rock. This was done by using a servo-controlled press modified to control the confining pressure in the triaxial tests and to measure the volume of hydraulic fluid displaced from Hoek's triaxial cell so that it could be related to the volumetric strain of the rock sample. More than 20 unconfined and confined compressive tests were performed on Amarelo País granite samples (Figure 2). The results were plotted and studied in relation to the most relevant parameters, including elastic, strength, and post-failure parameters.

The peak and residual strength envelopes were fitted using regression analysis techniques (Figure 3a). Information regarding the post-failure behaviour was obtained based on the full stress-strain results (σ_1, ε_1; σ_1, ε_3; and ε_v, ε_1) as shown in Figure 3b. In order to extend these observations to the behaviour of large-scale rock masses, the Hoek and Brown (1997) approach based on GSI (Marinos and Hoek, 2000) was adopted. According to Exdaktylos and Tsoutrelis (1993) and Cai *et al.* (2007) and our own observations (Arzúa, Alejano, and Walton, 2014), the residual strength of intact rocks, as interpreted from triaxial tests, could be similar to the that of jointed rock masses. It was also observed that the stress drop from peak to residual values, when confinement increases, results in a shallower slope (Figure 3b).

Statistical fitting of unconfined and triaxial strength results enabled the intact rock strength envelope (blue) to be fitted (Figure 3a and c) and estimation of the Hoek-Brown parameters of this rock as UCS= 76.59 MPa and m = 40.96. This, in turn, can be used to compute strength envelopes for different quality rock masses (*e.g.*, GSI 90 or 65, following the GSI approach), shown in green and orange colours respectively in Figure 3c. It is also possible to back-analyse the GSI value that would make the UCS of the rock mass equal to that estimated according to pillar formulae. Thus, for a 4 m wide and 8 m high pillar, and using the Hedley and Grant (1972) formula $\sigma_{pillar} = 0.74 \times \sigma_{ci} \times W^{0.5} \times H^{-0.75}$, a compressive strength of 23.8 MPa is estimated for the pillar, equivalent to that for a rock mass with GSI 79. This would lead to a strength envelope shown by the dotted grey line in Figure 3c.

Based on the assumption of scale-independent residual strength discussed above, it is possible to estimate the complete stress-strain response of the rock mass for different rock qualities and for the pillar. This behaviour for three

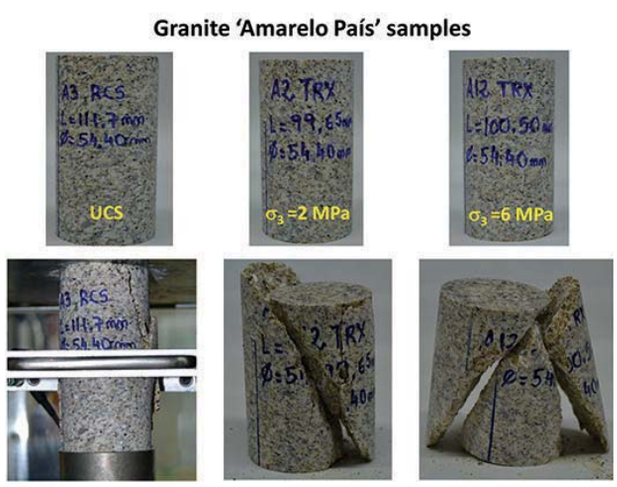

Figure 2—Samples of Amarelo País granite before and after strength testing under uniaxial compression (UCS), and triaxial compression (2 and 6 MPa) conditions

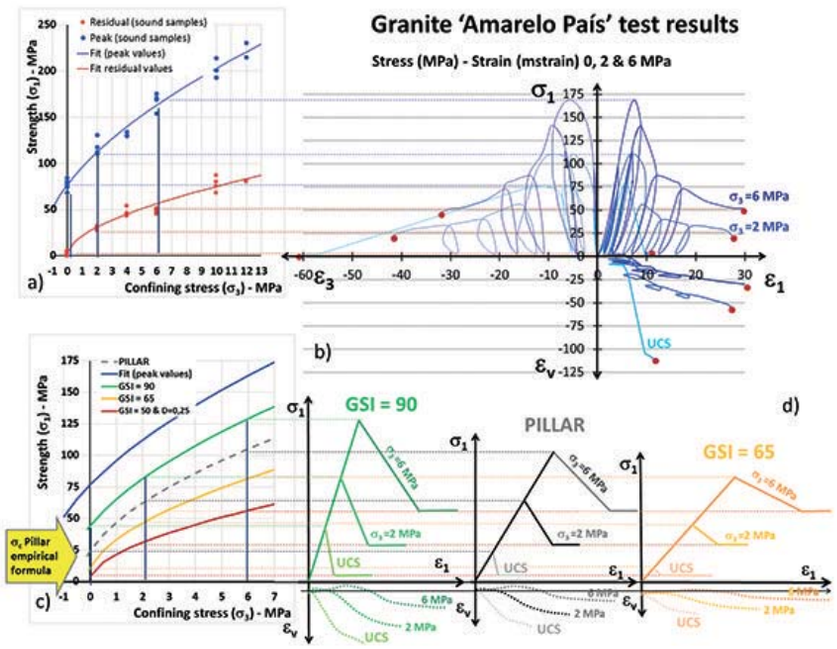

Figure 3—(a) Peak and residual Hoek-Brown strength envelopes for Amarelo País granite specimens, (b) complete stress-strain curve of three samples of Amarelo País granite specimens tested at 0, 2, and 6 MPa confinement, (c) peak and residual strength envelopes for Amarelo País granite samples (computed from actual tests); GSI 90 and GSI 65 Amarelo País granite rock masses (computed based on the GSI approach) and a pillar on Amarelo País granite (adjusting a value of UCS to an equivalent GSI so the UCS coincides with the value supplied by an empirical formula), (d) complete stress-strain curve for rock masses and pillar behaviour as derived from the GSI approach and observations

confinement levels is shown in Figure 3d. Note how a decrease in rock mass quality decreases dilation of the pillars. This dilation also becomes smaller as the confining stress increases. Although these estimates of pillar behaviour are first approximations only, they may provide insight on the effect of strapped pillars based on the strength testing of strapped rock specimens.

As a next step, we compared results obtained from the standard uniaxial strength test on Amarelo País granite specimens described above with results obtained from a specimen strapped using four steel cables of 3 mm thickness (Figure 4a and b). The complete stress-strain curves (Figure 4b) reflect similar trends to those observed for the Indiana limestone specimens. For the cabled specimen, dilation occurred in a more controlled fashion. Additionally, a significant residual strength, around 10 MPa was maintained by the strapped sample after 4% axial strain.

These results were used to estimate the residual strength of strapped specimens by fitting a GSI value, whereby the equivalent 'rock mass' uniaxial compressive strength was adjusted to that observed in the test as indicated by the observations of Cai *et al.* (2007). Accordingly, the estimated residual strength envelope for the cabled specimens and pillars (due to the fact that it is assumed that scale effects do not affect this strength) was obtained as the purple curve shown in Figure 4c. Similar to the description above, the peak pillar strength was obtained and the pillar behaviour (for a standard pillar and a strapped pillar) in terms of its complete stress-strain curve can be estimated for various confinement levels as shown in Figure 4d. Note that even if the pillars are unconfined, some confinement is usually present as shown by actual measurements (Maleki and Lewis, 2010; Tulu and Heasley, 2011) and numerical models (Duncan Fama, Trueman, and Craig, 1995).

The results presented in Figure 4 and associated considerations would indicate that strapping pillars with a reasonable number of steel cables does not affect their elastic (generally pre-peak) behaviour, whereas it does affect their post-failure behaviour by significantly increasing residual strength, controlling dilation, and slightly reducing brittleness. This increase in residual strength could possibly contribute to the stability of a room and pillar mine.

Description of the experimental room and pillar mine

General information about the mine

Initially mined in the early 20th century and again in the 1950s and 1960s, Santa Rosa is an old underground room and pillar mine. A haematite bed typically 2 m thick (but varying in thicknesses between 2 and 10 m due to thrust faulting) of Cambrian age is exploited. The current production is very small; around 10 000 t/a. The ore is crushed, classified, and sold as a paint additive.

The geological history of this sedimentary basin is complex. Locally, thrust faulting has thickened the bed in some locations, but the ore tends to follow a dip of around 15°. Some normal faults are present that limit the deposit in some locations and produce discontinuities in other areas. This makes the geology unpredictable, which together with the small production, causes mining to be concentrated in areas where the iron ore bed is considered to be the optimum thickness. This results in a number of scattered, irregular-shaped rooms being mined in the vicinity of the ramp. Planning of the future mining areas is difficult owing to the

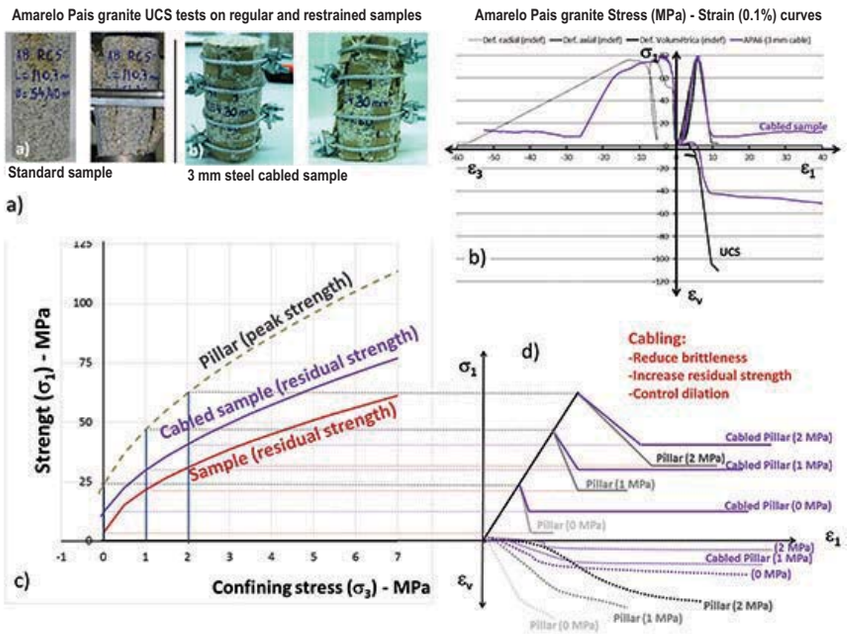

Figure 4—(a) Amarelo País granite specimens tested under uniaxial compression without and with four 3 mm steel cables, (b) complete stress-strain curves for unconfined and cabled Amarelo País granite specimens, (c) pillar peak and specimen (and pillar) residual (cabled and non-cabled) strength envelopes, (d) complete stress-strain curves for cabled and non-cabled pillars as derived from estimates and observations

small budget associated with the small production and the geological complexity of the deposit. Future mining is therefore planned based on drilling from the stopes and drifts, and reserves are delineated roughly one year ahead of current mining.

The rock mass in the immediate vicinity of the reef is bedded and contains four joint sets. This rock mass was originally highly discontinuous due to Carboniferous -age tectonic stresses (the Variscan or Hercynian orogeny). Subsequently, the rock was subjected to metamorphism of Alpine age that reassembled the rock mass and 'froze' the faults and joints. This has produced a good-quality rock mass (GSI in the range of 60–70). As a result, 4 m wide drifts and rooms up to 15 m long do not need to be supported. This is very convenient for reducing mining costs, and very few cases of instability (very local and small rockfalls) have been reported in these excavations (Figure 5).

A laboratory programme which involved UCS and triaxial strength tests was carried out to characterize the rocks found in the mine (haematite ore and dolomite). In July 2011, the authors conducted a first stability assessment of the mine. The overall stability of the rooms and 50 identified pillars was assessed using empirical approaches and preliminary numerical simulations. The roofs of the rooms were deemed to be stable, with only minor local falls of ground observed. These are associated with a green shale layer that tends to swell when subjected to humid conditions.

Pillar strength was computed by means of the formula proposed by Hedley and Grant (1972):

$$\text{Strength}_{\text{pillar}} = K \cdot W_{ef}{}^{0,5} \cdot H^{-0,75} \qquad [1]$$

K was estimated by averaging the UCS test results on standard samples recovered in different areas of the mine, inverting the formula above, and finally performing a scale correction associated with the strength scale formula proposed by Hoek and Brown (1980) accounting for a representative elementary volume of a cylinder with a diameter of 200 mm as suggested by Martin *et al.* (2014). It is relevant to note that this approach produced an average K value of $0.65\sigma_c$, equal to the estimate proposed by Esterhuizen *et al.* (2011) for sedimentary rock pillars in underground quarries. H refers to the height of the pillar and W_{ef} is the effective width, which is computed for isolated pillars as (Malan and Napier, 2011):

$$W_{ef} = \frac{4 \cdot A}{perimeter} \qquad [2]$$

where A is the area of the pillar.

The load on the pillars is estimated based on tributary area theory, which relates the pillar stress to the pre-mining stress and the extraction ratio by:

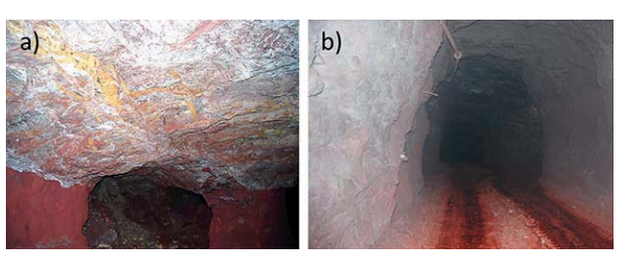

Figure 5—Typical excavations in Santa Rosa mine not needing reinforcement. (a) Shallow room more than 50 years old. Note the stability of the pillars and roof, although at the bottom a small fall of ground is observed. (b) Typical unsupported drift

$$\sigma_P = \frac{\sigma_v}{1-e} \quad [3]$$

where σ_P is the estimated pillar load, σ_v is the vertical pre-mining stress (equal to depth of the pillar multiplied by the mean specific weight of the overburden), and e is the extraction ratio. It should be noted that this is only a crude first approximation as the mining areas are small with a number of nearby abutments. Equation [3] therefore overestimates the stress on the pillars.

The factor of safety of the pillars is ultimately estimated as the ratio of pillar strength and average load. Only five pillars of more than 50 studied showed factors of safety smaller than 1.5. Two of these pillars were located in the deepest room of the mine (190 m deep) and were of irregular shape. These two pillars are discussed in more detail below.

Description of the mining area where pillar strapping was used

The mining area of interest is located in the deepest part of the mine. Figure 6a illustrates the plan view of this area at the time of the stability study. The subsequent observations in this area are summarized in Table I. It can be seen in Figure 6a that pillars *a* and *b* in this room had small dimensions, which according to the miners was a result of overbreak. Photographs of these pillars at the date of the visit are shown in Figure 7.

Factors of safety of 1.14 and 1.22 were estimated for pillars *a* and *b*. The other pillars appeared to be more stable, and this was confirmed by the higher factor of safety values (Table II). Pillar *b* was of particular concern due to the high density of joints in its lower part.

In the general stability study, it was observed that the post-failure behaviour of the haematite was more ductile (less brittle) than that of the dolomite rock of the roof and floor. Based on this consideration, it was evident that catastrophic pillar failure was not to be expected based on energy considerations (Figure 8) and according to Zipf (2001).

A few months after presenting the general stability study, the geometry of this mining area had changed substantially (cutting of pillars *e*, *g*, *h*, and *i*, see Figure 6b). It was reported by the mine in February 2012 that pillar *b* had collapsed, immediately followed by pillar *a*. Luckily, no other pillars were affected. Access to the area was limited due to

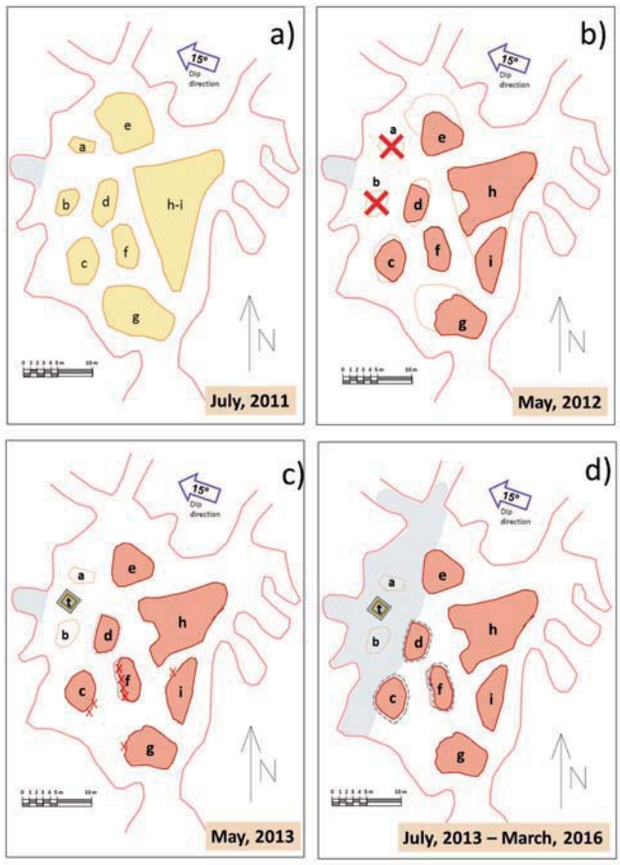

Figure 6—Plan view of the part of the mine investigated in detail. This is located at a depth of 190 m. The changes in this area with time are explained in the text

Figure 7—Photographs of pillars *a* and *b* during the visit conducted for the stability study (July 2011)

Table I

Key observations and actions over a period of time for the mining area analysed in this study

Date	Source	Observations or actions
July 2011	General visit to the mine	Identification of potentially unstable pillars *a* and *b*
February 2012	Report by miners	Collapse of pillars *a* and *b*. Cleaning of portions left
May 2012	Report by mine's engineer	Started monitoring first period, measurements during 3 months, unstable areas.
October 2012	Authors	Design proposal including timber crib and cabling of pillar *d*.
November 2012	Report by mine's engineer	Building of timber crib and cabling of pillar *d*
December 2012	Report by mine's engineer	Started monitoring second period, measurements during 5 months
March 2013	Visit to the room	Observations of the effect of the timber crib and cabling. Only slight damage on pillars observed.
May 2013	Visit to the room	Significant damage on pillar *f*. Significant damage on pillar *c*. Little damage on pillars *i* and *g*
June 2013	Report by mine's engineer	Cabling and meshing of pillars *f* and *c*. Resetting of the monitoring system working till now
June 2014	Visit to the room	Generally stable, slight damage on some pillars
January 2016	Visit to the room	The room is being filled. No further relevant damage observed

Table II

Estimates of factor of safety for the pillars in the room in July 2011 based on tributary area theory and Hedley and Grant (1972) strength calculations presented above

Pillar	Pillar area m^2	Supported area m^2	e %	Depth m	W_{eff} m	H m	Pillar stress MPa	Pillar strength MPa	FoS	W/h	Pillar stress / σ_c
a	13.08	73.54	82	190	3.06	3.5	29.9	34	1.14	0.87	0.392
b	19.50	96.00	80	190	3.97	4.5	26.2	32.1	1.22	0.88	0.343
c	34.65	92.06	62	190	4.84	3.5	14.3	42.8	3.03	1.38	0.185
d	29.66	89.07	67	190	4.41	3.5	16.0	40.9	2.56	1.26	0.209
e	63.01	132.40	52	190	6.93	3.5	11.18	51.17	4.58	1.98	0.146
f	42.01	123.59	66	190	5.63	3.5	15.65	46.15	2.95	1.61	0.205
g	107.9	204.98	47	190	8.89	3.5	10.11	58.0	5.74	2.54	0.133
h-i	139.86	216.01	32	190	9.32	3.5	8.22	59.4	7.23	2.66	0.108

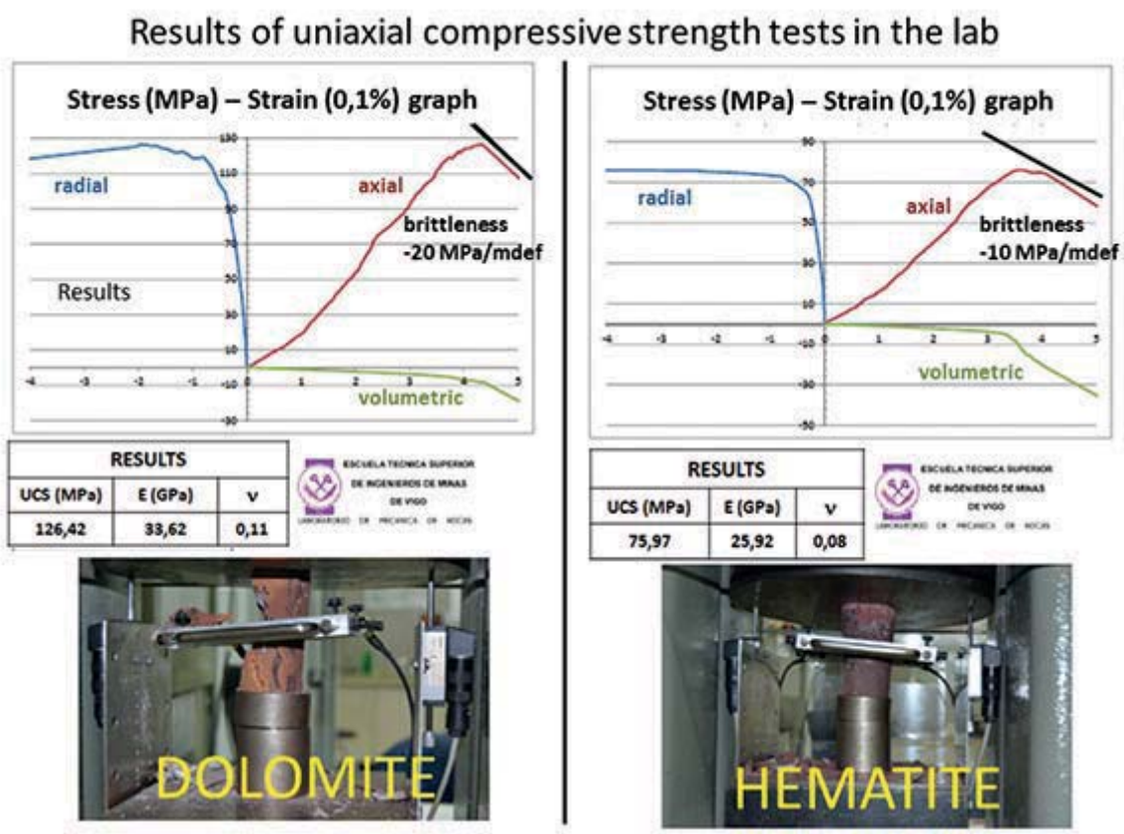

Figure 8—Stress-strain curves for rocks of the roof and pillar. The roof rock (dolomite) is more brittle than the pillar rock

safety regulations and a monitoring system with levelling control of various roof and pillar targets was established during May 2012.

A stability analysis of the unsupported roof span was performed (Figure 6b, where pillars *a* and *b* stood), showing compromised stability according to Mathews' stability graph method (Mathews *et al.*, 1980; Potvin, 1988). It was therefore recommended that a concrete and timber crib be built in the middle of the unsupported span (between the locations of collapsed pillars *a* and *b*). This timber crib needed a concrete base due to the fact that the area was to be flooded. It was also decided to strengthen pillar *d* with cable strapping as it was likely to be overloaded after the collapse of pillars *a* and *b*. The estimated factor of safety on this pillar was 1.23 after the collapse of pillars *a* and *b*.

The crib was designed and built within a few months, as Figure 9 illustrates. It was designed to avoid instability of the roof as well as to distribute vertical stress to the abutment of the room, avoiding overloading of the nearby pillars. Oak and pine wood railway ties or sleepers were found in the market with a uniaxial compressive strength over 30 MPa and Young's modulus in the range 8 to 10 GPa. During the preparation for this construction, the monitoring system was damaged. During the control period (from May to August, 2012), maximum vertical convergence rates of approximately 2 mm/month were measured at the east side of pillar *d*.

The lower part of pillar *d* was strapped with six steel torsion cables of 1 cm diameter separated by approximately 30 cm. These were fixed and stressed by means of turnbuckle hooks (Figure 10). Shortly after their installation, small

Strapping of pillars with cables to enhance pillar stability

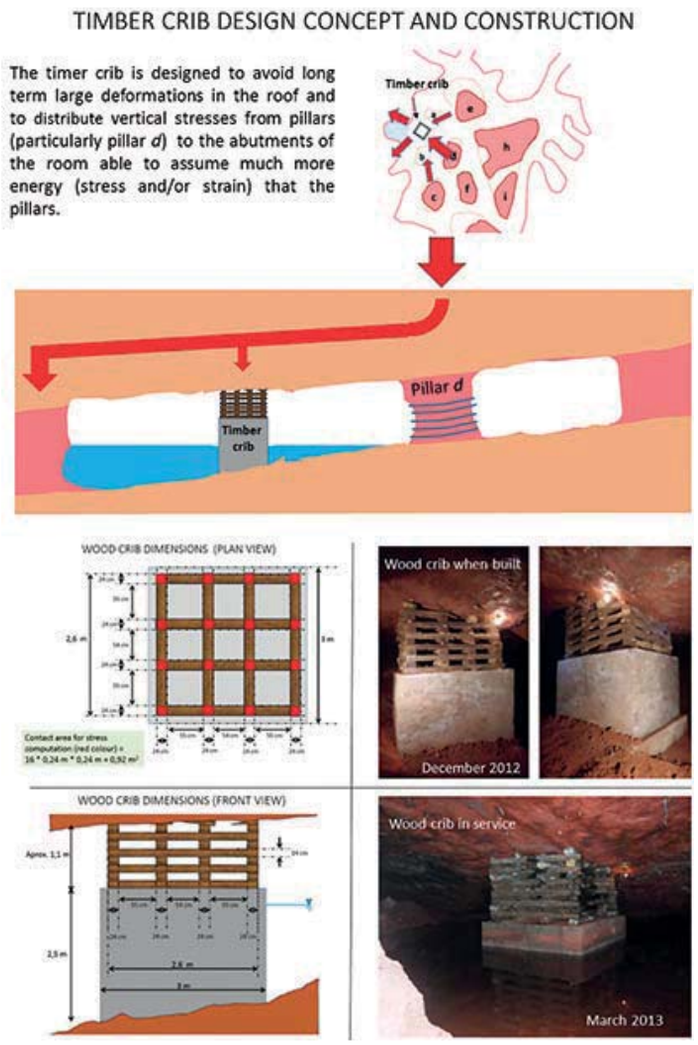

Figure 9—The timber crib design concept. Photographs of the crib just after construction in December 2012 (top right) and in service in March 2013 are (bottom right)

Figure 10—Different views of the strapped pillar *d* in March 2013

cracks were observed and the cables appeared to be under tension.

The remedial measures were completed by December 2012. Pumping was also stopped in the area due to mine requirements. The damaged monitoring system was reinstalled with locating targets in some pillars and roof positions. Levelling and measuring was carried out every month. For the period from December 2012 and May 2013, the data illustrated displacements of less than 3 cm on the pillar surfaces and lowering of the roof of around 1 cm in a

location between the timber crib and pillar *d*. Movement of measurement bases prevented further measurements and some falls of ground was observed. A further visit to the mine was therefore planned for March 2013.

During the visit in March 2013, it was observed that the cables on pillar *d* seemed to be effective. Even though some cracks appeared in the pillar, the cables were able to retain most of the detached blocks, thereby increasing confinement in the pillar (Figure 10). Small pieces of rock fell between the cables, so it was clear that for future strapping of pillars, it would be advisable to wrap the pillar in mesh before installing the cables.

A further visit in May 2013 was conducted to examine the condition of the pillars. Pillars *e* and *h* were intact, but slight scaling of pillars *i* and *g* was observed. Pillar *c* showed signs of more severe scaling and two significant blocks fell from this pillar (0.3 m (1 ft) side cubes) (Figure 11). The stability of pillar *f* was particularly poor, with significant scaling on its western side. This reduced its width – and consequently its section – by around 1 m (Figure 6c and 11).

Based on these observations, it was recommended that pillars *f* and *c* be strapped with mesh and cabling. This work was completed in June 2013. Additionally, the monitoring system was reset and displacement measurements were recorded every two to three months during the following 2½ years.

No significant instability was reported during the following year and a follow-up visit was made to the site during June 2014. Photographs of the strapped pillar *f* and of the intact pillar *e* taken during this visit ate shown in Figure 12. No movements or pillar instability was recorded during this inspection and it appears that the pillar support was functioning as intended. A further visit was conducted in June 2015 with similar observations, and it was decided to start filling this excavation with available waste material (scarce in this mine). A final visit in January 2016 indicated no further instability problems.

Figure 11—Condition of pillars *f* and *c* in March 2013

Data recorded by the monitoring system

The harsh conditions in underground mining environments make it particularly difficult to maintain these systems. Displacement monitoring systems consisting of laser measuring devices and a number of targets are particularly prone to damage as the targets can be accidently moved or disturbed. This happened twice in this particular case study.

As described above, a monitoring system was installed in May 2012 after the collapse of pillars *a* and *b*. This included targets on the pillars (visible in Figures 10 and 11 on pillars *d* and *c*) and on the roof in the more unstable areas as shown in the sketch in Figure 13. Three useful measurements were made with this initial system, giving vertical deformations rates in the roof up to 2 mm/month near pillar *d* (which was not strapped at the time). Two further measurements were recorded. Unfortunately the recording base shifted after this and further records were unreliable. A maximum displacement just over 1 cm was estimated for the period from May 2012 to November 2012, when pillar *d* was strapped.

The monitoring system was reinstalled in December 2012 using most of the same targets. At this stage the timber crib and strapping of pillar *d*. was completed. Five groups of monthly measurements were recorded before the system was

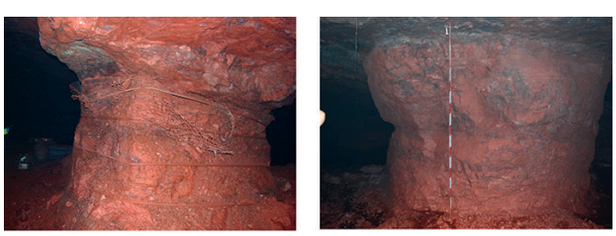

Cabled and meshed Pillar *f* – June 2014 **Intact pillar *e* – June 2014**

Figure 12—Condition of pillars *f* and *e* in June 2014

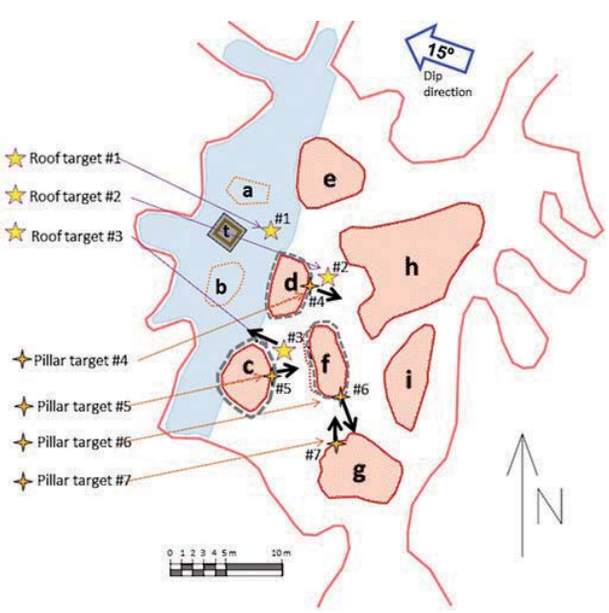

Figure 13—Plan view of the experimental site with the location of the monitoring targets in the roof and on the pillar sidewalls

lost again (caused by falls from pillar *f*). Maximum vertical velocities in the roof between pillars *c* and *f* of up to 2 mm/month were recorded. Pillar *f* was scaling at the time, so this deformation is interpreted as the result of this pillar slowly failing. In contrast, the vertical velocity near the strapped pillar *d* was now reduced to approximately 0.3 mm/month. It is therefore deduced that the strapping of pillar *d* effectively improved the stability of this pillar.

A third period of measurement started in June 2013 after the strapping of pillars *f* and *c*. The measurements recorded using the targets shown in Figure 13 are presented in Figure 14 for the roof and Figure 15 for the pillars. The period of recording was 700 days, after which the area seemed to reach a new state of equilibrium. A maximum vertical displacement of 1.5 cm for this period was observed in the roof.

In conclusion and as summarized in Table III, in the four-year period, a maximum total roof displacement of less than 5 cm was estimated. The iron ore bed in this area is 4 m thick, resulting in a vertical strain of the pillars of around 1.25% (12.5 millistrain). This is considered feasible, particularly for the strapped pillars, as the laboratory results indicated that values up to 5% are possible.

Graphical representation of pillar instability

A useful method to represent the stability of pillars was proposed by Martin and Maybee (2000) and consists of plotting pillars in terms of the ratios (pillar load/UCS) and (*W*/*H*) for a particular pillar height (4 m in this case). Such a graph was plotted for the pillars at the experimental site and is presented in Figure 16. A pillar is considered stable according to a particular empirical strength formula if it plots below the line of that formula.

The state of pillars in May 2011 (Figure 6a) is represented by a blue colour in Figure 16. This indicates that the pillars *a* and *b* were only slightly below the Hedley and Grant (1972) strength and therefore close to being unstable. The state of the other (some reshaped) pillars after the collapse in May 2012 (Figure 6b) is represented by the red colour in Figure 16. Pillar *d* appears to be close to instability and therefore required strapping. Furthermore, in May 2013 the state of pillar *c* and particularly *f* (the only one that had significantly changed because of the reduction of its size due to the scaling) also justified strapping. It is clear that this graphic representation, in conjunction with *in situ* observations, can be a useful and simple method to quantify and investigate the stability of underground pillars.

Finally, it is relevant to remark that in the process of development of this study, some assumptions were made out of necessity. This has to be often the case in large-scale rock pillar stability, where a certain degree of uncertainty is always to be expected.

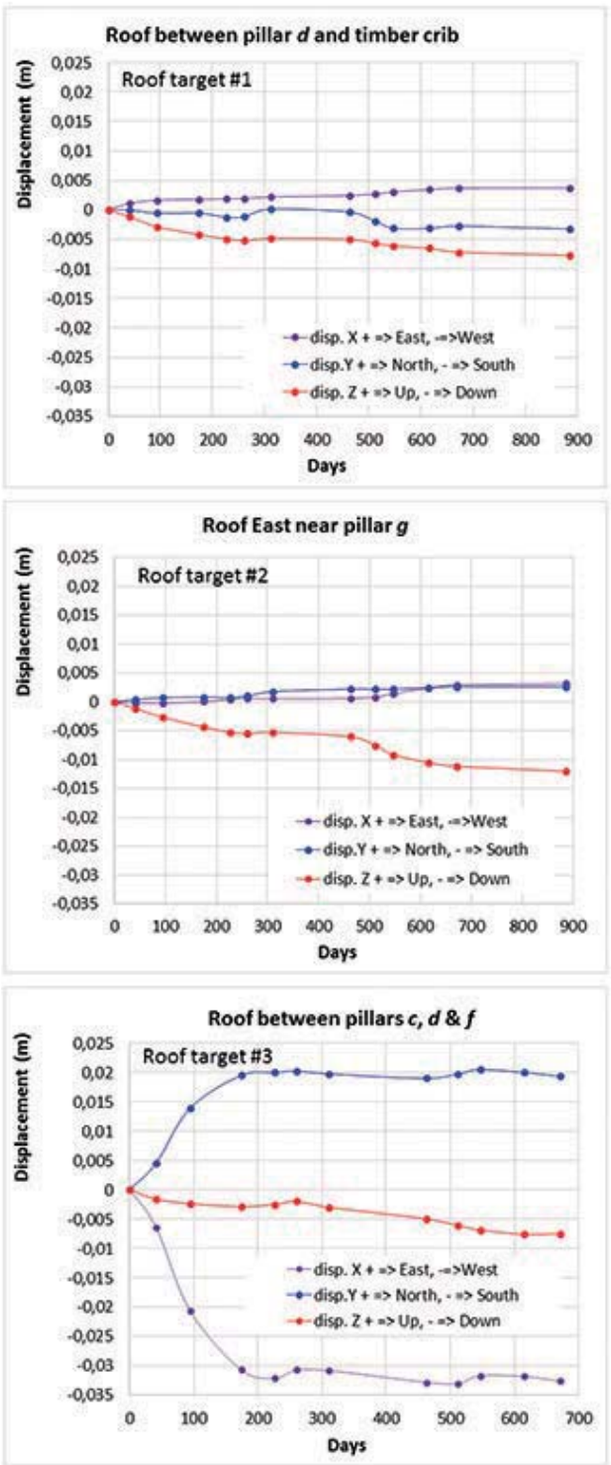

Figure 14—Displacements measured using the roof targets from June 2013 to the end of 2015

Discussion

As discussed above, the objective of the paper is not to propose a new pillar design method, but to describe a remedial support method for damaged or potentially unstable pillars. The technique was shown to be very useful in the Santa Rosa mine where the span of the experimental mining area was small. It should be noted that the proposed method will not be universally applicable as it will not prevent creep or extrusion phenomena. Furthermore, a recent collapse in a shallow hard-rock room and pillar mine in Africa indicated that even very heavy strapping of pillars will not prevent a collapse if the instability occurs on a mine-wide scale. In this particular mine, a thick shear layer with clay-like infilling was encountered in the deeper parts of the mine after very large spans had already been mined. This layer is shown in

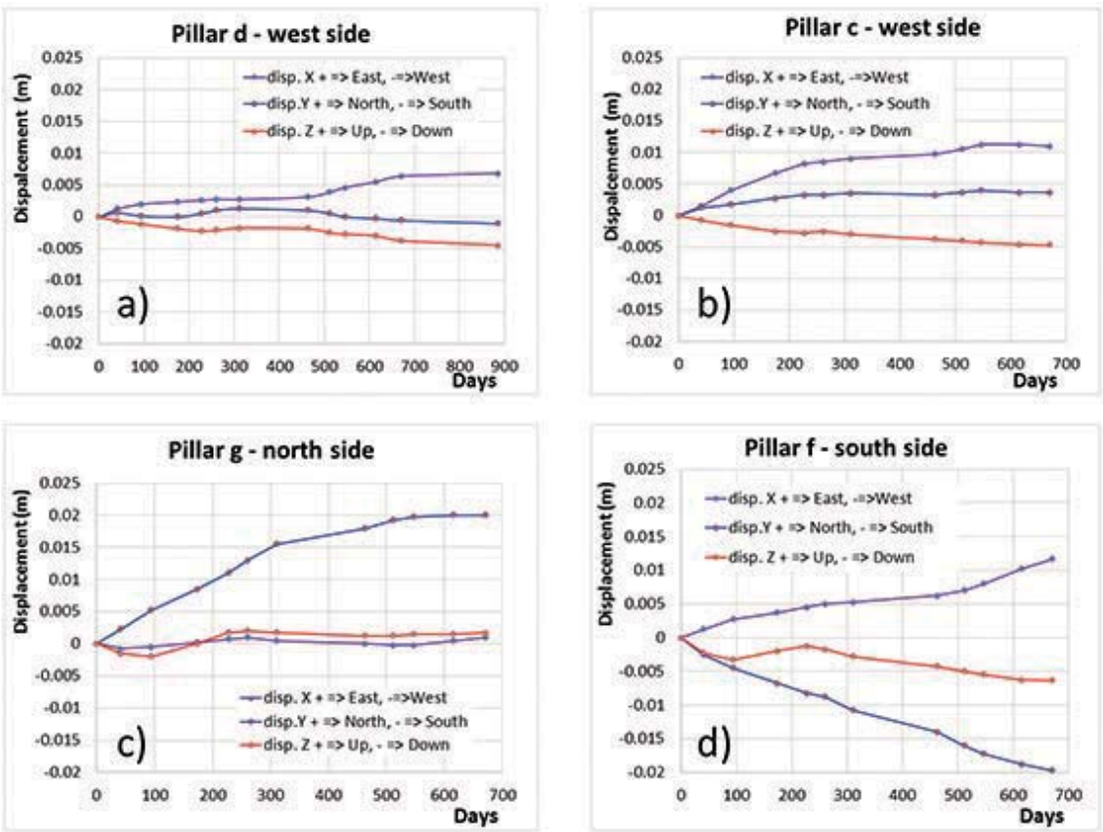

Figure 15—Displacements measured using the pillar targets from June 2013 to the end of 2015

Table III

Summary of monitoring data

	Vertical displacement (m)			
Roof target no.	**May 2012 to November 2012**	**December 2012 to May 2013**	**June 2013 to December 2015**	**Accumulated from May 2012 to - December 2015**
1	-0.006* (1 mm/month)	-0.006* (1 mm/month)	-0.008 (0.25 mm/month)	-0.02
2	-0.012* (2 mm/month)	-0.002* (0.3 mm/month)	-0.012 (0.4 mm/ month)	-0.036
3	-0.001* (0.2 mm/month)	-0.013* (2 mm/month)	-0.032 (5 mm/month the first 5 months, then 0.1 mm/month)	-0.046

*Estimated

Figure 17. The mine started collapsing in the deeper areas and the subsequent load transfer also affected the pillars in the shallower areas. It was then discovered that the shear zone occurred in the footwall in some of these areas. It was decided to strap the key pillars protecting the main roadways with very heavy support. The support consisted of a layer of shotcrete, bolting, mesh, steel strapping, and a further layer of shotcrete. This is shown in Figure 18. Unfortunately, this support did nothing to arrest the eventual collapse (Figure 19) and at least half of the mine and the main access roadways were lost.

Figure 20 (modified from Brady and Brown, 2006) shows typical pillar failure modes. If pillars are cut in massive rock with no weak contacts with the floor and roof, failure will occur by spalling from the pillar surfaces (Figure 20a). This leads to a progressive reduction in the width of the pillar and will increase the stress on the pillar. If the width/height ratio of a pillar is small, an inclined shear failure could develop (Figure 20b). If there are weak contacts between the pillar and the hangingwall and footwall, there will typically be internal axial splitting of the pillar (Figure 20c). If there is a joint set (or more than one) with a dip angle larger than the angle of friction, the pillar can yield due to slipping on the fractures (Figure 20d). If the joints are parallel to the principal axis of loading, the pillar may fail by buckling (Figure 20e).

It is hypothesised that for the first five cases in Figure 20, cabling will contribute to an increase in pillar stability. The deformation of the pillar will tension the cables, increasing the confining stress and, consequently, the pillar strength.

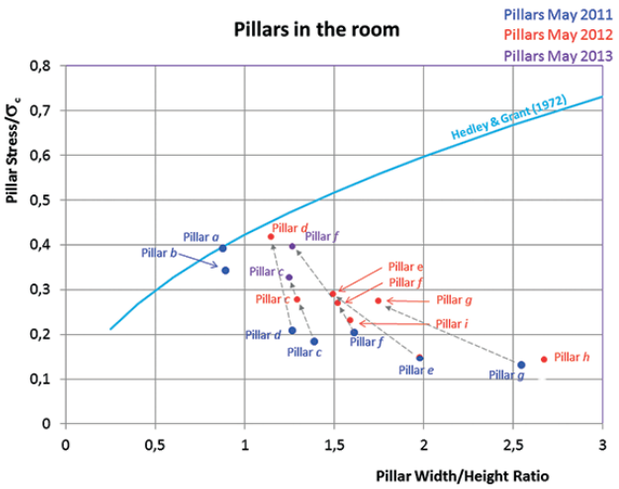

Figure 16—Graph representing the pillars in terms of the ratios (strength/UCS) and (W/H)

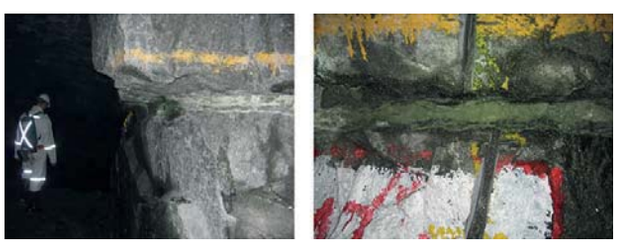

Figure 17—Shear zone with clay-like infilling in the middle of a pillar (left). A close-up of this layer is shown on the right

Figure 18—Strapping of the pillars in the mine shown in Figure 17. The strapping consisted of two layers of shotcrete, mesh, and steel straps

This concept should nevertheless be further tested for different conditions encountered in a variety of mines. If there is a weak material forming intermediate layers or filling the discontinuities as shown in Figure 20f, the proposed approach may prove ineffective as was illustrated by the mine

Figure 19—Typical damage to the supported pillars (left) and a roofbolt pulling through the bearing plate as the pillar continued to undergo dilation (right)

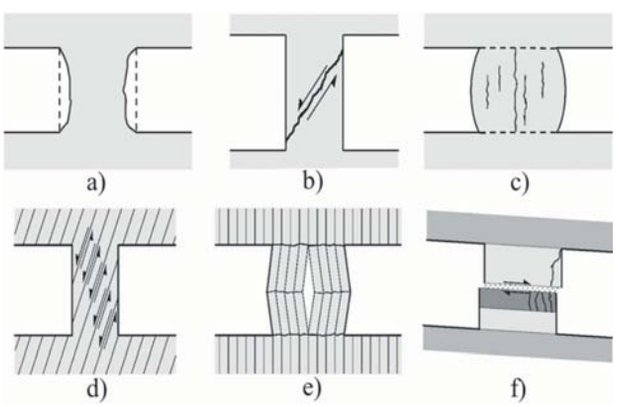

Figure 20—The modes of failure shown in (a) to (e) can possibly be arrested with the cabling method (after Brady and Brown, 2006). The mode of failure shown in (f) may not be corrected with the cabling method

collapse described above. It should be noted that for this particular collapse, some pillars may have failed according to the mechanism in Figure 20d where the shear zone was some distance into the footwall. It is very clear from this particular case study that no amount of pillar reinforcement will be successful in the case of such a large mine-wide instability.

Conclusions

Failing pillars may be encountered in room and pillar mines unless a very conservative design approach is followed. Remedial measures (shotcrete, rockbolting, strapping) have been adopted in some cases for failing pillars, but the success of these is doubtful based on reports in the literature. In this paper we investigated the usefulness of an inexpensive pillar strapping method that may assist in stabilizing individual failing pillars in isolated areas. Installing a number of cables around the pillar will increase its strength and ductility as it slightly increases the confinement, and minimize ongoing degradation.

Compressive strength tests were conducted in the laboratory on cabled rock specimens. This illustrated that the cabling increases the residual strength and ductility, which allows for large controlled deformations instead of catastrophic failure. The dilation of the cabled rock specimens was less than in comparable tests on unconfined specimens. The cabling did not affect the elastic properties and peak strength of the samples. As a theoretical exercise, the laboratory-scale observations were extended to larger scales by assuming that the residual strength is not dependent on scale and adopting the Hoek and Brown (1997) approach based on GSI (Marinos and Hoek, 2000).

As a first trial, this method was applied in a small haematite room- and- pillar mine. A room located at a depth of 190 m, which contained some scaling pillars, was stabilized by using meshing and cabling on the unstable pillars. The room remained stable for a period of 900 days when the final observations were made.

The method of strapping pillars using mesh and cabling seems useful for stabilizing individual pillars in areas where most of the other pillars are stable and the total mining spans are small. This concept should nevertheless be further tested for different conditions encountered in a variety of mines. If there is a weak material such as a clay layer traversing the pillar, the proposed approach may prove ineffective, as was illustrated by a recent mine collapse in Africa.

Acknowledgements

The authors wish to thank the Spanish Ministry of the Economy and Competitiveness for partial funding, awarded under Contract Reference No. BIA2014-53368-P, partially financed by ERDF funds from the EU. The mining engineers of Santa Rosa Mine are also acknowledged for their contribution to the case study presented in this manuscript.

References

Alejano, L.R., García-Bastante, F., Taboada, J., and Migliazza, R. 2012. Design of room and pillar exploitations of non-expensive minerals and ornamental rocks in Spain. *Harmonising Rock Engineering and the Environment - Proceedings of the 12th ISRM International Congress on Rock Mechanics.* pp. 1453–1456.

Arzúa, J. and Alejano, L.R. 2013. Dilation in granite during servo-controlled triaxial strength tests. *International Journal of Rock Mechanics and Mining Sciences*, vol. 61. pp. 43–56.

Arzúa, J., Alejano, L.R., and Walton, G. 2014. Strength and dilation of jointed granite specimens in servo-controlled triaxial tests. *International Journal of Rock Mechanics and Mining Sciences*, vol. 69. pp. 93–104.

Bieniawski, Z.T. 1992. A method revisited: coal pillar strength formula based on filed investigations. *Workshop on Coal Pillar Mechanics and Design*. US Bureau of Mines, IC 9315.

Brady, B.H.G. and Brown, E.T. 2006. Rock Mechanics for Underground Mining. 3rd edn. Springer.

Cai, M., Kaiser, P.K., Tasaka, Y., and Minamic, M. 2007. Determination of residual strength parameters of jointed rock masses using the GSI system. *International Journal of Rock Mechanics and Mining Sciences*, vol. 44, no. 2. pp. 247–265.

Chase, F.E., Zipf, R.K., and Mark, C. 1994. The massive collapse of coal pillars: case histories from the United States. West Virginia University, Morgantown, WV. pp. 69–80.

Dismuke, S.R. Forsyth, W.W., and Stewart, S.B.V. 1994. The evolution of mining strategy following the collapse of the Window Area at the Magmont Mine, Missouri. *Proceedings of the CIM Annual General Meeting*, District 6, Metal Mining, CIM Montreal, 1994. pp. 3–8.

Duncan Fama, M.E., Trueman, R., and Craig, M.S. 1995. Two- and three-dimensional elasto-plastic analysis for coal pillar design and its application to highwall mining. *International Journal of Rock Mechanics and Mining Sciences*, vol. 32. pp. 215–225.

Esterhuizen, G.S., Dolinar, D.R., and Ellenberger, J.L. 2011. Pillar strength in underground stone mines in the United States. *International Journal of Rock Mechanics and Mining Sciences*, vol. 48, no. 1. pp. 42–50.

Esterhuizen, G.S., Dolinar, D.R., Ellenberger, J.L., and Prosser, L.J. 2011. Pillar and roof span design guidelines for underground stone mines. *Information Circular* 9526. NIOSH. Pittsburgh, USA.

Esterhuizen, G.S. 2006. An evaluation of the strength of slender pillars. *SME Annual Meeting*, St. Louis, Missouri.

Exadaktylos, G.E. and Tsoutrelis, C. E. 1993. Scale effect on rock mass strength and stability. *Scale Effects in Rock Masses 93*. Pinto da Cunha, A. (ed.). Balkema, Rotterdam.

Grgic, D., Hommand, F., and Hoxha, D. 2003. A short- and long-term rheological model to understand the collapses of iron mines in Lorraine, France. *Computers and Geotechnics*, vol. 30, no. 7. pp. 557–570.

Hedley, D.G.F. and Grant, F. 1972. Stope-and-pillar design for Elliot Lake Uranium Mines. *Bulletin of the Canadian Institute of Mining and Metallurgy*, vol. 65. pp. 37–44.

Hedley, D.G.F., Roxburgh, J.W., and Muppalaneni, S.N. 1984. A case history of rock-bursts at Elliot Lake. *Proceedings of the 2nd International Conference on Stability in Underground Mining*. Szwilski, A.B. and Brawner, C.O. (eds). Society of Mining Engineers. pp. 210–234.

Hoek, E., and Brown, E.T. 1997. Practical estimates of rock mass strength. *International Journal of Rock Mechanics and Mining Sciences*, vol. 34, no. 8. pp. 1165–1187.

Hustrulid, W. 1976. A review of coal pillar strength formulas. *Rock Mechanics*, vol. 8. pp. 115-145.

Jaiswal, A. and Shrivatva, B.K. 2009. Numerical simulation of coal pillar strength. *International Journal of Rock Mechanics and Mining Sciences*, vol. 46, no. 4. pp. 779–788.

Khair, A.W. and Peng, S.S. 1985. Causes mechanisms of massive pillar failure in a southern West Virginia coal mine. *Mining Engineering*, vol. 37. pp. 323–328.

Lunder, P.J. and Pakalnis, R. 1997. Determination of the strength of hard rock mine pillars. *Bulletin of the Canadian Institute of Mining and Metallurgy*, vol. 68. pp. 55–67.

Madden, B.J., Canbulat, I., and York, G. 1998. Current South African coal pillar research. *Journal of the South African Institute of Mining and Metallurgy*, vol. 98. pp. 7–10.

Malan, D.F. and Napier, J.A.L. 2011. The design of stable pillars in the Bushveld Complex mines: a problem solved? *Journal of the Southern African Institute of Mining and Metallurgy*, vol. 111. pp. 821–836.

Maleki, H. and Lewis, J.C. 2010. Verification of in situ pillar strength for Utah coal seams. *Proceedings of the 44th US Rock Mechanics Symposium and 5th U.S-Canada Rock Mechanics Symposium*, Salt Lake City, 27–30 June 2010. American Rock Mechanics Association. 15 pp.

Mansurov, V.A. and German, V.I. 2009. Preparation and causes of major collapse at Annenskiy Mine (Kazakhstan). *Rock Engineering in Difficult Ground Conditions - Soft Rocks and Karst: Proceedings of EUROCK 2009 – the Regional Symposium of the International Society for Rock Mechanics.* pp. 809-814.

MARINOS, P. and HOEK, E. 2000. GSI: A geologically friendly tool for rock mass strength estimation. *Proceedings of the GeoEng2000 Conference*. Technomic, Lancaster, PA. pp. 1422–1442. .

MARTIN, C.D., LU, Y., LAN, H., and CHRISTIANSSON, R. 2014. Numerical approaches for estimating the effect of scale on rock mass strength. *Proceedings of the 7th Nordic Grouting Symposium and 2nd Nordic Rock Mechanics Symposium*. Ghoteburg, 13–14 November 2014. pp. 93–106.

MARTIN, C.D. and MAYBEE, W.G. 2000. The strength of hard rock pillars. *International Journal of Rock Mechanics and Mining Sciences*, vol. 37. pp. 1239–1246.

MATHEWS, K., HOEK, E., WYLLIE, D.C., and STEWART, S.B.V. 1980. Prediction of stable excavation spans for mining at depths below 1000 metres in hard rock. Report to Canada Centre for Mining and Energy Technology (CANMET), Department of Energy and Resources, DSS File No. 17SQ.23440-0-90210. Ottawa,

MURALI MOHAN, G., SHEOREY, P.R., and KUSHWAHA, A. 2001. Numerical estimation of pillar strength in coal mines. *International Journal of Rock Mechanics and Mining Sciences*, vol. 38, no. 8. pp. 1185–1192.

POTVIN, Y. 1988. Empirical open stope design in Canada. PhD thesis, Department of Mining and Mineral Processing, University of British Columbia.

SALAMON, M.D.G. and MUNRO, A.H. 1967. A study of the strength of coal pillars. *Journal of the South African Institute of Mining and Metallurgy*, vol. 68. pp. 56–67.

SIWAK, J.M. 1984. Carrières de craie du Nord de la France. Comportement des piliers et confortation par gunitage. (Shale quarries in northern France. Pillar behavior and shotcrete support). PhD thesis. Université des Sciences et Techniques de Lille. (In French).

TULU, I.B. and HEASLEY, K.A. 2012. Investigating abutment load. *Proceedings of the 31st International Conference on Ground Control*, Morgantown, WV. pp 150–159.

VAN DER MERWE, N. 2006. Beyond Coalbrook: what did we really learn? *Journal of the Southern African Institute of Mining and Metallurgy*. vol. 106. pp. 857–868.

WANG, J.-A., SHANG, X.C., and MA, H.T. 2008. Investigation of catastrophic ground collapse in Xingtai gypsum mines in China. *International Journal of Rock Mechanics and Mining Sciences*, vol. 45. pp. 1480–1499.

WOJTKOWIAK, F., RAI, M.A., and BONVALLET, J. 1985. Experimental studies in laboratory of different reinforcement methods to be applied on small mining pillars. *Bulletin of the International Association of Engineering Geology*, vol. 32. pp. 131–138. (In French).

ZINGANO, A.C., KOPPE, J.C., and COSTA, J.F. 2004. Colapso de pilares em mina subterrânea de carvão - mina do Barro Branco - Santa Catarina (Pillar collapse in an underground coal mine). *Congresso Brasileiro de Mina Subetrrânea*, Belo Horizonte. (In Portuguese).

ZIPF, R.K. 2001. Toward pillar design to prevent collapse in room-and-pillar mines. *108th Annual Exhibit and Meeting*, Denver, CO. Society for Mining, Metallurgy and Exploration, Littleton, Co. ◆

http://dx.doi.org/10.17159/2411-9717/2017/v117n6a4

Molecular modelling of tantalum in an aqueous phase

by M.J. Ungerer*, C.G.C.E. van Sittert*, D.J. van der Westhuizen*, and H.M. Krieg*

Synopsis

The transition metals tantalum (Ta) and niobium (Nb) are of significant importance, for example in the nuclear energy sector where they are used as cladding materials, as well as in capacitors and specialized materials. For these applications a high-purity metal is needed. The separation of Ta and Nb is always a challenge since they are found together in nature and have similar chemical and physical properties, resulting in costly and laborious separation processes. A technology that has been used successfully for the separation of these metals entails solvent extraction (SX)[1]. While separation was achieved in a previous SX study using a sulphuric acid (H_2SO_4) medium with the extractants diiso-octyl phosphinic acid (PA) and di-(2-ethylhexyl) phosphoric acid (D2EHPA), due to the absence of speciation data for Ta and Nb it is not clear how the separation occurred.

One method that might be suitable for determining the speciation of a reaction is molecular modelling. Calculations based on the density-functional theory (DFT) are now used not only for light elements and small molecules, but also metal complexes, heavy metals, and especially metal separation in SX[2]. In this study the aqueous phase used during SX was investigated by studying periodic systems of Ta, as a metal and in salt form, when it is in contact with H_2O and H_2SO_4. The results were used to predict the reaction mechanism occurring during SX. Results showed that (i) in a 1:1 acid-water ratio, the deprotonation of H_2SO_4 was endothermic, (ii) in a 1:5 ratio deprotonation was exothermic forming HSO_4^-, and (iii) in a 1:10 ratio double deprotonation occurred to form SO_4^{2-} exothermically.

Keywords

tantalum, niobium, solvent extraction, reaction mechanism, molecular modelling.

Introduction

Tantalum (Ta) and niobium (Nb) are two metals found in the same group (VB) of the periodic table of elements. Owing to their similar chemical and physical properties, they are difficult to separate. Ta and Nb are usually found together in various minerals, of which the most important are columbite ((Fe, Mn, Mg)(Nb, Ta)$_2O_6$) and tantalite ((Fe, Mn)(Nb, Ta)$_2O_6$) (Agulyanski, 2004). Ta is used in a variety of applications, including capacitors in electronic circuits, rectifiers, pins for bone fixtures, surgical and dental instruments, and in chemical heat exchangers (Krebs, 2006). For many applications, pure Ta is needed; however, increasing purity entails a proportional increase in production cost. One way of ensuring an economically viable process for the production of high-purity Ta is to find a cost-effective way to separate Ta and Nb.

Solvent extraction (SX) is used for the separation and purification of various metals, including copper (Bidari, Irannejad, and Gharabaghi, 2013), nickel (Noori *et al.*, 2014), iron (Li *et al.*, 2011), platinum group metals (PGMs) (Kumar *et al.*, 2008), zirconium (Biswas and Hayat, 2002), hafnium (Lee, Banda, and Min, 2015), and Ta, and Nb (Zhu and Cheng, 2011). Ungerer *et al.* (2014) studied the separation of Ta and Nb (in the form of MF_5) by SX using safer and more environmentally friendly chemicals and techniques. Although partial separation was achieved in a sulphuric acid (H_2SO_4) medium with the extractants diiso-octyl phosphinic acid (PA) and di-(2-ethylhexyl) phosphoric acid (D2EHPA), the main obstacle remained the lack of data on the speciation of Ta and Nb compounds, without which it was not possible to fully explain the separation data obtained.

One method that could be used for speciation of the compounds is computational methods for SX, which entails a step-by-step analysis of the extraction process on a molecular level and determination of the molecular reactions occurring during SX from a thermodynamic perspective, which could lead to the development of a new method for the analysis of Ta and Nb separation by SX.

[1] Narbutt, J. and Czerwinski, M. 1992. Computational chemistry in modelling solvent extraction of metal ions. *Solvent Extraction Principles and Practice.* Rydberg, J., Cox, M., Musikas, C., and Choppin, G.R. (eds). Wiley, New York. Chapter 16.

[2] Ungerer, M.J., van der Westhuizen, D.J., Lachmann, G., and Krieg, H.M. 2014. Comparison of extractants for the separation of TaF5 and NbF5 in different acidic media. *Hydrometallurgy*, vol. 144–145. pp. 195–206.

* *Chemical Resource Beneficiation (CRB), North-West University, Potchefstroom, South Africa.*

 ISSN 2225-6253. Paper received Apr. 2016; revised paper received Sept. 2016.

Molecular modelling of tantalum in an aqueous phase

In this study we propose the use of molecular modelling to determine the behaviour of Ta in a sulphuric acid medium. Reactions of H_2SO_4 and water (Equations [1] and [2]) and TaF_5 in H_2SO_4 (Equations [3] and [4]) were investigated.

$$H_2SO_4 + H_2O \rightarrow HSO_4^- + H_3O^+ \quad [1]$$

$$HSO_4^- + H_2O \rightarrow SO_4^{2-} + H_3O^+ \quad [2]$$

$$TaF_5 + H_2SO_4 + H_2O \rightarrow TaF_5.HSO_4^- + H_3O^+ \quad [3]$$

$$TaF_5 + H_2SO_4 \rightarrow TaF_4.HSO_4 + HF \quad [4]$$

Computational methods

For the molecular modelling of H_2SO_4 with H_2O (Equations [1] and [2]) as well as TaF_5 with H_2SO_4 (Equations [3] and [4]), both in an aqueous phase, the DMol3 module – a density functional theory (DFT) (Hohenberg and Kohn, 1964; Levy, 1979) quantum mechanical modelling method of the Materials Studio 6.1 software from Accelrys (2012) was used. For all the calculations on the different molecules, a geometry optimization (Perdew and Wang, 1992; Delley, 1992) was first performed with the generalized gradient-corrected approximation (GGA) with Perdew-Wang (1992) correlation functional (PW91). The basis set used was DNP (double-numeric polarization functions) with basis file 4.4 and OBS dispersion correction. The core treatment parameter was set to 'All Electron' and therefore all the calculations were done for the electrons as if they are valence electrons. Under the electronic properties, smearing of 0.005 Hartree (Ha) was also chosen (Delley, 1995) and the solvation model COSMO (conductor-like screening model) (Delley, 2006) was used, with water as the solvent with a dielectric constant of 78.54. COSMO was used to account for the surrounding of implicit H_2O molecules. After the geometry optimization, various properties were calculated using single-point energy calculations with the same settings as stated previously. The calculations were done in the aqueous phase at 0 K and the energy correction term was added to give Gibbs free energy values at 298.15 K.

Results and discussion

The relative energies for Reactions [1] and [2] are presented in Figure 1, where the dotted line represents the reaction energies when using a 1:1 H_2SO_4:H_2O ratio and the solid line when using a 1:5 H_2SO_4:H_2O ratio, where five explicit water molecules were added. For each line three points are presented, the first being the energy of the starting materials, the second the energy of the intermediate products, and the third the energy of the final products. When using a 1:1 H_2SO_4:H_2O ratio (dotted line) it can be seen that when one H_2SO_4 molecule reacted consecutively with two H_2O molecules to firstly form HSO_4^- and H_3O^+, and then SO_4^{2-} and $2H_3O^+$, 33.5 kJ/mol and 153.4 kJ/mol were needed respectively, indicating an endothermic reaction for both steps.

However, according to laboratory results and values from the literature, Reaction [1] is highly exothermic and Reaction [2] moderately exothermic. Steyl (2009) used DFT modelling (DMol^3 v.4.2) to show that when H_2SO_4 reacted with H_2O, five H_2O molecules were needed to form an outer sphere around the H_2SO_4 molecule to react to form HSO_4^-. Therefore a balanced reaction equation was modelled where five H_2O molecules reacted with H_2SO_4 as follows:

$$H_2SO_4 + 5H_2O \rightarrow HSO_4^- + H_3O^+ + 4H_2O \quad [5]$$

$$HSO_4^- + 4H_2O \rightarrow SO_4^{2-} + 2H_3O^+ + 3H_2O \quad [6]$$

According to Figure 1 (solid line) the reaction becomes exothermic, as expected, when sufficient water molecules are available. To determine the effect of adding further water molecules it was decided to model the H_2SO_4-H_2O system with 10 explicit waters surrounding the acid (Figure 1 – dashed line). After the geometry optimization of the 1:10 system, it was seen that double deprotonation of H_2SO_4 took place, without the formation of HSO_4^- as an intermediate step. The energy decrease to –816 kJ/mol indicates an exothermic reaction with a stabilized ion forming as the final product. As when using five H_2O molecules, the surrounding H_2O molecules stabilized the ion by hydrogen bonding. Ding and Laasonen (2004), using DFT modelling with PW91(DNP) as well as BLYP calculations, showed that when less than five H_2O molecules are present with H_2SO_4 the first deprotonation occurs exothermically, and when eight to ten H_2O molecules surround H_2SO_4, the second deprotonation also occurs, resulting in the formation of SO_4^{2-} with the other surrounding H_2O molecules forming hydrogen bonds and stabilizing the formed ions. Hammerich, Buch, and Mohamed (2008) used *ab initio* modelling methods and also showed that when ten H_2O molecules are present double deprotonation occurs, but also observed proton hopping between the different oxygen sites of HSO_4^- and the surrounding H_2O molecules. Although it is generally assumed that H_2SO_4:H_2O is a 1:1 reaction, it was shown that, energetically, from five to ten explicit H_2O molecules are needed for the reaction to occur. According to these results, the 1:10 reaction of H_2SO_4 in H_2O showed the best correlation to the real system.

In the second part of the investigation, the reaction of TaF_5 and H_2SO_4 in the presence of 1, 5 and 10 H_2O molecules was modelled at TaF_5:H_2SO_4:H_2O ratios of 1:1:1, 1:1:5, and 1:1:10. Since TaF_5 has a trigonal bipyramidal structure, the H_2SO_4 molecule will most likely approach from an equatorial position (where more space and best orbital overlap is available) to form $TaF_5.HSO_4^-$ (octahedral structure) before rearranging to $TaF_4.HSO_4$, where the HSO_4^- group can be either axial or equatorial (Figure 2).

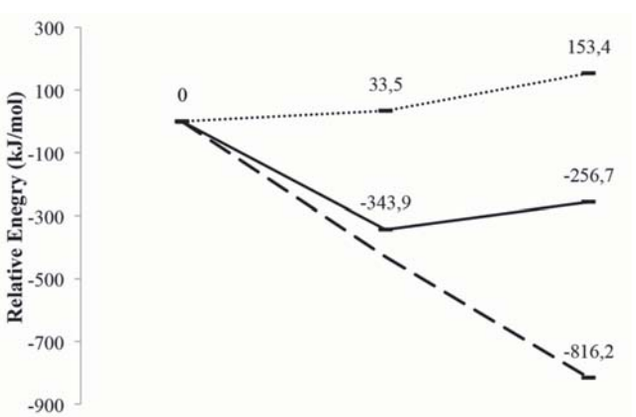

Figure 1—Relative reaction energy (kJ/mol) for H_2SO_4 and H_2O (dotted line is H_2SO_4:H_2O = 1:1; solid line is H_2SO_4:H_2O = 1:5; dashed line is H_2SO_4:H_2O = 1:10)

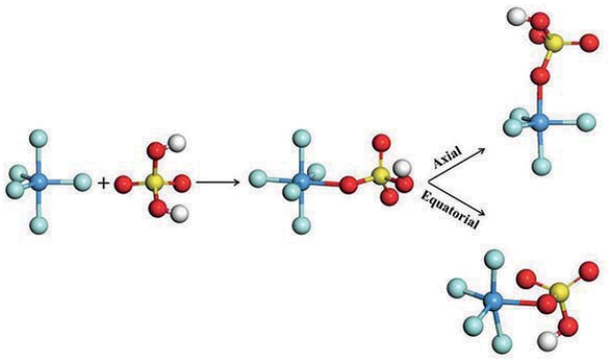

Figure 2—Possible reaction pathway of TaF_5 and H_2SO_4

As with Equations [1] and [2], it was expected that the relative reaction energies would be lower when adding explicit water molecules to Equations [3] and [4]. To confirm this, the same calculations done for Equations [1] and [2] were performed for Equations [3] and [4]. The relative energies of the reactions of TaF_5 with H_2SO_4 and H_2O are shown in Figure 3. The dotted line shows the energies for a TaF_5:H_2SO_4:H_2O ratio of 1:1:1, the solid line the energies for a TaF_5:H_2SO_4:H_2O ratio of 1:1:5, and the dashed lines the energies when the TaF_5:H_2SO_4:H_2O ratio is 1:1:10. Again, the first data point is the energy of the reagents, the second the energy of the intermediates, and the third the energy of the products.

As shown in Figure 2, the position of the HSO_4^- group can be either axial or equatorial. In Figure 3, for the 1:1:1 reaction (dotted line) 105 kJ/mol is needed for the HSO_4^- group to bond to TaF_5, before HF is evolved and $TaF_4.HSO_4$ is formed at 97.2 kJ/mol and 54.4 kJ/mol for the axial and equatorial positions respectively, indicating an endothermic reaction. However when using more H_2O (five molecules – solid line) –304.8 kJ/mol is needed to form $TaF_5.HSO_4^-$, indicating that a stable ion forms. The formation of $TaF_4.HSO_4$ in the axial position requires –158.6 kJ/mol, and in the equatorial position -203.5 kJ/mol, indicating an exothermic reaction. The same trend was observed as for the 1:1:1 reaction, where the molecule with the HSO_4^- group in the equatorial position was at a lower energy than when the group is axial. This is due to the orbital overlap that occurs between the HSO_4^- group and TaF_5 when the reaction takes place. Steyl (2009) obtained similar results.

The 1:1:10 reaction of TaF_5:H_2SO_4:H_2O was also modelled. Again, the HSO_4^- ion bonded axially and equatorially, and as with the 1 H_2SO_4:10 H_2O system, double deprotonation occurred. The intermediate molecule $TaF_4.HSO_4$ did not form, but the $TaF_4SO_4^-$ molecule formed and was stabilized by the surrounding H_3O^+ ions and H_2O molecules. This would imply that the 1:1:10 reaction scheme had the lowest energy and would therefore be energetically the most likely.

Furthermore, it was seen from the modelling results that when the HSO_4^- group was in the equatorial position it formed a bidentate bond to Ta, lowering the overall energy of the molecule and changing the oxidation state of Ta from 5+ to 4+ in both the 1:5 and the 1:10 system.

Conclusion

The reactions of H_2SO_4 with H_2O and TaF_5 with H_2SO_4 and H_2O were investigated. When modelling a 1:1 reaction of acid and water an endothermic reaction was observed. The modelling software COSMO was used to account for the surrounding implicit H_2O molecules. By adding five explicit H_2O molecules to the reaction, an exothermic reaction was observed for the reactions of H_2SO_4 with H_2O. This indicated that COSMO adds a correction term for the long-range interactions that could occur if these reactions occurred in water as a medium, but does not show or calculate the explicit reactions and hydrogen bonding that occur with H_2O in the short range. This hydrogen bonding stabilizes the molecules, resulting in lower energy values. With the addition of 10 explicit H_2O molecules a double deprotonation was observed with the formation of SO_4^{2-} stabilized by the surrounding hydrogen bonds. The same tendencies were observed for the reactions of TaF_5 with H_2SO_4 and H_2O, where the explicit H_2O molecules lowered the overall reaction energies, showing an exothermic reaction. The resulting ions were stabilized with the surrounding H_3O^+ ions and H_2O molecules.

Further investigations are needed to determine the side reactions and other geometries that may occur during these reactions, as well as the possible influence if a change in oxidation state occurs.

Acknowledgements

The author would like to thank the South African Nuclear Energy Corporation SOC Limited (Necsa) and the New Metals Development Network (NMDN) of the Advanced Metals Initiative (AMI) of the Department of Science and Technology (DST) for financial support, and the North-West University High Performance Computing (NWU-HPC) centre for the use of their facilities and their support.

References

Accelrys Software Inc. 2012. Material Studio Modelling Environment, version 6.1. San Diego.

Agulyanski, A. 2004. The chemistry of tantalum and niobium fluoride compounds. Elsevier, San Diego, Oxford, London.

Bidari, E., Irannejad, M., and Gharabaghi, M. 2013. Solvent extraction recovery and separation of cadmium and copper from sulphate solution. *Journal of Environmental Chemical Engineering*, vol. 1. pp. 1269–1274.

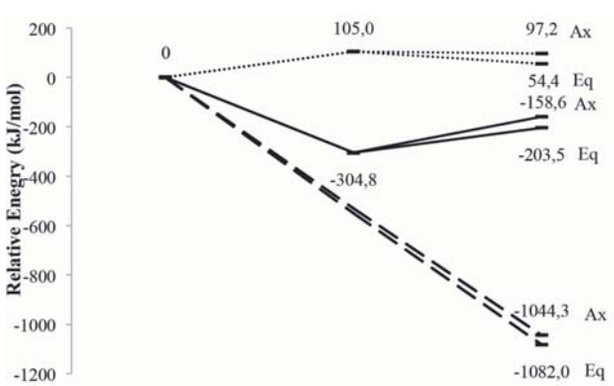

Figure 3—Relative reaction energy (kJ/mol) for TaF_5, H_2SO_4, and H_2O (dotted line is 1:1:1 reaction, solid line is 1:1:5 reaction, dashed line is H_2SO_4:H_2O = 1:1:10)

Biswas, R.K. and Hayat, M.A. 2002. Solvent extraction of zirconium(IV) from chloride media by D2EHPA in kerosene. *Hydrometallurgy*, vol. 63. pp. 149–158.

Delley, B. 1992. Ground-state enthalpies: evaluation of electronic structure approaches with emphasis on the density functional method. *Journal of Physical Chemistry A*, vol. 110. pp. 13632–13639.

Delley, B., and Scherrer, P. 1995. DMol, a standard tool for density functional calculations: review and advances *Modern Density Functional Theory: a Tool for Chemistry*. Seminario, J.M. and Politzer, P. (eds). *Theoretical and Computational Chemistry Series*, vol. 2. Elsevier.

Delley, B. 2006. The conductor-like screening model for polymers and surfaces. *Molecular Simulation*, vol. 32. pp. 117–123.

Ding, C.G., and Laasonen, K. 2004. Partially and fully deprotonated sulfuric acid in $H_2SO_4(H_2O)_n$ (n = 6 - 9) clusters. *Chemical Physics Letters*, vol. 390. pp. 307–313.

Hammerich, A.D., Buch, V., and Mohamed, F. 2008. Ab initio simulations of sulfuric acid solutions. *Chemical Physics Letters,* vol. 460. pp. 423–431.

Hohenberg, P. and Kohn, W. 1964. Inhomogeneous electron gas. *Physical Review B*, vol. 136. p. B864.

Krebs, R.E. 2006. The History and Use of Our Earth's Chemical Elements: A Reference Guide. 2nd edn. Greenwood Press, Westport, USA.

Kumar, J.R., Lee, H.I., Lee, J.Y., Kim, J.S., and Sohn, J.S. 2008. Comparison of liquid-liquid extraction studies on platinum(IV) from acidic solutions using bis(2,4,4-trimethylpentyl) monothiophosphinic acid. *Separation and Purification Technology*, vol. 63. pp. 184–190.

Lee, M.S., Banda, R., and Min, S.H. 2015. Separation of Hf(IV)–Zr(IV) in H_2SO_4 solutions using solvent extraction with D2EHPA or Cyanex 272 at different reagent and metal ion concentrations. *Hydrometallurgy*, vol. 152. pp. 84–90.

Levy, M. 1979. Universal variational functionals of electron densities, first-order density matrices, and natural spin-orbitals ans solution of the v-representability problem. *Proceedings of the National Academy of Sciences*, vol. 76. pp. 6062–6065.

Li, X., Wei, C., Deng, Z., Li, M., Li, C., and Fan, G. 2011. Selective solvent extraction of vanadium over iron from a stone coal/black shale acid leach solution by D2EHPA/TBP. *Hydrometallurgy*, vol. 105. pp. 359–363.

Narbutt, J. and Czerwinski, M. 1992. Computational chemistry in modelling solvent extraction of metal ions. *Solvent Extraction Principles and Practice*. Rydberg, J., Cox, M., Musikas, C., and Choppin, G.R. (eds.). Wiley, New York. Chapter 16.

Noori, M., Rashchi, F., Babakhani, A., and Vahidi, E. 2014. Selective recovery and separation of nickel and vanadium in sulfate media using mixtures of D2EHPA and Cyanex 272. *Separation and Purification Technology*, vol. 136. pp. 265–273.

Perdew, J.P., and Wang, Y. 1992. Accurate and simple analytic representation of the electron-gas correlation energy. *Physical Review B*, vol. 45. pp. 13244–13249.

Steyl, J.D.T. 2009. Kinetic modelling of chemical processes in acid solution at t≤200°C. (i) thermodynamics and speciation in H_2SO_4-metal (ii) SO_4-H_2O system. *Proceedings of Hydrometallurgy 2009*, Misty Hills, Muldersdrift, Gauteng 24–26 February. Southern African Institute of Mining and Metallurgy, Johannesburg. pp. 401–444.

Ungerer, M.J., van der Westhuizen, D.J., Lachmann, G., and Krieg, H.M. 2014. Comparison of extractants for the separation of TaF_5 and NbF_5 in different acidic media. *Hydrometallurgy*, vol. 144-145. pp. 195–206.

Zhu, Z. and Cheng, C.Y. 2011. Solvent extraction technology for the separation and purification of niobium and tantalum: a review. *Hydrometallurgy*, vol. 108. pp. 1–12. ◆

http://dx.doi.org/10.17159/2411-9717/2017/v117n6a5

Determination of magnitude completeness from convex Gutenberg-Richter graphs in the central portion of the Kiirunavaara mine

by M. Svartsjaern* and A. Eitzenberger*

Synopsis

This paper describes a study of seismic records from the Kiirunavaara mine footwall which were interpreted in relation with numerical models developed outside the study. Seismic data was retrieved from a portion of the mine and filtered with respect to the ratio between energy carried by an event's P (primary) and S (secondary) waves (*Es/Ep* ratio), local magnitude, and active mining depth. The data was analysed using *Es/Ep* ratios and Gutenberg-Richter graphs to determine the event origin, mechanisms, and minimum magnitude cut-off. The magnitude completeness was identified by studying the *b*-value stability and *b*-value differentiation between origin sets. It was shown that, by separating seismic events into the origin components shear, complex, and tensile based on *Es/Ep* ratios, a representative value for the magnitude completeness can be identified for a catalogue with a convex cumulative log curve. The majority of the events were shown to be of shear-slip origin based on the recorded *Es/Ep* ratios, with pure tensile events constituting only about 10% of the recorded data. Spatial and temporal event location patterns were studied and compared with numerical modelling results. The comparison showed a correlation between shear-slip seismic events and volumes experiencing high differential stresses in the lower part of the footwall. In the upper part of the footwall the results did not reveal any clear correlation between observed damage in drifts and seismic event locations. The concentration of seismic events in the lower portion of the footwall is discussed in the context of rock mass displacements. The results indicate a possible connection between mine seismicity at depth and damage observations in the drifts in higher non-seismic areas by seismic softening and subsequent lateral expansion of the rock mass.

Keywords

mine seismicity, event origin, failure mode, Gutenberg-Richter relationship, *Es/Ep* ratio.

Introduction

The general trend of increasing mining depths throughout the world implies an increase in mining-induced seismicity. Advances in monitoring techniques have allowed more seismic data to be collected and recorded, and its importance is generally accepted across various disciplines. This data has assisted in predicting the origin of seismic events and explaining the plausible underlying causes, and in so doing, aiding strategic mine planning.

The link between mining and recorded seismicity has been a focus of research for many years. Notable recent works include McKinnon (2006), who showed how even small stress changes from mining activities could activate seismic faults in volumes proportionally much larger than the mining area itself. These remote fault-slip events were also recognized by Richardson and Jordan (2002) as 'type B' events activated by long-term mining. The 'type B' events described by Richardson and Jordan (2002) were recognized primarily as originating from shear-type events which are commonly associated with mining-induced seismicity (Ortlepp, 2000). Shear-type and non-shear events are most typically distinguished by studying the ratios of energy carried by an event's P (primary) and S (secondary) waves. This relation is referred to as the *Es/Ep* ratio (Richardson and Jordan, 2002, Snelling, Godin, McKinnon, 2013; Xu *et al.*, 2014).

Separating seismic events by types and categories allows for detailed analysis on what are often otherwise significantly large data-sets. Simplification and analysis by filtering and clustering of seismic data is a common first step when analysing located events, as demonstrated by Lynch and Malovichko (2006), Richardson and Jordan (2002), Orlecka-Sikora *et al.* (2012), Xu *et al.* (2014), and Cesca, Sen, and Dahm (2014).

The basis for these analyses is the fact that a seismic or acoustic event is an indication of changes in rock mass properties due to fracture slip and growth (Shen *et al.*, 1995). Cai, Kaiser, and Martin (2001) and Shen *et al.* (1995) noted this fracture growth as a reduction of the rock mass matrix stiffness. This effect was also demonstrated by Young *et al.* (2004), who observed a reduction in the Young s modulus following recorded micro-seismicity. The correlation between fracture growth and subsequent stiffness reduction was used by Agliardi *et al.* (2013) to track progressive fracture growth leading up to rock mass failure by measuring changes in GSI (Geological Strength Index). Cai, Kaiser, and

* *Division of Mining and Rock Engineering, Department of Civil, Environmental and Natural Resources Engineering, Luleå University of Technology, Sweden.*

 ISSN 2225-6253. Paper received Jan. 2016; revised paper received Aug. 2016.

Martin (2001) used seismic data to directly characterize the rock mass damage. The potential of using seismic data for rock mechanical back-analysis was also explicitly recognized by Mendecki, Lynch, and Malovichko (2010).

The current study comprises a micro-seismic event database from the Kiirunavaara mine footwall which was filtered and analysed with respect to temporal and spatial distributions, as well as in the context of numerically calculated stress difference concentrations and displacements. A possible correlation between stress difference concentrations and seismic event clustering was earlier shown for the Creighton mine by Snelling, Godin, and McKinnon (2013), while Moss, Diachenko, and Townsend (2006) indicated an increase in seismicity near mobilized rock mass volumes in the Palabora mine pit slopes. The use of seismic data to track general rock mass damage is well documented and a variation of techniques for doing so can be found in a number of published studies (*e.g.* Cai, Kaiser, and Martin, 2001; Young *et al.*, 2004; Lynch and Malovichko, 2006; Xu *et al.* 2014; Abdul-Wahed, Al Heib, and Senfaute, 2006; Liang *et al.*, 2013; Ma *et al.*, 2013).

The state of the rock mass at the Kiirunavaara mine, particularly in the footwall, has previously been investigated by Singh, Stephansson, and Herdocia (1993), Lupo (1996), Sjöberg (1999), Henry and Dahner-Lindquist (2000), Villegas and Nordlund (2008, 2013), and Svartsjaern (2015). However, none of these studies have incorporated the mine's seismic event data. The mine started recording seismic events on a larger scale in 2008, after previously installing a minor system in 2003 following a trial system in 2000 (Henry *et al.*, 2001). Even though data was sparse, Henry *et al.* (2001) indicated the possibility of using a larger seismic system to track failure in the footwall rock mass. The study by Svartsjaern (2015) concentrated on rock mass response in the upper part of the footwall (0–600 m depth), while most of the seismic events have been located at depths greater than 600 m. The predominant mechanisms suggested by Henry *et al.* (2001) and Svartsjaern (2015) are closely related to the theory of rock mass softening through seismic events. Part of the seismic event database for the mine was therefore extracted for this study in an attempt to relate it to the footwall rock mass response described by Svartsjaern (2015) and ultimately connect it to plausible large-scale fracturing in this region. This is done by studying the location of seismic shear events with magnitudes above a reliable minimum magnitude cut-off.

The Kiirunavaara mine

The LKAB (Luossavaara-Kiirunavaara Aktiebolag) Kiirunavaara mine's orebody dips approximately 60 degrees to the east. The mine's infrastructure is located inside the footwall rock mass, as are the majority of the geophones constituting the current seismic monitoring system. Ore is currently extracted through sublevel caving (SLC) after transitioning from an open pit in the 1950s. The current main haulage level is located on level 1365 m, which corresponds to an actual depth below the ground surface of roughly 1100 m. The main orebody is mined from blocks designated with lead digits of 16 to 45, which correspond to Y-coordinates of 1600 to 4500 m. Mining of these blocks is currently performed between the (Z) levels 993 and 1051 m. For modelling purposes a mine section within the middle two-thirds of the strike length is commonly approximated as a 2D plane strain profile as seen in the north-south direction.

Underground mine seismic system

The primary objective of the seismic system is to track events that might be related to rockfalls and rockbursts in active production areas to gain insight into the mine seismicity. This has resulted in the bulk of the geophones being installed in close proximity to the mining areas, with fewer geophones in the upper 600 m of the rock mass. The arrangement of geophones with respect to depth is shown in Figure 1.

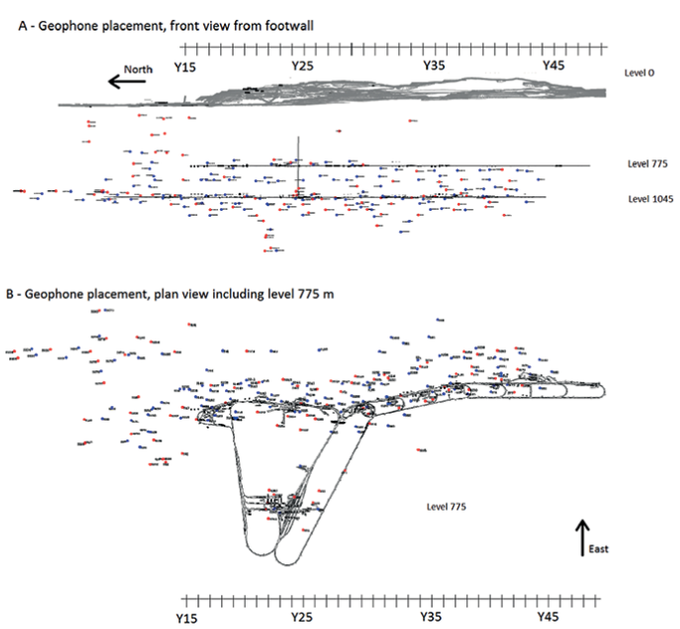

Figure 1—(A) Cross-section of geophone placement with respect to depth, (B) horizontal cross-section of geophone placement. Triaxial geophones are indicated by red, and uniaxial by blue circles (courtesy of LKAB)

The first set of geophones at Kiirunavaara was installed as a small test set-up in 2000 in an attempt to confirm field observations of footwall rock mass movements in the upper footwall and near the production level (Henry *et al.*, 2001). The data retrieved from this system was limited and the principles differed from subsequent systems as a transition was made from macro-seismic to micro-seismic sensors. Installation of the current (micro-seismic) system began in 2003. Since then, the number of geophones has been increased on a regular basis. A second large installation was performed in 2008 due to increased seismic risks, which made the system coverage mine-wide (relative to the production areas); the system was later significantly extended during 2012 and 2013. The current seismic system includes more than 210 geophones by which the mine strives to achieve a location accuracy of less than 20 m for -1.5 local magnitude events (Stöckel, Mäkitaavola, Sjöberg, 2013). Because of the different installation periods, the seismic data pre-dating 2008 was judged to be less reliable as it was recorded by much fewer devices. Data acquired from the earliest arrays (installed in 2000) was collected using only a few geophones and different principles. Consequently, co-analysis of old and new data is discouraged. Only data collected after 14 November 2008 was included in the current study.

Footwall rock mass deformation

The main footwall host rock is Precambrian-aged trachyandesite with UCS ranging from 140–300 MPa and RMR values in the range of 49–68 (Sandström, 2003). Despite the rock being relatively competent, damage on the decommissioned open pit footwall crest, as well as within the footwall rock mass, has been observed since the late 1980s. The current state of this large-scale damage pattern is described in Svartsjaern *et al.*, (2015), where it is proposed that the mappable damage in the footwall involves three stages as visualized in Figure 2A:

- Rock mass weaknesses formed near the production level are activated, resulting in mappable damage. The degree of visual damage and extent of the damaged volume depend on the confinement, resulting in a step-path-like extent boundary that travels outwards relative to the footwall contact with decreasing confinement
- Further up in the footwall, currently above level 740 m, the reduction in confinement has reached a magnitude which allows the damage extent boundary to reach the outer edge of the mining-induced rock mass weaknesses. Deformation in the de-stressed rock mass below level 740 m facilitates slip of natural ore-parallel structures on overlying levels, which results in fallouts related to these structures. The mappable damage in this fallout zone is caused mainly by activation of zones of weakness formed earlier within 'the damaged zone' and damage associated with structure contacts. Fresh fracture propagation is limited and the damage extent boundary moves away from the footwall contact by stepping from one structure group to the next (Figure 2B). The shear movement in these structure groups is observable up to around level 300 m, where the displacement seems to be absorbed by subvertical structures that daylight at the open pit footwall slope face (Figure 2A).

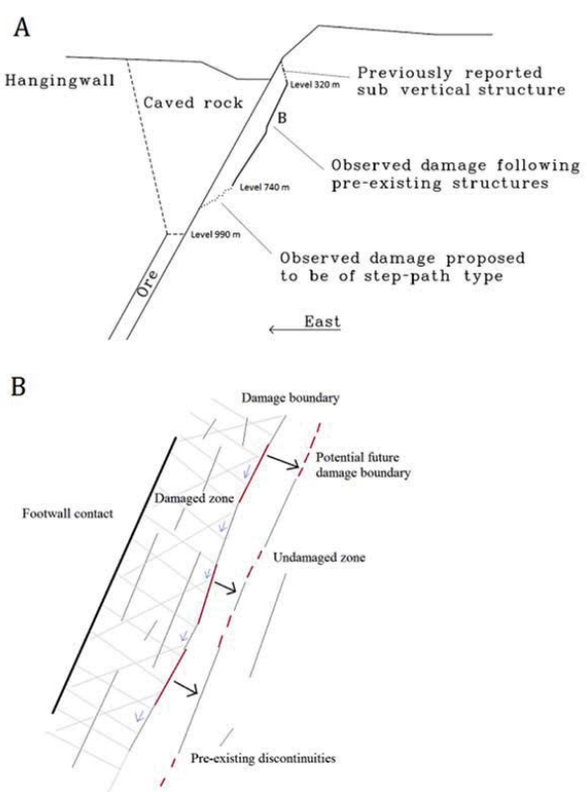

Figure 2—Footwall damage hypothesis as proposed by Svartsjaern *et al*. (2015)

Seismic data

Data-set

Due to the large quantity of seismic recordings collected throughout the mine, a limited volume was selected for detailed analysis. As it was opted to connect the study of the seismic data to on-site failure observations, the mine profile Y23 (refer to Figure 3) was chosen as the centre line of the studied block, which also coincides with the location of the central infrastructure. The mine infrastructure is relatively dense at these coordinates, which allows access to the rock mass on several levels. Seismic data was extracted for a polygonal volume incorporating the footwall and footwall/ore contact (including part of the hangingwall) covering depths between level zero (initial ground surface before mining) and the mine level 1400 m. The width was set to 400 m centred on the profile Y23, resulting in a 200 m data collection zone on the north and south sides of the model profile. With the imposed limitation, the data constituted 35 119 localized events with local magnitudes, according to Equation [1], of between -2.8 and 1.7 for the period 14 November 2008 to 13 February 2014.

$$M_L = 0.392 \cdot \log(\text{Seismic potency, m}^3) + 0.272 \cdot \log(\text{Seismic energy, J}) - 0.523 \quad [1]$$

As can be noted from Figure 3, two distinct areas of seismic activity are apparent; one near the production and footwall-ore contact and the other, shown as a vertical column, far into the footwall. The location of the far field column corresponds to the location of the mine skip shafts. Due to the likelihood of the far field data being generated by skip operations and not mining-induced seismic events it was decided to further spatially constrain the data by excluding the column location from the sets. The remaining events are referred to as 'the full catalogue' to differentiate between the entire studied volume and any data subsets within the sample. There are no orepasses located within the studied volume.

The source parameters of the seismic events were calculated by the Institute of Mine Seismology (IMS) based on the seismic records and accessed in a standardized text format supplied by LKAB. Production and development blasts were filtered from the data by IMS. Subsequent filtering and event analysis was performed using the IMS software Vantage (IMS, 2014).

Estimating the magnitude completeness and minimum magnitude cut-off

Larger magnitude events are more likely to be detected by a seismic system than small events due to the system sensitivity and wave attenuation. Thus for each seismic catalogue there is a limiting magnitude below which events might have occurred in the monitored area without being recorded. This limiting magnitude is called the minimum magnitude cut-off or critical magnitude (M_c or M_0). M_c is defined as the magnitude at which the slope of a cumulative Gutenberg-Richter graph (Gutenberg and Richter, 1949) first deviates from linearity. The slope at any M in the cumulative Gutenberg-Richter graph is defined by the Gutenberg-Richter power law, $\log N(M > M_c) = a - bM$, where a and b are seismic parameters and the slope is ultimately given by b. Naylor, Orfanogiannaki, and Harte (2010) describe procedures to identify M_c by studying the variation in b for different choices of $M = M_c$ following the assumption that b will exhibit an incremental increase while stepping through the cumulative Gutenberg-Richter graph for $M<M_c$ and stabilizing for $M \geq M_c$.

Following the recommendations by Naylor, Orfanogiannaki, and Harte (2010), b is estimated using the maximum likelihood technique where $b = \frac{\log_{10} e}{\bar{M} - (M_c - \Delta M/2)}$ and $\bar{M}$ is the mean magnitude in the examined set and ΔM equals the binning width (in this case 0.1). The values of b are calculated both for the full magnitude range $M>M_c$ and a truncated set where the bins containing less than 17% of the events fulfilling $M>M_c$ are ignored to minimize the influence from chance large-magnitude events. The calculated values

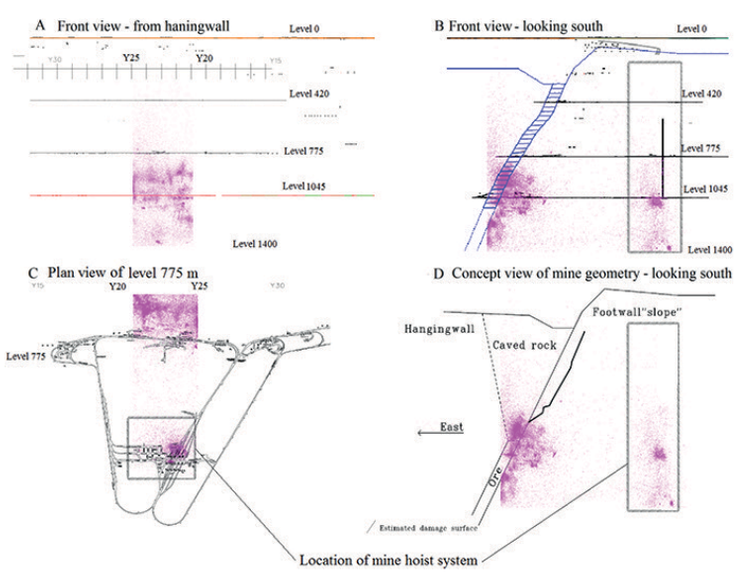

Figure 3—Visualization of spatial limitations imposed on seismic data; the grey rectangle outlines volumes affected by skip operations (Figure D was modified following Svartsjaern, 2015)

of *b* are also compared to the automatically calculated *b* from Vantage for the same seismic catalogue. To further reduce ambiguity in the estimate of *b* the truncated values for *b* are also averaged over two adjacent bins to account for any large frequency changes between the bins. The values of *b* for incremental steps from low to high magnitudes are shown in Figure 4 together with the *b* value increment for each step.

Based on the assumption of *b*-value stabilization at $M>M_c$, the *b* increment diagram in Figure 4 indicates an initial change in behaviour to relative stability at about M = -1.7, where the increment changes from a steadily increasing rise to a relatively stable constant increase. Setting M_c = -1.7 and applying the Gutenberg-Richter power law with the corresponding values for *b* results in fitted lines that overshoot the log-linear portion of the cumulative graph in all cases (manual and Vantage calculations). In effect, the occurrence of larger magnitude events is not realistically represented. No plateau in the absolute *b* value *vs.* M_c can be found in Figure 4. Instead, *b* increases incrementally for the entire magnitude range M<0, only to show a stabilization of the magnitude increment.

To investigate the possible influence of origin mechanisms on the *b*-value stability the data was filtered into three subsets; shear-slip component events with a *Es/Ep* ratio above 10 (Snelling, Godin, and McKinnon, 2013; Xu *et al.*, 2014), complex events containing both shear-slip and tensile/volumetric components with *Es/Ep* ratios between 3 and 10, and tensile-component-only events with *Es/Ep* ratios less than 3 (Hudyma and Potvin, 2010; Xu *et al.*, 2014). As evident in Figure 5, the calculated value for *b* does not differ significantly between the subsets for M < -1.0 and there is no arguable stabilization for any subset until M_c = 0. At M_c > -0.8 the different origin sets return clearly different *b*-values with a stable internal distance. At M = -1.0 the trend for the tensile events is to return a higher *b*-value for the same M than the other sets, followed by the complex set (less pronounced) containing both shear-slip and tensile components. This would be consistent with the indications by Hudyma (2008a) that events with tensile/volumetric origin will return higher *b*-values than shear-slip events. The trend is lost at M = 0. This is most likely due to the small number of tensile events in the remaining bins (68 out of 2513 total).

Two potential M_c values are studied further: M = -1.0 where the *b*-value for the different subsets start to diverge, and M = -0.8 where the differentiation between the *b*-values for the sets is significant and stable. The resulting fits for M_c

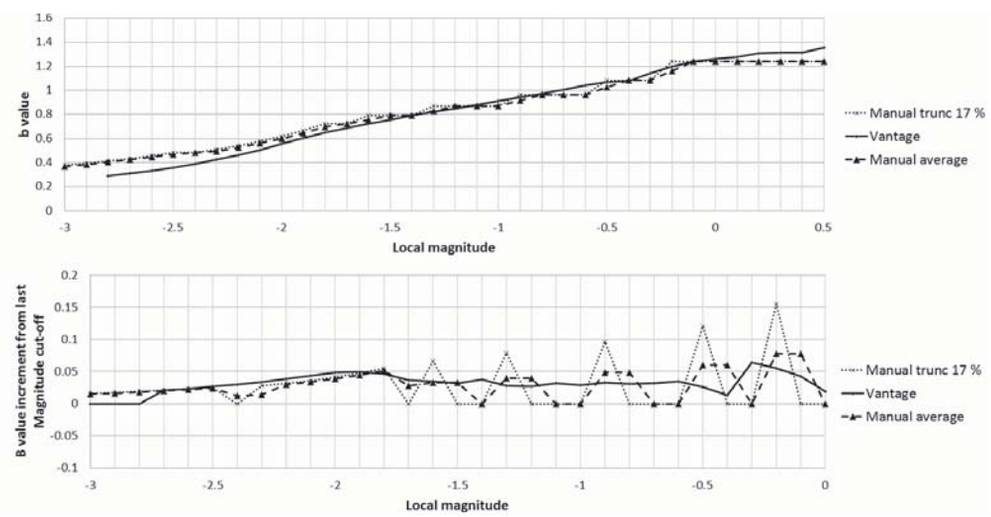

Figure 4—Values of *b* and relative change for incremental changes of M_c (zero and peak incremental values for the manual calculations most likely results from the bin width, as no interpolation between bins was implemented)

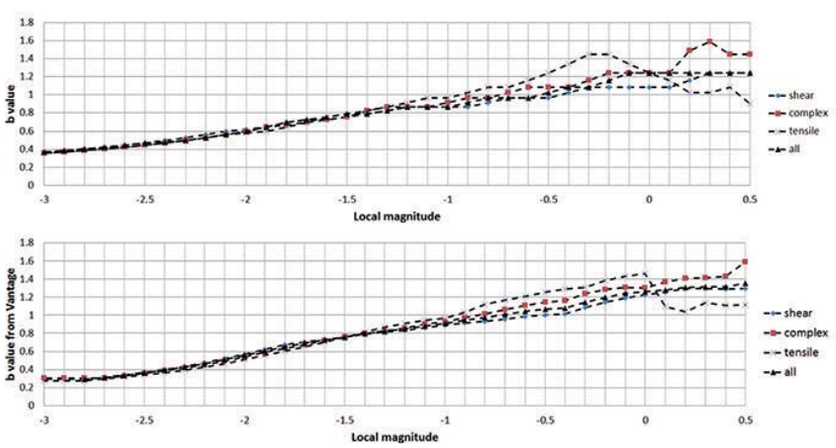

Figure 5—Calculated *b*-values using a 17% truncation and averaging over 2 magnitude bins (upper) and *b*-values by Vantage (lower)

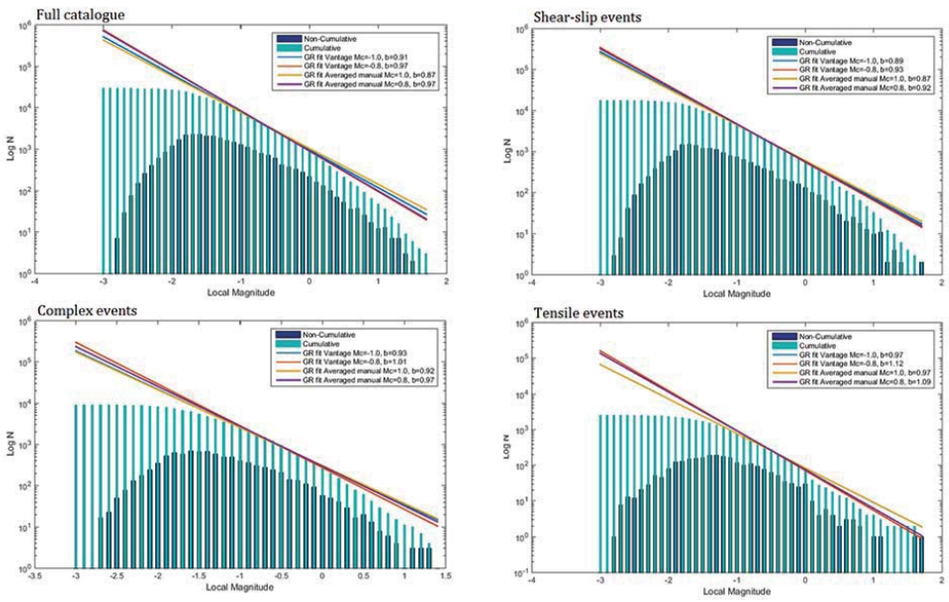

Figure 6—Fitted Gutenberg-Richter power law for all subsets using M_c = -1.0 (note that fitted lines for *b* may overlay)

= -1.0 and -0.8 are shown in Figure 6. As can be seen, the *b*-value adequately fits the log-linear portion of the cumulative graph, but there is still a tendency in all the subsets to over-represent the largest magnitudes.

In general, the calculated *b*-value fits well to the cumulative data plot. However, the representation is more weighted towards low-magnitude events, with some overrepresentation of higher magnitude events. The averaged truncated calculation, in which the bins containing less than 17% of the events with $M < M_c$ were ignored, results in virtually the same magnitude values as those automatically returned from Vantage (Figure 4 for M > -2) and shows a good fit to the plotted data. As evident from Figure 5, the value of *b* becomes unstable at M > 0. This break in trend is almost certainly due to undersampling of the events, since a complete catalogue of the potential large-magnitude events in the studied area is unlikely to be adequately recorded during the relatively short data collection period (approx. 5 years).

As discussed earlier, the resulting *b*-values differ between the subsets based on the inferred origin mechanism. As shown in Figure 6, when sorted by ascending *b*-value (manual average) the subsets are ordered shear component (0.87/0.92), complex (0.92/0.97), and tensile (0.97/1.09) for M_c =-1.0 and -0.8 respectively. The corresponding *b*-values from Vantage calculated using the same M_c are for the shear events (0.89/0.93), complex events (0.93/1.01), and tensile events (0.97/1.12) respectively. These results are in line with the expected outcome given the findings of Hudyma (2008a) that sets of shear-slip events will produce lower *b*-values than sets of tensile/volumetric origin. The order of the subsets represented in Figure 6 is reasonable as the complex events with *Es/Ep* ratios between 3 and 10 are assumed to contain both shear-slip and tensile components, thus this subset should, with adequate sampling, result in a *b*-value lying between the shear and tensile sets. This would indicate that the M_c < -0.8 for this case leads to an undersampling of the catalogue as no additional information becomes evident at the higher cut-off, and that M_c = -1.0 is the best estimate for the minimum magnitude cut-off and represents the magnitude completeness. At M_c = -1.0 the subsets are represented by 4465 (shear), 2536 (complex), and 781 (tensile) events.

Location error

Location error is a semi-fictitious number based on the difference between measured and theoretical arrival times (based on the velocity model used) for an event multiplied by a scaling number that is unique for each geophone. A combination of the values from the geophones that registered the event is then used to estimate an error for the estimated event location (defining the size of the sphere in which the event is likely to be located). As such, the location error is not a true and absolute measurement in metres but rather indicates the relative size of the volume of the 'event location sphere'. In this study the location error is automatically calculated and given as an output by the mine's seismic system.

The layout of the seismic recording system at the Kiirunavaara mine results in low azimuthal coverage of events located above level 700 m and beneath level 1200 m. In Figure 7 the individual events with M > -1.0 are plotted with respect to the calculated location error and depth. Error locations larger than 50 m were removed from the plot for visualization purposes (12 events). To further illustrate the

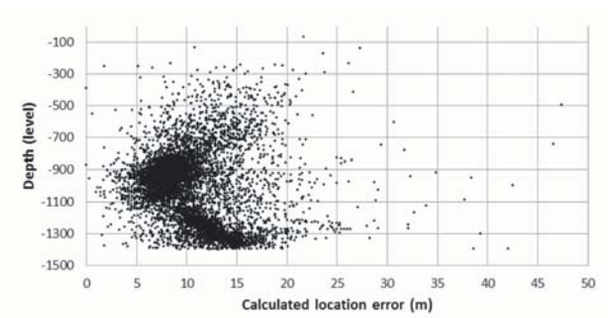

Figure 7—Distribution of location error *versus* mine level for events M > -1.0

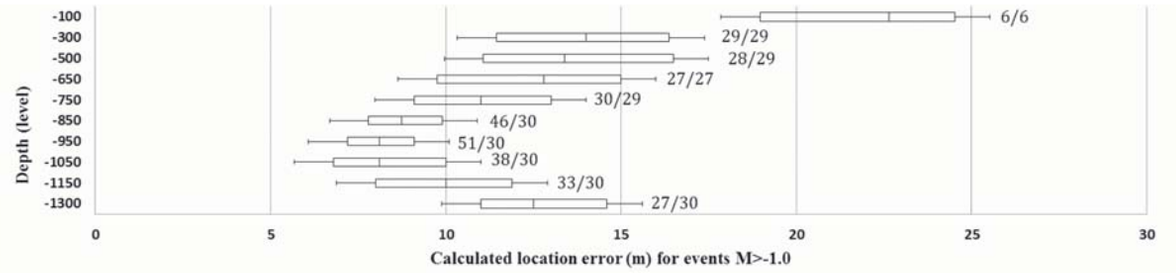

Figure 8—Box-whisker plot of calculated location error *versus* mine level for events M > -1.0., numbers indicate the average number per median number of triggered sensors for an event at the given depth

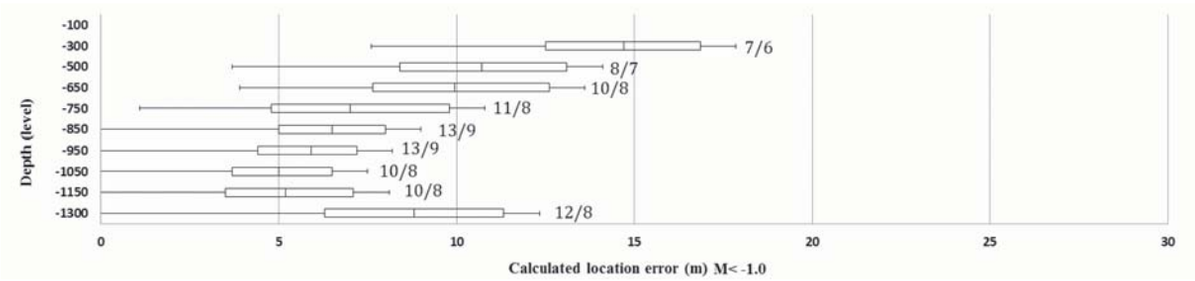

Figure 9—Box-whisker plot of calculated location error *versus* mine level for events M < -1.0. Numbers indicate the average number per median number of triggered sensors for an event at the given depth

depth-location error relationship the events are sorted with respect to the mine level and shown in Figure 8 as box-plot distributions (based on standard deviations). The box plots are based on first and third quartiles, median values, and on error standard deviations. Very few events are located within a calculated location error larger than 15 m, which is lower than the 20 m indicated as the mine accuracy threshold (Stöckel, Mäkitaavola, and Sjöberg, 2013). About 50% of the events have a calculated location error of less than 10 m. As evident in Figure 8, the most well-located data is found around level 950 m, which corresponds to the relative centre of the mine seismic system. Beneath the system the relative location error again increases to magnitudes similar to those above the system as fewer wave paths are intersected. The few events recorded in the footwall above level 300 m (floor of the decommissioned open pit) are poorly located.

A comparison of the calculated location error for events above and below the estimated cut-off magnitude, M_c = -1.0, shows the need to accurately determine the minimum magnitude cut-off. The event subset below the cut-off magnitude, as indicated in Figure 9, is reported as better located than the event subset with M > M_c (compare with Figure 8). As the recording of low-magnitude events is more sensitive to distance attenuation it is not surprising that the M < M_c events are more concentrated at the system installation levels (700–1200 m), as short travel distance is a prerequisite for the wave energy to be recorded. This is also apparent when comparing Figure 8 and Figure 9 with respect to the average number of triggered sensors for each event with respect to depth. Even though the low-magnitude events are more abundant, each event is (on average) picked up by fewer sensors. The representation of the low-magnitude events in space therefore becomes skewed to potentially form artificial clusters close to the sensor positions. As shown in Figure 8 and Figure 9, an event of M > -1.0 at level 950 m is on average picked up by 51 (median 30) sensors, while an event at the same level with M < -1.0 is picked up by only 13 (median 9) sensors. For both subsets the number of triggered sensors is likely to rise with an increase in magnitude, and events close to M = -1.0 will have similar statistics for both subsets. The location accuracy calculated from residuals can thus not be used to decide which event locations to use for analysis in place of the magnitude completeness.

Analysis of seismic parameters

As previously indicated, the events where the *Es/Ep* ratio suggests a shear-slip origin vastly outnumber the events where the *Es/Ep* ratio suggests a pure tensile origin. Taking into account the number of total events with M > -1.0, the predominant failure mechanism in the studied area could be argued to be shear failure as events, with indicated shear-slip origin corresponding to 57% (4465 out of 7782), complex origin 33% (2536 out of 7782), and tensile origin 10% (781 out of 7782) of the recorded events. It should be noted that the relative distribution might be influenced by the sensitivity of the seismic system, as shear origin events in general tend to be of larger magnitudes than tensile origin events. However, performing this simple origin analysis, based on the *Es/Ep* ratio only, on the full set of events without application of the lower minimum magnitude cut-off at -1.0 local magnitude did not affect the relative distribution between the sets by more than a few units of percentage. Without the minimum magnitude cut-off, events with indicated shear-slip origin correspond to 60% (17574 out of 29084), complex origin 31% (8997 out of 29084), and tensile origin 9% (2513 out of 29084) of the entire catalogue.

The calculated values for the seismic Gutenberg-Richter parameters (*b* and *a*) are presented for the estimated cut-off magnitudes in Table I. As can be noted, the *b*-value changes when a larger minimum magnitude cut-off is applied for the

Table I

Seismic and statistical data for calculating *b*

Suggested origin mechanism	Maximal local magnitude in set	Cut-off magnitude (M_c)	Number of included events / total events	Events M>M_c truncated when calculating *b**	*b/a* (averaged over two bins)
Full catalogue	1.7	-1.0	7782 / 29084	902	0.87 / 3.02
Full catalogue	1.7	-0.8	5399 / 29084	682	0.97 / 2.96
Shear-slip	1.5	-1.0	4465 / 17574	577	0.87 / 2.78
Shear-slip	1.5	-0.8	3071 / 17574	445	0.92 / 2.75
Complex (shear-slip + tensile)	1.3	-1.0	2536 / 8997	350	0.92 / 2.49
Complex (shear-slip + tensile)	1.3	-0.8	1768 / 8997	199	0.97 / 2.48
Tensile	1.6	-1.0	781 / 2513	93	0.97 / 1.93
Tensile	1.6	-0.8	560 / 2513	68	1.09 / 1.88

**Percentage of truncated events differs between sets as truncation was performed on complete bins of width 0.1 local magnitude; no interpolation was made to find 'partial bins'*

Table II

Variations in *b*-value over time as calculated in Vantage for M_c = -1.0

Year (full years)	*b* (open-ended magnitude)	*a* (open-ended magnitude)	Events included /total	#(events with M>Mc) shear/complex/tensile	% (events with M>Mc) shear/complex/tensile
2009	0.871	2.377	1759 / 5942	1015 / 555 / 189	58 / 32 /10
2010	0.934	2.314	1758 / 4839	1108 / 496/ 154	63 / 28 /9
2011	0.910	2.230	1375 / 4012	863 / 412 / 100	63 / 30 / 7
2012	0.904	2.145	1111 / 3886	650 / 355 / 106	59 / 32 /10
2013	0.961	2.075	1081 / 6678	478 / 434 / 169	44 / 40 /16

sets. This behaviour was explicitly shown also in Figure 6. The *b*-values calculated for M_c = -1.0 fit reasonably well to both large- and medium-to small-magnitude events but overestimate the occurrence of the largest events. The reason is that the 'linear' of the log cumulative graph of the studied catalogue is in fact not linear as assumed by the power law, which is most evident for the well-populated sets. This could be caused by either the *b*-value changing in time or by the analysed catalogue containing two or more 'seismic areas' with different parameters.

In Table II, the *b*- and corresponding *a*-values were calculated for the full catalogue with M_c = -1.0. With the applied M_c the *b*-value remains stable over the years 2010–2012 (note: only data for full years was studied). The seismic activity, indicated by *a*, however, decreases steadily from 2009 to 2013. The same trend can also be seen in the (total) number of events registered for each year as the numbers reduce from 2009 (with the most events) to 2012 (with the fewest events) followed by an apparent increase in events again in 2013. Note that it is the total number of events recorded that is on the rise, not the number of registered events with M > M_c. It is also indicated that the ratio of event origin type (given by the *Es/Ep* ratio) remains similar for 2009–2012, while the ratio between indicated shear and complex event origins significantly changed during 2013. It is likely that this is the result of the geophone installation campaign conducted during 2012 and 2013, with the new system fully operational in late 2013.

To investigate the influence of the 'extreme' years on the *b*-value the years 2009 and 2013 (refer to Table II) were filtered from the catalogue and the *b*-value was re-calculated. As shown in Figure 10, this action has no discernible effect on the calculated *b*-value with respect to M_c. The manually calculated *b*-value averaged over two bins stabilizes around M = -0.2 to 0, aligning with the Vantage calculation at -1.7 < M > -0.2 (deviation between returned values for the two calculation procedures is overall insignificant). The Vantage calculation again shows a stabilizing trend after M = -0.2. This is an indication that the convex decline of the cumulative log plot in the Gutenberg-Richter graph is not caused by variations of *b*-value in time, and that even though the seismic activity in the area studied is seemingly reducing, the magnitude distribution remains stable.

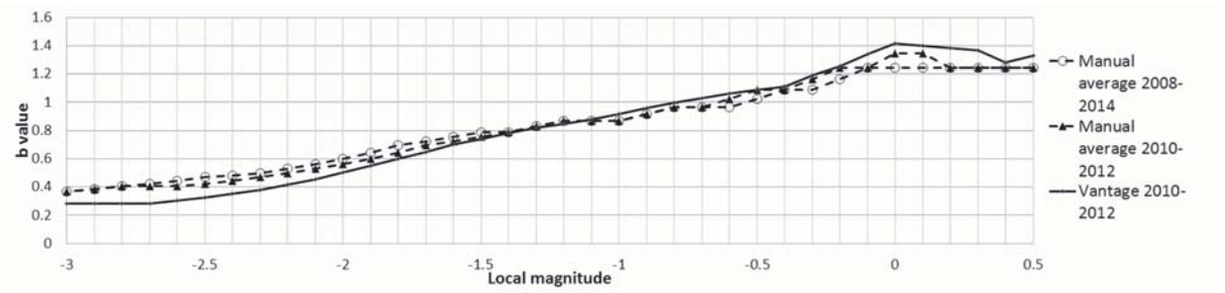

Figure 10—Comparison of *b*-value for catalogues 2008–2014 and 2010–2012 with respect to M_c

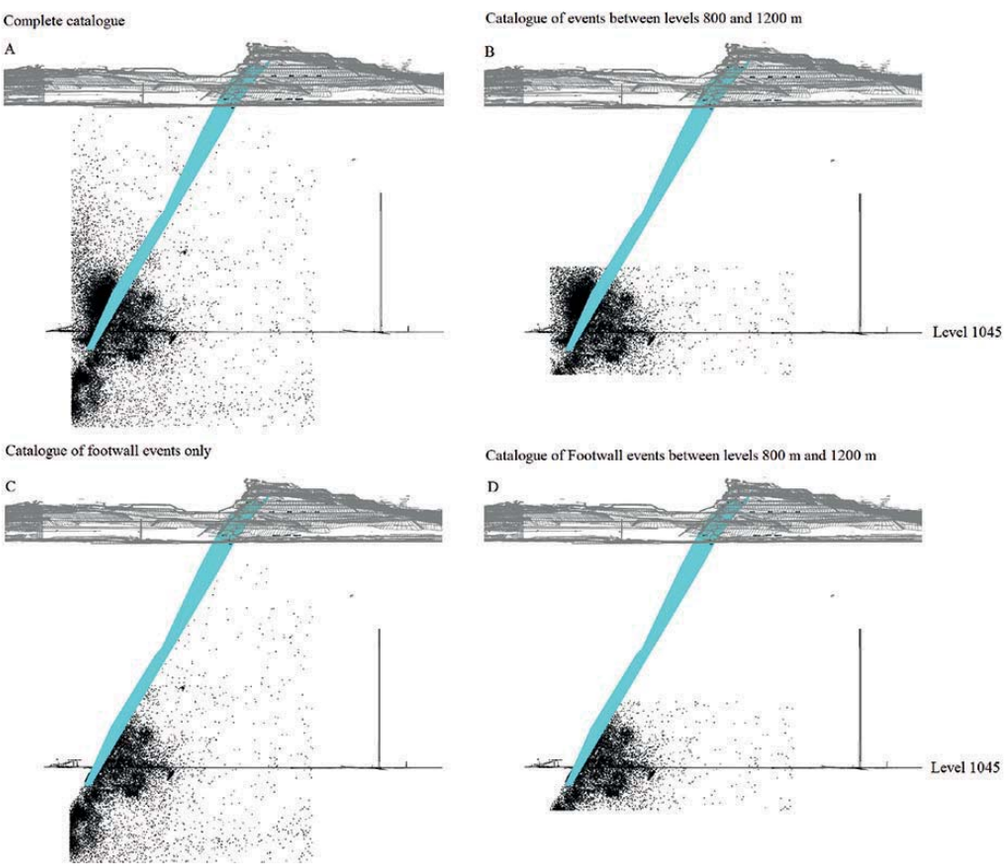

Figure 11—Spatial filtering of event catalogue for evaluation of changes in *b*-value. Orebody incline (footwall contact) between Y23 and Y25 is indicated by teal surface

In an attempt to identify any spatial variations in the *b*-value, the event catalogue without any magnitude restriction (Figure 11A) was filtered to include only specific regions in the studied volume. The regions studied were the depth intervals with small calculated location errors (Figure 11B, inside the seismic system boundaries), level 800–1200 m (see Figure 8), and events located in the footwall (Figure 11C, defined using the general orebody dip). Both spatial limits contain a majority of the catalogue but the data that is likely to have different properties has been omitted. In Figure 11B the events located outside the system, *i.e.,* the far field data, has been removed, while in Figure 11C the events originating in the caving hangingwall and flowing cave rock were excluded. In all cases (Figures 11A–D) the sharp line on the left indicates the boundary of the studied catalogue. As evident in Figure 12, on the *b*-value stability there is an apparent pivot point at M = -1.0, around which the filtered data seems to rotate compared to the unfiltered catalogue. For both spatial filters the difference with respect to the unfiltered catalogue at M < -1.0 is notable as both sets return nearly identical *b*-values which are both slightly higher than for the full catalogue. At M > -1.0 the 'footwall' filter (Figure 11C) does not seem to have any effect as the returned *b* is virtually identical to that of the full catalogue. However there is a noticeable effect from the depth filter (Figure 11B) as the corresponding *b* -alue does not increase as fast as for the full catalogue and for the 'footwall' filter. In fact, the increase in *b* value for the depth filter groups is negligible between M = -1.0 and -0.3. Combining both filters, *i.e.* evaluating only events located in the footwall and between levels 800 and 1200 m (Figure 11D) returns a *b*-value that is arguable stable between M = -1.7 and -0.4, whereafter it becomes

Determination of magnitude completeness from convex Gutenberg-Richter graphs

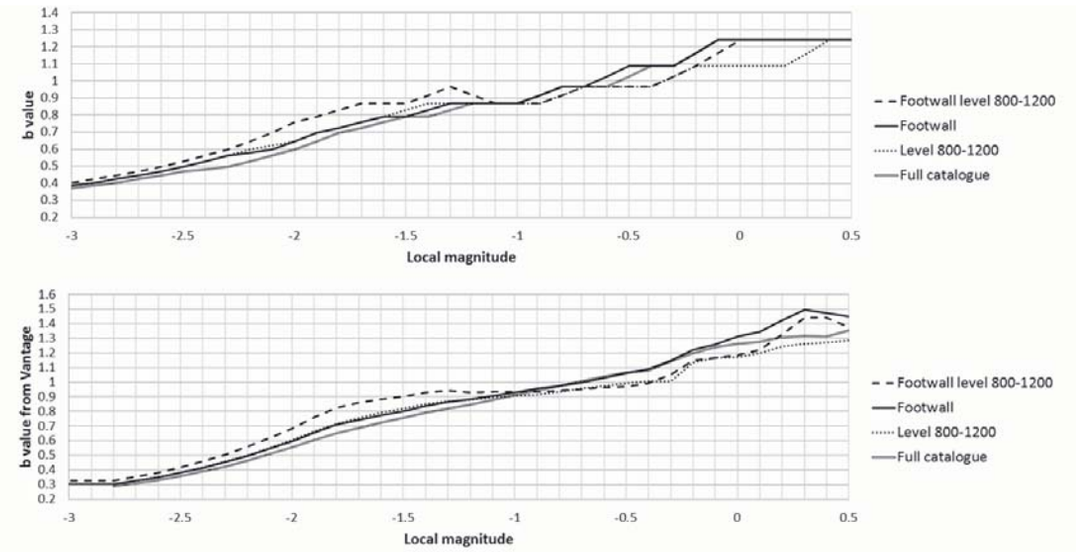

Figure 12—Calculated *b*-value *vs.* M_c with respect to spatial filtering of the event catalogue

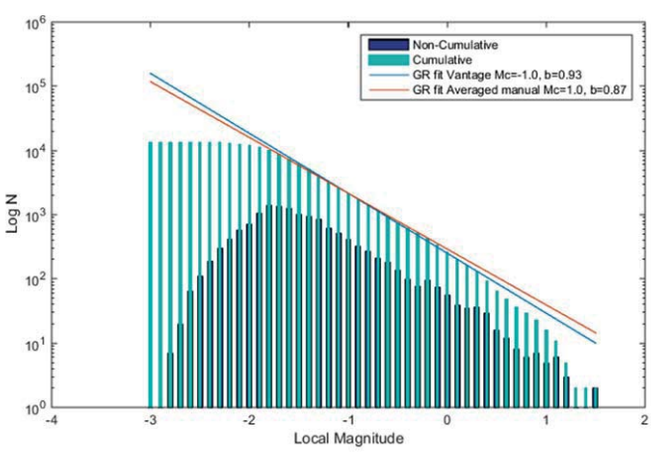

Figure 13—Gutenberg-Richter plot with fitted power law for events located in the footwall between levels 800 and 1200 m

unstable again, likely due to undersampling. The fitted power-law and the events from the combined filters are shown in Figure 13; the deviation from linearity due to undersampling shows as a 'drop' at M = 0.5.

The convex shape of the cumulative Gutenberg-Richter graph for the full event catalogue is concluded to be system-induced. By eliminating the events located outside the seismic array the convexity of the graph is eliminated and the remaining set fits the log-linear power law. The spatial filtering allowed for 13 608 out of 29 084 events to be analysed as one set with stable seismic parameters. The indicated M_c for the spatially filtered set is -1.7, while for the full set the *b*-value stability indicates M_c = -1.0. The significant difference is unsurprising given the apparent sensitivity of the calculated *b*-value with respect to the system spatial proximity. The *b*-values calculated for the spatially filtered set, 0.87–0.93, are in fair agreement with the *b*-values calculated for the full catalogue when considering also the event origin, *i.e.* M_c = -1.0, 0.87–0.91. The origin distribution within the double set is similar to the full catalogue with shear-slip, complex, and tensile events making up 68%, 26%, and 6% of the events with M > -1.0 respectively. Evaluating the *b*-value for each set at M_c = -1.0 returns (from Vantage) 0.94, 0.92, and 0.88 for shear, complex, and tensile events. As for the full catalogue, this is argued to be unreasonable due to the different origins.

As shown in Figure 14, the calculated *b*-values (for the double-filtered set with respect to the different event origins) do not start to differentiate significantly until M_c = -0.8, just as for the full catalogue (see Figure 5). Calculating for M_c = -0.8 again returns *b* = 0.92–0.94 for the full set, while the components from the different origins are sorted as; 0.87–0.92 (manual–Vantage), 0.97–0.99, and 1.00–1.02 for shear, complex, and tensile events respectively, with tensile events returning a higher value than shear-slip events as expected. The change in M_c from -1.0 to -0.8 has no significant effect on the origin distribution. The distribution of the origin mechanisms for the double-filtered set shows the same trend as the full catalogue (based on *Es/Ep* ratio), both showing a predominance of shear-slip component events.

The calculated value for the full catalogue based on the *b*-value stability alone was in this study subjective as the

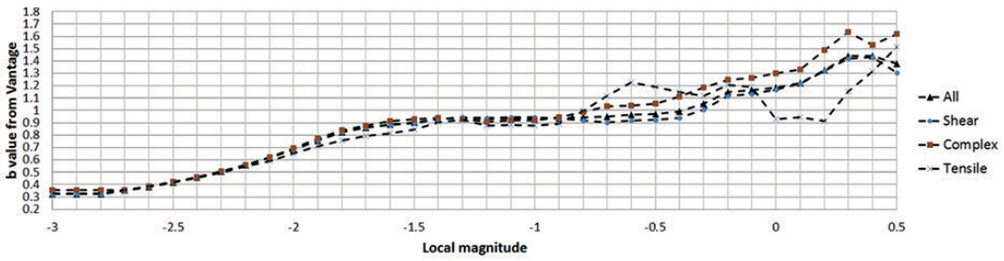

Figure 14—*b*-values with respect to M_c calculated in Vantage for origin-separated events

Gutenberg-Richter graph was convex. The convexity is shown to be system-dependent as different *b*-values are returned for the events located inside the confines of the seismic system than for the events located outside. The events located inside the systems fit well to the log-linear assumption of the Gutenberg-Richter power law as the graph shows negligible convexity. The *b*-value is common for all sets at a minimum magnitude cut-off of -1.0, which also results in fitted log-linear parameters that adequately represent the events located inside the system for events with M > -2.0. Identifying the magnitude at which the individual origin sets (shear, complex, and tensile events) can be separated by studying the individual *b*-values also suggests the magnitude completeness at M = -1.0. At M < -1.0 the different origin sets cannot be positively distinguished from each other, regardless of whether the studied volume contains the full catalogue or only the inside system events are studied. At M > -1.0 the events are sorted in ascending order of tensile, complex, and shear events by the returned *b*-value, as expected from literature experience. Moving the cut-off further to M_c = -0.8 does not reveal any additional seismic information but indicates the same trends as shown already at M_c = -1.0 for both the full catalogue and the subsets. The use of *b*-value differentiation based on origin mechanisms to identify the magnitude completeness thus seems to eliminate some of the system location dependency indicated for the *b*-value stability approach.

Analysis of event locations

The event catalogue was filtered with respect to a cut-off magnitude of -1.0 local magnitude. Events of lower magnitude were not incorporated as the non-differential *b*-values for M < -1.0 indicate that the events with lower magnitudes are not accurately represented in the studied catalogue. The event locations are analysed with respect to the footwall damage hypothesis proposed by Svartsjaern *et al.* (2015).

In Figure 15 the tensile event locations are coloured with respect to the main active production level at the time the event was recorded. Also shown in the figure is the simplified geometry of the mine at profile Y23, finalized production levels, and the conceptual boundary of the mappable damage to the infrastructure by Svartsjaern *et al.* (2015). The event locations show a significant scatter with little or no clustering above level 1200 m. Most of the events occur far below the production area and thus remote from the boundary of the systematically mappable damage. The far field scatter indicates general large-scale stress redistribution from the mining but no significant direct reaction to the excavation of each respective level. It is not possible to trace the outlines of the damage extent boundary from the tensile event locations. This result is in line with the proposed damage hypothesis, where mappable failure above the production level is proposed to be caused primarily by activation of previously formed zones of weakness, not by fresh fracture propagation.

Plotting only the shear events shows clear clustering; firstly near the active production level and secondly close to the footwall contact at level 1200–1400 m (Figure 16). There is no correlation between the shear event locations and the postulated shearing structure groups in the upper footwall, *i.e.,* above level 740 m. A likely reason would be that the structures are slipping continuously without any significant strain accumulation. Any energy released from continuous shearing along the natural structures in this area is then attenuated before being registered by the seismic system. The assumption of continuous slip is supported by a handful of vibrating wire joint shear gauges installed over individual joints in the upper footwall. The gauges indicate continuous subvertical shear of individual joints in the order of a few millimetres to fractions of a millimetre per year. Principal readings are shown in Figure 17.

The upper 'shear cluster' surrounds the production area shown in the footwall as a 'half cylinder' with the long axis parallel to the orebody strike. The cluster centre position moves downwards with the mining and shows increased scatter with increasing distance from the footwall contact. The stress difference within the cluster volume is relatively high as it coincides with the footwall 'slope toe'. Large differential stresses are indicated at one to two sublevels below the main mining level, together with a de-stressing zone above the mining level (Figure 18). Several events are located outside the high stress difference zone, but apart from the second clustering at levels 1200–1400 these events show large scatter. The stress difference plots, which were produced from the UDEC (Itasca, 2011) model designed by Svartsjaern *et al.* (2015), give a simplified but robust picture of the stress redistribution during mining.

The clustering of shear events near the production level, together with the deviatory stress plots, indicates a region of active fracturing at the footwall 'slope toe'. This supports the failure theory where mappable damage in the upper part of the footwall is postulated to be a symptom of a confinement-dependent response to rock mass damage formed earlier close to the production level. The event origin based on *Es/Ep* ratios suggests that the rock mass response to the stress redistribution is shear-dominated, since events with only shear-slip component follow the same pattern as events containing both shear-slip and tensile components (see Figure 19), while events with pure tensile components show significant scatter with no apparent clustering (Figure 15).

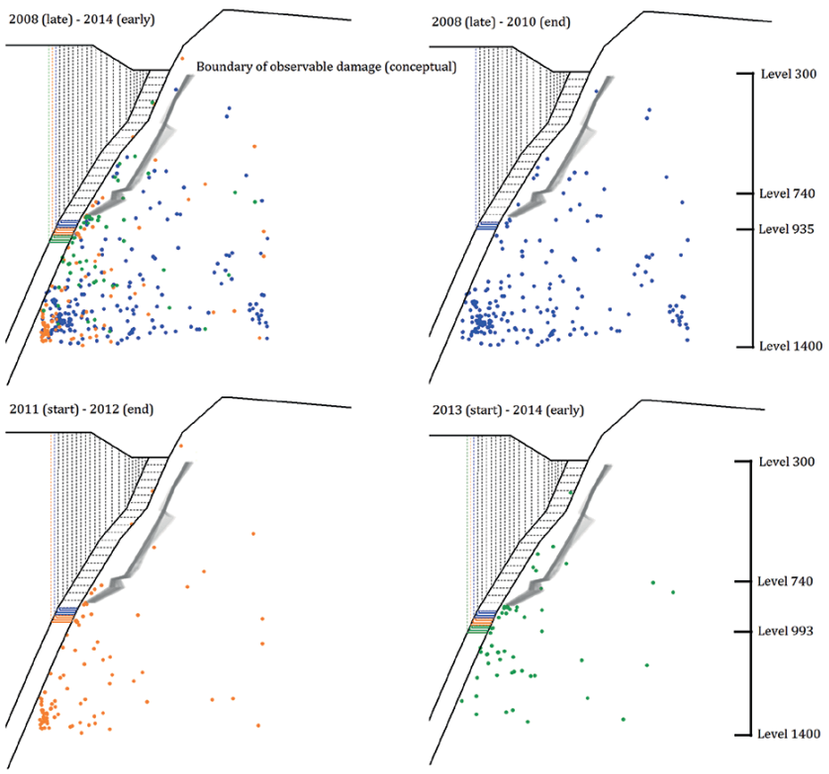

Figure 15—Tensile events (*Es*/*Ep* < 3) with M > -1.0 arranged with respect to main active production level based on date of record. Active production level is indicated by the (lowest) infilled field in the SLC zone, associated events are coloured in same palette

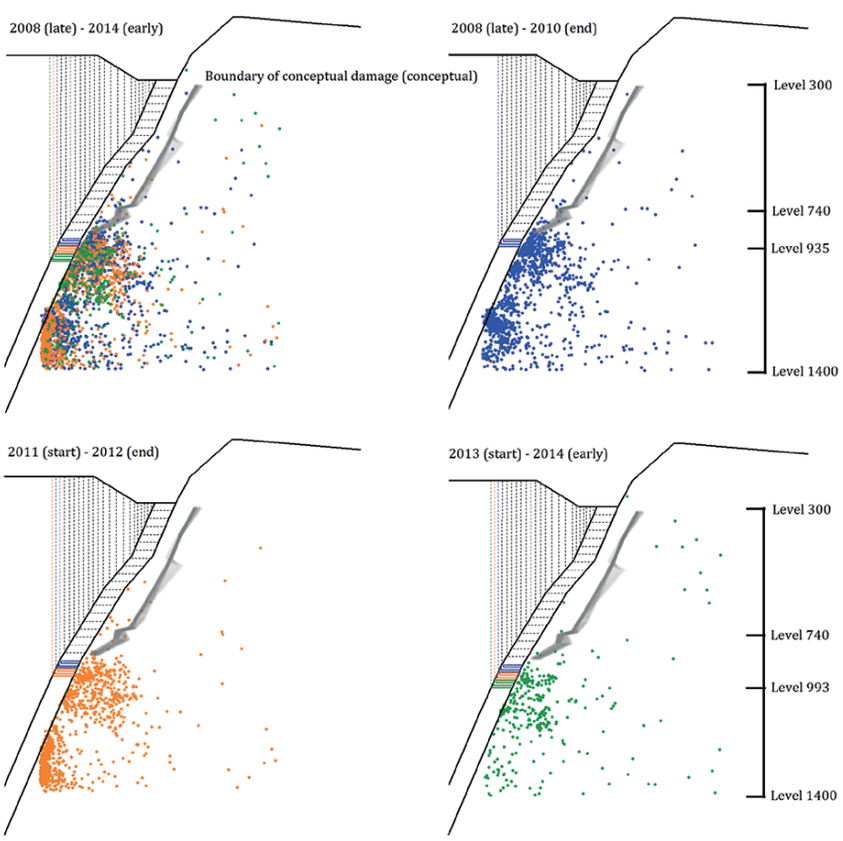

Figure 16—Shear events (*Es*/*Ep* > 10) with M > -1.0 arranged with respect to main active production level based on date of record. Active production level is indicated by the (lowest) infilled field in the SLC zone, associated events are coloured in same palette

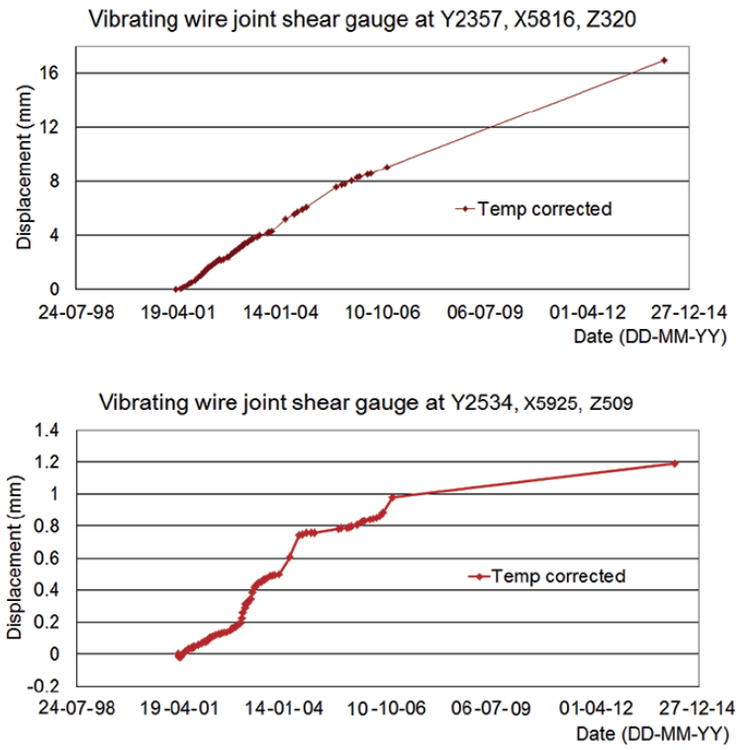

Figure 17—Principal vibrating wire joint shear gauge results from levels 320 and 509 m

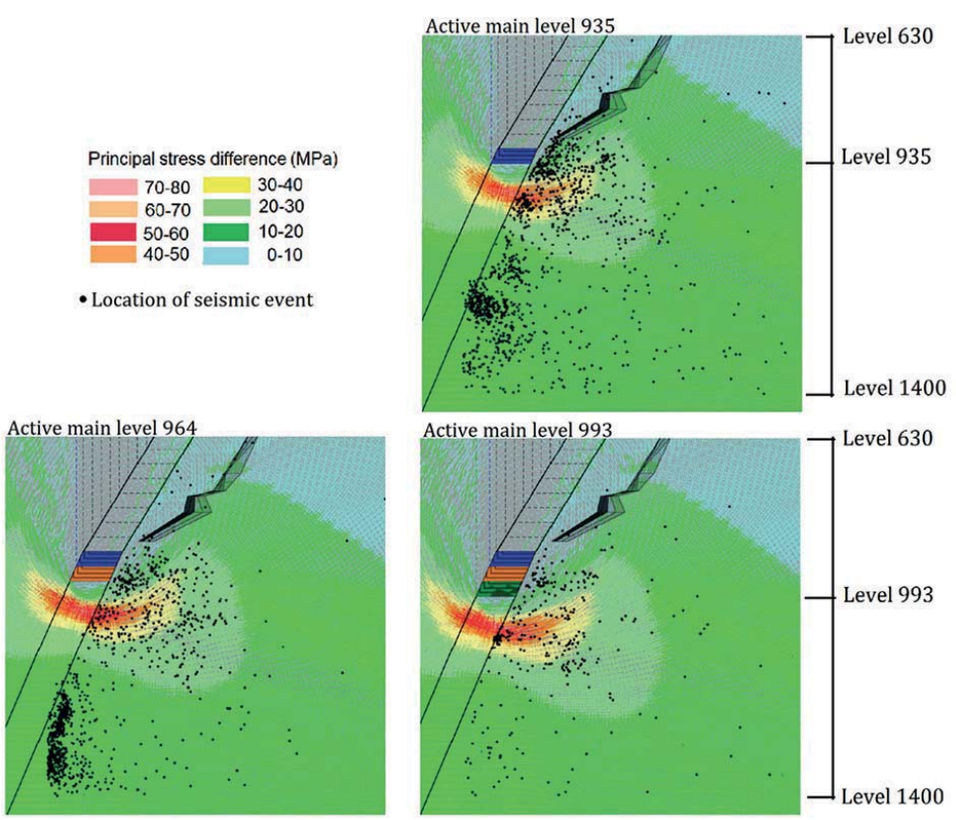

Figure 18—Shear events *(Es/Ep* > 10) with M > -1.0 arranged with respect to main active production level based on date of record. Active production level is indicated by the (lowest) infilled field in the SLC zone on background indicating principal stress difference

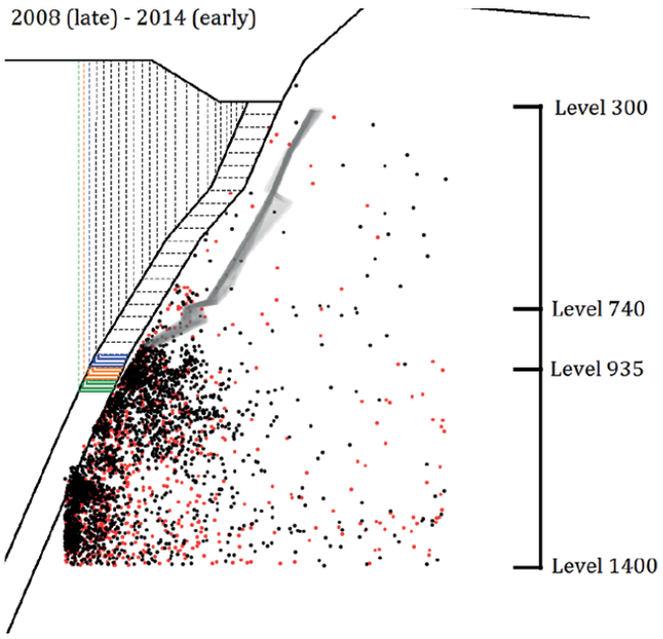

Figure 19—Shear (*Es/Ep* >10) and complex (*Es/Ep* 3-10) events with M > -1.0; shear events are black, complex events are red

The numerical model does not explain the origin of the lower cluster. The apparent 'disappearance' of the cluster for the mining step 964→993 is caused by the imposed spatial limit on the studied seismic catalogue as the cluster simply 'migrates' out of the studied volume. The origin and migration path of this cluster warrants further study, but possible explanations include footwall-ore contact interactions, development work connected to level 1365 (new haulage level commissioned in part during 2013), or possible activation of seismically significant structures.

Discussion

The analysed seismic event locations do not form explicit bridging patterns that could be directly linked to observed damage. Even so, the concentrations of seismic event locations close to the mining level could be considered in the context of seismic softening of the rock mass as described for the Creighton mine by Snelling, Godin, and McKinnon (2013). Seismic softening was earlier indicated for the Kiirunavaara mine by Henry *et al.* (2001) and a general reduction in rock mass integrity below the excavation level was anticipated by Svartsjaern (2015). The earlier damaged rock mass (Svartsjaern, 2015) is postulated to mobilize as the mining front passes the studied level due to loss of horizontal confinement resulting from replacing relatively stiff ore with low-stiffness cave rock from the hangingwall.

Stress analyses show that clustering of seismic events could indicate areas of high differential stresses. The formation of the deep-seated seismic cluster cannot be explained by the continuum numerical model utilized. It is, however, considered likely, based on the spatial location, that the cluster is related to some type of footwall-orebody interaction. Characteristic seismic sources related to formation of event clusters are described by Hudyma (2008b), including the activation of faults or similar brittle structures. Sandström (2003) describes the footwall-ore contact as containing a higher concentration of skarns and breccia and showing a lower RMR than the footwall in general. There is a potential for this contact zone to show a similar seismic response as a brittle fault with concentrated event localization. Some indications in this direction can be found in Henry *et al.* (2001), where the interpreted far field seismicity is proposed to originate from slip parallel to the orebody. Conclusive evidence of the influence of a footwall-ore contact fault-like zone is, however, currently not available. The fact that the indicated location of the deep-seated cluster (beneath level 1200 m) is well below the boundary of the seismic system, which reduces the location accuracy and entails a possible bias in event localization, should also be taken into account. Further analysis of the lower cluster, such as possible correlations with development drifting below the excavation level, was beyond the scope of this paper. This limitation was imposed for two major reasons; (i) the cluster was indicated at the spatial boundary of the data and it could not be tracked in full, and (ii) the cluster was indicated in a volume of low azimuthal coverage.

The tensile origin events recorded in the studied area indicate the occurrence of brittle failure in the form of fracture propagation through intact rock. The tensile events constituted only a minor portion of the event cloud and were scattered throughout a relatively large area. The location scatter indicates that brittle failure is not well confined to certain regions but is a sign of general stress changes in the footwall rock mass. Tendencies could be discerned for some clustering of tensile events at the intersection between the conceptual damage extent boundary proposed by Svartsjaern

(2015) and the SLC area, but the low number of events makes the correlation uncertain. Instead, the direction of the major virgin principal stress (perpendicular to the orebody) entails significant stress-redistribution in the footwall from the mining advance (Sandström, 2003). Thus, brittle failures throughout the footwall rock mass with wide scattered tensile event locations would be expected.

The non-tensile origin events were analysed with respect to numerically calculated displacements. The results indicate that clustering of seismic events in a volume changes from heavily confined (high differential stress) to de-stressing, which suggests inhomogeneous movement and dilatation. The relationship between mobilized wall regions and concentrations of seismicity was indicated for the Palabora open pit by Moss, Diachenko, and Townsend (2006). Rock mass movements resulting in the observed damage in the upper parts of the footwall could not be clearly traced by the analysed seismic data. The baseline for tracking rock mass failure using seismic recordings is that fracture growth and slip is accompanied by distinct micro-seismicity which can be picked up by the seismic arrays. Intrinsic to this approach is that slip along a plane is discontinuous over time. Elastic strain energy accumulates over a slip surface until the surface yields and shears, accompanied by the release of energy in form of micro-seismicity. However, if the slip is constant and continuous over time then very small amounts of elastic strain energy will accumulate. The energy released from small elastic strain buildups will also be inherently small and likely to fall below the recording threshold of the seismic arrays. The few available measurements of individual shearing structures on levels 320 and 509 m indicate continuous shear displacements in the order of a few millimetres to fractions of a millimetre per year. In addition, owing to the relatively large distance from the seismic system, near the production level, to the upper part of the footwall, the low-magnitude micro-seismicity that would be generated by the described process will attenuate before reaching the system.

The separation of event origins in terms of shear, shear-component, and tensile events based only on *Es/Ep* ratio does impose some limitations compared to a more in-depth analysis of origin parameters. The indicated thresholds used to differentiate between event origins should be considered as conceptual and some overlap between the groups with respect to the true origin is likely.

Conclusions

Seismic data was extracted for the central portion of the mine and analysed with respect to event origin determined using *Es/Ep* ratios and *b*-values from Gutenberg-Richter graphs. The analyses indicate that the majority of the events originate from shear-slip-type failures. The predominance of shear-slip events below the main excavation level agrees with the arguments presented by Svartsjaern (2015) that a confinement-dependent large-scale damage extent boundary is actively developing between level 740 m and the current main excavation level. However, it should be noted that the purpose of this study was not to predict where seismic events are likely to occur. Rather, the purpose was to use the recorded seismicity to track regions of active fracturing and failure in the footwall rock mass by clustering of seismic events. Hence, seismic records have been analysed in relation to the spatial and temporal patterns as well as to numerically calculated stresses. The following are the major findings of this study.

- By separating the seismic catalogue based on the event origins into shear, complex, and tensile events a representative *b*-value indicating the magnitude completeness can be identified for a convex Gutenberg-Richter graph by finding the minimum magnitude cut-off at which the *b*-values differ between the sets
- Clustering of shear events near the production level together with the differential stress plots indicates a region of active fracturing at the footwall 'slope toe'
- A predominance of seismic events with *Es/Ep* ratios above 10 observed below level 700 m indicate that the main failure mode of the rock mass below this level is shear-dominated. The second largest group of events contains both shear-slip and volumetric failure components (complex set)
- Continuous sliding along the discontinuities in the upper part of the footwall, where mappable damage has been documented, has so far not resulted in micro-seismicity with magnitudes large enough to be recorded by the seismic system
- The analyses have not revealed a direct correlation between seismic location data and observed damage resulting from large-scale deformations. It is, however, postulated that the seismic events lead to a softening of the rock mass, which in turn allows increased rock mass deformation on the upper levels in response to decreasing confinement.

Acknowledgements

The authors acknowledge the funding and data access granted for this study by LKAB. Thanks are also due to Centre of Mining and Metallurgy (CAMM) at Luleå University of Technology (LTU). The on-site contributions during data collection by the LKAB staff, in particular Karola Mäkitaavola and Mirjana Boskovic, are greatly appreciated. Finally, the authors wish to thank Adjunct Professor Jonny Sjöberg (Itasca Consultants AB), Professor Savka Dineva (LTU), as well as Associate Professor David Saiang (LTU) for valuable comments related to this paper.

References

Abdul-Wahed, M.K., Al Heib, M.A., and Senfaute, G. (2006. Mining-induced seismicity: Seismic measurement using multiplet approach and numerical modeling. *International Journal of Coal Geology*, vol. 66. pp. 137–147.

Agliardi, F., Crosta, G.B., Meloni, F., Valle, C., and Rivolta, C. 2013. Structurally-controlled instability, damage and slope failure in a porphyry rock mass. *Tectonophysics,* vol. 605. pp. 34–47.

Cai, M., Kaiser, P.K., and Martin, C.D. 2001. Quantification of rock mass damage in underground excavations from microseismic event monitoring. *International Journal of Rock Mechanics and Mining Sciences*, vol. 38. pp. 1135–1145.

Cesca, S., Sen, T.A., and Dahm, T. 2014. Seismicity monitoring by cluster analysis of moment tensors. *Geophysical Journal International*, vol. 196. pp. 1813–1826.

Gutenberg, B. and Richter, C.F. 1949. Seismicity of the Earth. Princeton University Press, Princeton, NJ.

Henry, E. and Dahner-Lindqvist, C. 2000. Footwall stability at the LKAB's Kiruna sublevel caving operation, Sweden. *Proceedings of Massmin 2000*, Brisbane, Queensland, Australia. Australasian Institute of Mining and Metallurgy, Melbourne. pp. 527–532.

Henry, E., Plouffe, M., Côté, M., and Sandström, D. 2001. Rock mass response to mining induced over-stresses in a sublevel caving operation case study at the Kiruna mine, Sweden. *Proceedings of MineSpace 2001*, Quebec City, Canada. CIM, Montreal.

Hudyma, M. 2008a. Appendix A: Mine seismology concepts. *Generic Seismic Risk Management Plan for Underground Hardrock Mines*. Australian Centre for Geomechanics, Nedlands, WA.

Hudyma, M. 2008b. Analysis and Interpretation of clusters of seismic events in mines. Doctoral thesis, University of Western Australia.

Hudyma, M., and Potvin, Y.H. 2010. An engineering approach to seismic risk management in hardrock mines. *Rock Mechanics and Rock Engineering,* vol. 43. pp. 891–906.

IMS. 2014. Vantage. Institute of Mine Seismology.

Liang, Z., Xu, N., Ma, K., Tang, S., and Tang, C. 2013. Microseismic monitoring and numerical simulation of rock slope failure. *International Journal of Distributed Sensor Networks*, vol. 2013, no. 5. http://journals.sagepub.com/doi/pdf/10.1155/2013/845191

Lupo, J.F. 1996. Evaluation of deformations resulting from mass mining of an inclined orebody. Doctoral thesis, Colorado School of Mines.

Lynch, R.A., and Malovichko, D.A. 2006. Seismology and slope stability in open pit mines. *Proceedings of the International Symposium on Stability of Rock Slopes in Open Pit Mining and Civil Engineering*. South African Institute of Mining and Metallurgy, Johannesburg. pp. 375–390.

Ma, K., Tang, C-A., Xu, N-W., Liu, F., and Xu, J-W. 2013. Failure precursor of surrounding rock mass around cross tunnel in high-steep rock slope. *Journal of Central South University*, vol. 20. pp. 207–217.

McKinnon, S.D. 2006. Triggering of seismicity remote from active mining excavations. *Rock Mechanics and Rock Engineering*, vol. 39, no. 3. pp. 255–279.

Mendecki, A.J., Lynch, A.R., and Malovichko, D.A. 2010. Routine micro-seismic monitoring in mines. *Proceedings of the Australian Earthquake Engineering Society 2010 Conference*, Perth, Western Australia. pp. 33.

Moss, A., Diachenko, S., and Townsend, P. 2006. Interaction between the block cave and the pit slopes at Palabora mine. *Journal of the South African Institute of Mining and Metallurgy*, vol. 106. pp. 479–484.

Naylor, M., Orfanogiannaki, K., and Harte, D. 2010. Exploratory data analysis: magnitude, space and time. Community Online Resource for Statistical Seismicity Analysis. doi: 10.5078/corssa-92330203

Orlecka-Sikora, B., Lasocki, S., Lizurek, G., and Rudzinski, Ł. 2012. Response of seismic activity in mines to the stress changes due to mining induced strong seismic events. I*nternational Journal of Rock Mechanics and Mining Sciences*., vol. 53. pp. 151–158.

Ortlepp, W.D. 2000. Observation of mining-induced faults in an intact rock mass at depth. *International Journal of Rock Mechanics and Mining Sciences*, vol. 37. pp. 423–436.

Richardson, E., and Jordan, T. H. 2002. Seismicity in deep gold mines of South Africa: implications for tectonic earthquakes. *Bulletin of the Seismological Society of America*, vol. 92, no. 5. pp. 1766–1782.

Sandström, D. 2003. Analysis of the virgin state of stress at the Kiirunavaara mine. Licentiate thesis, Luleå University of Technology.

Shen, B., Stephansson, O., Einstein, H.H., and Ghahrema, B. 1995. Coalescence of fractures under shear stresses in experiments. *Journal of Geophysical Research*, vol. 100. pp. 5975–5990.

Singh, U.K., Stephansson, O.J., and Herdocia, A. 1993. Simulation of progressive failure in hangingwall and footwall for mining with sub-level caving. *Transactions of the Institution of Mining and Metallurgy*, vol A102. pp. A188–A194.

Sjöberg, J. 1999. Analysis of large scale rock slopes. Doctoral thesis, Luleå University of Technology.

Snelling, P.E., Godin, L., and McKinnon, S.D. 2013. The role of geologic structure and stress in triggering remote seismicity in Creighton mine, Sudbury, Canada. *International Journal of Rock Mechanics and Mining Sciences*, vol 58, February 2013. pp. 166–179.

Stöckel, B-M., Mäkitaavola, K., and Sjöberg, J. 2013. Hangingwall and footwall slope stability issues in sublevel caving. *Proceedings of Slope Stability 2013*, Brisbane, Australia. Australian Centre for Geomechanics, Perth, WA. pp. 1045–1060.

Svartsjaern, M. 2015. Predominant failure mechanisms at the kiirunavaara mine footwall. Licentiate thesis, Luleå University of Technology.

Svartsjaern, M., Eitzenberger, A., Saiang, D., and Nordlund, E. 2015. Conceptual numerical modeling of large scale footwall behavior at the Kiirunavaara mine, and implications for deformation monitoring. *Rock Mechanics and Rock Engineering*. DOI: 10.1007/s00603-015-0750-x

Villegas, T., and Nordlund, E. 2008. Numerical simulation of the hangingwall subsidence using PFC2D. *Massmin 2008: Proceedings of the 5th International Conference and Exhibition on Mass Mining*. Luleå University of Technology. pp. 907–916.

Villegas, T., and Nordlund, E. 2013. Numerical analyses of the hangingwall failure due to sublevel caving: study case. *International Journal of Mining and Mineral Engineering*, vol. 4, no. 3. pp. 201–223.

Xu, N.W., Dai, F., Liang, Z.Z., Zhou, Z., Sha, C., and Tang, C.A. 2014. The dynamic evaluation of rock slope stability considering the effects of microseismic damage. *Rock Mechanics and Rock Engineering*, vol. 47. pp. 621–642.

Young, R.P., Collins, D.S., Reyes-Montes, J.M., and Baker, C. 2004. Quantification and interpretation of seismicity. *International Journal of Rock Mechanics and Mining Sciences*, vol. 41. pp. 1317–1327. ◆

http://dx.doi.org/10.17159/2411-9717/2017/v117n6a6

Comparison of the effect of particle size on the flotation kinetics of a low-rank coal using air bubbles and oily bubbles

by Y. Liao*, Y. Cao*, C. Liu†, Y. Zhao†, and G. Zhu†

Synopsis

The effect of particle size on the flotation kinetics of a low-rank coal was compared using air bubbles and oily bubbles. Five kinetic models were applied to the data from the tests to derive the relationships between the flotation rate constant, the ultimate recovery, and the particle size fraction. The results show that oily bubble flotation (OBF) resulted in a lower ash content and higher combustible recovery than air bubble flotation (ABF), especially for the -125 μm size fraction. It was found that the flotation of a low-rank coal in individual size fractions using air bubbles and oily bubbles can be best described by a first-order model with rectangular distribution of tendency to float and the classical first-order model respectively. OBF yielded higher ultimate combustible and ultimate ash recoveries. The flotation rate constants for OBF were higher in all the models except for the fully mixed reactor model. The ultimate recovery values and modified rate constants first increased and then decreased as the size fraction decreased. The trend of the flotation rate constants as a function of the size fraction was similar in all the models except for the fully mixed reactor model.

Keywords
particle size, flotation kinetics, low-rank coal, oily bubble, air bubble.

Introduction

Froth flotation is a physical-chemical separation method that is widely used in coal beneficiation for the separation of fine coal particles from associated minerals in water slurries. Since the cumulative recovery of a component in the concentrate is proportional to flotation time, the flotation process can be considered as a time-rate recovery process (Emad, Mohammad, and Bahram, 2010). Therefore, the general mathematical flotation models that incorporate both a recovery and a rate function can describe flotation time-recovery profiles.

The kinetics of coal flotation, as a measure of coal recovery as a function of time, have been studied in detail by many researchers. Different kinetic models have been proposed and published in the literature. The order and the rate constant are strongly dependent on the flotation conditions, such as the particle size and size distribution, the bubble concentration, the reagent concentrations, and the operating parameters (Zhang *et al.*, 2013). The particle size has been reported to affect the flotation kinetics to a great extent (Yoon, Luttrell, and Asmatulu, 2002; Ntengwe and Witika, 2011). Numerous researchers have studied the aspects of flotation kinetics while paying special attention to particle size (Meftuni and Ibrahim, 1997; Rubinstein and Samygin, 1998; Graeme, 2012). However, the effect of particle size on the flotation kinetics of a low-rank coal has been relatively little discussed.

It is difficult to achieve a high yield or combustible matter recovery by flotation of fine low-rank coal, due to the poor hydrophobicity. The presence of polar hydroxyl, carbonyl, and phenol groups and some peroxide-type oxygenated moieties on the surface of low-rank coal decreases the coal hydrophobicity (Xia, Yang, and Liang, 2013). Researchers have investigated many ways to improve the floatability of low-rank coal by using pretreatment prior to flotation and surfactant additions during flotation. Recently, Xia and Yang (2013) designed an oily bubble flotation process using oily bubbles instead of the conventional air bubbles to increase the flotation recovery of low-rank/oxidized coal. The oily bubble flotation (OBF) process yielded a higher combustible matter recovery and lower ash content than the conventional air bubble flotation (ABF) process.

An oily bubble is an air bubble covered with a thin layer of kerosene containing collectors (Liu *et al.*, 2002). The OBF process has been successfully applied in bitumen flotation. A superior performance was noted when using OBF, compared to the use of conventional ABF, when applied to

* *National Engineering Research Center of Coal Preparation and Purification, China University of Mining and Technology, Xuzhou, Jiangsu, PR Chinan.*

† *School of Chemical Engineering and Technology, China University of Mining and Technology, Xuzhou, Jiangsu, PR China.*

 ISSN 2225-6253. Paper received Nov. 2015; revised paper received Feb. 2016.

bastnaesite, apatite, dolomite, and quartz (Zhou *et al.*, 2014, 2015). The mechanisms by which oily bubbles improve flotation performance have been studied by various methods. Su, Xu, and Masliyah (2006) observed that oily bubbles could attain a much higher contact angle and decrease the induction time between bubbles and particles. Zhou *et al.* (2014) found that the attachment between bastnaesite particles and reactive oily bubbles could be predicted well by the DLVO theory (named after Boris Derjaguin, Lev Landau, Evert Verwey, and Theodoor Overbeek) only within a restricted pH range, due to the absence of hydrophilic interaction repulsion and chemical interaction forces. In spite of the apparent importance of these observations, very little work has been done on the kinetics of the OBF process.

In the present paper, the effect of particle size fraction on the flotation kinetics of a low-rank coal is compared using conventional ABF and OBF Five kinetic models were selected to evaluate the effect of particle size fraction on the kinetic parameters. The flotation performance of ABF and OBF was also evaluated on the basis of the selected indices.

Experimental

Materials

The coal sample, a sub-bituminous coal, was obtained from the Daliuta coal preparation plant, Shendong Mine Area of China. The moisture content was 8.71%, and the ash content 16.91% on an air-dry basis. The proximate and ultimate analyses of the sample are given in Table I.

The sample was crushed, ground, and screened into five narrow size fractions: +500, -500+250, -250+125, -125+74, and -74 μm. Each size fraction was weighed and analysed for ash, then stored in plastic bags until required for flotation tests. Table II shows the particle size and ash distribution of the sample. The yield of the coarse particle size (+250 μm) was 10.44% with 16.26% ash. The -250+74 μm size fraction that was suitable for flotation constituted about 55.83% of the sample. The fine (-74 μm) particles accounted for 33.73% of the total. It is important to note that the ash content of the -74 μm size fraction was high, at about 20.26%.

Kerosene was used as the collector and 2-octanol as the frother.

Table I

Proximate and ultimate analyses of the coal sample

Proximate analysis (wt%, ad)				Ultimate analysis (wt%, daf)				
M	V	A	FC	C	H	O	N	S
8.71	27.89	16.91	46.49	78.75	5.6	12.73	1.74	1.18

Ad = air-dry basis; daf = dry ash-free basis; M = moisture content; A = ash content; V = volatile matter; FC = fixed carbon.

Apparatus

An experimental apparatus was designed for the OBF, consisting of a flotation cell, an electrical heating jacket, a four-necked flask, a calibrated flow meter, a thermocouple, and a syringe (Figure 1). Kerosene was injected into the flask via the syringe. The flask was heated in the electrical jacket to a temperature of about 240°C. The thermocouple was used to measure the flask's temperature. When kerosene was injected into the flask, it instantly vapourized due to the high temperature, and the air stream containing the kerosene vapour was sucked into the pipes connected with the flotation cell. The air flow rate was regulated by a control valve, dependent upon the readings of the calibrated flow meter. By this process, the vapourized kerosene was cooled, and huge amounts of kerosene drops were created. When the air stream entered the flotation cell, fine bubbles were generated by the cell rotor device. As the kerosene drops collide with the air bubbles, since both streams are hydrophobic, the air bubbles become coated with kerosene. This mechanism is enhanced by the molecular movement of the kerosene drops, enabling dispersion of the drops and coverage of the bubble surface as the oily bubbles are formed.

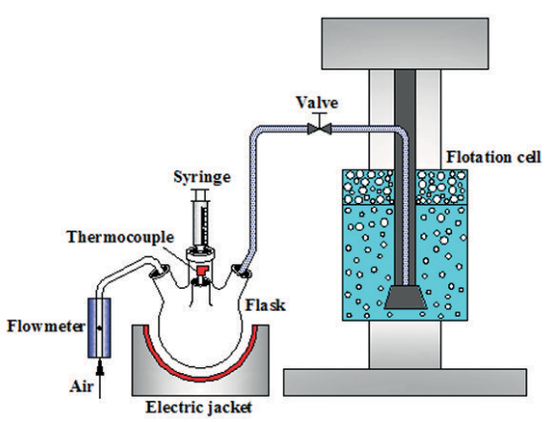

Figure 1—Experimental apparatus for oily bubble flotation test work

Table II

Size and ash distribution of the coal sample

Size fraction, μm	Yield, %	Ash, %	Cumulative oversize, %		Cumulative undersize, %	
			Yield	Ash	Yield	Ash
+500	2.71	18.9	2.71	18.9	100	17.03
-500+250	7.73	15.33	10.44	16.26	97.29	16.97
-250+125	29.12	15.02	39.56	15.35	89.56	17.12
-125+74	26.71	15.43	66.27	15.38	60.44	18.13
-74	33.73	20.26	100.00	17.03	33.73	20.26
Total	100.00	17.03				

Comparison of the effect of particle size on the flotation kinetics

Methods

The flotation tests were conducted on size fractions of +500, -500+250, -250+125, -125+74, and -74 μm using oily bubbles and conventional air bubbles. All the tests were conducted in a 1.5 L XFD flotation cell using 120 g of coal at a pulp density of 7.4% solids, with a kerosene (collector) dosage of 5 kg/t (kilograms reagent per ton coal) and 0.5 kg/t 2-octanol (frother). The impeller speed was 1800 r/min and the air flow rate was set at 2 L/min.

For the conventional flotation tests, the slurry was first agitated in the flotation cell for 3 minutes. The requisite amount of kerosene and 2-octanol was then added and the slurry was conditioned for an additional 3 minutes. Flotation was started by introducing air. Froth samples were collected after 0.5, 1, 2, 3, and 5 minutes of flotation.

A similar procedure was conducted for the OBF tests, except that only 2-octanol was added before introducing air. The flask was preheated to 240°C and a requisite amount of kerosene was held in the syringe. When the valve was opened, the kerosene was injected into the flask. The kerosene instantly vapourized and passed through the tube along with the air to the flotation cell.

The flotation products were filtered, dried, weighed, and analysed for ash. The combustible matter and ash recoveries were calculated from the following equations (Gupta, Banerjee, and Mishra, 2009; Liao *et al.*, 2015):

$$\varepsilon_C(\%) = [W_C(100\text{-}A_C)/W_F(100\text{-}A_F)]\times 100 \quad [1]$$

$$\varepsilon_A(\%) = (W_C A_C/W_F A_F)\times 100 \quad [2]$$

$$SE\,(\%) = \varepsilon_C - \varepsilon_A \quad [3]$$

where ε_C is the combustible recovery, ε_A the ash recovery, SE the separation efficiency, W_C the weight of the concentrate (%), W_F the weight of the feed (%), A_C the ash content of the concentrate (%), and A_F is the ash content of the feed (%).

In this work, five kinetic flotation models (Chaves and Ruiz, 2009; Zhang *et al.*, 2013) were selected to study the effects of particle size on low-rank coal flotation using oily bubbles and conventional air bubbles, as shown in Table III. The combustible and ash recoveries after 0.5, 1, 2, 3, and 5 minutes of flotation time were fitted to the five kinetic models. Origin 8.0 graphing and analysis software was used to simulate the flotation rate constant (k), the ultimate recovery (ε_∞), and the correlation coefficient (R^2) based on the Levenberg-Marquardt (LM) algorithm.

Results and discussion

Effect of particle size on flotation performance

The influence of the particle size on the concentrate ash and combustible content is illustrated in Figure 2. For both ABF and OBF, the coarse size fraction (+250 μm) yielded the lowest ash content and combustible recovery. The combustible recovery from the intermediate size fraction (-250+74 μm) was much higher than that from the coarse and the fine (-74 μm) size fractions. The fine size fraction yielded an intermediate combustible recovery, but the ash content was highest. Moreover, it is obvious that OBF is superior to ABF for all size fractions in terms of lower ash content and higher combustible recovery. For the -125+74 μm size fraction, ABF has potential to give a product with 11.10% ash content and 66.47% combustible recovery after 5 minutes of flotation. With OBF, the product ash content can be reduced further to 9.37% with 93.63% combustible recovery after 5 minutes of flotation. Similar results have been reported for numerous mineral flotation processes (Peng and Li, 1991; Xia and Yang, 2013; Su, Xu, and Masliyah, 2006). This may be attributed to the fact that with oily bubbles the contact angle is increased and the induction time between bubbles and particles decreased.

The effect of particle size on flotation performance in ABF and OBF is further compared in Figure 3, where the cumulative values in the final concentrate after 5 minutes of flotation is taken as the measure. The ash content in concentrate for OBF is lower than that for ABF at different size fractions, particularly for the -74 μm size fraction. At the same time, OBF results in a higher combustible recovery, ash recovery, and separation efficiency for all the size fractions, in particular the -125 μm size fraction. The ash content of the concentrate increases with decreasing particle size in both ABF and OBF, while the combustible recovery, ash recovery, and separation efficiency first increase and then decrease. The difference in ash content for both ABF and OBF becomes more pronounced as the particle size decreases. A similar trend can be seen for ash recovery. It is interesting to note that for both the combustible recovery and ash recovery, the difference between ABF and OBF first increases and then

Table III

Flotation kinetic models

No.	Model	Formula
1	Classical first-order model	$\varepsilon(t) = \varepsilon_\infty[1-\exp(-k_1 t)]$
2	First-order model with rectangular distribution of tendency to float	$(t) = \varepsilon_\infty\left\{1-\frac{1}{k_2 t}[1-\exp(-k_2 t)]\right\}$
3	Fully mixed reactor model	$\varepsilon(t) = \varepsilon_\infty(1-\frac{1}{1+t/k_3})$
4	Second-order kinetic model	$\varepsilon(t) = \frac{\varepsilon_\infty^2 k_4 t}{1+\varepsilon_\infty k_4 t}$
5	Second-order model with rectangular distribution of tendency to float	$\varepsilon(t) = \varepsilon_\infty\left\{1-\frac{1}{k_5 t}[\ln(1+k_5 t)]\right\}$

$\varepsilon(t)$ = fractional recovery at time t, ε_∞ = fractional ultimate recovery, k = flotation rate constant

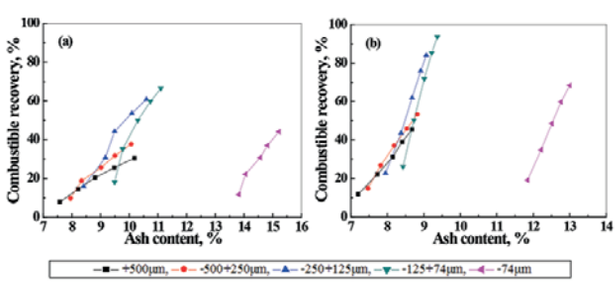

Figure 2—Effect of size fraction on flotation performance: (a) air bubble flotation; (b) oily bubble flotation

Comparison of the effect of particle size on the flotation kinetics

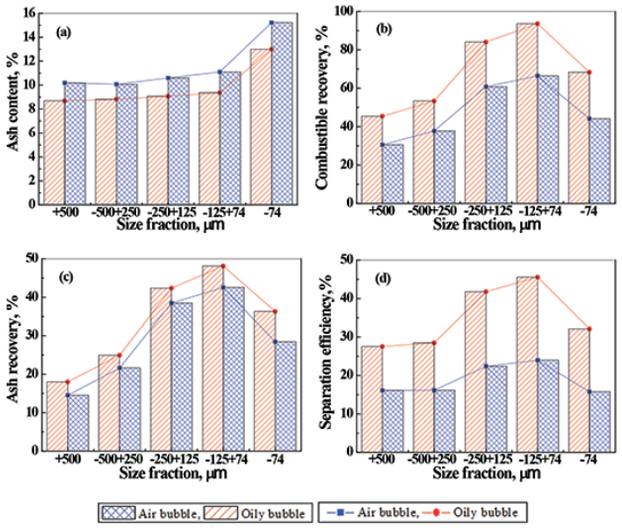

Figure 3—Comparison of flotation performance between air bubble and oily bubble flotation: (a) ash content; (b) combustible recovery; (c) ash recovery; (d) separation efficiency

decreases with decreasing particle size, with the greatest difference in the -125+74 μm size fraction. OBF therefore shows better flotation performance compared to ABF, especially for the -125 μm size fraction.

Effect of particle size on flotation kinetics

The combustible recovery, ash recovery, and separation efficiency for different size fractions as a function of flotation time are shown in Figures 4–6. These figures clearly illustrate that for all the size fractions, combustible recovery, ash recovery, and separation efficiency increase with increasing flotation time, with the rate of increase becoming less with increasing time. It is also observed that for a given flotation time, combustible recovery, ash recovery, and separation efficiency first increase and then decrease with decreasing particle size, with the maximum values being for the -125+74 μm size fraction. Moreover, the combustible recovery, ash recovery, and separation efficiency are higher for OBF than for ABF at the same flotation time for all the size fractions, which indicates that OBF has better kinetics.

The test results related to the combustible and ash recoveries *versus* flotation time at different size fractions for both ABF and OBF were fitted to the five flotation kinetic models using Origin 8.0 analysis software. The fractional ultimate recovery (ε_∞), flotation rate constant (k), and the correlation coefficient (R^2) are given in Tables IV and V.

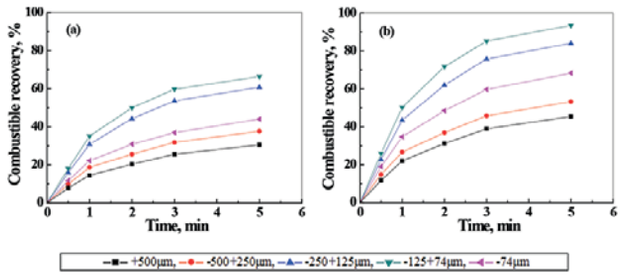

Figure 4—Combustible recovery to concentrate for different size fractions as a function of flotation time: (a) air bubble flotation; (b) oily bubble flotation

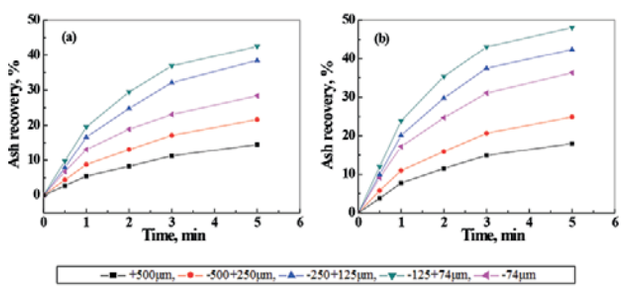

Figure 5—Ash recovery to concentrate in different size fractions as a function of flotation time: (a) air bubble flotation; (b) oily bubble flotation

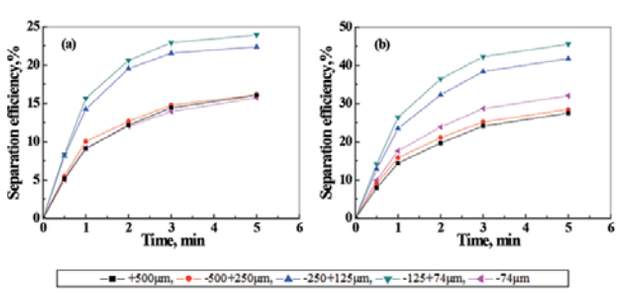

Figure 6—Separation efficiency in different size fractions as a function of flotation time: (a) air bubble flotation; (b) oily bubble flotation

Table IV

Fitted results of air bubbe flotation by different size fractions

Model		+500 μm		-500+250 μm		-250+125 μm		-125+74 μm		-74 μm		Mean of R^2
		E	*k*	*E*	*k*	*E*	*k*	*E*	*k*	*E*	*k*	
Combustible	Model 1	32.31	0.541	39.34	0.576	63.55	0.620	68.92	0.668	45.53	0.601	0.9962
	Model 2	38.10	0.968	46.17	1.040	74.45	1.121	80.34	1.217	53.26	1.093	0.9970
	Model 3	43.71	2.158	52.65	1.986	84.53	1.832	90.55	1.663	60.52	1.878	0.9966
	Model 4	51.42	0.00636	59.55	0.00641	84.57	0.00645	90.72	0.0066	68.37	0.00588	0.9936
	Model 5	52.29	0.782	60.32	0.930	96.57	1.013	100.00	1.166	69.14	0.989	0.9956
Ash	Model 1	17.90	0.328	25.10	0.386	43.10	0.447	46.06	0.524	30.36	0.506	0.9972
	Model 2	21.95	0.547	30.41	0.657	51.82	0.770	54.76	0.919	36.01	0.895	0.9974
	Model 3	26.80	4.249	36.37	3.424	61.17	2.860	63.47	2.323	41.69	2.374	0.9972
	Model 4	31.74	0.00558	41.21	0.00564	61.22	0.0057	63.57	0.0068	47.83	0.0066	0.9958
	Model 5	32.04	0.404	42.97	0.511	71.70	0.619	73.54	0.778	48.24	0.763	0.9968

Table V

Fitted results of oily bubbe flotation by different size fractions

Model		+500 μm		-500+250 μm		-250+125 μm		-125+74 μm		-74 μm		Mean of R^2
		E	*k*	*E*	*k*	*E*	*k*	*E*	*k*	*E*	*k*	
Combustible recovery	Model 1	47.90	0.567	55.30	0.605	87.81	0.643	97.01	0.689	70.83	0.624	0.9971
	Model 2	56.37	1.017	64.65	1.100	100.00	1.191	100.00	1.373	82.73	1.137	0.9898
	Model 3	64.46	2.044	73.31	1.856	100.00	1.284	100.00	1.285	93.61	1.791	0.9720
	Model 4	65.80	0.0071	73.75	0.0072	100.00	0.0079	100.00	0.0104	93.86	0.00591	0.9847
	Model 5	74.00	0.900	83.65	1.003	100.00	1.450	100.00	1.722	100.00	1.195	0.9317
Ash recovery	Model 1	20.12	0.445	27.38	0.468	45.56	0.550	50.90	0.602	38.61	0.544	0.9975
	Model 2	24.18	0.768	32.70	0.816	53.99	0.971	59.89	1.076	45.61	0.968	0.9973
	Model 3	28.51	2.862	38.20	2.646	62.24	2.178	68.35	1.928	52.42	2.167	0.9962
	Model 4	34.28	0.00716	42.34	0.00725	62.38	0.00732	68.50	0.0075	55.60	0.0073	0.9950
	Model 5	35.39	0.555	44.47	0.678	71.85	0.835	78.38	0.955	60.39	0.843	0.9953

As evident from the results in Table IV, in general, the mean correlation coefficients (R^2) for the five kinetic models are greater than 0.9900, which indicates that all the models give an excellent fit to the experimental data for ABF. The highest mean correlation coefficients for combustible and ash recoveries are 0.9970 and 0.9974 respectively, which are both obtained by Model 2. As shown in Table V, the mean correlation coefficients of all kinetic models fitted to combustible recovery by OBF are lower, except for Model 1, with a mean R^2 greater than 0.9900. However, the mean correlation coefficients of the five kinetic models fitted to ash recoveries of OBF are all higher than 0.9950, with Model 1 having the highest value of 0.9975. Therefore, we conclude that the flotation of this low-rank coal in individual size fraction using air bubbles and oily bubbles can be described by the first-order model with rectangular distribution of tendency to float and classical first-order model, respectively.

As evident from Tables IV and V, the ultimate recovery values increase from Model 1 to Model 5. The ultimate recovery values for OBF are higher than those for ABF in a given size fraction for both combustible and ash recovery calculations. At the same time, the flotation rate constants for OBF are higher than those for ABF at a given size fraction for all the models except Model 3. Moreover, the size fraction strongly influences the ultimate recovery value and flotation rate constant. The trend of the ultimate recovery values as functions of the size fraction are similar to the test data, as shown in Figures 4 and 5, respectively. The flotation rate constant also first increases and then decreases as the size fraction decreases in all of the models except Model 3. Similar findings have been reported in investigations of the kinetics of waste coal flotation and reverse flotation of lignite (Sokolovic, Stanojlovic, and Markovic, 2012; Zhang *et al.*, 2013).

Xu (1998) suggested a modified rate constant, K, the product of ε_∞ and k, and proposed a quantity called the selectivity index (SI) to compare results of flotation kinetics experiments. K can be written as:

$$K = \varepsilon_\infty \times k \quad [4]$$

The modified rate constants were used to define a new quantity, *viz.*, the selectivity index (*SI*) or the relative modified rate constant of combustible matter (K_C) over that of ash (K_A). The selectivity index is calculated by the following equation (Natarajan and Nirdosh, 2009):

$$SI = K_C/K_A \quad [5]$$

Modified rate constants and selectivity indices were used to compare the selectivity between ABF and OBF. Table VI presents the calculated values of modified rate constant and selectivity index (*SI*). As seen, the modified rate constants K_C and K_A at first increase and then decrease with decreasing size fraction in both ABF and OBF, with the maximum K_C and K_A obtained in the intermediate size fraction (-125+74 μm). However, the selectivity index decreases as the size fraction decreases in both cases, with the minimum *SI* obtained for the fine size fraction of -74 μm. These results can be used to explain the trend of flotation performance as a function of the size fraction, as previously discussed.

Conclusions

Flotation tests on a low-rank coal were carried out to investigate the differences in performance and kinetics between air bubble flotation (ABF) and oily bubble flotation (OBF). The model fitting was performed using five flotation kinetic models to estimate the relationships between the flotation rate constant, the ultimate recovery, and the particle size fraction. The conclusions drawn from this study are as follows.

(1) OBF is superior to ABF in terms of ash content and combustible recovery, especially for the -125 m size fraction
(2) The first-order model with rectangular distribution of tendency to float provides the best fit to the experimental data for ABF, and the classical first-order model the best fit for OBF. OBF yields higher ultimate recovery values for combustible matter and lower ash recovery values. The flotation rate constants for OBF are higher in all the models except the fully mixed reactor model
(3) Size fraction strongly affects the flotation kinetics of low-rank coal. The ultimate recovery values and modified rate constants first increase and then decrease as the particle size decreases. The trend of the flotation rate constants as functions of the size fraction is similar in all the models except the fully mixed reactor model.

Recommendations

Further research should be conducted on the oily bubble

Comparison of the effect of particle size on the flotation kinetics

Table VI

Calculated values of modified rate constants and selectivity index (SI)

Parameter	Air bubble					Oily bubble				
	+500 µm	-500+250 µm	-250+125 µm	-125+74 µm	-74 µm	+500 µm	-500+250 µm	-250+125 µm	-125+74 µm	-74 µm
K_C	36.8790	48.0250	83.4368	97.8018	58.2047	27.1375	33.4316	56.4967	66.8384	44.1900
K_A	12.0112	19.9811	39.9263	50.3450	32.2301	8.9635	12.8134	25.0503	30.6379	20.9957
SI	3.0704	2.4035	2.0898	1.9426	1.8059	3.0275	2.6091	2.2553	2.1816	2.1047

concept. For a larger scale application of the oily bubble concept, the energy consumption for high-temperature heating has to be taken into account in a comprehensive economic analysis. Collectors with lower boiling points can decrease the energy required for high-temperature heating so as to further reduce the costs associated with oily bubble flotation. These collectors need to be considered in future research to increase the economic advantage of the oily bubble concept. In addition, it is important to find a more economical and efficient way to produce the oily bubbles. The properties of the oily bubbles and the air bubbles, such as zeta potential, induction time, and bubble size, should be further investigated in order to explain the advantages of oily bubble flotation and the flotation mechanism.

Notation

A_C Ash content of the concentrate, %
A_F Ash content of the feed, %
k Flotation rate constant, minute^{-1}
K Modified rate constant, %/minute
K_A Modified rate constant of combustible matter, %/minute
K_C Modified rate constant of ash matter, %/minute
R^2 Correlation coefficient
SE Separation efficiency, %
SI Selectivity index
W_C Weight of concentrate, g
W_F Weight of feed, g
$\varepsilon(t)$ Fractional recovery at time t, %
ε_A Ash recovery, %
ε_C Combustible recovery, %
ε Ultimate recovery, %

Acknowledgements

This research was supported by the Fundamental Research Funds for the Central Universities (Grant no. 2015QNB16).

References

Chaves, A.P. and Ruiz, A.S. 2009. Considerations on the kinetics of froth flotation of ultrafine coal contained in tailings. *International Journal of Coal Preparation and Utilization*, vol. 29. pp. 289–297.

Emad, A., Mohammad, K., and Bahram, R. 2010. A study on the effect of particle size on coal flotation kinetics using fuzzy logic. *Expert Systems with Applications*, vol. 37. pp. 5201–5207.

Graeme, J.J. 2012. The effect of surface liberation and particle size on flotation rate constants. *Minerals Engineering*, vol. 36–38. pp. 132–137.

Gupta, A.K., Banerjee, P.K., and Mishra, A. 2009. Influence of chemical parameters on selectivity and recovery of fine coal through flotation. *International Journal of Mineral Processing*, vol. 92, no. 1. pp. 1–6.

Liao, Y.F., Cao, Y.J., Huang, S.M., He, J., Zhang, X.B., Li, S.L., and Shao, S.G. 2015. Water carrying property of flotation frothers and its effect on fine coal flotation. *International Journal of Coal Preparation and Utilization*, vol. 35, no. 2. pp. 88–98.

Liu, J., Mak, T., Zhou, Z., and Xu, Z. 2002. Fundamental study of reactive oily-bubble flotation. *Minerals Engineering*, vol. 15. pp. 667–676.

Meftuni, Y. and Ibrahim, S. 1997. Effect of the hydrophobic fraction and particle size in the collectorless column flotation kinetics. *Colloids and Surfaces A: Physicochemical and Engineering Aspects,* vol. 121. pp. 9–13.

Natarajan, R. and Nirdosh, I. 2009. Effect of molecular structure on the kinetics of flotation of a Canadian nickel ore by N-arylhydroxamic acids. *International Journal of Mineral Processing*, vol. 93. pp. 284–288.

Ntengwe, F. and Witika, L.K. 2011. Optimization of the operating density and particle size distribution of the cyclone overflow to enhance the recovery of the flotation of copper sulphide and oxide minerals. *Journal of the Southern African Institute of Mining and Metallurgy*, vol. 111, no. 4. pp. 295–300.

Peng, F.F. and Li, H.R. 1991. Oil-coated air bubble flotation to improve coal flotation rate and recovery. *Preprint no. 91-77:1. Society for Mining, Metallurgy, and Exploration, Inc.*, Littleton, CO.

Rubinstein, J.B. and Samygin, V.D. 1998. Effect of particle and bubble size on flotation kinetics. *Recent Advances in Coal Processing*, no. 2. pp. 51–80.

Sokolovic, J.M., Stanojlovic, R.D., and Markovic, Z.S. 2012. The effects of pretreatment on the flotation kinetics of waste coal. *International Journal of Coal Preparation and Utilization*, vol. 32. pp. 130–142.

Su, L., Xu, Z., and Masliyah, J. 2006. Role of oily bubbles in enhancing bitumen flotation. *Minerals Engineering*, vol. 19. pp. 641–650.

Xia, W.C., Yang, J.G., and Liang, C. 2013. A short review of improvement in flotation of low rank/oxidized coals by pretreatments. *Powder Technology*, vol. 237. pp. 1–8.

Xia, W.C. and Yang, J.G. 2013. Experiment design of oily bubble in oxidized coal flotation. *Gospodarka Surowcami Mineralnymi*, vol. 29, no. 4. pp. 129–135.

Xu, M.Q. 1998. Modified flotation rate constant and selectivity index. *Minerals Engineering*, vol. 11, no. 3. pp. 271–278.

Yoon, R.H., Luttrell, G.H., and Asmatulu, R. 2002. Extending the upper particle size limit for coal flotation. *Journal of the South African Institute of Mining and Metallurgy*, vol. 102, no. 7. pp. 411–415.

Zhang, H.J., Liu, J.T., Cao, Y.J., and Wang, Y.T. 2013. Effects of particle size on lignite reverse flotation kinetics in the presence of sodium chloride. *Powder Technology*, vol. 246. pp. 658–663.

Zhou, F., Wang, L.X., Xu, Z.H., Liu, Q.X., and Chi, R.A. 2014. Interaction of reactive oily bubble in flotation of bastnaesite. *Journal of Rare Earths*, vol. 32, no. 8. pp. 772–778.

Zhou, F., Wang, L.X., Xu, Z.H., Liu, Q.X., and Chi, R.A. 2015. Reactive oily bubble technology for flotation of apatite, dolomite and quartz. *International Journal of Mineral Processing*, vol. 134. pp. 74–81. ◆

http://dx.doi.org/10.17159/2411-9717/2017/v117n6a7

The geoscience education pipeline in South Africa: Issues of skills development, equity and gender

by A. Cameron* and G. Drennan*

Synopsis

South African mining operations depend on the skilled professionals produced through the tertiary education sector. In geoscience courses at the University of the Witwatersrand, which lead into the mining sector, there has been a significant increase in student intake over the past 15 years. This increase has been characterized by a radical shift in demography: in classes where white male students once formed the majority, black female students are now in the majority. This demographic shift appears closely linked to policies addressing issues of social justice and transformation in post-apartheid South Africa. We document this change and consider the role played by employment equity legislation (as in the Mining Charter) and corporate social investment strategies in the mining industry, notably through bursaries offered to black female students. We also look at the changing needs of the industry, where the critical need for managerial skills, not just technical knowledge, is highlighted through data from surveys of past students and industry managers. Our findings indicate the need for a curriculum adjustment to meet these changing requirements, as well as more rigorous selection criteria for bursars than simply gender, race, and appropriate matric results.

Keywords
geoscience education, student demographics, skills development, equity, gender, bursaries.

Introduction

The South African economy has historically been linked to mining and the exploitation of mineral resources. South African mining operations are dependent on the professional labour that is produced through the tertiary education sector, with critical thinking, teamwork, and the art of negotiation having been identified as the crucial skills required for this industry (Sideropoulos, 2014).

Over the past three decades the South African system of education has gone through a period of dysfunction that it is struggling to rectify (Maphai, 2014). This has impacted on the levels of academic preparedness of students applying for places in higher education. Concurrently, government and university policies have widened access to higher education in response to the need to address issues of social injustice and transformation related to South Africa's history of apartheid. As a result, the number of students admitted to universities has increased dramatically. In the School of Geosciences at the University of the Witwatersrand (Wits), the increase in student numbers has been accompanied by a significant change in demographics: classrooms which in the past were dominated by white males have given way to classrooms in which black females are often in the majority. This demographic shift is related to legislation such as the Mineral and Petroleum Resources Development Act and the Broad-based Socio-Economic Empowerment Charter, developed to reshape the socio-economic and equity frameworks of the country (Botha and Cronjé, 2015). Requirements aimed at transformation in terms of management, skills development, and employment equity, together with corporate social investment (CSI) requirements, have resulted in bursaries being made available to attract students from designated groups, which in turn has increased the number of black students, and notably black female students, taking courses in geosciences. However, due to the economic downturn, instability in the mining industry has recently resulted in the downsizing of some mines, with international investors pulling out of South Africa. This instability resulted in devastating strikes across all sectors of the mining industry (Stewart, 2013) and in Marikana, an important platinum mining area, the strike culminated in a deadly shoot-out between miners and police. The resulting tensions spilled over into the gold mining sector, resulting in further strike action, shaft closures, and retrenchments. These challenges have implications not only for the mining industry in South Africa, but for the tertiary education providers whose graduates would have been absorbed into the mine-related workforce.

* *The University of the Witwatersrand, Johannesburg, South Africa.*
 ISSN 2225-6253. Paper received May 2016; revised paper received Aug. 2016.

The geoscience education pipeline in South Africa

Background

Mining in South Africa has traditionally been recognized as 'man's work'. However, mining supports a white-collar industry in addition to the blue-collar labour force, and it is the white-collar work that students seeking tertiary qualifications now aspire to. Job opportunities include mining or rock engineering, geology and technical valuation, consulting and management. To maintain the required supply of skilled personnel, large mining companies have recognized the need to support students, firstly by assisting them to meet the entry standards required by universities, and secondly, by providing bursaries for those who make it into the system. A research report commissioned by Anglo Platinum (Besharati, 2014) has revealed, however, that massive investment in education by mining companies (for example R100 million in the period 2010 to 2014 by Anglo Platinum) has had little impact on schooling throughput rates or the quality of learning. Such investment has been undertaken, as explained by Maphai (2014) in the keynote address at the presentation of the report, because '... the country cannot address equality without addressing the economy, and we cannot address the economy without addressing education'.

Although the mining industry is not required by law to involve itself in education, it is required, in the context of addressing equity and social justice in South Africa's post-apartheid democracy, to fulfil quotas related to gender equity. Mines are also required to fulfil corporate social investment (CSI) obligations. One way to address these needs is to supply students with bursaries, and our records in the School of Geosciences at Wits report a steady increase in the number of students enrolling for degrees that are geared to take them into the mining sector. Students are keen to earn qualifications that will lead to perceived sustainable livelihoods and are thus willing recipients of bursaries, even when they have no intention of following a career in the mining industry. This is not a new phenomenon, however. Hillman (1996) referred two decades ago to the poor throughput rates in mining engineering at Wits, which were associated with failure or dropout rates. He indicated that mining bursaries were taken as a stopgap while the recipients settled into the university and explored the availability of bursaries for other degrees, notably in commerce, law, and medicine (Hillman, 1996, p. 80). At that time of writing, however, the demographic patterns were different to what they are today. Classes are now not only dominated by black students, but significantly, black female students are usually in the majority. These changes in South African student demographics are in stark contrast to the American geosciences experience, as reported by Huntoon and Lane (2007), where the lack of students from diverse ethnic and racial backgrounds is lamented.

The Anglo Platinum research report (Besharati, 2014) also alerted us to the skills that the industry seeks in employees. We have become increasingly concerned about the poor performance of black male students in our courses, and the report served to make us reflect on how our programmes were preparing students for the conditions of work they would encounter. We became interested in how access to bursaries might have affected students' choice of university courses and wanted to find out what mining companies other than Anglo Platinum saw as critical skills for the industry. We wanted to be able to establish how our courses met these needs and whether there was a need to redesign the curriculum. We were interested especially in the views of female students regarding what kinds of challenges they anticipated they would encounter in the mining industry.

These concerns led us to investigate changes in demographics and throughput in geoscience courses at Wits. We begin in this paper by reporting on how these have changed between 1992 and 2013. We then look at the role of bursaries and scholarships in relation to these shifts in demographics and examine the consequences of such changes in terms of performance (throughput) and 'fit' for the industry. We further report on what senior managers from different sectors of the industry believe are the most important skills required by graduates. We compare their views with those of current and former students regarding the most important skills needed in the industry and how these skills are/were developed through their courses at Wits. This leads to a discussion about the current geosciences curriculum and how courses could be redesigned to more explicitly develop the skills identified as critical by industry, especially in relation to issues of equity and the increase of females in the geosciences education pipeline. These curriculum concerns are raised at a time when universities are hard-pressed to maintain standards as well as the throughput rates required by the state, and also when higher education policy in South Africa requires the alignment of courses into a national framework for the purposes of articulation (HEQSF, 2015). This alignment does, however, provide the opportunity for curriculum responsiveness in higher education in relation to changing needs.

Research method

Three research questions were used to guide this study:

- How has student diversity changed over the past 15 years, especially with regard to the geosciences?
- How have bursary allocations been affected by social justice issues, particularly in relation to CSI requirements and gender equity?
- What are the skills required by the industry and how are these being met by current geosciences curricula, particularly with regard to female students?

To respond to the first research question, data on student intake from 1992 to 2014 was obtained from the Wits Academic Information on Students Unit (AISU). These data were analysed to establish the changes in admissions with reference to race and gender over the 15-year period. Data on throughput, also linked to race and gender, were also obtained from the School of Geosciences records. A decision was taken for the purpose of this paper to focus on black and white students only, as the numbers of students from other population groups taking courses in geology is very small.

To gather data on our questions related to bursaries and skills, we selected three groups of respondents. The first group was made up of students taking a third-year course in Ore Body Modelling (GEOL 3028). This sample was purposely selected as the course they attend is a compulsory course for mining engineering students, but is taught in the

School of Geosciences by Geology lecturers. It is a course that was developed in collaboration with the School of Mining Engineering in response to industry needs, and was first offered in 2002. The second group of respondents was made up of students who had graduated from Wits, and had worked, or were currently working, in the mining industry. The third group comprised senior managers in the industry who had employed graduates from the Wits School of Geosciences. Representatives from the gold, coal, platinum, and diamond sectors, as well as independent consultants, were included in this group. The second and third groups were convenience samples (Patton): since contact had been maintained with these people, they were accessible for the purposes of this research.

Three sets of questionnaires were created to survey the different sample groups (see Appendix). These questionnaires were submitted for non-medical ethics clearance to the Wits Ethics Committee, together with the required information regarding the process that would be used to collect the data, *i.e.* that respondents would be informed of the purpose of the survey; that their participation would be voluntary; and that their responses would be anonymous. Having been granted ethics clearance (Protocol H14/08/01), the questionnaires were distributed by e-mail to former students and senior managers, and through a paper-based survey to students enrolled in the Ore Body Modelling course in 2014 at a pre-arranged time after a lecture. The return rate on this survey was 91%, with 115 students out of a class of 126 completing the survey. Five former students and nine industry employers responded to the questionnaires e-mailed to them, with four of the nine managers electing to respond in narrative form rather than by answering each of the questions individually.

Results

Student diversity and throughput

Diversity: changes in student demographics 1992 – 2014

Between 1992 and 2014, black students dominated the intake into first-year Geology (GEOL 1000), the start of the Geosciences pipeline. There were significant swings in the intake of black male students from 1992, but overall the trend for this group was one of increase, with black male students usually making up more than half the class. Figure 1 shows that from representing more than half the class in the 1990s, the number of black male students increased in the early 2000s to over 60%, and then declined.

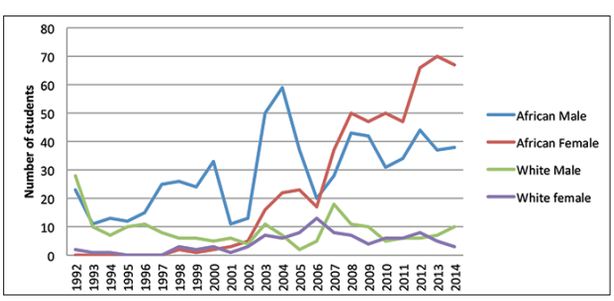

Figure 1—Changes in student demographics (race and gender) in GEOL 1000 (first-year Geology), 1992–2014

The most striking demographic change, however, was in the number of black females enrolling in Geology. The first black female students were enrolled in 1998, and ten years later they were the dominant group in the class. By 2013, black females represented nearly 60% of the class. The number of white students remained relatively low, but there was also a slight increase in the number of white females registering for first-year Geology. The number of Coloured and Indian students enrolling for these courses was very low, so data on these groups have been omitted.

Throughput rates

Two sets of data were accessed to provide a view of throughput rates affecting the Geosciences education pipeline in relation to gender and race.

The first set of data (Figure 2) focuses on throughput rates for Geology 1 (GEOL 1000). This data shows the relative success and failure rates with regard to race and gender at the start of the Geosciences tertiary education pipeline. Failure is most pronounced in the case of black males; 44% of these students failed over the years considered in this study. In contrast, the failure rate for white males was 12.5%. The average failure rate for black females was 37%, while that for white females was 8%.

The second set of data obtained in order to highlight specifically throughput rates for a course leading to careers in the mining industry, came from the Ore Body Modelling course (GEOL 3028) (see Figure 3).

Black male students were consistently the dominant group taking the Ore Body Modelling course over the period 2002 to 2013. From 2006, however, there was an increase in the number of black females, with this group being more successful academically than their male counterparts. As is evident from Figure 3, few white students take this course.

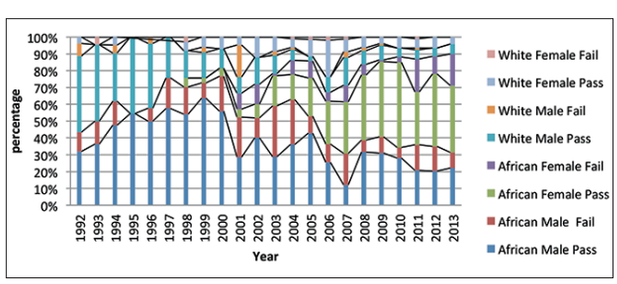

Figure 2—Throughput rates for first-year Geology (GEOL 1000) by race and gender, 1992–2013

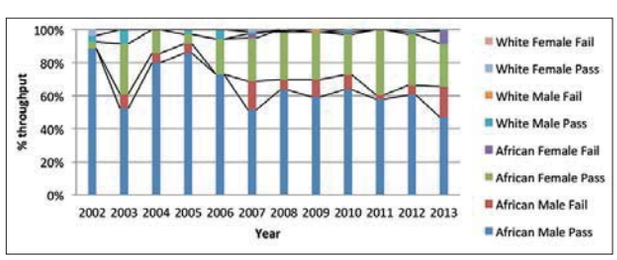

Figure 3—Throughput rates for 'Ore Body Modelling' (GEOL 3028) by race and gender, 2002–2013

Table I

Gender distribution of bursaries allocated to students taking the Ore Body Modelling course

Bursary obtained	Yes	No
Female	23	12
Male	50	30
Total	73	42

Bursary allocations and factors influencing career choice

Bursaries

The students taking the Ore Body Modelling course were asked to indicate whether they were the recipient of a bursary, and if so, which company or organization was the sponsor. Of the 115 who responded, 73 (63%) were bursars (see Table I).

Bursaries had been obtained from a wide variety of sponsors, including the gold, coal, copper, and platinum sectors, Eskom and Sasol, and even foreign companies such as Platinum Australia. The greatest number of bursaries (in terms of both male and female students) was secured from the Mining Qualifications Authority (MQA).

Students were asked in the survey to explain the process that led to their being granted a bursary. The most notable feature from the responses, particularly as far as the female students were concerned, was that there was no procedure other than simply submitting an application. Of the remaining students, some had been invited for an interview and one or two noted that they were required to take medical and psychometric tests. This indicates that in most cases, neither the mining companies offering bursaries nor the MQA had any idea of the suitability of the recipient.

Proximity to a mine as a factor influencing career choice

One of the significant observations in the Anglo Platinum report (Besharati, 2014) was that proximity to a mine had an influence on students choosing to study for a career in this sector. We were interested in whether this applied to our students. Responses to the questions regarding this are shown in Tables IIa and IIb.

Thirty-one of the 115 students in the sample confirmed they grew up close to a mine, while 49 indicated they had not. Fifteen of the male students indicated that growing up close to a mine had significantly affected their choice of career, while eight said this had no influence on their choice. Of the eight female students who grew up close to a mine, six indicated that proximity to the mine had influenced their choice to go into mining. The one female student who did not live near a mine, and did not have a bursary, explained that 'most of the mining companies prefer students from the mining community', indicating her belief that not living close to a mine had put her at a disadvantage in obtaining a bursary. However, the two female students who claimed that growing up near a mine had made no difference to their choice of a career, had nevertheless applied for and had obtained bursaries relating to mining. Although our sample is small, it shows agreement with the findings of the Besharati (2014) report, that growing up near a mine serves to heighten awareness of mining as a possible career option.

Skills: requirements and development

The three most important skills required for success in the workplace that were identified at the presentation of the Anglo Platinum report were critical thinking, teamwork, and the 'art of negotiation' (Sideropoulos, 2014). Students in the Ore Body Modelling course, as well as the former students, were asked to indicate how well they were prepared in the development of these skills during their undergraduate years. Results are shown in Table III.

Most students (both current and former) reported that they had been at least reasonably prepared for teamwork and critical thinking, as the majority ranked these skills above 5 (midway on the scale). In contrast, there was a wide range of ranking for development of the 'art of negotiation'.

The specific courses identified by the Ore Body Modelling students as best serving their development of the three skills were as follows:

- Critical thinking skills: A first-year course (MIN1001) entitled 'Critical Thinking'
- Teamwork: A second-year course, Mine Ventilation and Transportation (MINN 2004), and a third-year course, Surveying (MINN 2002) were identified by many of the students as contributing to the development of this skill. Both courses have joint projects and practical work which require students to work in groups

Table IIa

Influence of proximity to a mine on career choice of students taking the Ore Body Modelling course. The first number in each category refers to the number of students without a bursary, while the number in brackets refers to the number of students with a bursary. The numbers in bold indicate the total for each category

Home location		Close to mine		Not close to mine	
Gender		Male	Female	Male	Female
Influence on career choice	Yes	6 +(9)=**15**	1+(5)=**6**	1+(3)=**4**	1=(0)=**1**
	No	2+(6)=**8**	0+(2)=**2**	11+(19)=**30**	5+(9)=**14**

Table IIb

Influence of proximity to a mine on career choice of students taking the Ore Body Modelling course, where responses were not given in full. The first number in each category refers to the number of students without a bursary, while the number in brackets refers to the number of students with a bursary. The numbers in bold indicate the total for each category

Did not grow up close to a mine but response to influence on career choice was not given	Male	7+(10)=**17**
	Female	6+(3)=**9**
No response to location given, but student indicates that location where they grew up had no influence on career choice	Male	3+(3)=**6**
	Female	0+(3)=**3**

Table III

Student opinions on skills development offered in undergraduate geology courses. Values in the table represent the number of students scoring each skill at that level

Skill	Scale	1 (no preparation)	2	3	4	5	6	7	8	9	10 (excellent preparation)	No response
Critical thinking	Female	0	1	1	1	5	4	8	9	3	3	0
	Male	1	1	0	3	6	10	13	20	12	13	1
	Former students	0	0	0	1	0	1	0	0	2	1	0
Teamwork	Female	0	0	0	2	3	3	9	9	7	2	0
	Male	1	2	0	2	7	11	0	13	12	13	1
	Former students	0	0	0	0	0	1	3	1	0	0	0
Art of negotiation	Female	3	2	2	4	6	2	5	6	3	2	0
	Male	7	1	1	5	12	11	15	10	6	8	4
	Former students	1	0	1	1	0	1	0	0	1	0	0

Current students: females n = 35; males n = 80.
Former students (all female) n = 5.

- Art of negotiation: No particular single course was identified that had been of assistance in developing this skill, and several students indicated that it had not been developed at all. Many students did not offer input in relation to this skill, which may indicate that they did not fully understand what was meant.

The former students had not undertaken the same courses as the current students, as there had been ongoing changes in the structure of the degree over the period covered by the study. Thus students in the Ore Body Modelling course felt that the Mine Ventilation and Transportation and Surveying courses had contributed significantly to their teamwork skills, whereas the former students, who had not done these courses, referred to the importance of fieldwork in developing both teamwork ability and critical thinking. Senior industry managers extended the skills mentioned by Sideropoulos (2014) to include other skills, such as interpersonal, communication, and technical skills, and emotional intelligence.

Discussion

Student diversity and throughput

Over the period 1992 to 2015, the overall demographic profile of the university shifted profoundly with regard to race and gender. The number of female students gaining admission increased from 1999 and now outnumbers males: from being in the minority, black students have become the dominant race group, comprising 75% of the student body in 2015 (Kupe, 2015). The Science Faculty intake has reflected similar trends. With regard to students entering the Geosciences pipeline, admission to training for the mining industry was initially dominated by male students, with more or less equal numbers of black and white males being accepted into first-year Geology between 1992 and 1996. From 1997 the pattern changed, with the number of black male students increasing and the number of white males decreasing. As with the overall trends, the most significant shift in diversity in the Geosciences has been in relation to black female students: from 2003, their numbers steadily increased and by 2007 black females were the dominant demographic group taking the introductory Geology course. Over the years, there has been little change in terms of the few Coloured and Indian students registering for courses in the Geosciences, as mining has not been a preferred career choice for either males or females in these groups.

The demographic shifts outlined above are associated with changes in South Africa's political landscape, as education and industry have responded to the need for transformation, particularly with regard to race and gender. New policies and legislation introduced to bring about this transformation include the Mining Charter, which addresses the need to include women in mining and to distribute wealth across a broad a spectrum of previously disadvantaged South Africans. In recognition of the new opportunities that were opening up in South Africa's post-apartheid landscape, a number of women have been appointed to serve at Ministerial level in the field of Minerals and Energy: Phumzile Mlambo-Ngcuka was the first female appointed to this position in 1999, followed successively by Lindiwe Hendricks, Buyelwa Sonjica, and Susan Shabangu, whose appointment ran until 2014, ending 15 years of continuous female leadership. The Skills Development Act (No. 98 of 1999) led to the establishment in 2010 of Sector Education and Training Authorities (SETAs), and levies from these, and corporate social investment programmes, led to money being invested in bursary programmes. This was to encourage and assist young people from designated groups to enter tertiary education institutions and thus provide a pipeline of graduates back into industry. The past two decades have thus seen a significant increase in not only black students, but especially black female students, as previously disadvantaged individuals gain access to, and the financial means to engage in, tertiary education.

However, the pass rates highlight that access and finance alone do not lead to success. The reasons behind the high failure rates, particularly among black students, have been the subject of much research in South Africa. The legacy of apartheid and the ongoing dysfunction in state schooling have been well documented (DBE Diagnostic Report, 2014). Consistent with national statistics, our data shows the

highest failure rate is among black students, with black males performing at a lower level than black females with failure rates of 44% and 37% respectively. The lowest failure rates are among white females (8%), and white males (12.5%), but few white females register for Geology and the number of white males who do so is declining.

Our interest lies in what may underlie the significant increase in black females in a preserve traditionally dominated by white males. We believe the answer lies at least partially in the availability of bursaries as a result of national policies and CSI regulations that require investment that addresses South Africa's gender and race inequalities.

Bursaries

The results from the 2014 Ore Body Modelling (GEOL 3028) course survey indicate that bursary opportunities are a major factor behind students choosing a career in mining. In our sample, 21 of the 31 students who grew up near a mine indicated that proximity to the mine had influenced their career choice. Clearly, knowledge of the mining environment plays a role in awareness of the opportunities and lifestyles associated with mining, and consequently in the choice of a career, as suggested by Besharati (2014). Our data show that whether they grew up close to a mine or not, in each case the students with bursaries outnumbered those without, with 65% of the male students and 70% of the female students holding bursaries. Thus out of the 115 students in our sample, 72 held bursaries. The 2004 Mining Charter set a target of 10% representation by women by 2009, but only 6% was achieved by that time (Mining Charter Assessment Report, 2015, p. 28). A new target of 10.5% by 2014 was then set, with bursaries as one of the mechanisms to enable achievement of this target. Bursaries offered, for example, by the South African Department of Mineral Resources for the start of study in 2017 were restricted to female South African citizens from a disadvantaged background, with preference given to those from rural areas, and with Grade 12 results that included a 75% pass rate in Mathematics and Physical Science and 60% for English (http://www.dmr.gov.za/bursaries.html). These specifications accord with our analysis of responses to the questionnaire by the GEOL 3028 students, who indicated from their own experience that bursaries were closely tied to matric results; coming from a previously disadvantaged background; and gender. In contrast to students in the 2014 sample, our former students (all female) described a very rigorous bursary application process. They went through mine visits, internships, interviews, and medical tests before being awarded their bursaries. One of the former students recalled how she was exposed to deep-level mining as a test of whether she would be able to cope: 'They [the geologists] took me to the worst possible places underground just to see if I was really into the whole mining scene'. This rigorous screening has now been replaced by criteria that are more closely aligned to equity agendas than the needs and realities of mining. One of the GEOL 3028 students explained: 'The bursary (sic) was short of people around the time I applied. I just got called.'

In our view, however, many female students over the past few years, including a number in the 2014 class, will not satisfy the medical requirements for underground work. The guidelines on thermal stress given by the Department of Minerals and Energy (2002, p. 47) indicate that a body mass of 50 kg or less makes a person 'unsuitable for work in hot environments'. Equally, if the body mass index (BMI) is greater than 35, the person concerned is deemed unsuitable for work in the environments experienced in mining. BMI is an important measure of body fat, with a high BMI being associated with low heat tolerance. At the same time, a small body frame and lack of physical strength is compromising in the physically demanding underground environment, which also requires heavy protective clothing (Fox, 2016). Students who are slightly built thus carry a limiting attribute that would have been noticed had the bursary allocations required both an interview and a medical. Students who otherwise meet the criteria but are overweight could also be limited, but have opportunity to meet the criteria through weight-loss programmes. Of all the 73 students in the sample group holding a bursary, only five underwent a medical examination (three females and two males). In terms of the 'soft skills' highlighted by senior managers as critical for success in the mining industry, none of the 2014 class described undergoing aptitude tests that would screen for suitability and attitudinal fitness for the mining industry.

The drive to recruit students from the appropriate groups to enable large corporations to meet their Broad Based Black Economic Empowerment (BBBEE) obligations appears to have translated into a 'loosening up' of the bursary application and award processes. Our understanding is that in the current context, the allocation of bursaries is driven by corporate social investment requirements and social justice agendas, and that the follow-through to students actually entering the mining industry is of less consequence than the need to satisfy transformation agendas. The increasing numbers of females accessing bursaries and requiring training for employment in this industry also places a responsibility on higher education to take account of the environment in which they will work. We noted in the introduction to this paper that mining has traditionally been a male-dominated environment. With the increase in the number of females entering the industry there is a need for appropriate curriculum development that will help them achieve success in their work. At the same time, bursary providers need to allocate bursaries in a way that leads to return on investment, not only for them, but for the lecturers who invest time and effort in developing the intellectual capital and the skills necessary for career success, and who themselves are judged according to student pass rates. Thus students who have not been carefully selected with regard to suitability and intention to go into mining make return on investment problematic, for the mining companies and the MQA, who award the bursaries, and for the lecturers who teach the bursars.

Skills needed in the workplace

The concerns noted by senior industry managers about how graduates adapt (or do not adapt) to the world of work indicated that there are many more skills required than those mentioned at the Anglo Platinum presentation. Given the opportunity to express their views about what is needed of incoming graduates, the managers had great difficulty in restricting themselves to just three important skills, which was what was asked for in the survey. They went to great lengths to describe what they believed was needed, and how they experienced the attitude of incoming recruits. 'There is a great need for realism and modesty, and acknowledgement that their qualification is merely a certificate to get into the

field of play' was a comment made by one of the managers and echoed by others. The harshness of the environment was also pointed out: 'Mining is still dominated by an autocratic, mostly insensitive leadership style. Therefore a graduate needs to be mature enough to absorb the pressure without reaching breaking point.' Additional skills identified were 'tempered expectations' and 'personal adaptability and accountability'. One of the managers, the chief geologist at an Anglo Platinum mine, wrote extensively about the need for interpersonal skills, emotional intelligence, good communication skills, adaptability, and technical skills. Other challenges that had little to do with the content knowledge associated with a degree included frustrations related to 'the expectation new recruits have for acknowledgement'; an 'air of expectation and deserving'; and the 'sense of being better than the next person'. All referred to attributes of maturity and a willingness to continue to learn, which appeared to be lacking.

Our analysis of student responses to the development of the three core skills identified in the Anglo Platinum presentation revealed that students believed they were being trained in the first two of the skills, *i.e.* critical thinking and teamwork, but that the 'art of negotiation' was not covered in the courses they were taking. However, we question the validity of this response. We believe that students, the majority of whom are second-language English speakers, may have made a superficial connection between the name of a course and the skill that was being sought. The MIN 1001 course, for example, which is called 'Critical Thinking', was identified by many students as having developed their ability to think critically. In the same way, 'teamwork' was associated with courses where they were required to work in groups.

There were some important mismatches between the students' expectations of what a future in mining would hold for them and the senior managers' expectations of attributes that graduates would bring to the workplace. Most of the male students indicated that they would remain in the mining industry, rather than use their degrees to transfer into another line of industry as was noted by Hillman (1996). They anticipated attaining management positions and were clear that their intention was to 'make money'. Most of the female students indicated they did not intend staying on in the mining sector. The few who indicated that they would stay were like their male counterparts in seeing themselves in management positions, driven by the idea of making money. Ironically, the group least likely to stay in mining is now the only group eligible for bursaries, at least from the South African Department of Mineral Resources.

However, a few of the female students were committed to the career they had chosen. One of them said 'I am privileged in that I am a black woman pursuing mining. That is what the mining sector wants.' This indicates awareness of the potential and power in this field for women, inherent in their gender and race, but the majority of the female students were worried about the instability and violence that had affected the mining sector, much more so than their male counterparts. They felt that despite efforts to change the profile of mining, it was still a 'hostile place' dominated by males. This 'place', according to the mine managers, requires self- and interpersonal management; emotional intelligence; technical and communication skills; tempered expectations and ambitions; realism and modesty. But for the female students, additional skills were needed. One wrote: 'I have grown a good set of balls (not literally) in the sense these courses challenged me, but I manned up and met the challenge. I fought with them and fighting symbolises strength'. Another commented '… most important: develop a thick skin! The mining environment is a harsh and abrasive one, with a culture that is still significantly different to that of big cities. A strong personality is needed in order not to get personally affected. Secondly: strengthen your backbone. It is important to have confidence in your work. Do not allow yourself or your work to be undermined. Find yourself a mentor. If you love what you do, you will be just fine.'

Curriculum development to address industry recommendations

National legislation in post-apartheid South Africa has served as a catalyst for change, not only with regard to industry, but also in education. In a drive to facilitate articulation between institutions and to provide for the recognition of prior experience and learning, universities are required to make their curricula not only 'more relevant, while remaining internationally competitive' but should be 'transformative, innovative, relevant and appropriate, (speaking) to our national and continental issues and priorities' (Kupe, 2015, p. 1).

The failure rates in geoscience courses affect especially black students. The failure rates (averaged over 21 years) are 22% for black males, 27% for black females, 12.5% for white males, and 8% for white females. This has a substantial impact on the subsidy earned by the university. Female students are more likely to graduate than male students, but they are also less likely to go into mining as a career. Curriculum change needs to address the fears that were expressed by female students, the declining throughput rates of male students, and the issues raised by the former students, to prepare them to deal with the environment they will encounter. But there is also need for change in the culture of the industry. Former students who were speaking from experience made the following remarks: 'It was a huge culture shock. The reception of African females coming into the mining industry is not always a warm one, especially from the older generations'. 'I have been assaulted in the cage and nothing was done by the company or human resources'. 'Retrenchment was a reality; the alternative was being put into an unfamiliar position'. The former students also spoke about the need to 'think on your feet, be adaptable and flexible' and noted that a sense of 'discrimination and being looked down upon' was common. What is disturbing is that of the five former students who responded to the survey, one had already left mining, and of the others, only one wanted to remain in the industry. The Mining Charter therefore needs to address not only issues of gender representation in the sector, but the conditions of service. Transformation in the industry requires not simply an increase in the number of women in mining, but rather a shift in culture, where human dignity and respect for all people prevails, whether they are male or female. However, this is not a new phenomenon. It has been an issue since the mining industry started in South Africa (Ncube-Hein, 2016)

The benefit of having embarked on research that sought to document and understand the needs of the geosciences education pipeline, with a view to aligning more closely with industry needs, is that such curriculum development is now

underway, driven by the Higher Education and Qualification Sub-Framework (HEQSF). The objective of the HEQSF is to create a single, integrated national framework for learning achievements (CHE, 2013). The curriculum development that has been undertaken for this national objective is incorporating the needs highlighted by industry, but also has to take into account changes in the tertiary education sector, including increases in student numbers without significant increases in teaching staff. The focus by industry on the development of soft skills is particularly challenging in that many of these skills are affective, requiring relationship development and additional time.

Conclusion

The general understanding of higher education in the sciences is that it will serve to develop the knowledge and skills of students to a point where, upon graduation, they are deemed fit for the relevant workplace. Bursaries and scholarships are awarded by industry to worthy students to enable them to pursue dreams of higher education and provide a pipeline of appropriately trained students for the industry. But this ideal does not always work out. Nearly two decades ago Hillman (1996, p. 77) recommended that, in terms of mining students, it was a 'matter of urgency' that some method of assessing students' commitment to the industry be instituted, which would benefit both industry and higher education. He was concerned that applicants for bursaries are 'stretching this opportunity to the point of dishonesty, and are, in effect, milking the system dry' (p. 80).

Hillman was writing of the situation before the advent of the Mining Charter in 2002 and the BBBEE scorecards that have resulted in the drive to recruit women, through bursaries, into work environments known to be hostile to women. While one of the senior managers claimed from his experience over the past 10 years that 'females were more intelligent and consistently derived better results than the male students', finding a fit between the workplace environment and the aspirations of students, especially in regard to challenges related to women in mining, requires more than bursaries being allocated on the basis of gender, economic disadvantage, and minimum Grade 12 results.

In this study, which looked at how student diversity has changed over the past 15 years with regard to the geosciences education pipeline, we have shown how equity and social justice imperatives have impacted on bursary allocations, significantly increasing the number of female students registering for mining engineering. Our findings indicate that in the current economic environment, male students are more likely to actually go into mining than female students, but that bursaries for male students are now harder to come by.

We recommend that a more rigorous process is put into place before students are awarded a bursary—one that involves mine visits, internships, interviews, and medical tests, for both male and female applicants. At the same time, mine owners and managers need to address the hostility encountered by women in the mining environment, and universities need to impart the skills needed for success through curricula that take into consideration the many affective attributes needed for success in mining—whether these relate to men or women. Assessing students more carefully in terms of admission and the allocation of bursaries will also create a better teaching and learning environment, resulting in a supply of graduates more suited to an industry that continues to be vital to South Africa's economy.

References

Besharati, N. 2014. The impact of mining operations, corporate social initiatives, school interventions and other social-economic factors on education outcomes in South Africa. Challenges in evaluating development effectiveness. Platinum and Passes. *SA Mining and Education Stakeholder Conference*, Wits School of Governance, Parktown, Johannesburg, 23 May 2014.

Botha, D. and Cronje, J.F. 2015.: Women in mining: A conceptual framework for gender issues in the South African mining sector. *South African Journal of Labour Relations*, vol. 39, no. 1. pp. 10–37.

Council on Higher Education (CHE). 2013. The Higher Education Qualifications Sub-Framework. Pretoria.

Cornish, L. 2013. Women climb the ladder: Equality, it's the name of the game: women in mining. *Inside Mining*, vol. 2, no. 2. pp. 40–43. http://reference.sabinet.co.za/webx/access/electronic_journals/sh_mining/sh_mining_v6_n2_a14.pdf [Accessed 18 June 2015].

Cornish, L. 2014. Transformation muse - Anglo American: women in mining. *Inside Mining*, vol. 7, no. 2. pp. 32, 33. http://reference.sabinet.co.za/sa_epublication_article/sh_mining_v7_n2_a14 [Accessed 18 June 2015].

Department of Education. 2014. National Senior Certificate Examination Diagnostic Report. Pretoria.

Department of Mineral Resources. 2016. Bursaries. http://www.dmr.gov.za/bursaries.html [Accessed 22 February 2016].

Department of Mineral Resources. 2015. Mining Charter Assessment Report. http://www.dmr.gov.za/publications/viewcategory/262-mining-charter-assessment-report-2015.html [Accessed 22 February 2016].

Department of Minerals and Energy. 2002. Guideline: thermal stress. Mine Health and Safety Inspectorate. Reference number 16/3/2/4-A2. h [Accessed 22 February 2016].

Fox, F. 2016. South African Society of Occupational Medicine. Personal communication, 8 February, 2016.

Hillman, J.C. 1996. Increasing black representation in mining engineering: the need for a new approach. *Journal of the South African Institute of Mining and Metallurgy*, vol. 96, March/April. pp. 77–81.

Huntoon, J.E. and Lane, M.J. 2007. Diversity in the geosciences and successful strategies for increasing diversity. *Journal of Geoscience Education* vol. 55, no. 6. pp. 447–457.

Kupe, T. 2015. Progress on the implementation of Wits' transformation plan. VCO Circular, 1 October, 2015. University of the Witwatersrand.

Le Roux, T. and Naude, A.M.E. 2009.: Communicating with diversities: female employees in the South African platinum-mining industry. *Communicare*, vol. 28, no. 1. pp. 24–49.

Maphai, V. 2014. Keynote address. *SA Mining and Education Stakeholder Conference*, Wits School of Governance, Parktown, Johannesburg, 23 May 2014.

Ntombela, D. 2014. Women in mining face challenges: women in mining. Inside Mining, vol. 7, no. 6. pp. 30-31. http://reference.sabinet.co.za/print_document?printFT=true&printMD=true [Accessed 18 June 2015].

Ncube-Hein, K. 2016. School of Geosciences, University of the Witwatersrand. Personal communication.

Patton, M.Q. 1990. Qualitative Evaluation and Research Methods (2nd edn). Sage Publications, Newbury Park, CA.

Sideropoulos, E. 2014. Introduction to the SA Mining and Education Stakeholder Conference, Wits School of Governance, Parktown, Johannesburg 23 May 2014.

Stewart, P. 2013. The 2012 strike wave, Marikana and the history of rock drillers in South African mines. http://www.global-labour-university.org/fileadmin/GLU_Column/papers/no_121_Stewart.pdf [Accessed 18 June 2015]. ◆

Appendix

Student Questionnaire

The Geoscience Education Pipeline: issues of Skills Development, Equity and Gender

Please Note: *Participation in this survey is voluntary. All responses will be treated confidentially and all correspondence will be protected. Data collected will be used for the purpose of a research paper only. No individual student names will be mentioned in the paper. Thank you in advance for your participation.*

1) Which course are you currently taking in the School of Geosciences?

_____

2) Why did you choose to do this course?

_____
_____
_____

3) Do you have a bursary to study this course? If so, which company is sponsoring you?

_____
_____

4) What was the process you went through to obtain this bursary (i.e. how did you secure this bursary)?

_____
_____
_____
_____
_____
_____
_____
_____

5) What are your plans once you graduate?

_____
_____
_____
_____
_____
_____

6) South Africa has recently experienced the longest strike involving the mining sector in its history. How does the uncertainty associated with this aspect of mining contribute to how you see your future in the mining sector?

_____
_____
_____
_____
_____
_____
_____

7) How well do you think you have been prepared by the University in the following skills areas? (which have been identified by the mining sector as the 3 most important attributes necessary for their employees)

Tick the most appropriate answer (0 = not at all, 10 = excellent preparation).

SKILL	1	2	3	4	5	6	7	8	9	10
Critical thinking										
Team work										
Art of negotiation										

8) Which course/topic in your curriculum best prepared you for.....?

a. Critical thinking_____
_____

b. Team work
_____
_____

c. Art of negotiation_____
_____

9) Please comment on what it was that you gained from these courses/topics that prepared you for critical thinking, team work and the art of negotiation.

_____
_____
_____
_____
_____
_____
_____
_____
_____
_____
_____

10) What kind of work do you anticipate you will be doing once you graduate?

_____
_____
_____
_____
_____
_____
_____

11) What kind of challenges (as a woman) do you anticipate you would need to overcome once you join the work place?

_____
_____
_____
_____
_____
_____

Thank you for your participation and good luck for the future!

Gillian Drennan (School of Geosciences)
Ann Cameron (Science Teaching and Learning Centre)

The geoscience education pipeline in South Africa

Past Student Questionnaire

The Geoscience Education Pipeline: issues of Skills Development, Equity and Gender

Please Note: *Participation in this survey is voluntary. All responses will be treated confidentially and all correspondence will be protected. Data collected will be used for the purpose of a research paper only. No individual names of past students will be mentioned in the paper. Thank you in advance for your participation.*

1) Why did you choose to study Geology?

_____

_____

2) Did you have a bursary to study Geology? If so, which company sponsored you?

_____

_____

3) What was the process you went through to obtain this bursary (i.e. how did you secure this bursary)?

_____

_____

4) What is your current position? What work do you now do?

_____

_____

5) South Africa has experienced the longest strike involving the mining sector in history. How does the uncertainty associated with this aspect of mining contribute to how you see your future in the mining sector?

_____

_____

6) How well do you think you were prepared at University in the following skills (which have been identified by the mining sector as the 3 most important attributes necessary for their employees)?
Tick the most appropriate answer (0 = not at all, 10 = excellent preparation).

SKILL	1	2	3	4	5	6	7	8	9	10
Critical thinking										
Team work										
Art of negotiation										

7) Can you remember which course/topic in your curriculum best prepared you for.....?

a. Critical thinking_____

_____

b. Team work

_____

_____

c. Art of negotiation_____

_____

Please comment on why you think these courses/topics made a difference in preparing you for the world of work.

_____

_____

8) What kind of challenges (as a woman) have you encountered once you joined the work place?

_____

_____

9) What words of advice / encouragement / warning might you offer to young female students who are currently studying in this field?_____

_____

Thank you for your participation and good luck for the future!

Gillian Drennan (School of Geosciences)
Gillian.Drennan@wits.ac.za
Ann Cameron (Science Teaching and Learning Centre)
Ann.Cameron@wits.ac.za

Company Questionnaire

The Geoscience Education Pipeline in South Africa: issues of Skills Development, Equity and Gender.

Please note: *all responses will be treated confidentially and will be used for the purpose of the paper only. No company names will be mentioned in the paper. Should you wish to receive a copy of our paper we would be pleased to send you one.*

1) What do you think are the 3 most important skills necessary for a graduate entering your sector?

2) In terms of selection of students for bursaries, what are the criteria you use for allocation (e.g. matric results, gender, equity imperatives)?

3) Does your company see any return on investment with respect to bursary allocation, especially from females, and if so, how much return?

4) In your opinion, what is currently missing in the tertiary training that you believe would improve the articulation between university and industry?

5) Do Mining Houses see any difference between graduates from different curricula i.e from different Universities)?

6) Are there any BEE (or other redress/social justice) guidelines related to gender and bursary allocation?

http://dx.doi.org/10.17159/2411-9717/2017/v117n6a8

Direct block-support simulation of grades in multi-element deposits: application to recoverable mineral resource estimation at Sungun porphyry copper-molybdenum deposit

by S.A. Hosseini*, O. Asghari*, and X. Emery†

Synopsis

Recoverable mineral resources assessment has become a standard geostatistical application in the mining industry, with various geostatistical techniques currently available. This investigation aimed to improve the prediction at the Sungun deposit and to obtain mineral resource models capable of handling (i) the change of support from drill-hole composites to selective mining units (SMUs), (ii) the multivariate nature of the ore control selection criteria that involves both copper and molybdenum grades; and (iii) the local uncertainty on the true (unknown) grades. The solution presented in this paper is to use direct block-support sequential cosimulation in order to construct a set of alternative outcomes of the copper and molybdenum grades on block support over the deposit, with no need for storing point-support values, hence with a considerable gain in memory management and CPU time. The grade realizations so obtained are then processed to calculate the uncertainty in the mineral resources that can be recovered above given cut-off grades, both globally and on a block-by-block basis.

Keywords
direct block support cosimulation, recoverable resources estimation, local uncertainty, Sungun porphyry copper-molybdenum deposit.

Introduction

Geostatistical methods are widely used by mining companies to determine a resource model of the tonnage and head grade of a potential orebody, which is one of the first and most critical inputs underpinning any mining project. The prediction of the grade, tonnage, and recoverable metal for a particular mining plan and the corresponding financial forecast constitute the main technical risks in mineral resource evaluation. The conventional approach to this problem is to predict the mineral grade for constant volumes relevant to the mining plan and to base the recoverable mineral resource calculations on those predictions. Alternatively, one can directly predict the local variability in the mining block grades based on a spatial distribution model (David 1988; Rossi and Deutsch 2014). Multiple realizations can also be constructed by conditional simulation, providing a more complete representation of block grade uncertainty, as well as the uncertainty over multiple blocks. Simulation methods allow quantification of the uncertainty of the mineral resource prediction risks in downstream studies such as mine design, mine planning, or operational optimization studies; the risk assessment is achieved after applying transfer functions to the conditional simulation models (Dimitrakopoulos 2012; Rossi and Deutsch 2014).

Recoverable mineral resource prediction and simulation models should be capable of handling: (1) a change of volumetric support, which is a common and critical issue in modelling regionalized variables such as mineral grades as, invariably, the volumetric support of the available data (*e.g.,* drill-hole composites) is much smaller than the blocks on which the model is based (Emery and Ortiz, 2011); (2) the multivariate nature of the ore control selection criteria (Montoya *et al.*, 2012); (3) the local uncertainty, which refers to the probability distributions of the actual values at specific locations (Khan and Deutsch 2015). The solution is therefore to construct a multivariate block-support simulation and a post-processing aimed at producing a multivariate recoverable mineral resource evaluation.

The usual approach used for simulating grade values onto a block support consists in performing point-support simulation on a dense grid that covers the region of interest, and then averaging within relevant selective mining units (SMUs) or blocks in order to develop a simulated block-support (Boucher and Dimitrakopoulos, 2009; Emery, 2009; Emery and Ortiz, 2011). This procedure has two computational disadvantages: it is time-consuming and requires a significant amount of computer memory. An alternative is direct block-support simulation, which avoids simulating onto a grid that discretizes the blocks. This idea, as originally proposed by Journel and Huijbregts (1978), is based on separate simulation and conditioning steps. Boucher and Dimitrakopoulos (2009)

* *Simulation and Data Processing Laboratory, School of Mining Engineering, University College of Engineering, University of Tehran, Tehran, Iran.*

† *University of Chile, Chile.*

 ISSN 2225-6253. Paper received Dec. 2015; revised paper received Mar. 2017.

expanded on direct block simulation by adding a decorrelation method (minimum/maximum autocorrelation factors), which allows reproduction of the spatial relationships between cross-correlated variables. Emery (2009) presented a computer program for direct block simulation that also accounts for the 'information effect', produced by misclassifications when selecting blocks as ore or waste, based on whether or not the predicted grade values exceed a threshold (Chilès and Delfiner 2012). Two algorithms for the direct block cosimulation of cross-correlated random fields are also presented by Emery and Ortiz (2011): the first one is a variation of sequential Gaussian cosimulation, with no need for storing point-support values; the second is a direct block simulation algorithm based on a spectral approach that incorporates a change-of-support model into the simulation process. In this study, the direct block sequential Gaussian cosimulation is applied to the Sungun copper-molybdenum data-set, and a practical implementation of direct block-support simulation for multi-element deposits is presented.

Principle of block-support sequential Gaussian cosimulation

The sequential algorithm proposed by Emery and Ortiz (2011) uses a change-of-support model to directly simulate block-support values. It is versatile enough to incorporate several coregionalized variables and to handle heterotopic data-sets, *i.e.,* data-sets for which not all the variables are measured at all the data locations. It consists of the following steps:

1. For each variable of interest, transform the original point-support grade data into normal scores values with a mean of 0 and variance of 1
2. Fit a linear model of coregionalization (Wackernagel 2003) for the spatial structure of the normal scores data. In multi-element deposits for which the grades of K elements are of interest, the set of $K(K+1)/2$ direct and cross-variograms must be calculated, then fitted by the linear model of coregionalization (LMC). This leads us to model all direct and cross-variograms from the same pool of basic variogram models $\lambda_n(\mathbf{h})$ ($n = 1,\ldots, nst$) with a unit sill:

$$\Gamma(\mathbf{h}) = \sum_{n=1}^{nst} \mathbf{B}_n \gamma_n(\mathbf{h}) \quad [1]$$

   where $\mathbf{h}$ stands for a lag separation vector, $\Gamma(\mathbf{h})$ for the $K \times K$ matrix of direct and cross-variograms at lag $\mathbf{h}$, and each $\mathbf{B}_n$ is a real-valued, symmetric, positive semidefinite coregionalization matrix. The anisotropy and range parameters are fitted in the specification of each constituent nested structure $\lambda_n(\mathbf{h})$. Automated or semi-automated procedures are often used for fitting of a linear model of coregionalization to ensure that the requirements of positivity of the coregionalization matrices are met
3. Divide the simulation domain into non-overlapping blocks
4. Select a block v in the domain among the blocks not yet simulated. Selection can be made according to a regular sequence or randomly
5. At a set of nodes $\{\mathbf{x}_1,\ldots,\mathbf{x}_M\}$ discretizing the block v, simulate Gaussian random fields that follow the linear model of coregionalization fitted at step (2), conditionally to the original point-support normal scores data and to the previously simulated block-support data located in and around this block (see next step for detail). The conditioning can be based on simple or ordinary cokriging, the latter being less sensitive to departures from ideal stationarity conditions than the former (Emery, 2007, 2009)
6. Average the simulated point-support Gaussian values ($Y_k(\mathbf{x}_i)$ with $k = 1\ldots K$ and $i = 1\ldots M$) within the block, which provides block-support data to be used for further conditioning along the simulation path (step 5):

$$Y_k(v) = \frac{1}{M}\sum_{i=1}^{M} Y_k(\mathbf{x}_i) \quad [2]$$

   The direct and cross-covariance functions of the point- and block-support Gaussian random fields can be derived from the linear model of coregionalization fitted at step (2). Indeed, for any pair of indices k, $k \in \{1,\ldots, K\}$, one has the following:

• Point-to-point covariance:

$$\mathrm{cov}\{Y_k(\mathbf{x}), Y_{k'}(\mathbf{x}')\} = \sum_{n=1}^{nst} \mathbf{B}_n(k,k')(1-\gamma_n(\mathbf{x}-\mathbf{x}')) \quad [3]$$

• Point-to-block covariance:

$$\mathrm{cov}\{Y_k(\mathbf{x}), Y_{k'}(v')\} = \frac{1}{M}\sum_{i=1}^{M}\sum_{n=1}^{nst} \mathbf{B}_n(k,k')(1-\gamma_n(\mathbf{x}-\mathbf{x}'_i)) \quad [4]$$

where $\{\mathbf{x}'_1,\ldots,\mathbf{x}'_M\}$ are a set of nodes discretizing block v'.

• Block-to-block covariance:

$$\mathrm{cov}\{Y_k(v), Y_{k'}(v')\} = \frac{1}{M^2}\sum_{i=1}^{M}\sum_{j=1}^{M}\sum_{n=1}^{nst} \mathbf{B}_n(k,k')(1-\gamma_n(\mathbf{x}_i-\mathbf{x}'_j)) \quad [5]$$

where $\{\mathbf{x}_1,\ldots,\mathbf{x}_M\}$ and $\{\mathbf{x}'_1,\ldots,\mathbf{x}'_M\}$ discretize blocks v and v', respectively.

   Provided with these covariance functions between the Gaussian random fields at both point and block supports, it is straightforward to write the cokriging equations needed for the conditioning stage at step (5)
7. Back-transform the simulated point-support Gaussian values within the block and average them to obtain simulated block-support values for the original grade variables:

$$Z_k(v) = \frac{1}{M}\sum_{i=1}^{M} Z_k(\mathbf{x}_i) = \frac{1}{M}\sum_{i=1}^{M} \phi_k(Y_k(\mathbf{x}_i)) \quad [6]$$

   where ϕ_k is Gaussian transformation function associated with the k-th grade variable, *i.e.,* the function that converts the Gaussian values into grade values. Note that the block-support grade data is not used in the conditioning stage at step (5) and that the block-support Gaussian data (Equation [2]) is used instead
8. Go back to step (4) until all the blocks are simulated.

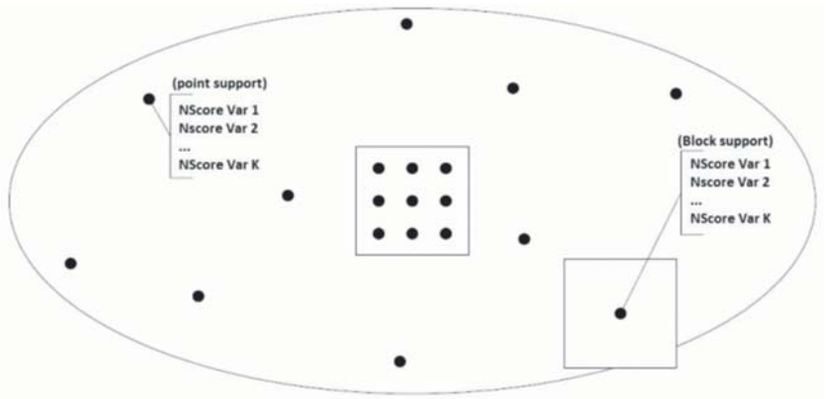

Figure 1—Search neighborhood for direct block cosimulation (target block located in the centre of the neighborhood)

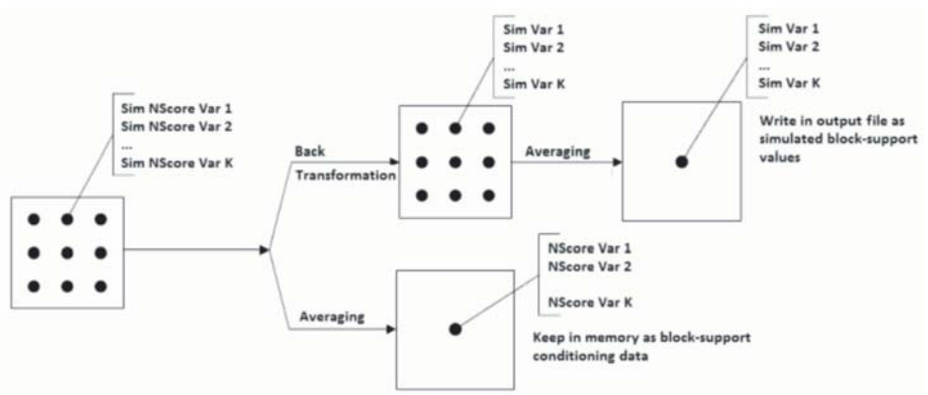

Figure 2—Process for cosimulation on block support

Because the simulated point-support Gaussian values are not stored and only block-support information is retained at steps (6) and (7), the above algorithm reduces the memory storage requirements of traditional sequential simulation. Also, the search for nearby conditioning data at step (5) is faster, as the number of previously simulated data is considerably fewer when using block-support data instead of point-support data. A graphical summary of the process for searching data and for simulating Gaussian and grade values is given in Figures 1 and 2, and a schematic example is provided in the Appendix.

Sungun copper deposit

Geological description

The Sungun porphyry copper-molybdenum deposit is located in the Eastern Azarbaijan Province, NW Iran, in the northwestern part of a NW-SE trending Cenozoic magmatic belt (the Sahand-Bazman Belt). The Sungun porphyries occur as calc-alkaline stocks and andesitic to dacitic dikes. Sungun is actually a skarn-porphyry deposit, and is called the Sungun porphyry copper-molybdenum deposit due to the large metal content in its porphyry section and the presence of molybdenum. This deposit is composed of quartz monzonite (major intrusive bodies) and diorite-granodiorite, which have been injected into Eocene volcano-sedimentary and Cretaceous carbonate rocks. The emplacement of the Sungun stock took place in several intrusive pulses associated with hydrothermal activity (Hezarkhani, 2006). The arrangement of alteration and mineralization domains is complicated and does not conform to the simple models of porphyry systems. (Asghari and Hezarkhani, 2008; Soltani, Afzal, and Asghari, 2014; Talebi, Asghari, and Emery, 2015). During the alteration and mineralization in Sungun, three different hydrothermal fluids were present: (1) hydrothermal fluids that were derived magmatically and were characterized by high temperatures and moderate to high salinities caused potassic alteration and Cu ± Mo mineralization, (2) a mixture of magmatic fluid with a predominantly meteoric fluid, resulting in lower temperatures and salinities, that was responsible for sericitization at higher levels and transition alteration at depth, and (3) a relatively oxidized meteoric water which produced a peripheral propylitic alteration zone outside the core of potassically altered rock. (Hezarkhani and Williams-Jones, 1998; Tahmasebi, Hezarkhani, and Mortazavi, 2010). Four alteration zones can be identified Sungun: (1) potassic, (2) propylitic, (3) phyllic, and (4) argillic (Hezarkhani and Williams-Jones, 1998). Two elements are of interest for resource modelling: copper (Cu) as the main product, and molybdenum (Mo) as a by-product.

Data-set

A set of 31 533 diamond drill-hole samples, distributed in a volume of about 1200 m × 1100 m × 1000 m, were available for the study (Figure 1). Copper and molybdenum grades

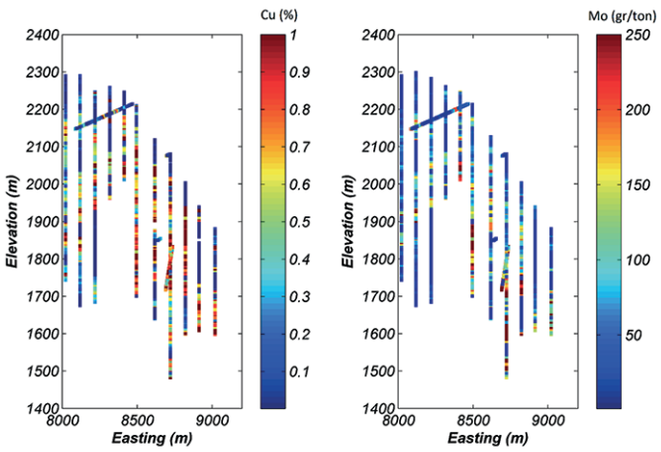

Figure 3—One cross-section (northing 4800 m ± 20 m) of available drill-hole data: copper grade (left) and molybdenum grade (right)

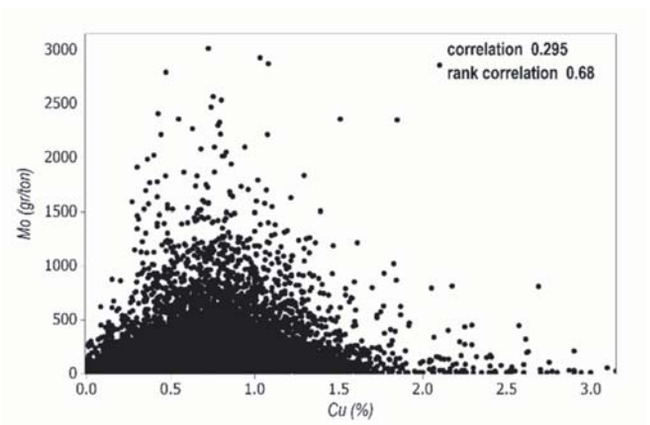

Figure 4—Scatter plot of copper and molybdenum grades (drill-hole data)

Table I

Basic statistics of assayed grades

Variable	Mean deviation	Standard	Minimum	Maximum	Number of data
Copper grade (%)	0.41	0.45	0.001	23.5	24 949
Molybdenum grade (g/t)	109.73	222.95	1	6258	29 786

have been analysed with a proper QA/QC process in order to ensure data accuracy, and composited to 2 m lengths. Table I indicates the basic statistics of the composited data. It is seen that the two grades have not been measured for all the samples and the data-set is therefore partially heterotopic. The linear coefficient of correlation between copper and molybdenum grades is 0.30, but this correlation rises to 0.53 after transforming the grades into normal scores. Also, the Spearman rank correlation coefficient is equal to 0.68, indicating a significant dependence between copper and molybdenum grades (Figure 4). These correlation coefficients can be explained by the minerals associations present in the Sungun deposit, especially in the potassic alteration zone. Several main vein groups have been identified, for instance quartz + molybdenite + anhydrite + K-feldspars + pyrite + chalcopyrite and quartz + chalcopyrite + pyrite ± molybdenite (Hezarkhani and Williams-Jones, 1988).

Cosimulation of grades at a block support

In the following analyses, it is of interest to construct a set of realizations of the copper and molybdenum grades over the deposit that match the known values at the sample locations, mimic the spatial variability of the true unknown values at unsampled locations, and reproduce the spatial dependence between the grades, as described by their cross-variogram (Chilès and Delfiner, 2012; Wackernagel 2003). The steps for constructing the realizations using block-support sequential Gaussian cosimulation are as follows:

- Declustering of the original data to obtain representative distributions of the grade variables
- Normal scores transformation of copper and molybdenum grades
- Calculation of the sample variograms of the normal scores data along the recognized directions of anisotropy (horizontal plane and vertical direction)
- Fitting of a linear model of coregionalization, using nugget, exponential, and spherical structures (Figure 5). The fitted model is presented in Equation [7], where the horizontal and vertical ranges are indicated in brackets

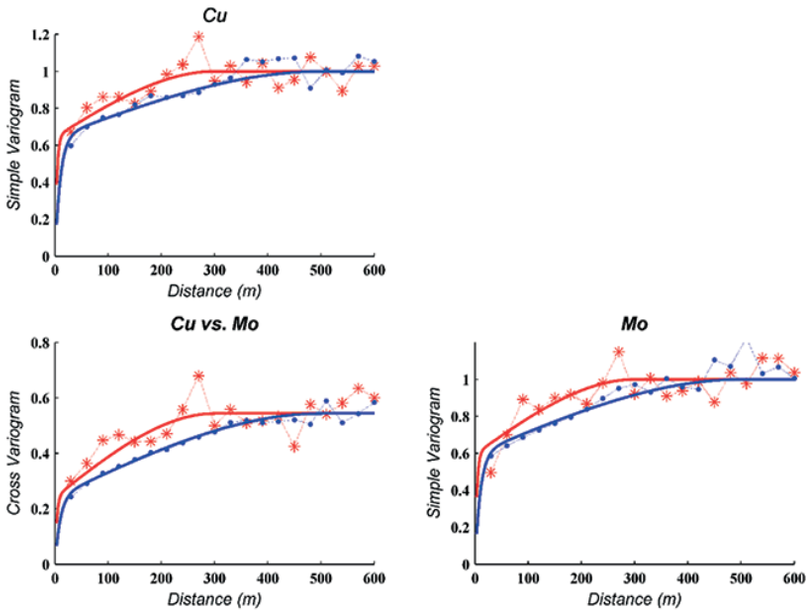

Figure 5—Sample (dashed lines) and modelled (solid lines) direct and cross-variograms of normal scores transforms of copper and molybdenum grades, along horizontal (red) and vertical (blue) directions

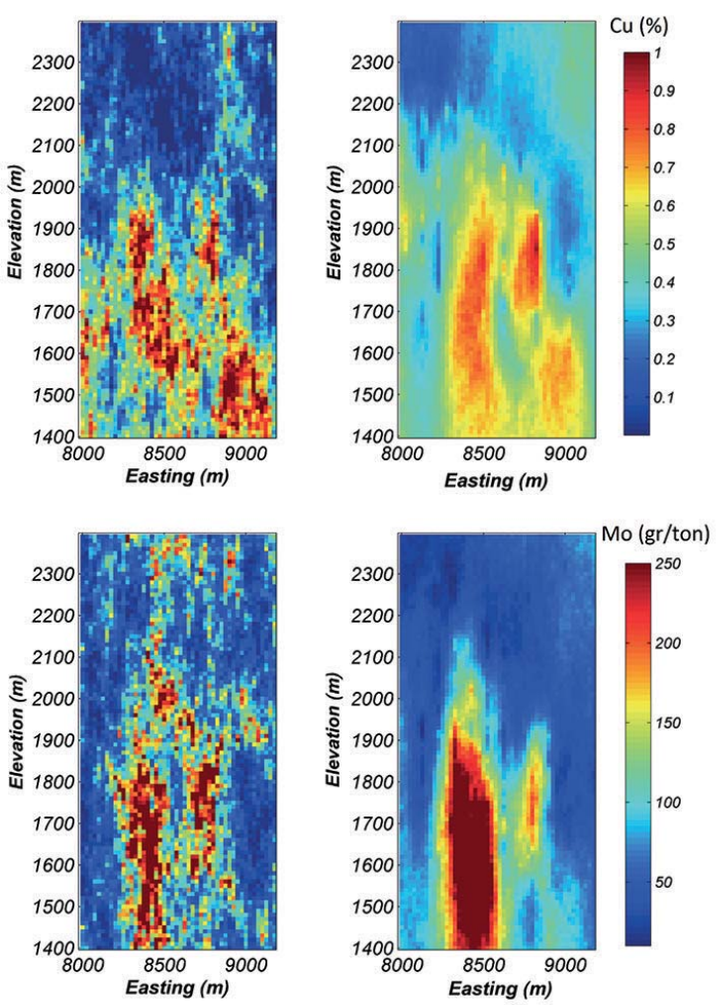

Figure 6—Maps of simulated copper (top) and molybdenum (bottom) grades for realization #1 (right) and maps of expected copper and molybdenum grades (average of 100 realizations) (left)

$$\begin{pmatrix} \gamma_{Cu} & \gamma_{Cu-Mo} \\ \gamma_{Cu-Mo} & \gamma_{Mo} \end{pmatrix} = \begin{pmatrix} 0.001 & 0.001 \\ 0.001 & 0.007 \end{pmatrix} nugget + \begin{pmatrix} 0.643 & 0.0241 \\ 0.241 & 0.588 \end{pmatrix} \exp(10m, 30m) + \begin{pmatrix} 0.356 & 0.302 \\ 0.302 & 0.403 \end{pmatrix} sph(300m, 500m) \quad [7]$$

This is a licit model of coregionalization, insofar as the three coregionalization matrices are symmetric and positive semidefinite. For practicality, a semi-automated technique has been used to fit the sill matrices of each nested structure based on the calculated sample variograms (Goulard and Voltz, 1992; Emery, 2010)

- Definition of a regular grid covering the domain, with 48 × 47 × 100 blocks of size 25 m × 25 m × 10 m, which represent the size of the SMUs. Each grid block is furthermore discretized into 5 × 5 × 2 points
- Construction of 100 conditional realizations of the copper and molybdenum grades using direct block-support sequential Gaussian cosimulation, as explained in the previous section.

Since each block is discretized into $M = 50$ points, the direct simulation approach reduces the size of the problem (storing of simulated values and search for nearby data) by a factor of 50 with respect to the traditional point-support simulation followed by block averaging. The gain is thus very attractive from a computational point of view in order to account for the change of support from the point-support samples to the SMU support. No information effect is taken into account in this work, but it could be incorporated if a pattern of production data were available to predict the block-support grade for ore/waste classification (Emery and Ortiz, 2011).

For both elements of interest (copper and molybdenum grades), the maps of the first realization and of the average of 100 realizations for a selected section at northing 4800 m are displayed in Figure 6. As can be expected, the latter maps smooth the variability and display much smaller contrasts and fluctuations than the former, which are intended to reproduce the 'true' SMU grade variability at all spatial scales. This fact can be corroborated by examining the statistics of the simulated block-support grades (Table II), which show a higher dispersion and larger range of the simulated grades for the individual realizations than for the average of 100 realizations. However, due to the support effect (Chilès and Delfiner, 2012), the variability of the simulated grades is smaller than that of the original point-support data (Table I). Likewise, the linear correlation coefficient between the simulated copper and molybdenum grades (0.62) is higher than that of the original data (0.30), which is also a consequence of the support effect that smooths small-scale variability and therefore enhances the correlation between both variables (Figure 7, left). It is noteworthy that the rank correlation coefficient of the point-support data does not change significantly with the simulated block-support grades (0.71 *vs.* 0.68). For comparison, if copper and molybdenum grades are simulated separately, as if these two variables were independent, the rank correlation coefficient between the simulated block-support grades would drop to 0.22, much lower than that of the original data (Figure 7, right), hence the importance of jointly simulating both variables to reproduce their dependence relationships.

Table II

Basic statistics of simulated block-support grades

Variable	Block model	Mean	Standard deviation	Minimum	Maximum
Copper grade (%)	Realization 1	0.41	0.30	0.003	4.43
	Realization 2	0.36	0.22	0.004	2.76
	Average of 100 realizations	0.38	0.13	0.08	1.11
Molybdenum grade (g/t)	Realization 1	109.2	138.22	7.65	2977
	Realization 2	96.9	97.05	8.19	1421
	Average of 100 realizations	99.6	61.30	18.98	579.2

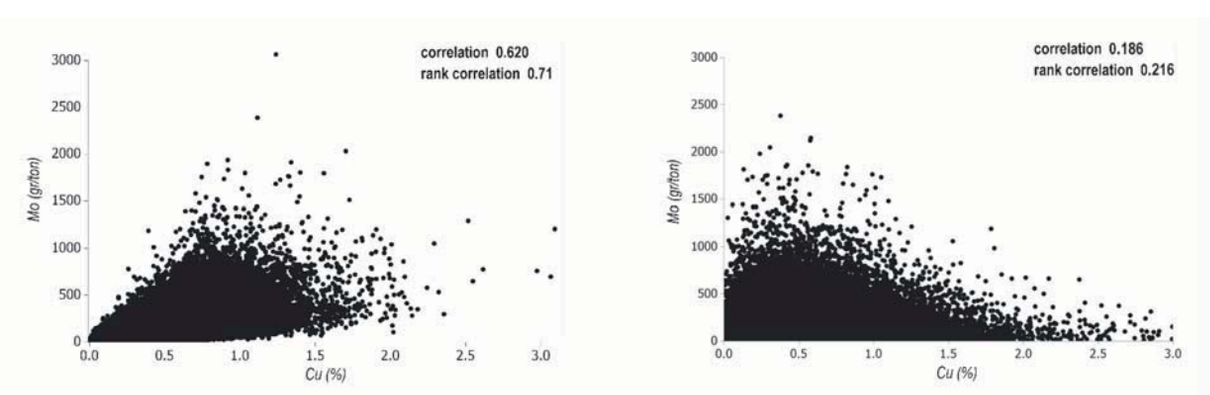

Figure 7—Scatter plots of copper and molybdenum simulated block-support grades (left: cosimulation, right: independent simulation)

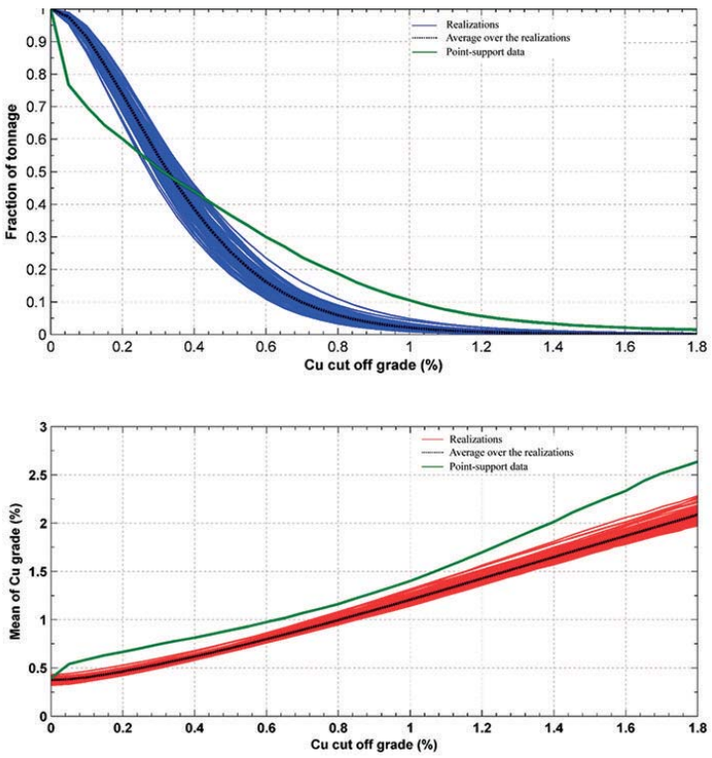

Figure 8—Tonnage (top) and mean copper grade (bottom) recovered after applying a cut-off on the block-support copper grade, calculated for each realization (solid coloured lines) and averaged over all the realizations (black line). The curves associated with the point-support data are superimposed (green curves)

Assessing global uncertainty on recoverable resources

For each realization, the recoverable copper and molybdenum mineral resources above given cut-off grades are calculated. The expected recoverable mineral resources are then defined by an average over the realizations. The analysis of uncertainty of grade, tonnage, and metal curves by long-term planning engineers can be carried out to understand the recoverable mineral resource scenarios at different cut-offs. The tonnages and mean copper grades above different cut-offs for all realizations and their averages are shown in Figure 8, together with the curves associated with the original copper data at the sample support. It can be seen that the tonnage curve of the data decreases faster at low cut-offs, and slower at high cut-offs, than that of the block-support realizations, and that, at a zero cut-off, the mean grades for both the point-support data and the block-support realizations are comparable. These results are consistent with the change-of-support theory, as the point-support and block-support distributions of the copper grade should have the same mean value and the former should be more selective than the latter (Chilès and Delfiner, 2012), and demonstrate that the realizations are unbiased and correctly reproduce the support effect.

Since the mineralization comprises more than one metal of economic value (copper and molybdenum), the two grades can be converted to a single value or 'equivalent grade'. Typically the minor metals are converted and added to the grade of the major metal. In the present case, the equivalent copper grade is defined as

$$Z_{eq} = Z_{Cu} + Z_{Mo}\, F_{eq} \quad [8]$$

where Z_{Cu} is copper grade, Z_{Mo} molybdenum grade, and the equivalent factor is equal to

$$F_{eq} = \frac{(s_{Mo} - r_{Mo})\, y_{Mo}}{(s_{Cu} - r_{Cu})\, y_{Cu}} \quad [9]$$

with s the selling price, r the refinery cost, and y the recovery for each metal, *i.e.*

$$F_{eq} = \frac{(32000 - 4500)0.8}{(5300 - 1000)0.85} = 6.02$$

The grade-tonnage curves based on different cut-offs on the equivalent copper grade are calculated for all the realizations (Figure 9). These curves can be used for ore/waste selection and for finding the optimum cut-off grade (Osanloo and Ataei, 2003; Ataei and Osanloo, 2003).

A complete mineral resources model should include a predicted grade, tonnage, and metal above respective cut-offs and a detailed assessment of uncertainty and the consequences of such uncertainty (Dimitrakopoulos, 1997). Now, since each realization constitutes a plausible outcome for the deposit, the 'true' tonnage and grade curves should lie within the set of simulated curves (although uncertainty with regard to model parameters, including uncertainty on inferred variograms, used as inputs to the simulation remains additional unquantified uncertainty). The realizations thus provide an image of the uncertainty on the mineral resources: a risk analysis can be performed with the simulated curves

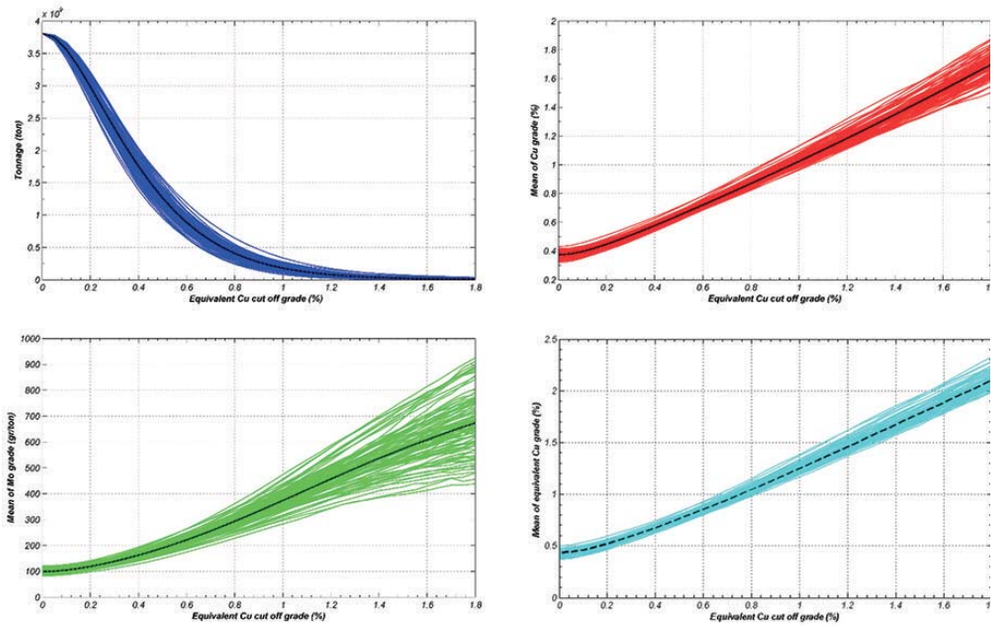

Figure 9—Tonnage (top left), mean copper grade (top right), mean molybdenum grade (bottom left), and mean of equivalent copper grade recovered after applying a cut-off on the block-support equivalent copper grade, calculated for each realization (solid coloured lines) and averaged over all the realizations (black line

(Figures 8 and 9) in order to assess the worse and the best scenarios, with no need for (or in addition to) the traditional classification of mineral resources into Measured, Indicated, or Inferred. Also, one can assess the uncertainty on the mineral resources after applying a cut-off without generating biased conclusions (Emery, Ortiz, and Rodríguez, 2006).

Assessing local uncertainty on recoverable resources

The results obtained from direct block conditional simulation can also be used for measuring uncertainty in the prepared models on a block-by-block basis, by providing cumulative distribution functions for the copper and molybdenum grades of each SMU. Important parameters extractable from such cumulative distribution functions include the conditional variance, the conditional coefficient of variation, the conditional interquartile range, and probability intervals (Dimitrakopoulos, Godoy, and Chou, 2009), which measure the level of uncertainty on the SMU grades.

For instance, Figure 10 displays the conditional coefficient of variation at the support of SMUs, calculated

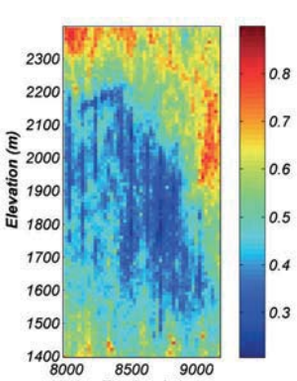

Figure 10—Local coefficient of variation of the block-support copper grade

with 100 realizations of the block-support copper grade for the selected section at northing 4800 m. This coefficient constitutes an appropriate measure for classifying the resources for a considered uncertainty level (Emery, Ortiz, and Rodríguez, 2006; Dimitrakopoulos, Godoy, and Chou, 2009). The areas located in the top and bottom parts of the region displayed in Figure 10 correspond to sparsely sampled areas, in which the uncertainty in the true grades turns out to be higher than in densely sampled areas (Figure 4).

Conclusions

The objective of the approach developed for Sungun was to remove current limitations of conventional techniques for determining the recoverable mineral resources and to ensure robust mineral resource models capable of handling (1) the change of support from the data support (drill-hole composite) to the target SMU block; (2) the multivariate nature of the ore control selection criteria, which involve not only copper but also molybdenum; and (3) the uncertainty in the actual (unknown) block grades. The solution presented in this paper is to construct a set of alternative block grade models using direct block-support cosimulation. Regarding the sought objectives, the proposed approach is remarkably simple, depending on a few key parameters (essentially, the transformation functions from grades to normal scores and the coregionalization model for the normal scores data).

Block-support cosimulation has interesting applications for predicting recoverable resources. It allows a full and proper characterization of the variability of the key elements at all spatial scales within the orebody. The post-processing of the realizations allows for measurement of the uncertainty in the resources recoverable above any cut-off, at both global and local scales, and provides a characterization of the risk attached to the mining project due to the uncertainty on the mineral resources. These are useful tools that can be incorporated into exploration, exploitation, and scheduling of the Sungun porphyry deposit.

Acknowledgements

The authors are grateful to Sungun copper mine for providing the data-set used in this work. This work was partially supported by the Chilean Commission for Scientific and Technological Research, through Projects CONICYT / FONDECYT / REGULAR / N°1130085 and CONICYT PIA Anillo ACT 1407.

References

Asghari, O. and Hezarkhani, A. 2008. Applying discriminant analysis to separate the alteration zones within the Sungun porphyry copper deposit. *Journal of Applied Sciences*, vol. 8, no. 24. pp. 4472–4486.

Ataei, M. and Osanloo, M. 2003. Determination of optimum cutoff grades of multiple metal deposits by using the golden section search method. *Journal of the South African Institute of Mining and Metallurgy*, vol. 103, no. 8. pp. 493–499.

Boucher, A. and Dimitrakopoulos, R. 2009. Block simulation of multiple correlated variables *Mathematical Geosciences*, vol. 41. pp. 215–237

Chilès, J.P. and Delfiner, P. 2012. Geostatistics: Modeling Spatial Uncertainty. 2nd edn. Wiley, New York

David, M. 1988. Handbook of Applied Advanced Geostatistical Ore Reserve Estimation. Elsevier, Amsterdam.

Davis, M.W. 1987. Production of conditional simulations via the LU triangular decomposition of the covariance matrix. *Mathematical geology*, vol. 19, no. 2. pp. 91–98

Dimitrakopoulos, R. 1997. Conditional simulations: tools for modelling uncertainty in open pit optimisation. *Optimizing with Whittle*. Whittle Programming (Pty) Ltd, Perth. pp 31–42.

Dimitrakopoulos, R. 2012. Advances in orebody modelling and strategic mine planning. *Spectrum Series 17*. Australasian Iinstitute of Mining and Metallurgy, Melbourne. 345 pp.

Dimitrakopoulos, R., Godoy, M., and Chou, C.L. 2009. Resource/reserve classification with integrated geometric and local grade variability measures. *Proceedings of Orebody Modelling and Strategic Mine Planning 2009.* Australasian Institute of Mining and Metallurgy, Melbourne. pp. 207–214.

Emery, X. 2007. Conditioning simulations of Gaussian random fields by ordinary kriging. *Mathematical Geology*, vol. 39, no. 6. pp. 607–623.

Emery, X. 2009. Change-of-support models and computer programs for direct block-support simulation. *Computers and Geosciences*, vol. 35, no. 10. pp. 2047–2056.

Emery, X. 2010. Iterative algorithms for fitting a linear model of coregionalization. *Computers and Geosciences*, vol. 36, no. 9. pp. 1150–1160.

Emery, X. and Ortiz, J.M. 2011. Two approaches to direct block-support conditional co-simulation. *Computers and Geosciences*, vol. 37, no. 8. pp. 1015–1025.

Emery, X., Ortiz, J.M., and Rodríguez, J.J. 2006. Quantifying uncertainty in mineral resources by use of classification schemes and conditional simulations. *Mathematical Geology*, vol. 38, no. 4. pp. 445–464.

Goulard, M. and Voltz, M. 1992. Linear coregionalization model: tools for estimation and choice of cross-variogram matrix. *Mathematical Geology*, vol. 24, no. 3. pp. 269–286.

Hezarkhani, A. 2006. Petrology of intrusive rocks within the sungun porphyry copper deposit, Azarbaijan, Iran. *Journal of Asian Earth Sciences*, vol. 27, no. 3. pp. 326–340.

Hezarkhani, A. and Williams-Jones, A.E. 1998. Controls of alteration and mineralization in the sungun porphyry copper deposit, Iran: evidence from fluid inclusions and stable isotopes. *Economic Geology*, vol. 93. pp. 651–670.

Journel, A.G. and Huijbregts, C.J. 1978. Mining Geostatistics. Academic Press, New York.

Khan, K.D. and Deutsch C.V. 2015. Practical incorporation of multivariate parameter uncertainty in geostatistical resource modeling. *Natural Resources Research*. pp. 1–20.

Montoya, C., Emery, X., Rubio, E., and Wiertz, J. 2012. Multivariate resource modelling for assessing uncertainty in mine design and mine planning, *Journal of the Southern African Institute of Mining and Metallurgy*, vol. 112. pp. 353–363.

Osanloo, M., and Ataei, M. 2003. Using equivalent grade factors to find the optimum cut-off grades of multiple metal deposits. *Minerals Engineering*, vol. 16, no. 8. pp. 771–776.

Rossi, M.E. and Deutsch, C.V. 2014. Mineral Resource Estimation. Springer, New York.

Soltani, F., Afzal, P., and Asghari, O. 2014. Delineation of alteration zones based on Sequential Gaussian Simulation and concentration-volume fractal modeling in the hypogene zone of Sungun copper deposit NW Iran. *Journal of Geochemical Exploration*, vol. 140. pp. 64–76.

Tahmasebi, P., Hezarkhani, A., and Mortazavi, M. 2010. Application of discriminant analysis for alteration separation; Sungun copper deposit, East Azerbaijan, Iran. *Australian Journal of Basic and Applied Sciences*, vol. 6, no. 4. pp. 564–576.

Talebi, H., Asghari, O., and Emery, X. 2015. Stochastic rock type modeling in a porphyry copper deposit and its application to copper grade evaluation. *Journal of Geochemical Exploration*, vol. 157. pp. 162–168.

Wackernagel, H. 2003. Multivariate Geostatistics—An Introduction with Applications. Springer, Berlin. ◆

Appendix

Consider the simulation for a target block v discretized into M points $\{\mathbf{x}_1 \dots \mathbf{x}_M\}$. For the sake of simplicity, the example is restricted to a single Gaussian random field Y_1 and to the use of simple kriging to derive the conditional distributions, but the formalism can be extended to more random fields and/or to ordinary kriging.

Suppose that one finds two point-support data (located at $\mathbf{u}_1$ and $\mathbf{u}_2$) and two block-support data (located at blocks v_1 and v_2) in the neighborhood of block v. The simple kriging system can be written as:

$$\begin{pmatrix} C(\mathbf{u}_1,\mathbf{u}_1) & C(\mathbf{u}_1,\mathbf{u}_2) & C(\mathbf{u}_1,v_1) & C(\mathbf{u}_1,v_2) \\ C(\mathbf{u}_2,\mathbf{u}_1) & C(\mathbf{u}_2,\mathbf{u}_2) & C(\mathbf{u}_2,v_1) & C(\mathbf{u}_2,v_2) \\ C(v_1,\mathbf{u}_1) & C(v_1,\mathbf{u}_2) & C(v_1,v_1) & C(v_1,v_2) \\ C(v_2,\mathbf{u}_1) & C(v_2,\mathbf{u}_2) & C(v_2,v_1) & C(v_2,v_2) \end{pmatrix} \begin{pmatrix} \lambda_{1,1} & \cdots & \lambda_{1,M} \\ \lambda_{2,1} & \cdots & \lambda_{2,M} \\ \omega_{1,1} & \cdots & \omega_{1,M} \\ \omega_{2,1} & \cdots & \omega_{2,M} \end{pmatrix} = \begin{pmatrix} C(\mathbf{u}_1,\mathbf{x}_1) & \cdots & C(\mathbf{u}_1,\mathbf{x}_M) \\ C(\mathbf{u}_2,\mathbf{x}_1) & \cdots & C(\mathbf{u}_2,\mathbf{x}_M) \\ C(v_1,\mathbf{x}_1) & \cdots & C(v_1,\mathbf{x}_M) \\ C(v_2,\mathbf{x}_1) & \cdots & C(v_2,\mathbf{x}_M) \end{pmatrix}$$

where the right-hand-side member contains the data-to-target covariances (given by Equations [3] and [4]), while the left-hand-side member contains the data-to-data covariance matrix (given by Equations [3] to [5]) and the matrix of kriging weights, in which $\lambda_{i,j}$ (respectively, $\omega_{i,j}$) indicates the weight assigned to the data at $\mathbf{u}_i$ (respectively, at v_i) when predicting the Gaussian random field at $\mathbf{x}_j$. The simple kriging prediction at location $\mathbf{x}_j$ is therefore:

$$Y_1^{SK}(\mathbf{x}_j) = \lambda_{1,j} Y_1(\mathbf{u}_1) + \lambda_{2,j} Y_1(\mathbf{u}_2) + \omega_{1,j} Y_1(v_1) + \omega_{2,j} Y_1(v_2)$$

On the other hand, the variance-covariance matrix of kriging errors is:

$$\boldsymbol{\Sigma}^{SK} = \begin{pmatrix} C(\mathbf{x}_1,\mathbf{x}_1) & \cdots & C(\mathbf{x}_1,\mathbf{x}_M) \\ \vdots & & \vdots \\ C(\mathbf{x}_M,\mathbf{x}_1) & \cdots & C(\mathbf{x}_M,\mathbf{x}_M) \end{pmatrix} - \begin{pmatrix} \lambda_{1,1} & \cdots & \lambda_{1,M} \\ \lambda_{2,1} & \cdots & \lambda_{2,M} \\ \omega_{1,1} & \cdots & \omega_{1,M} \\ \omega_{2,1} & \cdots & \omega_{2,M} \end{pmatrix}^T \begin{pmatrix} C(\mathbf{u}_1,\mathbf{x}_1) & \cdots & C(\mathbf{u}_1,\mathbf{x}_M) \\ C(\mathbf{u}_2,\mathbf{x}_1) & \cdots & C(\mathbf{u}_2,\mathbf{x}_M) \\ C(v_1,\mathbf{x}_1) & \cdots & C(v_1,\mathbf{x}_M) \\ C(v_2,\mathbf{x}_1) & \cdots & C(v_2,\mathbf{x}_M) \end{pmatrix}$$

Accordingly, one can simulate the Gaussian random field at locations $\mathbf{x}_1 \dots \mathbf{x}_M$ by putting (Davis, 1987):

$$\begin{pmatrix} Y_1(\mathbf{x}_1) \\ \vdots \\ Y_1(\mathbf{x}_M) \end{pmatrix} = \begin{pmatrix} Y_1^{SK}(\mathbf{x}_1) \\ \vdots \\ Y_1^{SK}(\mathbf{x}_M) \end{pmatrix} + \sqrt{\boldsymbol{\Sigma}^{SK}} \begin{pmatrix} U_1 \\ \vdots \\ U_M \end{pmatrix}$$

where $\sqrt{\boldsymbol{\Sigma}^{SK}}$ is a square root matrix or the Cholesky factor of $\boldsymbol{\Sigma}^{SK}$, while $U_1 \dots U_M$ are standard normal random variables, independent between themselves and independent of all the existing values of Y_1, either at point or block support. The simulated block-support value $Y_1(v)$ that will be used as a conditioning data in the subsequent steps of sequential simulation is finally obtained by averaging $Y_1(\mathbf{x}_1) \dots Y_1(\mathbf{x}_M)$, as per Equation [2], while the simulated value for the original grade variable on block v, $Z_1(v)$, is obtained by applying Equation [6]. $Y_1(\mathbf{x}_1) \dots Y_1(\mathbf{x}_M)$ and $Z_1(v)$ are not used in the subsequent steps of the simulation process.

Conference Announcement

SAIMM
THE SOUTHERN AFRICAN INSTITUTE OF MINING AND METALLURGY

MMMA

The Southern African Institute of Mining and Metallurgy
&
Mine Metallurgical Managers Association is proud to host the

WATER 2017
CONFERENCE
lifeblood of the mining industry

10–11 July 2017 Conference
12 July 2017 Technical Visit — Eastern Basin Plant

Emperors Palace, Hotel Casino Convention Resort Johannesburg

BACKGROUND

The mining industry is faced with a number of challenges regarding the use, recycling and management of their water resources. Some affected parties are unaware that the legislation around the use of water has become more onerous and strict controls have been put in place. This includes the requirements for the application of water use licences.

The scarcity of water in the Southern African region is a fact and the availability of water is a major consideration in the development of mining ventures across the sub-continent. The water authorities throughout the region have developed strategies to address the needs of the mines and their surrounding communities.

Acid Mine Drainage has been a reality for quite some time and with the 'closure' of mines on the Witwatersrand it has become a major issue for communities in Gauteng. A number of initiatives have been put in place to address the challenge and the enormity of the task has taken many by surprise.

The use of fresh water alone is no longer an option and users have to consider alternatives in the treatment and recycling of water. Major advances have been made in the processing of water yet these options have not been shared with the engineers on the mines.

TOPICS

The Conference will include but not be limited to the following topics:

- Legal requirements, amendments, and compliance
- What is required to obtain a water licence
- Acid mine drainage
- Status of water supply
- New technology in proccessing and recovering of water
- Treatment plants
- Water analysis
- Wetlands
- Agriculture *vs.* Mining
- Case studies
- Research.

OBJECTIVE

- To sensitise the mining and metallurgical industry to the requirements of the new legislation
- Share the overall water distribution strategy across the sub-continent
- Introduce new technology for the processing and recycling of water
- Report on various initiatives in the reclaiming of water
- Update interested parties on the status of the Acid Mine Drainage threat.

WHO SHOULD ATTEND

- Senior and operational management of mines
- Engineers responsible for mine water management
- Regional and national officials from DoE, DMR, DWS, and DEA
- Companies and individuals offering water related solutions
- Researchers
- Environmentalists and NGOs
- Agricultural sector.

Sponsor LANXESS Energizing Chemistry
LANXESS Chrome Mining (Pty) Ltd.

SAIMM
THE SOUTHERN AFRICAN INSTITUTE OF MINING AND METALLURGY

For further information contact:
Camielah Jardine Head of Conferencing • Saimm
P O Box 61127, Marshalltown 2107
Tel: +27 (0) 11 834-1273/7 E-mail: camielah@saimm.co.za
Website: http://www.saimm.co.za

http://dx.doi.org/10.17159/2411-9717/2017/v117n6a9

The needle penetration test for predicting coal strength

by S. Kahraman*, A.S. Aloglu†, B. Aydin*, and E. Saygin*

Synopsis

The coal strength parameter is used in operations such as the selection and design of mechanical excavators and coal crushing/grinding equipment. However, coring or cutting prismatic specimens from coal for the standard strength tests is difficult, and sometimes not possible. For this reason a method for the indirect determination of coal strength from easy tests would be useful. In this study, the predictability of coal strength from the needle penetration test was investigated. This is a very easy and practical test method. Point load and needle penetration index (NPI) tests were carried out on coal specimens from Çayırhan coalfield in Turkey. The point load indexes were converted to the uniaxial compressive strength (UCS) values by using the general conversion factor. The UCS and NPI values were evaluated using regression analysis. A strong linear relationship was found between the two parameters. The conversion factor for the UCS-NPI ratio is 0.35 for the tested coal samples. It is concluded that the UCS of coal can be predicted from the NPI.

Keywords

coal, uniaxial compressive strength, needle penetration index.

Introduction

Knowledge of coal strength is important for the selection and design of mechanical excavators and coal crushing and grinding equipment. Uniaxial compressive strength of coal is used in designing pillar dimensions in room and pillar mining. Coals always contain bedding planes and cleats; they are also brittle and fragile. Therefore, coring or cutting prismatic specimens from coal for the standard strength tests is difficult, and sometimes not possible. For this reason, a method for the estimation of coal strength from easy tests would be useful.

The needle penetration test is a nondestructive index test that is applicable both in the field and the laboratory and does not require any special sample preparation. The test has been used for the estimation of physical and mechanical properties of weak or soft rocks (Okada *et al.*, 1985; Yamaguchi *et al.*, 1997; Takahashi, Noto, and Yokokawa, 1988; Uchida *et al.*, 2004; Aydan *et al.*, 2006; Aydan, Watanabe, and Tokashiki, 2008; Aydan, 2012; Erguler and Ulusay, 2007; Park, Obara, and Kan, 2011; Ulusay and Erguler, 2012; Aydan and Ulusay, 2013; Aydan. Sato, and Yagi, 2014). This study investigates the predictability of coal strength from the needle penetration test.

Previous studies

The needle penetration test was originally developed by MARUTO Testing Machine Company (1999) for estimating the uniaxial compressive strength (UCS) of soft rocks. Several researchers have used the needle penetration index (NPI) to estimate the uniaxial compressive strength of rocks (Okada *et al.*, 1985; Yamaguchi *et al.*, 1997; Takahashi, Noto, and Yokokawa, 1988; Uchida *et al.*, 2004; Aydan *et al.*, 2006; Aydan, Watanabe, and Tokashiki, 2008; Aydan, 2012; Erguler and Ulusay, 2007; Park, Obara, and Kan, 2011; Ulusay and Erguler, 2012). Some researchers have also investigated the relations between the NPI and other rock properties such as tensile strength, Young's modulus (Aydan, 2012; Aydan and Ulusay, 2013; Aydan, Sato, and Yagi, 2014), and P- and S-wave velocities (Aydan, 2012; Aydan, Sato, and Yagi, 2014), cohesion, and friction angle (Aydan, Sato, and Yagi, 2014).

Ulusay and Erguler (2012) evaluated a database consisting of a total of 725 UCS–NPI data pairs from previous studies and additional tests and suggested the following relationship between UCS and NPI:

$$UCS=0.4NPI^{0.929} \quad [1]$$

where the UCS is measured in megapascals and the NPI in newtons per millimetre.

Although Equation [1] is not linear, Aydan (2012) found the following linear relationship for different rock types such as tuff, sandstone, pumice, limestone, and lignite measures (lignite, mudstone, siltstone, marl, loam):

$$UCS=0.2NPI \quad [2]$$

Aydan (2012) also stated that the conversion factor for the UCS-NPI relation

* *Mining Engineering Department, Hacettepe University, Ankara, Turkey.*

† *CINER Group, Ankara, Turkey.*

 ISSN 2225-6253. Paper received June 2016; revised paper received Sept. 2016.

ranges between 0.06 and 0.7, and the relationship should be evaluated individually for each rock group to improve the correlations.

Recently, Aydan and Ulusay (2013) derived the following relation for Derinkuyu tuff:

$$UCS=0.3NPI \quad [3]$$

Geology and sampling

Coal samples were provided from the Çayırhan underground lignite mine located in Çayırhan Town of Nallıhan County, 122 km west of Ankara, Turkey (Figure 1).

The Cayirhan coal basin comprises a Miocene series termed M1, M2, M3, and M4 and Pliocene formation (Figure 2). Coal seams are located in the M1 formation, which is some four kilometers wide and approximately 25 km long, elongated in a southwest to northeast direction (Haciosmanoglu, 2004). There are two lignite seams – seams 1 and 2 – in the basin, which vary in thickness from 1.7 to 2.0 m. The two seams are separated by an interburden with a thickness of 1.3–2.0 m in the western part of the area and 0.5–0.7 m on the eastern side (Aydin and Kaygusuz, 2001).

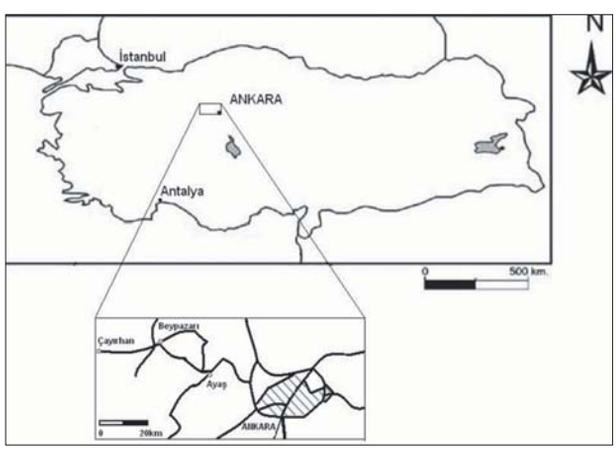

Figure 1—Location of Çayırhan coal mine

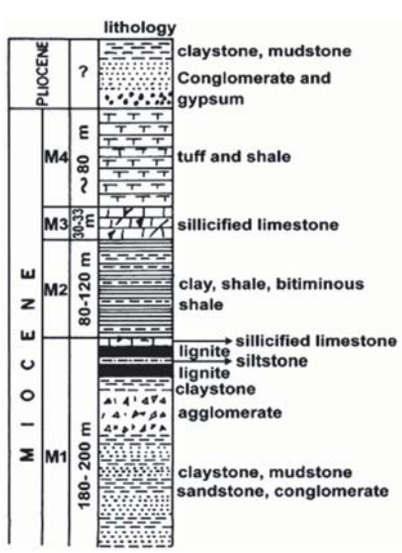

Figure 2—Vertical cross-section of the Cayirhan coal basin (Aydin and Funfstuck, 1988)

The dry ash-free carbon content of the coals varies between 61% and 80%, which is a very large range, from lignite to high-volatile C bituminous coal rank. The average bed moisture of the samples was 24.3%, which puts them in the sub-bituminous coal rank. The major inorganic mineral phases found in the raw coal are clinoptilolite, analcime, and pyrite, with variable minor amounts of quartz, albite-anorthite, gypsum, marcasite, illite, dolomite, and apatite (Whateley *et al.*, 1996).

Several researchers have carried out mechanical and physical tests on Cayirhan coal. Their results are summarized in Table I.

The mine was visited and the block samples of coals were collected from the ten different locations (Table II, Figure 3) and transported to the laboratory for testing.

Table I

Mechanical and physical properties of Çayirhan coal

UCS (MPa)		Tensile strength (MPa)		Density (g/cm^3)		Source
Lower coal bed	Upper coal bed	Lower coal bed	Upper coal bed	Lower coal bed	Upper coal bed	
8.6	7.9	2.10	2.60	---	---	Tiryaki *et al.* (2001)
10.2	7.1	2.15	1.94	1.53	1.53	Keles, 2005
12.1	10.8	1.29	1.07	1.38	1.37	Bilim, 2007

Table II

Sampling locations

Code	Sampling location	Sampling point
1	Roadway D210/3	316th metre
2	Roadway D210	136.5th metre
3	Roadway D210	136.5th metre
4	Roadway D210/2	321st metre
5	Access gallery D210	300th metre
6	Ventilation gallery D	1111.75th metre
7	Roadway G 510	1542nd metre
8	Roadway G 510	1551st metre
9	Ventilation gallery D	1106.75th metre
10	Ventilation gallery D	112.75th metre

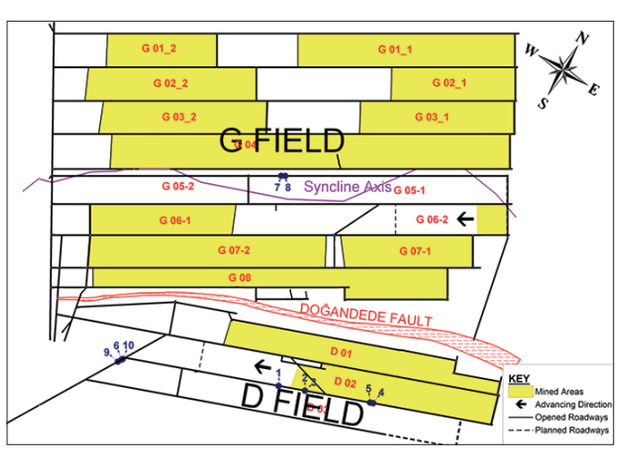

Figure 3—Mine plan showing the sampling locations

Figure 4—Some of the test specimens used in the point load tests

Point load test

Since the coal samples were weak, intact samples could not be prepared for the uniaxial compressive strength test. For this reason point load testing was selected for the strength test. About 70 prismatic test specimens were prepared from the coal blocks by diamond sawing (Figure 4). However, only 46 test results were accepted due to invalid failure modes observed in numerous specimens during testing due to the brittle nature of coal.

After calculating point load index values, the results were corrected to a specimen diameter of 50 mm. Franklin (1985) suggests that the ratio between the UCS and point load index is approximately 22 for different rock types. Therefore, point load index values were multiplied by 22 and converted to the UCS values.

Needle penetration test

The needle penetrometer was developed by MARUTO Co. in Japan to estimate the UCS of soft rocks. It is a lightweight portable device with a weight of about 700 g. The needle is a hardened steel, 0.84 mm diameter rod with a conical tip. The major components of the device are a plunger, chuck, penetration scale (0–10 mm in 1 mm graduations), load scale (0–100 N in 10 N graduations), load indicator ring, cap (removable; spare penetration needles contained in the grip), penetration needle, and spring mounted in the penetrometer grip as shown Figure 5.

The needle of the penetrometer is pushed into the rock until a force of 100 N is reached and the penetration depth is measured from the position of the plunger on the penetration scale. The maximum penetration depth (10 mm) may be attained for softer and saturated rocks before the maximum penetration force is reached. In this case, the test stops at this depth, the penetration load is read from the load scale, and the NPI is calculated from the following equations:

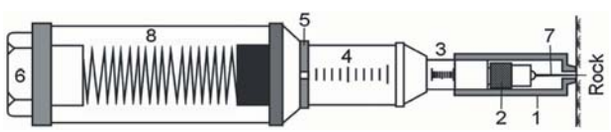

Figure 5 – The needle penetrometer. (1) plunger, (2) chuck, (3) penetration scale, (4) load scale, (5) load indicating ring, (6) cap, (7) penetration needle, and (8) spring (Tiryaki *et al.*, 2001)

For $F = 100$ N and $D \leq 10$ mm $\quad NPI = 100/D$ [4]

For $D = 10$ mm and $F \leq 100$ N $\quad NPI = F/10$ [5]

where NPI is the needle penetration index (N/mm), F is the applied load (N), and D is the depth of penetration (mm) (Ulusay *et al.*, 2014).

The needle penetration tests were carried out on the coal samples that failed in the point load tests (Figure 6). The tests were carried out on the top and bottom surfaces of the specimens at least four times and the results averaged to pair up with the corresponding UCS values for that particular specimen.

Results and discussion

The descriptive statistics of the test results are listed in Table III. The skewness values of each test are also given. In

Figure 6—The needle penetration test

Table III

Descriptive statistics of the test results

Statistical parameter	UCS (MPa)	NPI (N/mm)
Number of data	46	184
Minimum value	1.00	1.00
Maximum value	16.04	51.30
Average value	6.59	18.18
Standard deviation	± 3.64	± 12.69
Skewness	0.45	1.19

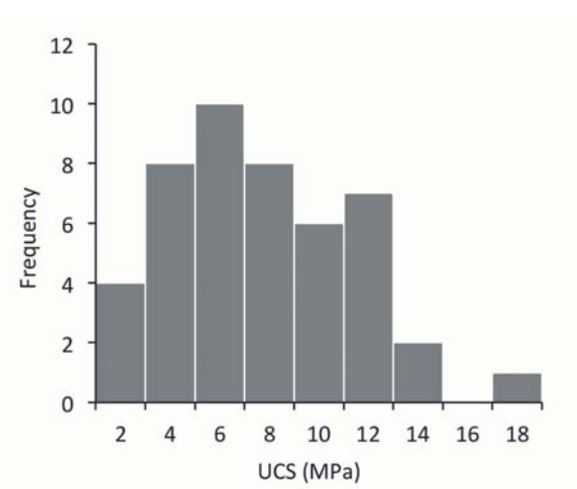

Figure 7—Histogram plot for the UCS data

addition, histogram plots of the UCS and NPI values are presented (Figures 7 and 8). The skewness values and histogram plots indicate that the data for UCS and NPI show fairly normal distributions.

The UCS and average NPI values were analysed using the method of least-squares regression. Linear approximation was executed to check the correlation between the UCS and NPI, as shown in Figure 9. The UCS increases with increasing NPI. The equation and the correlation coefficient of the relation (r) are:

$$UCS=0.35NPI \qquad r = 0.81 \qquad [6]$$

Although the data points are a bit scattered, the correlation coefficient is high enough for the estimation purposes. The scattering is probably due to the brittle nature of the coal.

Aydan (2012) showed that the conversion factor for the UCS-NPI relationship ranged between 0.06 and 0.7 and most of the data points were concentrated around the regression line with a slope of 0.2. In this study, the conversion factor of 0.35 (Equation [6]) falls in the range defined by Aydan (2012). In order to make a comparison, Equations [1]–[3] and [6] were plotted (Figure 10). Equation [6] indicates almost the same trend as the models derived by Ulusay and Erguler (2012) and Aydan and Ulusay (2013). There is a small difference between Equation [6] and the model derived by Aydan (2012). The derivation of a general equation for all rock types is difficult. Aydan (2012) stated that the conversion factor for the UCS-NPI relationship should be evaluated for each rock group separately in order to improve the correlations.

The correlation coefficient of the derived equation is good, but this does not necessarily identify a valid model. For this reason, the validation of the relationship was checked by the *t*-test and the *F*-test.

The significance of r values can be determined by the *t*-test, assuming that both variables are normally distributed and observations are chosen randomly. The test compares the computed *t*-value with the tabulated *t*-value using the null hypothesis. In this test, a 95% level of confidence was chosen. If the computed *t*-value is greater than tabulated *t*-value, the null hypothesis is rejected. This means that r is significant. If the computed *t*-value is less than tabulated *t*-value, the null hypothesis is not rejected. In this case, *r* is not significant. As seen in Table III, the computed *t*-value is greater than tabulated *t*-value. Therefore, it can be said that the derived equation is valid according to the *t*-test.

The significance of regressions was determined by the analysis of variance. In this test, a 95% level of confidence was chosen. If the computed *F*-value is greater than tabulated *F*-value, the null hypothesis is rejected, and there is a real relationship between the dependent and independent variables. The computed *F*-value is greater than the tabulated *F*-value, as shown in Table IV. Therefore, it is concluded that the derived equation is valid according to the *F* -test.

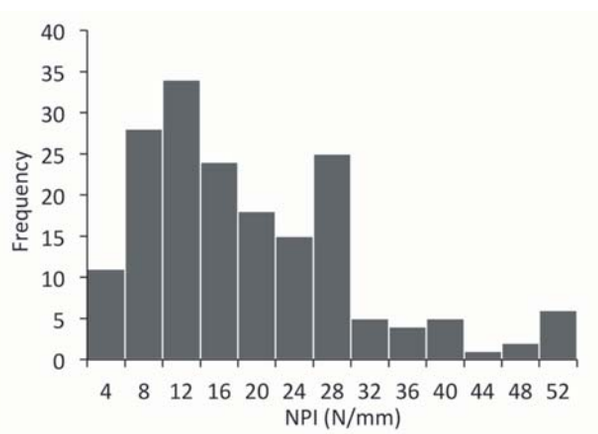

Figure 8—Histogram plot for the NPI data

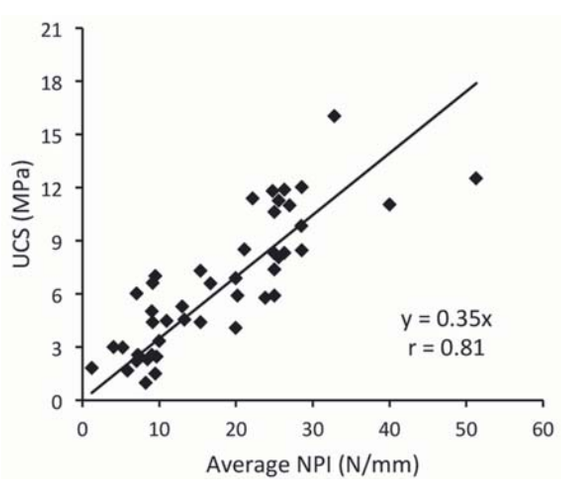

Figure 9—Correlation between the UCS and NPI for Cayirhan coal

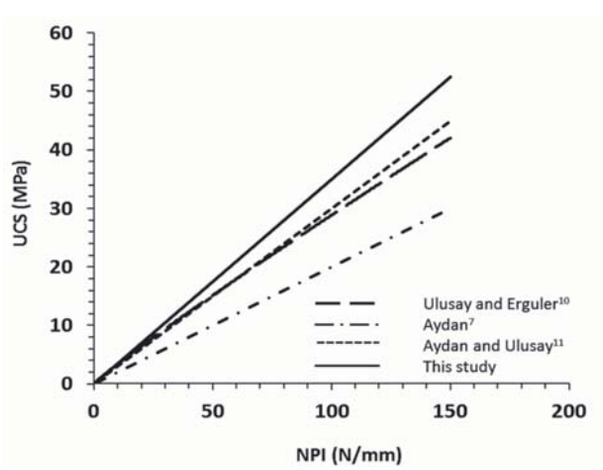

Figure 10—Comparison of conversion factors for the UCS-NPI relation: this study (Equation [6]) and the previous models

Table IV

***t*- and *F*-test results for Equation [6]**

t-table	*t*-test	*F*-table	*F*-test
± 2.01	10.13	3.94	49.19

Conclusions

Point load and the needle penetration index tests were carried out on Çayirhan coal specimens in the laboratory in order to investigate the predictability of coal strength from the needle penetration index.

The regression analysis indicated that there is a linear relationship between uniaxial compressive strength and the needle penetration index, and the correlation coefficient is high. The statistical tests also show that the derived relationship is significant. The derived correlation shows a similar trend to those found in the literature. It is concluded that the strength of Çayirhan coal can be predicted easily from the needle penetration index by using the derived correlation. Further research is necessary to check if the derived equation is valid for other coal types.

Acknowledgement

The authors thank TUBITAK (the Scientific and Technological Research Council of Turkey) for the support of the project (Project No. 114M836). We also thank the CINER Group for providing samples.

References

AYDAN, O. 2012. The inference of physico-mechanical properties of soft rocks and the evaluation of the effect of water content and weathering on their mechanical properties from needle penetration tests. *Proceedings of the 46th US Rock Mechanics and Geomechanics Symposium*, Chicago, IL, 24–27 June 2012. Paper no. ARMA12- 639. American Rock Mechanics Association, Alexandria, VA. [on CD].

AYDAN, O. and ULUSAY, R. 2013. Geomechanical evaluation of Derinkuyu antique underground city and its implications in geoengineering. *Rock Mechanics and Rock Engineering,* vol. 46. pp. 731–754.

AYDAN, O., SEIKI, T., ITO, T., ULUSAY, R., and YUZER, E. 2006. A comparative study on engineering properties of tuffs from Cappadocia of Turkey and Oya of Japan. *Proceedings of the Symposium on Modern Applications of Engineering Geology*. Turkish National Group of Engineering Geology, Denizli, Turkey. pp. 425–433.

AYDAN, O., WATANABE, S., and TOKASHIKI, N. 2008. The inference of mechanical properties of rocks from penetration tests. *Proceedings of the 5th Asian Rock Mechanics Symposium (ARMS5)*, Tehran, Iran, 24–26 November 2008. International Society for Rock Mechanics, Lisbon, Portugal. Vol 1. pp. 213–220.

AYDAN. O., SATO, A., and YAGI, M. 2014. The inference of geo-mechanical properties of soft rocks and their degradation from needle penetration tests. *Rock Mechanics and Rock Engineering*, vol. 47. pp. 1867–1890.

AYDIN, Y. and FUNFSTUCK 1988. Beypazari Project report. *Proceedings of the Sixth Coal Congress of Turkey*. Chamber of Mining Engineers of Turkey, Ankara. pp. 53–71 (in Turkish).

AYDIN, Y. and KAYGUSUZ, Y. 2001. Evaluation of single-slice and twin-face operations of Cayirhan lignite seams. *Proceedings of the 17th International Mining Congress and Exhibition of Turkey (IMCET 2001)*, Ankara, Turkey, 19–22 June 2001. Chamber of Mining Engineers of Turkey, Ankara. pp. 567–573.

BILIM, N. 2007. Çayırhan yeraltı kömür oca ında kazı makinalarının performanslarının ara tırılması ve kayaç özellikleri ile ili kilendirilmesi. [Investigation of the performance of excavators in Çayirhan underground coal mine as related to rock properties] PhD thesis, Selcuk University, Konya, Turkey. 270 pp. (In Turkish).

ERGULER, Z.A. and ULUSAY, R. 2007. Estimation of uniaxial compressive strength of clay-bearing weak rocks using needle penetration response. *Proceedings of the 11th Congress of the International Society of Rock Mechanics,* Lisbon, Portugal. Vol 1. pp. 265–268.

FRANKLIN, J.A. 1985. Suggested method for determining point load strength. *International Journal of Rock Mechanics and Mining Sciences & Geomechanics Abstracts*, vol. 22, no. 2. pp. 51–60.

HACIOSMANOGLU, M.E. 2004. Development of a subsidence model for Cayirhan coal mine. MSc thesis. Middle East Technical University, Ankara, Turkey. 154 pp.

KELES, S. 2005. Cutting performance assessment of a medium weight roadheader at Cayirhan coal mine. MSc thesis, Middle East Technical University, Ankara, Turkey. 58 pp.

Maruto TESTING MACHINE COMPANY. 1999. Instructions for SH-70 Penetrometer (NANGAN-PENETOROKEI). Tokyo, 4 pp. (in Japanese).

OKADA, S., IZUMIYA, Y., IIZUKA, Y., and HORIUCHI, S. 1985. The estimation of soft rock strength around a tunnel by needle penetration test. *Journal of the Japanese Society of Soil Mechanics and Foundation Engineering*, vol. 33, no. 2. pp. 35–38. (In Japanese).

PARK, Y., OBARA, Y., and KAN, S.S. 2011. Estimation of uniaxial compressive strength of weak rocks using needle penetrometer. *Proceedings of the 12th ISRM International Congress on Rock Mechanics*, Beijing, 18–21 October 2011. International Society for Rock Mechanics, Lisbon, Portugal. pp. 795–798.

TAKAHASHI, K., NOTO, K., and YOKOKAWA, I. 1988. Strength characteristics of Kobe formation in Akashi Strata (No. 1). *Proceedings of 10th Japan National Conference on Geotechnical Engineering*. Japanese Geotechnical Society. pp. 1231–1232. (In Japanese).

TIRYAKI, B., ATASOY, K., YASITLI, N.E., EYUBOGLU, A.S., and AYDIN, M.Z. 2001. Studies in the relationships between hardgrove grindability and some rock index tests on Cayirhan coals. *Proceedings of the 17th International Mining Congress and Exhibition of Turkey (IMCET 2001)*, Ankara, Turkey, 19–22 June 2001. Chamber of Mining Engineers of Turkey. pp. 451–458.

UCHIDA, N., ETOH, Y., ONO, H., and MIURA, N. 2004. Strength evaluation of deep mixing soil–cement by needle penetration test. *Journal of the Japanese Society of. Soil Mechanics and Foundation Engineering*, vol. 52, no. 7. pp. 23–25. (In Japanese).

ULUSAY, R. and ERGULER, Z.A. 2012. Needle penetration test: evaluation of its performance and possible uses in predicting strength of weak and soft rocks. *Engineering Geology*, vol. 149–150. pp. 47–56.

ULUSAY, R., AYDAN, O., ERGULER, Z.A., NGAN-TILLARD, D.J.M., SEIKI, T., VERWAAL, W., SASAKI, Y., and SATO, A. 2014. ISRM suggested method for the needle penetration test. *Rock Mechanics and Rock Engineering*, vol. 47. pp. 1073–1085.

WHATELEY, M.K.G., QUEROL, X., FERNANDEZ-TURIEL. J.L., and TUNCALI, E. 1996. Zeolites in Tertiary coal from the Cayirhan mine, Beypazari, Turkey. *Mineralium Deposita*, vol. 31. pp. 529–538.

YAMAGUCHI, Y., OGAWA, N., KAWASAKI, M., and NAKAMURA, A. 1997. Evaluation of seepage failure response potential of dam foundation with simplified tests. *Journal of the Japanese Society of Engineering Geology*, vol. 38, no. 3. pp. 130–144. ◆

Entrepreneurship in Mining Forum

A Focus on New Business in Mining

25–26 July 2017 • De Beers, Johannesburg

YOUNG PROFESSIONALS COUNCIL

THE SOUTHERN AFRICAN INSTITUTE OF MINING AND METALLURGY

TOPICS

Business Development **Procurement and Compliance** **Finance**

ABOUT THE EVENT

The Young Professionals Council of the Southern African Institute of Mining and Metallurgy is bringing you two days of high impact Forums with top industry speakers and thought leaders talking about business opportunities in mining for small and medium sized businesses. Join one or all four Forums to interact with a panel of industry practitioners and business experts. Be part of the new wave of entrepreneurs taking advantage of the exciting business opportunities in mining.

Four exciting Forums at only R1250.00 per forum

FORUM 1 - DECIDE TO ACT NOW

Business Development 1

The Mining Industry is at the heart of the South African Economy and offer opportunities for innovative thinkers and entrepreneurs. Attend this forum to hear from business leaders and entrepreneurs about the opportunities that exist in the mining industry as it transforms itself as part of Industry 4.0 and adopts the latest digital and systems thinking.

- **Keynote:** Invention to Reality
- Industry 4.0 open opportunities in Mining
- The mining landscape for Entrepreneurs
- Women in Mining
- **Panel Discussions:** What opportunities exist for Entrepreneurs in the Mining Industry.

FORUM 2 - KNOW THE RULES OF THE GAME

Procurement and Compliance

This session will aim at transferring knowledge to the delegate on what are the rules of playing the game. These sessions will give the delegate the advantage of participating in discussions with businesses in the industry regarding policies around procurement with a focus on purchasing goods and services from small businesses and local suppliers. The delegate will leave this session prepared to become a successful business partner to the mining industry.

- **Keynote:** Opportunities for doing business in the Mining Industry
- Regulatory framework for local procurement
- Managing the supplier, client relationship (case studies)
- Processes and procedures followed by mines to procure goods and services from small businesses
- **Panel Discussion:** Challenges faced by small businesses to supply mines and how to overcome them.

FORUM 3 - ENABLE YOURSELF

Finance

One of the biggest challenge in having a successful business remains financing it. This forum aims to inform, educate, and advise young entrepreneurs on where to go and how to access available funding schemes suitable for their businesses. Experts will give advice and guidance on proper channels and procedures to assist in the challenging entrepreneurial journey of heading a thriving and successful business. It is a great learning platform from those who have insights in different funding models and their particular requirements. For attendees, this is also a perfect opportunity of networking and knowledge sharing with likeminded people.

- **Keynote:** Financing options for business start-ups (Risks and Benefits)
- What financial model works for my business?
- Strategies to attract more investors
- Knowing the most common financing pitfalls and avoiding them
- **Panel discussion:** Starting, growing and sustaining your business financially.

FORUM 4 - DO IT RIGHT

Business Development 2

This session will aim at transferring knowledge to the delegate on what are the right moves to stay ahead of the game. These sessions will give the delegate the advantage of participating in discussions with businesses in the industry that have walked to path to success and have speakers will share their experiences along the journey. The delegate will leave this session prepared for the challenges of entrepreneurship equipped with the knowledge to confidently take their business to the next level.

- **Keynote:** What does it take for an idea to become a reality?
- If I could do it all again, what would I do better?
- Keeping your hand on the pulse
- Join the crowd or stand alone?
- **Panel Discussion:** How do you contribute from your success back to the community, and how has that contributed back to you?

EXHIBITION/SPONSORSHIP

Sponsorship opportunities are available. Companies wishing to sponsor or exhibit should contact Head of Conferencing

For further information contact:

Camielah Jardine Head of Conferencing, Saimm, Tel: +27 (0) 11 834-1273/7 E-mail: camielah@saimm.co.za, Website: http://www.saimm.co.za

http://dx.doi.org/10.17159/2411-9717/2017/v117n6a10

Synthesis of 3-hydroxy-2-naphthyl hydroxamic acid collector: flotation performance and adsorption mechanism on bastnaesite

by Z. Yang*, W. Wu*, and X. Bian*

Synopsis

The synthesis of 3-hydroxy-2-naphthyl hydroxamic acid (H2O5) as a collector for bastnaesite is described. The flotation performance of H2O5 with respect to bastnaesite was investigated by flotation tests, measurements of the surface adsorption capacity, and polarizing microscopy. The results indicated that H2O5 exhibits superior collecting performance compared with direct flotation recovery of bastnaesite, with recoveries above 90% at pH 8–9. The adsorption mechanism of H2O5 on bastnaesite was studied by solution chemistry analysis and ζ-potential tests. The results showed that the adsorption of H2O5 is associated with the types and concentrations of hydrolysis products of rare earth cations on the bastnaesite surface. At pH 8–9, the hydrolysis-dominant components $RE(OH)^{2+}$ and $RE(OH)_2^{+}$ of the rare earth cations were adsorbed onto the bastnaesite surfaces, which were considered to be the major positive active points and were beneficial to chemical adsorption of the reagents. The pH range of 7–10 was optimum for bastnaesite floatability, and the adsorption of H2O5 on bastnaesite was by means of chemical adsorption through formation of a five-membered ring chelate.

Keywords

3-hydroxyl-2-naphthyl hydroxamic acid (H2O5), flotation, bastnaesite, chemical adsorption.

Introduction

The rare earth elements (REEs) have long been known as 'industrial gold' and are widely used in the petroleum, chemical, ceramic, metallurgical, and permanent magnet material industries because of their special physicochemical properties (Chen, 2011; Krishnamurthy and Guptac, 2002; Esquivel, Bohe, and Pasquevich, 2002; Abrahami, Xiao, and Yang, 2015). Demand for REEs is growing in response to continuous advances in science and technology. Currently, most REEs are extracted from bastnaesite ($(Ce,La)CO_3F$) (Chelgani *et al.*, 2015; Yosry, 1990), which is recovered from rare earth ores by flotation. Typically, hydroxamic acids are used as bastnaesite collectors (Xu, 2015; Ren, 1997; Mousumi and Venugopal, 2016). Research into the mechanism of interaction between hydroxamic acids and bastnaesite is important for improving the recoveries of bastnaesite. However, there have been few studies that examine this mechanism.

Compared to other available collectors, hydroxamic acid has been shown to have better selectivity for bastnaesite. Hydroxamic acids (R–CO–NHOH) are much weaker acids than the corresponding carboxylic acids with identical carbon chains (Jiang *et al.*, 2010; Buglyo *et al.*, 2007; Wu and Zhu, 2006; Herrera, 2003). However, hydroxamic acids are better at selecting chelating metal ions (Wang, Liu, and Miller, 2008; Griffith *et al.*, 2011). The two O atoms in the carbonyl and hydroxyl groups of a hydroxamate molecule bond with a metal cation to form a five-membered ring structure (Chelgani *et al.*, 2015). Researchers have reported on the surface complexes of hydroxamic acid and metal species on the mineral surfaces (Jiang *et al.*, 2010; Wu and Zhu, 2006). This research has led to the wide use of hydroxamic acids such as octyl hydroxamic acid and salicylhydroxamic acid as collectors for flotation recovery of metal oxide minerals, including copper (Lee, 1998), tin (Sreenivas and Padmanabhan, 2002) and rare earth minerals (Zhou *et al.*, 2015a; Jordens *et al.*, 2014).

Flotation is a complex physical and chemical process in which collectors play a decisive role. Flotation is a useful approach for fine-grained rare earth occurrences. Other physical separation methods (*e.g.* magnetic, gravity) have been proven to be impractical. There have been a number of investigations of flotation processes for bastnasite ores (Cai *et al.*, 2009). In each case conditions, including a suitable collector and pH, have been established for the flotation of the desired minerals and depression of unwanted minerals.

In our study, we used H2O5, which was synthesized in a laboratory, as a hydroxamic acid rare earth collector. We investigated the effects of H2O5 dosage and the flotation pH on pure bastnasite. Further, we studied the collecting property and adsorption mechanism of H2O5 on the surface of bastnasite.

* *School of Metallurgy, Northeastern University, Shenyang 110819, Liaoning,China.*

 ISSN 2225-6253. Paper received Oct. 2016; revised paper received Apr. 2017.

Materials and methods

Materials

Minerals

Hand-picked, high-purity bastnaesite was obtained from Baotou, Mongolia, China, and ground using a porcelain mill. The ground samples were wet-sieved to separate the particles that were less than 74 μm for flotation tests. A portion of this fraction was further ground in an agate mortar to obtain particles less than 5 μm for the zeta potential measurements.

Reagents

Analytical-grade HCl and NaOH were used as pH modifiers. Analytical-grade 3-hydroxy-2-naphthyl methyl acid, $NH_2OH{\cdot}HCl$, methanol, and H_2SO_4 were used to synthesize the collector. Distilled water with a pH of 6 to 7 was used to prepare all reagent solutions and for the flotation tests. Pine oil provided by Baogang Corporation (Inner Mongolia, China)was used as a frother. The 3-hydroxy-2-naphthyl hydroxamic acid collector was synthesized in the laboratory using the following method.

- *Synthesis of 3-hydroxy-2-naphthyl methyl acid methyl ester*—3-hydroxy-2-naphthyl methyl acid (1; 18.8 g, 0.1 mol) was reacted with methanol (16.0 g, 0.5 mol) in the presence of concentrated sulphuric acid (0.76 mL, 0.014 mol) at 65°C for 6 hours. The unreacted methanol was then removed under reduced pressure and 3-hydroxy-2-naphthyl acid methyl ester (2; 17.3 g) was obtained with 85.2% yield.
- *Synthesis of 3-hydroxy-2-naphthyl hydroxamic acid*—Sodium hydroxide (8.8 g, 0.2 mol) and hydroxylamine hydrochloride (7.64 g, 0.1 mol) were dissolved in water (50 mL). Within 0.5 hours, 3-hydroxy-2-naphthyl acid methyl ester (2; 20.3 g, 0.1 mol, dissolved in 60 mL methanol) was added at 50°C. The mixture was stirred for 8 hours at 50°C, then methanol was removed from the reaction mixture under reduced pressure, the residue was acidized with 3 mol/L HCl, and 3-hydroxy-2-naphthyl hydroxamic acid (3;16.4 g) was obtained with 71.2% yield.

The synthesis route is shown schematically in Figure 1.

Experimental

Flotation tests

Flotation tests were carried out using an XFD-0.1L flotation machine (mechanical agitation) with a 100 mL plexiglass cell. The impeller speed was fixed at 1500 r/min. The pH values of the pulp were measured by a PHS-3E pH meter. All the flotation tests were carried out at 25°C. For each test, 20.0 g mineral samples were placed in the cell with 100 mL distilled water at 25°C. After adding the required amount of collector (H205), the pulp was agitated for 2 minutes and the pH was then adjusted to a designated value with hydrochloric acid or sodium hydroxide solution before flotation. Flotation was conducted for 5 minutes. The concentrates and tailings were weighed after filtration and drying, respectively.

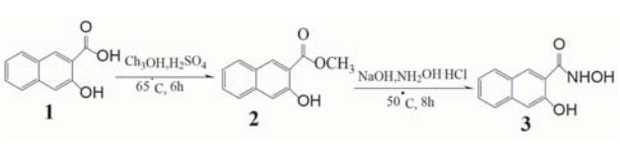

Figure 1—Synthesis route for 3-hydroxy-2-naphthyl hydroxamic acid

Zeta potential tests

The zeta potential tests were carried out using a JS94H electrophoresis apparatus (Beckman Coulter Inc., USA). 100 mg of -5 μm mineral samples were added to 40 mL of aqueous solution with or without 0.6 g/L H205, and then stirred for 15 minutes. The pH values were adjusted using HCl or NaOH solutions. Each sample was measured five times independently, and the average value was taken. For pH measurements, the samples were allowed to equilibrate for 5 minutes before measurement. To avoid zeta potential hysteresis, fresh samples were prepared for acidic and basic zeta potential measurements at 25°C.

Adsorption of H205 on the mineral surface

The H205 concentration in the aqueous solutions was measured by a UV-V double-beam UV-2100 spectrophotometer from Labtech Co. (China). Bastnaesite samples (1.0 g) with 0.6 g/L of H205 were measured at different pH values. The residual concentration of the surface collector solution was measured and then converted to the amount of H205 adsorbed on the bastnaesite surfaces. The samples were stirred for 5 minutes at 25°C, at a certain pH value, and then filtered and the residual concentration of H205 in the filtrate measured.

Results and discussion

Flotation results

Figure 2 showed the relationship between the recovery of bastnaesite and H2O5 dosage when the pH was adjusted to 8 using sodium hydroxide. The recovery increased with increasing H2O5 concentration, reaching a maximum of about 96% at an H2O5 dosage of 0.6 g/L. This demonstrates that bastnaesite has good floatability in the H2O5 flotation system.

Figure 3 shows the effect of pH on bastnaesite recovery at an H2O5 dosage of 0.6 g/L. At pH values of 7–10, the bastnaesite retained relatively good floatability and the recovery rates were all above 80%.

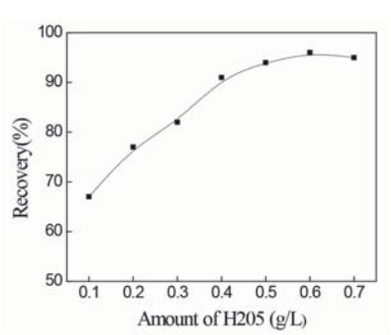

Figure 2—Relationship between floatability of bastnaesite and H2O5 dosage, at pH 8

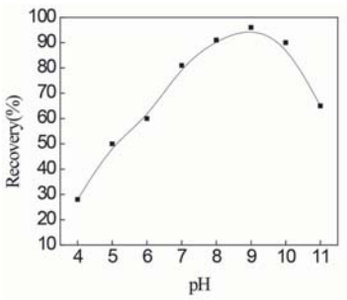

Figure 3—Effect of pH on the floatability of bastnaesite at 0.6 g/L H2O5

Polarizing microscopy

Figures 4–6 show images of bastnaesite flotation froth at an H205 dosage of 0.6 g/L and at pH values of 2, 8, and 13, respectively. It can be seen that many bastnaesite particles adhered to the bubble surfaces at pH 8, whereas the particles did not adhere to the bubble surfaces at pH 2 and pH 13.

Amount of H2O5 adsorption on bastnaesite surfaces

Figure 7 shows the effect of pH on the adsorption of H2O5 on the bastnaesite surfaces at an initial collector concentration of 0.6 g/L. At pH 2, adsorption of H2O5 was approximately zero. With increasing pH the adsorption rose sharply, reaching a maximum at pH 8, and then decreasing sharply to approximately zero at pH 12. Thus, it can be seen that the preferable pH range for H2O5 adsorption on the bastnaesite surfaces is 7 to 9, which is in accordance with the results of the flotation tests.

Solution chemistry analysis of the flotation process

H2O5 is a very weak acid – even weaker than carbonic acid (Xu, Xu, and Wang, 2002; Chi and Wang, 2014). According to the soft and hard acid-alkaline (HSAB) theory (Xu, Xu, and Wang, 2006), hydroxamic acid forms relatively unstable chelates with alkali metals, alkaline earth metals, and other ions. However, it forms relatively stable chelates with transition metals such as the REEs, iron, copper, and other hard acid metal ions. In these chelates, the chemical bonds between the metal ions and the hydroxamic acid are substantially coordinate-covalent bonds (Che *et al.*, 2004a, 2004b). The crystal surface characteristics of the minerals are closely associated with the floatability. The hydroxamic acid and lattice ions on the surfaces of the rare earth minerals are formed into a complex with a coordinate-covalent bond. This complex is strongly hydrophobic, and renders the minerals floatable when the mineral surfaces are covered. The chelate formed by the complex and the alkali metals or alkaline-earth metals and other ions is of an ionic type and is weakly hydrophobic, and therefore has relatively poor floatability in hydroxamic acid systems (Fuerstenau, 1985; Jordens, Chen, and Waters, 2013; O'Brien *et al.*, 1997; Sreenivas and Padmanabhan, 2002). According to this principle, using H2O5 as the collector, a rare earth concentrate suitable for further processing (above 50% rare earth oxides) can be obtained from complex rare earth ores by flotation.

In the flotation pulp system the conditions for interaction between the flotation reagents and the minerals are determined by the dissolution of the minerals, dissociation reactions of the reagents, hydrolysis reactions of the dissolved components, and chemical reactions of the flotation reagents. The chemical behaviour of the solution dominates the conditions and various balanced relations of these reactions (Ananthapadmanabhan and Somasundaran, 1985).

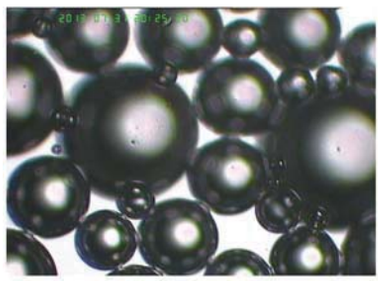

Figure 4—Bastnaesite flotation froth at pH 2, H205 dosage 0.6 g/L

Figure 5—Bastnaesite flotation froth at pH 8, H205 dosage 0.6 g/L

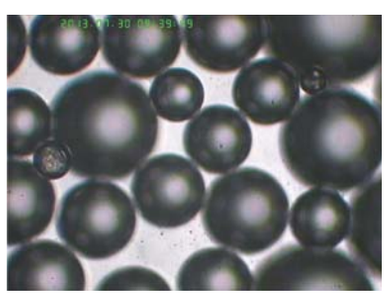

Figure 6—Bastnaesite flotation froth at pH 13, H205 dosage 0.6 g/L

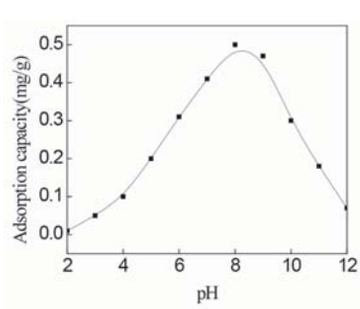

Figure 7—Effect of pH value on the adsorption of H2O5 on the bastnaesite surfaces at H2O5 dosage of 0.6 g/L

Once the minerals contact water, they will be dissolved. This is relevant to the properties of both the minerals and the solution. The dissolved mineral components will also undergo different chemical reactions to form a variety of chemical components, thereby affecting the surface properties of the minerals (Pugh, 1991).

After bastnaesite has been cracked and dissociated, rare earth cations are exposed on the surfaces of the lattices. Studies have shown that these ions have a relatively high hydration energy and easily undergo hydration in aqueous solutions to form hydroxyl-complex ions with strong surface activities, and can be strongly adsorbed in the compact layer (Stern layer) of the double electrode layer of bastnaesite, which affects the surface zeta potential of bastnaesite (Fuerstenau, 1983). In aqueous solutions, the rare-earth metal cations are hydrolysed. Ce^{3+} can be taken as an example. Figure 8 shows the hydrolytic equilibrium diagram in the aqueous solution at a Ce^{3+} concentration of 1×10^{-3} mol/L.

The hydrolysis reaction of Ce^{3+} in the aqueous solution can be written as follows (Ren *et al.*, 1997):

$$Ce^{3+} + H_2O \rightarrow Ce(OH)^{2+} + H^+ \quad K_1 = 10^{5.9}$$

$$Ce(OH)^{2+} + H_2O \rightarrow Ce(OH)^{+}_2 + H^+ \quad K_2 = 10^{5.8}$$

$$Ce(OH)^{+}_2 + H_2O \rightarrow Ce(OH)_3 + H^+ \quad K_3 = 10^{4.3}$$

$$Ce(OH)_3 + H_2O \rightarrow Ce(OH)^{-}_4 + H^+ \quad K_4 = 10^{2.0}$$

As shown in Figure 8, different hydrolysis products of the rare earth cations predominate in aqueous solution at different pH conditions, and their levels of concentration affect the chemical adsorption of the reagents. At pH<9, the dominant hydrolysis components are $Ce(OH)_2^+$, $Ce(OH)^{2+}$, and Ce^{3+}. At pH>9, the dominant hydrolysis components are $Ce(OH)_3$ and $Ce(OH)_4^-$, and the concentrations of $Ce(OH)^{2+}$ and Ce^{3+} began to decrease. At pH 8–9, the dominant components are $Ce(OH)_2^+$ and $Ce(OH)^{2+}$. This pH range is also the best for bastnaesite flotation (as shown in Figure 3). Hydroxamic acid anions dissociated from H2O5 undergo a chemical adsorption reaction with the hydroxy complexes on the surfaces of bastnaesite to form a stable five-membered ring complex, as shown in Figure 9. As a result, bastnaesite became hydrophobic (He and Vaisey, 2012). The OH- concentration in the pulp gradually increased at pH>9. According to the 'chemical reaction hypothesis' or the 'solubility product hypothesis' proposed by Taggart and Plaksins for flotation reagents (Hu, 2014), a $Ce(OH)_3$ cover film forms on the surfaces of bastnaesite, which prevents the combination of hydroximic acid ions with rare earth ions and reduces the recovery rate of bastnaesite. In an acidic medium (pH<7), the dominant hydrolysis component of the rare earth ion is Ce^{3+}. Theoretically, hydroximic acid could react with Ce^{3+} to form the chelate (Liu *et al.*, 1989). However, in this pH range bastnaesite had very poor floatability (as shown in Figure 3), indicating that the dominant hydrolysis component, Ce^{3+}, was unfavourable to flotation. According to the coordinated complexation reaction theory of coordination chemistry (Luo, 2012), as the pH of the flotation pulp is adjusted by addition of hydrochloric acid, Cl^- and hydroxamic acid in the pulp are adsorbed onto the surfaces of the minerals competitively to reduce the floatability. Furthermore, because hydroxamic acid is weaker than carbonic acid, when the pH is lowered, fewer hydroxamic acid ions dissociate from the pulp. According to the coordinated complexation reaction theory (Luo, 2012), when the concentration of ionic hydroxamic acid was reduced, the coordination capability with the ions on the bastnaesite surfaces was also lowered. This means that any acidic conditions are unfavourable for bastnaesite floatation.

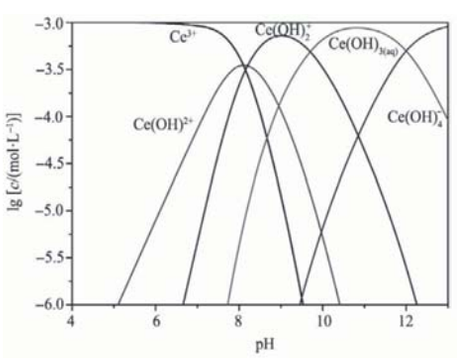

Figure 8—Aqueous solution equilibria for Ce^{3+} at 10^{-3} mol/L total solution concentration (Wang *et al.*, 2014)

Zeta potential analysis

Figure 10 shows the relationship between the zeta potential and pH. The isoelectric point (IEP) of pure bastnaesite was at pH 8.1. After bastnaesite reacted with H2O5, the zeta potential moved in the negative direction and the IEP moved from pH 8.1 to 6.6, which suggests that H205 ions were adsorbed on the bastnaesite surfaces. The collector was adsorbed on the mineral surfaces in an ionic form by either chemical adsorption or physical adsorption as a result of electrostatic attraction forces. In the pH range greater than the IEP, H2O5 could still be adsorbed onto the surfaces of the negatively charged bastnaesite to produce a higher negative potential. Therefore, we can conclude that H2O5 ions were not electrostatically adsorbed onto the surfaces of the bastnaesite, but entered the compact double-electrode layer of the bastnaesite by chemical adsorption.

Zeta potential that becomes more negative in the presence of a collector is associated with the compositions of both collector and the bastnaesite-water interface at different pH values. The organic compounds that contain hydroxamic acid groups (-CONHOH) have an affinity for REEs (Zhou, 2015). Since the pKa of H205 is about 7.0 (Che *et al.*, 2004a, 2004b), the polar group in H205 registers mainly as neutral hydroxamic acid groups (-CONHOH) at pH <7.0, and the H205 anion ($C(O^-)N(O^-)$) at pH >7.0. When H205 was introduced into the pulp at different pH values, its species

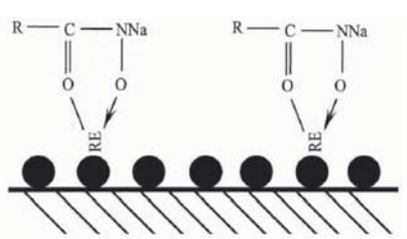

Figure 9—Action mode of H205 and bastnaesite (R=)

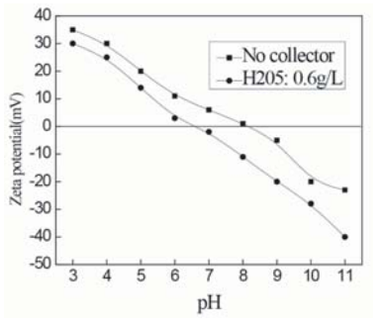

Figure 10—Relationship between zeta potential and pH

with more negative charge possibly replaced H_2O, OH^-, or O^{2-} in the bastnaesite/water interface, thus resulting in the zeta potential of the minerals declined (Zhou *et al.*, 2015a, 2015b; Jiang, Li, and Feng, 2011). The IEP of bastnaesite was at pH 8.0 (as shown in Figure 10). Since both bastnaesite and H205 are negatively charged at pH >8.0, the adsorption of H205 on the surfaces of bastnaesite has to overcome the electrostatic repulsion. However, H205 could be adsorbed on the bastnaesite surfaces at pH >8.0, so the collection of H205 to bastnaesite was a result of the chemical adsorption, which formed a five-membered ring chelate. At pH<8.0, because the IEP of bastnaesite in the absence of H205 was about pH 8.0. (as shown in Figure 10), bastnaesite is positively charged. H205 may adsorb on the bastnaesite surfaces by physical adsorption or chemical adsorption. The change in zeta potential could reflect the interaction between collector and mineral. In the presence of H205, the zeta potential of bastnaesite particles became more negative, inferring that H205 can adsorb onto bastnaesite surfaces.

Conclusions

1. H2O5 has a good collecting property for bastnaesite. The bastnaesite has relatively good floatability in the range of pH 7–10 and the best floatability at approximately pH 9
2. Chemical analysis of the mineral solution showed that the types and concentrations of the hydrolysis products of the rare earth cations on the surfaces of bastnaesite affect the floatability of the minerals. In aqueous solution at pH 8–9, the major hydrolysis products $RE(OH)^{2+}$ and $RE(OH)_2^+$ are the main positive active points and are adsorbed to the surfaces of the bastnaesite. At pH <7, the major hydrolysis product is RE_3^+, which is unfavourable for collection and considered to be the main negative active point. At pH >9, the major hydrolysis products are $RE(OH)_3$ and $RE(OH)_4^-$, which are adsorbed onto the bastnaesite surfaces. This is unfavourable for floatation and is also considered to be a main negative active point
3. Zeta potential analysis indicates that at pH 8–9, H2O5 is adsorbed chemically on the surface of the bastnaesite to form stable five-membered ring chelate. At pH <8.0, bastnaesite is positively charged and H205 may adsorb on the mineral surfaces by either physical or chemical adsorption.
4. Surface adsorption measurements indicate that the preferable pH range for H2O5 adsorption on bastnaesite surfaces is pH 7–10. H2O5 adsorption reaches its maximum value at pH 8.

Bastnaesite is a typical oxidized mineral, which is usually associated with fluorite, apatite, haematite, and quartz. According to our conclusions, H2O5 has a good collecting property for bastnaesite. The flotation performance of bastnaesite with H2O5 was best at pH 8–9. Water glass and sodium carboxymethyl cellulose (CMC) as depressants of gangue minerals (fluorite, apatite, haematite, and quartz), with H2O5 as collector, are recommended for bastnaesite flotation.

Open- and closed-circuit flotation experiments were carried out under the optimum conditions so as to simulate the industrial flotation process. The factors influencing the flotation process, such as the pulp concentration, mineral particle size, flotation temperature, and H205, depressant, and frother additions, were investigated to establish the optimum flotation conditions.. Preliminary tests covering gravity and magnetic separation were also conducted. Although flotation is the main concentration method for rare earth ores, other unit operations such as magnetic and gravity separation prior to flotation may obtain better results.

Acknowledgments

The authors acknowledge the support of the Major State Basic Research Development Program of China (973 program) (2012CBA01205).

References

Abrahami, S.T., Xiao, Y., and Yang, Y. 2015. Rare-earth elements recovery from post-consumer hard-disc drives. *Mineral Processing and Extractive Metallurgy*, vol. 124, no. 2. pp. 106–115.

Ananthapadmanabhan, K.P. and Somasundaran, P. 1985. Surface precipitation of inorganics and surfactants and its role in adsorption and flotation. *Colloids and Surfaces*, vol. 13. pp. 151–167.

Buglyo, P., Nagy, E.M., Farkas, E., Sovago, I., Sanna, D., and Micera, G. 2007. New insights into the metal ion–peptide hydroxamate interactions: metal complexes of primary hydroxamic acid derivatives of common dipeptides in aqueous solution. *Polyhedron*, vol. 26. pp. 1625–1633.

Cai, Z.L., Cao, M.L., Che, L.P., Yu, Y.F., and Hu, H.Y. 2009. Study on the beneficiation process for recovering rare-earth from the LIMS tailing of HIMS rougher concentrate after magnetizing roasting in Baogang concentrator. *Metal Mine*, vol. 7. p. 155 (in Chinese).

Chelgani, S., Chehreh A., Rudolph, M.A., Leistner, T.A., and Gutzmer, J.A. 2015. A review of rare earth minerals flotation: monazite and xenotime. *International Journal of Mining Science and Technology*, vol. 25. pp. 877–883.

Che, L.P., Yu, Y.F., Pang, J.X., Yuan, J.Z., and Zhang, F.G. 2004a. Application and trend of hydroximic acid as collectors on flotation of RE minerals. *Chinese Rare Earths*, vol. 25, no. 3. pp. 49–54 (in Chinese).

Che, L.P., Yu, Y.F., Pang, J.X., Yuan J.Z., and Wang X.T. 2004b. Synthesis and properties of hydroxamic acid collectors and their mechanism in the flotation of rare earth minerals. *Chinese Rare Earths*, vol. 25, no. 6. pp. 74–81 (in Chinese).

Chen, Z.H. 2011. Global rare earth resources and scenarios of future rare earth industry. *Journal of Rare Earths*, vol. 29, no. 1. pp. 1–5.

Chi, R.A. and Wang, D.Z. 2014. Mineral Processing of Rare Earth. 1st edn. Science Press, Beijing, China (in Chinese).

Esquivel, M.R., Bohe, A.E., and Pasquevich, D.M. 2002. Carbochlorination of cerium dioxide. *Mineral Processing and Extractive Metallurgy Review*, vol. 111, no. 3. pp. 149–155.

Fuerstenau, D.W. 1985. Adsorption of hydroxamate collectors on semisoluble minerals. Part II: Effect of temperature on adsorption. *Colloids and Surfaces*, vol. 15. pp. 137–146.

Fuerstenau, D.W. 1983. The adsorption of hydroxamate on semi-soluble minerals. Part I: Adsorption on barite, calcite and bastnaesite, *Colloids and Surfaces*, vol. 8. pp. 103–119.

Griffith, D.M., Szocs, B., Keogh, T., Suponitsky, K.Y., Farkas, E., Buglyo, P., and Marmion, C.J. 2011. Suberoylanilide hydroxamic acid, a potent histonedeacetylase inhibitor: its X-ray crystal structure and solid state and solution studies of its Zn(II), Ni(II), Cu(II) and Fe(III) complexes. *Journal of Inorganic Biochemistry*, vol. 105. pp. 763–769.

Herrera, R.U. 2003. Recent developments and advances in formulations and applications of chemical reagents used in froth flotation. *Mineral Processing and Extractive Metallurgy Review*, vol. 24, no. 2. pp. 139–182.

He, X. J. and Vaisey, M. 2012. Development and research on Mt Weld rare earth ore, Australia. *Proceedings of the XXVI International Mineral Processing Congress*, New Delhi, India, 23-28 September. Indian Institute of Mineral Engineers. pp. 5860–5890.

Hu, Y.H. 2014. Mineral Flotation. Cha Sha, China (in Chinese).

Jiang, Y., Zhou, L., Zhou, X., and Zhao, B. 2010. Novel condensed ring carboxylic acid studied in the flotation behavior of diaspora and aluminosilicates. *Separation Science and Technology*, vol. 45. pp. 2475–2480.

Jiang, Y R., Li, W., and Feng, R. 2011. Preparation and performance of 4-alkyl-4,4- bis(hydroxyl carbamoyl) carboxylic acid for flotation separation of diaspore against aluminosilicates. *Minerals Engineering*, vol. 24, no. 14. pp. 1571–1579.

Jordens, A., Marion, C., Kuzmina, O., and Waters, K.E. 2014. Surface chemistry considerations in the flotation of bastnasite. *Minerals Engineering*, vol. 66-68. pp. 119–129.

Jordens, A., Chen, Y.P., and Waters, K.E. 2013. A review of the beneficiation of rare earth element bearing minerals. *Minerals Engineering*, vol. 41. pp. 97-114.

Krishnamurthy, N. and Guptac, K. 2002. Rare earth metals and alloys by electrolytic methods. *Mineral Processing and Extractive Metallurgy Review*, vol. 22, no. 4–6. pp. 477–507.

Lee, J.S., Nagaraj, D.R., and Coe, J.E. 1998. Practical aspects of oxide copper recovery with alkyl hydroxamates. *Minerals Engineering*, vol. 11. pp. 929–939.

Liu, G.H., Wu, H.B., Liu, J., Shi, X.G., and Liu, Q.B. 1989. Stability constants of compound of rare earth with hydroxamic acid. *Journal of Inorganic Chemistry*, vol. 5, no. 2. p. 30 (in Chinese).

Luo, Q.H. 2012. Coordination Chemistry. Science Press, Beijing, China (in Chinese).

Mousumi, G. and Venugopal, R. 2016. Modeling of flotation process-an overview of different approaches. *Mineral Processing and Extractive Metallurgy Review*, vol. 37, no. 2. pp. 120–133.

O'Brien, E.C., Le, R.S., Vaillain,J., Fitzgerald, D.J., and Nolan, K.B. 1997. Metal complexes of salicylhydroxamic acid and O-acetylsalicyl hydroxamic acid. *Inorganica Chimica Acta*, vol. 266, no, 1. pp. 117–120.

Pugh, R.J. 1991. The interaction of polyethylene oxide non-ionic surfactant layers adsorbed on hydrophobic minerals. *International Journal of Mineral Processing*, vol. 33, no. 1–4. pp. 307–320.

Ren, J., Lu, S., Song, S., and Niu, J. 1997. New collector for rare earth mineral flotation. *Minerals Engineering*, vol. 10. pp. 1395–1404.

Sreenivas, T. and Padmanabhan, N. P. 2002. Surface chemistry and flotation of cassiterite with alkyl hydroxamates. *Colloids and Surfaces A*, vol. 205, no. 1–2. pp. 47–59.

Wang, C.H., Qiu, X.Y., Hu, Z., Wang, T., and Li, H.W. 2014. Flotation mechanism of bastnaesite by salicylhydroxamic acid. *Journal of the Chinese Society of Rare Earths*, vol. 32, no. 6. pp. 727–733.

Wang, X.M., Liu, J., and Miller, J.D. 2008. Adsorption and self-assembly of octyl hydroxamicacid at a fluorite surface as revealed by sum-frequency vibrational spectroscopy. *Journal of Colloid and Interface Science*, vol. 325. pp. 398–403.

Wu, X.Q. and Zhu, J.G. 2006. Selective flotation of cassiterite with benzohydroxamic acid. *Minerals Engineering*, vol. 19. pp. 1410–1417.

Xu, H.F., Zhong, H., Tang, Q., Wang, S., Zhao, G., and Liu, G.Y. 2015. A novel collector2-ethyl-2-hexenoic hydroxamic acid: Flotation performance and adsorption mechanism to ilmenite. *Applied Surface Science*, vol. 353. pp. 882–889.

Xin, Q.Y., Pei, W.W., and Xu, R.Q. 2006. Basic Organic Chemistry. Chemical Industry Press, Beijing, China (in Chinese).

Xu, J.Q., Xu, X.J., and Wang, J.W. 2002. Synthesis of 1-hydroxy-2-naphthylhydroximic acid and application to collecting rare earth minerals. *Nonferrous Metals*, vol. 54, no. 3. pp. 72–73 (in Chinese).

Yosry, A.A. 1990. Extraction and refining of high purity terbium metal from rare earth resources. *Mineral Processing and Extractive Metallurgy Review*, vol. 7, no. 2. pp. 95–114.

Zhou, F., Yan, C.J., Wang, H.Q., Sun, Q., and Wang, Q.Y. 2015a. Flotation behavior of four C18 hydroxamic acids as collectors of rhodochrosite. *Minerals Engineering*, vol. 78. pp. 15–20.

Zhou, F., Wang, L.X., Xu, Z.H., Liu, Q.X., and Chi, R.A. 2015b. Reactive oily bubble technology for flotation of apatite, dolomite and quartz. *International Journal of Mineral Processing*, vol. 134. pp. 74–81. ◆

http://dx.doi.org/10.17159/2411-9717/2017/v117n6a11

In-pit crusher location as a dynamic location problem

by M. Paricheh*, M. Osanloo*, and M. Rahmanpour*

Synopsis

The cost efficiency and high reliability of semi-mobile or combined in-pit crushing-conveying (IPCC) and truck systems, compared to conventional truck-shovel systems alone, make them more attractive for use in modern mining operations. Semi-mobile systems, which are the most common systems in open-pit mining, combine the advantages of both systems such that fewer trucks are required, operating costs are lowered, and the operation is environmentally sound. One major aspect of utilizing this system is determining the location of the in-pit crusher and the timing of relocations. Facility location models are rarely used in the mining sector, but these models may be used for solving the in-pit crusher location problem. To this end, the main parameters affecting the IPCC location in open pit mines are reviewed and examples given of how they are applied to a dynamic location-relocation problem. Subsequently, the model is implemented for Sungun copper mine in Iran and the number and the exact time of relocations of the IPCC units determined.

Keywords

open pit mining, in-pit crusher, IPCC system, dynamic location problem, relocations timing.

Introduction

Nowadays, compared to the last century, metal prices are more volatile, average and cut-off grades have decreased, and stripping ratios increased. From a mining engineering point of view, many ore deposits with simple access and low capital and operating costs have been exhausted. The remaining deposits are located at depth, with no easy access, which requires high initial capital costs (Osanloo, 2012). Mining at great depths and high tonnages is possible only through open pit mining. Today, more than 80% of open pit mines in the world use a shovel-truck system for loading-hauling operations (Osanloo, 2010).

With increasing depth, haulage distances increase and the number of loads per truck decreases. As a result, fuel, tyre, and depreciation costs per ton increase. Owing to these factors, open pit mining at great depth (300 to 1000 m) using shovel-truck systems faces some technical and economic problems. In-pit crushing-conveying (IPCC) systems have been known in the mining industry for many decades. The idea was introduced in 1956 in Germany. Today, the cost efficiency and high reliability of IPCC make it more appealing than conventional shovel-truck operation, especially in longer life projects with lengthy transportation distances and high production rates (Koehler, 2003). Since 1956, different aspects of this system have been reviewed by many researchers. Barua and Lanergan (1985) developed a computer program that compares the tonnage aspects of various conveyor layouts. They believed that to maximize the economic benefit of lower haulage costs associated with in-pit conveying, one must first minimize the cost of the flatter slope, which is expressed in terms of additional stripping or tied-up ore. Dos Santos and Stanisic (1987) evaluated the design of a high-angle conveyor at the Majdanpek copper mine. Then, Sturgul (1987) applied GPSS (general purpose simulation system) to find the best location of an in-pit crusher. Zimmermann (2006) believes that IPCC presents an opportunity for better and cheaper production. In this context, he considered the applications, case studies, and the economic effects of fully mobile crushing and conveying systems. Konak, Onur, and Karakus (2007) discussed the effects of pit geometry and mine access requirements on crusher site selection, based mainly on minimum haulage distance. They established a trial-and-error process and applied their method to an aggregate mine. Turnbull and Cooper (2009) and Morrison and Lourel (2009) evaluated the IPCC system, and sought to document the options that might be employed to transporting and dumping operations and rank them in terms of their applicability at any mine and their overall practicality. Also, they determined the types of IPCC that would be most appropriate for particular mining operations. Rahmanpour *et al.*, (2014) studied the factors influencing the choice of a proper location of an IPCC and

* *Department of Mining and Metallurgical Engineering, Amirkabir University of Technology, Tehran, Iran.*

 ISSN 2225-6253. Paper received Oct. 2015; revised paper received Feb. 2017.

investigated in-pit crusher location as a single hub location problem. Roumpos *et al.*, (2014) developed a model for the ideal location of the distribution point of the belt conveyor in continuous surface mines. The model was applied to different scenarios for a lignite deposit with simplified geometry and geology, considering a spatial analysis perspective.

Apart from choosing a suitable type of crushing and conveying system, the system location should also be optimized to reduce operating costs. The crusher site dictates the haulage length for both parts (conveyor and truck) of an IPCC system and the haulage system capacity. The capital and operating costs of an IPCC system thus depend strongly on the crusher locations (Roumpos *et al.*, 2014). Since open pit mining is dynamic in nature and is based on pushback strategy, periodical relocation of the in-pit crusher is inevitable, depending on the production plan. Thus, one major aspect of utilizing this system is to determine the optimum crusher location and the times of relocation. This problem has not been considered yet. Given the nature of open pit mining, in-pit crusher location is essentially a dynamic problem. This paper endeavours to model the problem as a facility location–relocation problem (FLRP). FLRP is a dynamic location model that helps decision-makers to select the initial location and the subsequent relocations. Location-relocation models find the optimum location of a facility in some distinct periods. Each period varies from others and has an individual condition. The model is verified by data gathered from Sungun copper mine in Iran.

Haulage systems in open pit mines

In a conventional system, the materials inside the pit are excavated and loaded onto trucks and transferred to the crushers, stockpiles, or waste dumps according to the type of material (ore or waste). In most cases, the primary crusher is situated at the edge of the pit. This system is known as an ex-pit crusher. Trucks are well suited to short hauls (less than two miles) and selective mining and dumping (Osanloo, 2010). However, as the mine deepens, they are faced with problems such as:

- Increased haulage distance, requiring more trucks and capital (trucks of 360 t payload cost more than US$3 million
- As the number of trucks increases, dispatching will become a concern
- Increasing maintenance, repair, and operational costs
- Increasing labour requirement and more supervision.

Haulage costs are always a significant part of capital and operating costs in large open-pit mines. According to Tutton (2009), in a typical large, deep mine using a conventional shovel-truck system, haulage costs constitute more than 45% of total operating costs, and about 40–50% of total capital costs (Figure 1). One way of reducing the haulage costs is to shorten the haulage distance by bringing the dumping points (*i.e.* primary crusher) into the pit. This system is known as in-pit crushing. In-pit crushers can be classified as:

- Semi-mobile operation (known as discontinuous systems): this involves a primary crushing unit inside the pit together with a shovel-truck system. After crushing, the materials is hauled by conveyor to the predetermined destination (processing plant or waste dump). This system is the best option for large open-pit mines (Tutton, 2009)
- Fully mobile operation, where shovels and a mobile crusher are combined. This system has the best productivity and availability. Fully mobile crushing systems are appropriate for horizontally developing surface mines. Figure 2 shows the alternatives for transportation systems in open pit mines.

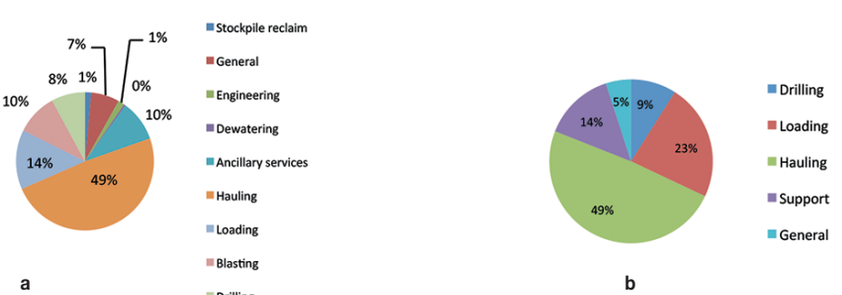

Figure 1—(a) Distribution of capital costs, and (b) distribution of operating cost in large open pits (Tutton, 2009)

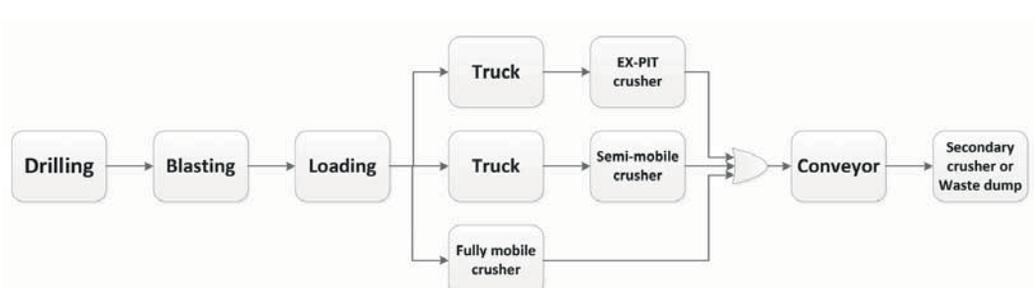

Figure 2—Conventional transportation systems in open pit mines (Tutton, 2009)

Table I

Factors affecting optimum location and relocation time for IPCCs

No.	Factor
1	Haulage distances and truck operating costs
2	Mine schedule and block sequences
3	Rate of increase in haulage costs with increasing haulage distance and time (predicted haulage cost)
4	Conveyor operating cost (per ton) vs. truck operating cost (per ton)
5	Additional haulage cost in relation to pit depth
6	Cost for relocation of the system (including engineering, disassembling, installation, labour, transportation, and overhead costs, as well as costs of purchasing additional conveyor and associated equipment)
7	Scheduled hours and time required for the relocation

Main factors affecting in-pit crusher location

An IPCC system must satisfy two competing criteria in order to be the most appropriate selection for a deep open-pit mine: (1) it should technically be able to deliver the required material to the out-of-pit system, and (2) be acceptably cost-effective during the operational phase. One major factor in the cost-efficiency of the IPCC system is the optimal in-pit crusher location. Table I summarizes the different criteria that affect the optimal location and time for relocation of an in-pit crusher.

Minimizing the overall haulage operating costs and relocation costs throughout the mine life is the main goal of this investigation. For this purpose:

- The in-pit crusher should be at an optimum distance from the faces and also from waste dumps or plant
- Based on the mine production plan, the amount of material that must be hauled from each working face should be considered. These factors force the in-pit crusher to be located in the centroid of the available working faces (Konak, Onur, and Karakus, 2007; Stughul, 1987; Rahmanpour, 2014). Hence, the capital and operating costs of the truck fleet are reduced
- In addition, the transportation costs increase rapidly each year, not only as a result of wage inflation but also as a result of the increment in haulage distances. In brief, haulage cost is a function of haulage length and time (Benito and Dessoreault, 2008; Roumpos *et al.*, 2014). In the case of open pit mining, to derive a function for haulage cost predictions, one needs to know the mine schedule and have comprehensive information about the haulage system. Thereby, the predicted haulage costs through the mine life will be more realistic
- The conveying distance (or conveying costs) from in-pit crusher to an ex-pit destination is another factor that affects haulage costs. With the lower costs of conveyor transport compared to trucking, the in-pit crusher can be at a greater distance from the plant or waste dump site. These conveying costs have not yet been incorporated into the in-pit crusher location problem
- In addition, since extra energy is required by trucks to haul material over a vertical distance, it is necessary to assign a factor into the haulage cost function to consider the extra cost of moving material from the lower benches (Konak, Onur, and Karakus, 2007)
- Owing to the inherent features of open pit mining, the in-pit crusher should be relocated periodically. These repeated displacements take time and add costs to the project. These costs and time intervals should be considered in terms of yearly investment costs and annual operating hours (Morris, 2008). Considering these parameters, the operating and relocating costs can be minimized through optimizing the in-pit crusher location using dynamic location models.

Mathematical model

Facility location problems (FLPs) are combinatorial optimization problems that help strategic management and decision-making. Combinatorial optimization is the process of finding the optimal solution for problems within a region of feasible solutions. Furthermore, real-world location problems are often large in scale, and are not solvable to optimality within a reasonable time and effort (Rayco, Francis, and Tamir, 1999). FLPs are divided into two main categories: (1) static facility location problems (SFLPs) and (2) dynamic facility location problems (DFLPs). The problem is called static as long as the factors and parameters are fixed and constant with the planning time horizon. If the parameters change during the planning horizon and if there is a considerable amount of capital required for development, then the problem is called dynamic. In most DFLPs, decision-makers must not only select robust locations, which will effectively serve changing demand over time, but must also consider the timing of expansions and relocation in the long term. From a general viewpoint, FLPs are subdivided in terms of two elements: space and time. Continuous-space, discrete-space, and network-space location problems are addressed under the category of SFLPs. On the other hand, timespans constitute the main parts of DFLPs. DFLPs are subdivided into (1) dynamic deterministic facility location problems, (2) facility location/relocation problems (FLRPs), (3) multi-period facility location problems (MPFLPs), (4) time-dependent facility location problems (TDFLPs), (5) stochastic facility location problems, which are relatively similar to probabilistic facility location problems, and (6) fuzzy facility location problems. It should be noted that some types of DFLPs (especially FLRPs, MPFLPs, and TDFLPs) can be converted to each other (many references consider them as a single model: Arabani and Farahani, 2012; Farahani, Drezner, and Asgari, 2009; Erlenkotter, 1981). According to the affecting factors in the previous section, to effectively handle probable changes of open pit mining in a crusher location problem, a dynamic model seems to be indispensable. Additionally, time-dependent parameters involving haulage costs can be predicted easily. Then, it is possible to model the problem by one of the FLRP, MPFLP, or TDFLP models. This paper uses the FLRP model. The binary linear programming form of a dynamic location-relocation problem for determination of the in-pit crusher location is given in Equation [1]. Notations of the model are defined in Table II.

Table II

Notations of the FLRP model

Notation	Explanation	Unit/value
r	Number of periods	-
p	Number of candidate locations	-
mk	Number of destinations or faces in period k	-
F_{kij}	Total haulage operating cost from face i to candidate point j in period k	$
C_k	Relocation cost, including engineering, disassembly, installation, labour, transportation, and overhead costs, as well as also costs of purchasing additional conveyor and associated equipment	$
z_{kj} and y_k	Binary decision variables	0 or 1

Objective function:

$$Z = Min \sum_{k=1}^{r}\sum_{j=1}^{p}\sum_{i=1}^{m_k+1} F_{kij} z_{kj} + \sum_{k=2}^{r} C_k y_k \qquad [1.1]$$

subject to:

$$y_k = 0.5\sum_{j=1}^{p}\left|z_{kj} - z_{(k-1)j}\right| \qquad \forall k \qquad [1.2]$$

$$\sum_{j=1}^{p} z_{kj} = 1 \qquad \forall k \qquad [1.3]$$

$$z_{kj}, y_k = 0 or 1, \quad \forall k, j \qquad [1.4]$$

Equation [1.1] is the objective function of the model, and is defined as the minimization of the total haulage costs. The first part of the objective function is the operating costs, and the second part is the relocation costs of the IPCC. In order to consider the operating costs of the conveyor from the candidate point j to the mill in period k, the value one is added to the third sigma. In the case of system relocation, Equation [1.2] embeds the relocation costs into the model. The constraint in Equation [1.3] ensures that only one of the candidate locations can be selected as the IPCC location. As stated in Equation [1.4], the decision variables are all binary.

The term F_{kij} is a function of material tonnage in each period and haulage costs per ton in that period. Furthermore, the haulage costs itself (F_{kij}) is a function of haulage distance (d) and time (t). In other words, F_{kij} is a function of haulage distance (d), time (t), and the amount of material to be hauled (Equation [2]):

$$F_{kij}\ ;\ \ F_{kij}(d,t) = T_{kij} \cdot f_{kij}(d,t) \qquad [2]$$

where T_{kij} and F_{kij} are the total amount of material and haulage costs per ton of materials in period k that should be hauled from site i to destination j, respectively.

Prior to applying Equation [2], the truck haulage cost functions should be estimated using any available method, such as that of O'Hara (1980). For the conveyor system, the results of similar investigations at other mine sites should be used or a function developed with respect to local parameters. When the total haulage costs are estimated and substituted in Equation [1], the model can be used to optimize the in-pit crusher location in each period.

Case study

Sungun copper mine (SCM) is a porphyry deposit and is located in the northwest of Iran. SCM is the second largest copper mine in Iran, with a resource estimated at up to 806 Mt at an average copper grade of 0.62%. The total mineable reserve of the deposit is about 388 Mt at an average grade of 0.67% Cu, and the stripping ratio is equal to 1.8:1. In the first five years, the annual production is 7 Mt, and it reaches 14 Mt in the remaining years. The mined area of SCM is 38.2 km^2, half of which will be completely disturbed during the first 27 years of mine life. Some mine infrastructure, including the industrial mine site, concentration plant, belt conveyors, and crushing site are located near the current pit limits. The Pakhir and Sungun rivers flow through the mine area and join the Mian-cafe River and the Ilgene-chai River. The valley of Pakhir on the northern side of the pit is used as a waste dump area. Waste dumps are on the same level as the mine bench into Pakhir. The ore is hauled to an ex-pit crusher on the southeast edge of the pit on horizon 1987 m (Kavoshgaran, 2003). The waste haulage distance will increase from 1 to 3 km by the end of the mine life, but the ore haulage distance increases to more than 5 km. Because the waste haulage distance is less than the economical travel distance for trucks (less than 2 miles) throughout the mine life, the dynamic location problem is applied for ore crusher locations. The economic and technical parameters of SCM that have been used in this study are shown in Table III.

Haulage distance calculations

One primary concern with the installation of an IPCC system is how the conveyors exit the pit. A tunnel, dedicated conveyor ramp, and existing haul roads are three ways by which the conveyors can exit the pit (Turnbull and Cooper, 2009; Morrisson and Lourel, 2009). A feasibility study will determine the best method; then the conveyor specifications (length, angle, and width) and corresponding haulage costs can be calculated. In this case study, the existing haul roads were selected for routing the conveyor to the pit exit located on level 1987 in the southeast part of mine site. The level is located in the mid-point of the mine depth. Currently, an ex-

Table III

Economic and technical parameters of SCM

Type	Parameter	Value	Unit
Economic parameters	Cost of 1.6 m width conveyor (Mular, 1992)	3000	$ per metre
	Conveyor shipping and installing cost (Mular, 1992)	25	% of conveyor price
	Electricity price	0.03	$/kW
	Worker wage	667	$ per man per month
Technical parameters	Conveyor capacity	4000	t/h
	Ramp width	25-30	m
	Ramp grade	8 -10	%
	Max. crusher output size	25	cm
	Existing ex-pit crusher level	1987	m
	First bench level	2362	m
	Pit bottom level	1600	m
	Conveyor width	160	cm
	Ore density	2.3	t/m^3
	Bench height	12.5	m

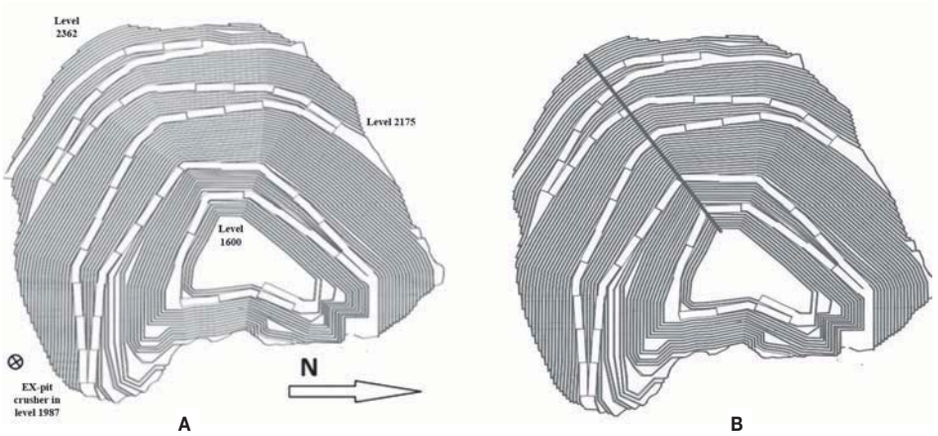

Figure 3—(a) Plan view of pit and ex-pit crusher, and (b) centroid line of all levels

pit crusher is located at this level at a distance of 270 m from the southern edge of the pit. An overland conveyor line with a length of 1171 m moves the crushed ore to the concentration plant southwest of the pit.

Considering these issues, if an IPCC is installed in the mine, then the ore should be hauled daily and dumped into an in-pit crusher. After crushing, the ore will be discharged onto a discharge conveyor, which will discharge the crushed ore onto movable conveyors. These conveyors will haul the ore over the existing haul roads out of the pit and deliver the material onto the overland conveyor which goes directly to the concentration plant. Three belts are thus required to complete the transportation process from the pit to concentration plant. Figure 3a shows a plan view of the pit and the location of the ex-pit crusher. According to the model, the first step is the determination of some candidate location for the crusher. The mine production plan indicates extraction levels and the ore tonnage to be mined. In order to simplify the problem, the geometric centre of each level is assumed as a candidate crusher location. Figure 3b shows the centroid line of all mine levels.

Generally speaking, if the IPCC system is going to be applied in the middle of the mine life, then it should be used after the first payback period. This is due to the fact that it would be unwise to reinvest in a project that has not yet returned its initial investment. For this reason, due to a 5-year payback period at Sungun, one can investigate the application of IPCC system from the 6th year. Then, depending on the time of the IPCC's application, the dynamic location problem will determine the optimum locations for the remaining years. To improve the solution time, it is assumed that the in-pit crusher should be placed between the highest and lowest levels of mining in each year. Thus, some penalty values are added to each level outside of this boundary. As an example, the distance from the mining point in the 6th year (centroid of each level) to the candidate point (centroid of each level) in the same year is given in Table IV. For the remaining mine life, these distances are calculated according to the available mine plan.

Table IV

Distance from each candidate level to each mining level in 6th year (m)

Year 6	Candidate level for in-pit crusher												
Extraction level		1962	1950	1937	1925	1912	1900	1887	1875	1862	1850	1837	1825
	1962	575	1570	1488	1469	1482	1792	2155	2431	2769	3189	3062	2948
	1950	1570	575	1148	1128	1142	1452	1815	2090	2429	2849	2722	2607
	1937	1488	1148	580	720	733	1044	1407	1682	2020	2441	2314	2199
	1925	1469	1128	720	580	413	723	1087	1362	1700	2120	1994	1879
	1912	1482	1142	733	413	595	410	773	1049	1387	1807	1680	1566
	1837	3062	2722	2314	1994	1680	1690	1727	1702	1713	1833	585	1265
	1825	2948	2607	2199	1879	1566	1575	1612	1587	1599	1718	1265	615

Incremental truck haulage cost function

In order to apply the model (Equation [1]), the haulage cost should be specified. To do that, two new mathematical models are developed for prediction of truck and conveyor haulage costs per ton as a function of distance. The unit cost can be calculated by dividing the hourly truck cost by the resulting truck productivity. Truck performance is typically expressed in terms of the hourly production rate (tons per hour), and is calculated considering truck payload and truck total cycle time, which includes spot, load, haul, turn, dump, empty return, wait, and delay times (Benito and Dessoreault, 2008). This method requires comprehensive information on

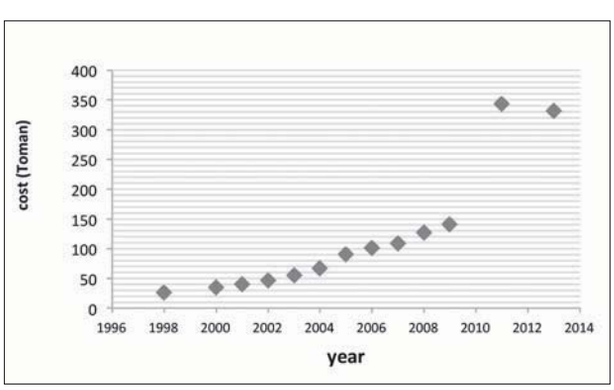

Figure 4—Transportation cost per year (tomans per cubic metre per 500 m)

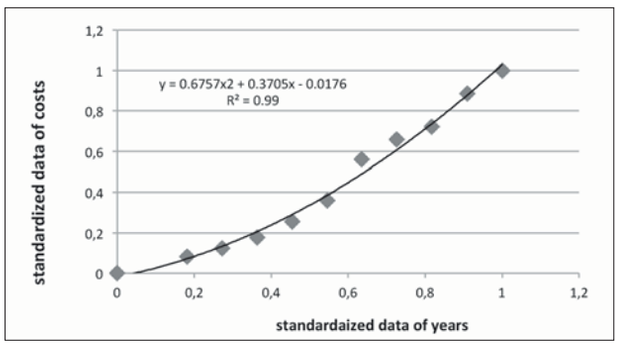

Figure 5—Best fit curve to the standardized data

each component of haulage cost. In this research, annual haulage cost data provided from 1998 to 2013 by the Vice Presidency of Strategic Planning & Supervision of I.R. Iran (VPSPSI) is used for prediction of truck haulage cost. VPSPSI provides the basic cost structure for contracting companies in all fields. The transportation costs by truck per 500 m per cubic metre are shown in Figure 4. To calculate the haulage cost for distances beyond 500 m, these costs are increased linearly. After normalizing and smoothing the data, the best curve fitted to the data is selected for prediction of haulage cost per cubic metre per metre. Figure 5 shows the best fit to the normalized data. Moreover, some coefficients such as overhead, road, equipment, weather, and contractor factors are added to the basic costs by contractors who will attend the biddings (Table V). To convert haulage cost from tomans per ton to dollars per ton, the exchange rate is assumed to be 3000 units per dollar.

Finally, the predicted truck haulage cost function per ton of ore per metre in SCM is modelled as in Equation [3]:

$$f(d,t) = \left[\left(0.6757*\left(\frac{t-1998}{2009-1998}\right)^2+0.3705*\left(\frac{t-1998}{2009-1998}\right)-0.0176\right)*(140-26)+26\right]*\left(\frac{1.3*1.3*1.2*1.04*1.05*d}{500*2.3*3000}\right) \quad [3]$$

where d is distance in metres, t is year, and f is the annual haulage cost (per ton per metre).

Incremental conveyor haulage cost function

The conveyor is an inseparable part of the IPCC system. Thus, its design and specifications are very important. Initially, conveyor components for carrying ore in SCM are designed according to the standards of the Conveyor Equipment Manufacturers Association (CEMA). Conveyor operating cost includes spare parts, maintenance, labour, and electricity costs. Calculation of electricity cost depends on belt tension and power consumption. Labour, maintenance, and spare parts costs are considered as a percentage of the initial investment cost. After calculation of conveyor power consumption in terms of conveyor length, the incremental annual haulage cost function per ton for the conveyor system is formulated (Equation [4]).

$$f(d,t) = (P_{KW}*\text{AOPH}*0.03+(2*2*10^6*12)/3000+0.06*d*3000*C_{index}(t))/14*10^6 \quad [4]$$

where f is yearly conveyor operating cost per ton per unit length of the conveyor, P_{KW} is power required for transportation of ore over a distance of d metres, AOPH is the yearly operating hours (in this case 3600 h), $C_{index}\ (t)$ is the predicted Marshall and Swift cost index for the year t, and $14*10^6$ is the yearly ore production of Sungun. The Marshall and Swift equipment cost index was created to facilitate comparisons between two previous quarters or years. Index comparisons are developed by dividing the index for the date for which a cost is desired by the index for the date of the known cost and multiplying the resulting factor by the known cost (Mular, 1992).

Table V

Conventional coefficients

Coefficient	Value (%)
Overhead factor	1.3
Road factor	1.3
Equipping factor	1.2
Weather factor	1.04
Contractor factor	1.05

Results

The dynamic location mathematical model presented in Equation [1] is adapted to match the case of Sungun. In this case, r is equal to 22 (from year 6 to 27), p is equal to 47 (number of candidate levels) and C_k is equal to $1.5 million (average of all probable periodic investment costs for additional conveyors plus 25% of this cost as engineering, disassembling, relocating and assembling costs). Then, Equations [3] and [4] are applied to calculate the yearly haulage operating cost from each face to candidate levels from year 6 to the end of mine life. The problem is modelled and solved in GAMS (General Algebraic Modeling System). GAMS is a high-level modelling system for mathematical optimization which is designed for modelling and solving linear, nonlinear, and mixed integer optimization problems. Input parameters in an Excel® sheet are sent to the software as a 145*47 matrix. Cplex optimizer is used to solve the model. Cplex is a solver that is designed to solve large and difficult problems quickly with minimal user intervention. Depending on the time of application of the IPCC system in the mine, the solution will provide the crusher location and optimum time for the system relocations. A sensitivity analysis was performed for the parameter of relocation costs.

Optimum locations for the in-pit crusher in different years of mine life, depending on the time of applying the system, are shown in Table VI. The first column shows the years, and the first row presents the year when the IPCC system is applied. Each number in the table presents the optimum level where the IPCC system should be installed. As an example, if the system is used from the 10th year, in the first year the in-pit crusher should be located on level 1975, and in the next year it should be relocated to level 1925. Similarly, the in-pit crusher should be located on 12 different levels to the end of mine life and the system should be relocated 11 times.

Running time in seconds (Intel® Core™ i5-2450 CPU at 2.5 GHz) was less than 300 seconds. By increasing the number of periods and the corresponding faces and candidate points, the numbers of variables increases, but this does not change the running time significantly.

Table VI

Optimum locations depending on time for application of the system

Year of mine life considered for system application

Year	6	7	8	9	10	11	12	13	14	15	16	17	18	19	20	21	22	23	24	25	26	27
6	1912																					
7	1912	1912																				
8	1912	1912	1912																			
9	1912	1912	1912	2025																		
10	1975	1975	1975	2025	1975																	
11	1925	1925	1925	1925	1925	1925																
12	1925	1925	1925	1925	1925	1925	1912															
13	1887	1887	1887	1887	1887	1887	1887	1887														
14	1825	1825	1825	1825	1825	1825	1825	1825	1825													
15	1825	1825	1825	1825	1825	1825	1825	1825	1825	1800												
16	1912	1912	1912	1912	1912	1912	1912	1912	1912	1912	1912											
17	1912	1912	1912	1912	1912	1912	1912	1912	1912	1912	1912	1875										
18	1862	1862	1862	1862	1862	1862	1862	1862	1862	1862	1862	1875	1862									
19	1812	1812	1812	1812	1812	1812	1812	1812	1812	1812	1812	1812	1812	1812								
20	1812	1812	1812	1812	1812	1812	1812	1812	1812	1812	1812	1812	1812	1812	1775							
21	1775	1775	1775	1775	1775	1775	1775	1775	1775	1775	1775	1775	1775	1775	1775	1775						
22	1775	1775	1775	1775	1775	1775	1775	1775	1775	1775	1775	1775	1775	1775	1775	1775	1750					
23	1737	1737	1737	1737	1737	1737	1737	1737	1737	1737	1737	1737	1737	1737	1737	1737	1750	1737				
24	1725	1725	1725	1725	1725	1725	1725	1725	1725	1725	1725	1725	1725	1725	1725	1725	1725	1725	1725			
25	1700	1700	1700	1700	1700	1700	1700	1700	1700	1700	1700	1700	1700	1700	1700	1700	1700	1700	1700	1700		
26	1650	1650	1650	1650	1650	1650	1650	1650	1650	1650	1650	1650	1650	1650	1650	1650	1650	1650	1650	1650	1650	
27	1650	1650	1650	1650	1650	1650	1650	1650	1650	1650	1650	1650	1650	1650	1650	1650	1650	1650	1650	1650	1650	1637

Discussion

The four most applicable methods that can be used to exit the conveyor from the pit include a dedicated ramp slot, high-angle conveyor, tunnel, and existing truck ramps. Only the last method is considered in this paper. It is a well-known fact that when the existing haul roads are used to handle the materials, extra width would be needed to accommodate both truck and conveyor haulage routes. It is worthwhile to note that the truck fleet would be smaller after the primary crusher moves into the pit. In this situation, the transportation process will be easier to manage because of the lower traffic volume. To increase the final pit slope, in some cases, reducing road widths may be considered. On the other hand, incorrect haul road width at certain places causes bottlenecking and increased truck travelling times. A separate investigation of this aspect is needed. However, in this paper, it is assumed that the existing haul roads do not need to be widened in order to accommodate both conveyor and trucks on the same route.

As stated previously, the crusher must be in the centroid of the working faces. Relocation of the in-pit crushing station is required when the haulage distances become uneconomic for trucks. So, the other most important parameter affecting the problem is the relocation cost of the crusher, which involves the costs associated with disassembling the equipment, conveyor and crusher relocation costs, and the cost of purchasing additional equipment to increase the length of the conveyors. There must be a trade-off between these two costs (*i.e.* haulage operating cost and relocation cost). The crusher would not be relocated if the haulage operating costs can be reduced, since crusher relocation would not offset the relocation costs. More scenarios for relocation costs are considered to show other aspects of the proposed mathematical optimization model. The results are illustrated in Table VII. Changes in the value of this parameter in a range of $1 million to $5 million do not change the optimum locations significantly. However, increasing this parameter up to $30 million reduces the number of relocations.

According to Table VI, depending on the year the mine installs the system, the exact timings of IPCC relocations are optimized. It is worth noting that, while there are some changes in the initial years, the optimum IPCC location in each year is somewhat independent of the IPCC's application time. The changes in the initial years are highlighted in Table VI.

The results in Tables VI and VII show that displacements occur most frequently in the final years. This means that the mine becomes deeper and operating costs are increased more rapidly than the earlier years.

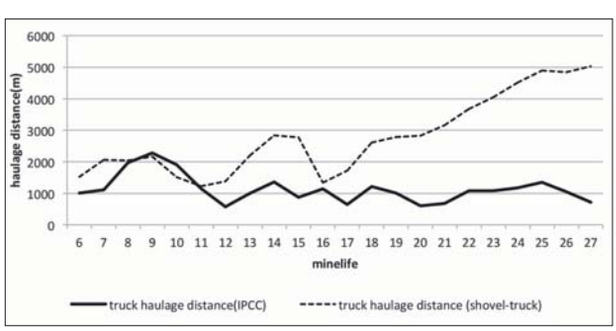

Figure 6—Comparison of truck haulage distances for both systems

Table VII

Results of the sensitivity analysis of relocation cost

Year	Scenario 1 (relocation cost $5 million)	Scenario 2 (relocation cost $10 million)	Scenario 3 (relocation cost $15 million)	Scenario 3 (relocation cost $30 million)
6	1912	1912	1962	1962
7	1912	1912	1912	1962
8	1912	1912	1912	1962
9	1912	1912	1912	1962
10	1975	1925	1912	1962
11	1925	1925	1912	1962
12	1925	1925	1912	1962
13	1887	1887	1887	1887
14	1825	1825	1825	1825
15	1825	1825	1825	1825
16	1912	1912	1912	1912
17	1912	1912	1912	1912
18	1862	1862	1862	1862
19	1812	1812	1812	1812
20	1812	1812	1812	1812
21	1775	1775	1775	1775
22	1775	1775	1775	1775
23	1737	1737	1737	1737
24	1725	1725	1725	1725
25	1700	1700	1700	1700
26	1650	1650	1650	1650
27	1650	1650	1650	1650
No. of relocations	12	11	11	10

After determination of the best location and best time for relocation of the in-pit crusher, an accurate comparison of IPCC vs. pure truck systems will be possible. The comparison of the total haulage distance in the shovel/truck and IPCC systems is shown in Figure 6. In this figure, the IPCC is applied in the mine from the 6th year. In the case of the shovel/truck system, the total haulage distance will reach to more than 3000 m after year 20. However, in the case of the IPCC system, the total haulage distance by trucks inside the pit is always about 1000 m. Thus, the IPCC system requires fewer trucks than the shovel/truck system. According to the results, this will save about $150 million by the end of the mine life.

As the pit continues to deepen, additional movable conveyors will be installed at a lower elevation to dump on to the first conveyors. Therefore, the conveyor's periodical investment cost depends not only on the additional drive pulleys and motors needed, but also on the extra length of conveyor needed and the corresponding costs. These costs are a part of the relocation costs, which are considered here as an average of all probable scenarios for the extra conveyor required. This is calculated in the conveyor design process and preparing the input cost matrix (*i.e.* trucking, conveying, and relocation cost matrix) of the mathematical model. The capital costs of the IPCC system (purchasing the in-pit semi-mobile crusher and initial required conveyor length, engineering, commissioning, assembling, *etc.*) are not part of the crusher location and relocation problem. They are main factors affecting the time of application of IPCC.

Three main belt conveyor paths are required in the case study. The first one passes from the crusher to the ramping system, the second via the ramp system up to the pit rim, and the last across the rim (the existing ex-pit crusher) to the concentration plant. In this case, because of the special ramping system (switchback) additional transfer points may be required and extra costs may be incurred; however, this was not considered in this paper.

Conclusion

In-pit crushing-conveying (IPCC) has received renewed interest and is being reviewed by mining researchers worldwide. As pits become deeper and strip ratios increase, cost pressure on operations means that alternatives that incur lower operating costs become more attractive. Factors such as fuel prices, skilled labour shortages, truck costs, vehicle incidents, and greenhouse gas emissions force mining companies to change their transportation systems. Apart from choosing a suitable type of crushing and conveying system, the location of the system should also be optimized to reduce operating and capital costs. In addition, determination of the optimum time for relocating the system has not been considered to date. This time plays an important role in mine plan and cost reductions. In this study, determination of the optimum locations and optimum times for relocations of an in-pit crusher was studied as a dynamic location problem. The proposed method was implemented in a case study for Sungun copper mine.

According to Sungun's mining schedules and extraction sequences, haulage distances were calculated in each year. Two models were then developed to predict the haulage cost per ton per metre for both truck and conveyor systems. These models enable the mine planner to easily estimate the haulage costs with regard to increased haulage distance and times.

Application of the IPCC system from year 6 will decrease the haulage costs by about 6% compared to the conventional shovel-truck system. This equates to about $150 million through the mine life. In this case all the parameters were predicted using available data. In some cases, collecting the data is relatively hard, or even no data may be available, and the main parameters of the problem are likely to be uncertain during the planning horizon, and therefore models considering uncertainty would be of interest in such conditions. Future research should also be focused on dealing with the uncertainties.

References

Arabani, A.B. and Farahani, R.Z. 2012. Facility location dynamics: An overview of classifications and applications. *Computers & Industrial Engineering*, vol. 62, no. 1. pp. 408-420. DOI: 10.1016/j.cie.2011.09.018

Benito, R. and Dessoreault, S. 2008. Estimation of incremental haulage cost by mining historical data and their influence in the final pit limit definition. *Mining Engineering*, vol. 60, no. 10. pp. 44–49.

Dos Santos, J. 1987. In-pit crushing and high angle conveying in Yugoslavian copper mine. *International Journal of Surface Mining*, no. 1. pp. 97–104.

Erlenkotter, D. 1981. A comparative study of approaches to dynamic location problems. *European Journal of Operational Research*, vol. 6, no. 2. pp. 133–143.

Farahani, R. Z., Drezner, Z., and Asgari, N. 2009. Single facility location and relocation problem with time dependent weights and discrete planning horizon. *Annals of Operations Research*, vol. 167, no. 1. pp. 353–368.

Kavoshgaran Consulting Engineers. 2003. Sungun copper mine design report. Tehran. [In Persian}.

Koehler, F. 2003. In-pit crushing system the future mining option. *Proceedings of Mine Planning and Equipment Selection (MPES) 2003*, Kalgoorlie, Western Australia. Australasian Institute of Mining and Metallurgy, Melbourne. pp. 371–176.

Konak, G., Onur, A.H., and Karakus, D. 2007. Selection of the optimum in-pit crusher location for an aggregate producer. *Journal of the Southern African Institute of Mining and Metallurgy*, vol. 107, no. 2. pp. 161–166.

Lonergan, J.E. and Barua, S.L. 1985. Computer-assisted layout of in-pit crushing/conveying systems. *Proceedings of the SME-AIME Fall Meeting*, Albuquerque, New Mexico, October.

Morriss, P. 2008. Key production drivers in in-pit crushing and conveying (IPCC) studies. *Proceedings of Surface Mining 2008*, Southern African Institute of Mining and Metallurgy, Johannesburg. pp. 23–34.

Morrisson. D. and Lourel, I. 2009. In-pit crushing and conveying. *Proceedings of the Iron Ore Conference*, Perth, WA. Australasian Institute of Mining and Metallurgy, Melbourne. pp. 13–26.

Mular. A.L. 1992. Mining and Mineral Processing Equipment Costs and Preliminary Capital Cost Estimates. Canadian Institute of Mining, Metallurgy and Petroleum, Montreal

O'Hara, T.A. 1980. Quick guides to evaluation of ore bodies. *CIM Bulletin*, vol. 73, no. 814. pp. 78–99

Osanloo, M. 2010. Surface Mining Methods. 3rd edn (revised version), vol. 2. Amirkabir University of Technology, Tehran.

Osanloo, M. 2012. Future challenges in mining division, are we ready for these challenges? Do we have solid educational program? *Proceedings of the 23rd Annual General Meeting of the Society of Mining Professors*, Poland. pp. 29–39.

Rahmanpour, M., Osanloo, M., Adibee, N., and AkbarpourShirazi, M. 2014. An approach to determine the location of an in-pit crusher in open pit mines. *International Journal of Engineering (IJE) Transactions C*, vol. 27, no. 9. pp. 14475–1484.p

Rayco, M.B., Francis, R.L., and Tamir, A. 1999. A p-center grid-positioning aggregation procedure. *Computers and Operations Research*, vol. 26, no. 10. pp. 1113–1124.

Roumpos, C., Partsinevelos, P., Agioutantis, Z., Makantasis, K., and Vlachou, A. 2014. The optimal location of the distribution point of the belt conveyor system in continuous surface mining operations. *Simulation Modeling Practice and Theory*, vol. 47. pp. 19–27

Schroder, D. 2003. The use of in-pit crushing and conveying methods to significantly reduce transportation costs by truck. *Proceedings of CoalTrans Asia 2003*, Bali International Conventional Center, 8-11 June. Indonesian Coal Mining Association.

Stughul, J. 1987. How to determine the optimum location of in-pit movable crushers. *International Journal of Mining and Geological Engineering,* vol. 5. pp. 143–148

Turnbull, D. and Cooper, A. 2009. In-pit crushing and conveying (IPCC) – a tried and tested alternative to trucks, *Proceedings of the AusIMM New Leaders' Conference*. Australasian Institute of Mining and Metallurgy, Melbourne. pp. 59–66.

Tutton, D. and Streck, W. 2009. The application of mobile in-pit crushing and conveying in large, hard rock open pit mines. *Proceedings of the Mining Magazine Congress*, Niagara on the Lake, White Oaks Centre, Toronto, Canada.

Zimmermann, E. 2006. Mobile crushing and conveying in quarries – a chance for better and cheaper production. *Proceedings of the International Symposium on Continuous Surface Mining*, Aachen. pp. 1–7. ◆

Conference Announcement

SAIMM
THE SOUTHERN AFRICAN INSTITUTE OF MINING AND METALLURGY
ZIMBABWE BRANCH

The SAIMM Zimbabwe Branch are proud to host

BUILDING A ROBUST MINERAL INDUSTRY

Thriving under prolonged low commodity price environment

3–4 August 2017
Cresta Lodge, Msasa, Harare

BACKGROUND

Mineral products remain pivotal to the development of the global economy, despite experiencing prolonged periods of low mineral commodity prices in recent times. Stakeholders in the industry have responded with innovative practices and technologies that continue to build a robust industry that not only survives but thrives under 'the new normal' commodity price environment.

OBJECTIVES

- To bring together stakeholders in the mineral industry to discuss ways of building a robust mineral industry that thrives despite a prolonged low global mineral commodity price environment
- To share the latest developments in the standards, practices and technologies introduced to strengthen the mineral industry sector under low global mineral commodity prices
- To improve understanding of new and existing technologies, leading to growth and sustainable resource extraction through all global mineral commodity price cycles.

MINERAL TYPES

- Platinum group minerals
- Gold bearing ores
- Base metal ores
- Energy minerals, gas and diamonds

WHO SHOULD ATTEND

- Accountants
- Auditors
- Decision makers in the private sector, government and parastatals
- Economists
- CEOs
- Directors
- Heads of divisions/departments
- Managers
- Geologists
- Mining engineers
- Metallurgists
- Mineral economists
- Project and maintenance engineers

EXHIBITION/SPONSORSHIP

Sponsorship opportunities are available. Companies wishing to sponsor or exhibit should contact the Conference Co-ordinator.

The Southern African Institute of Mining and Metallurgy
BUILDING A ROBUST MINERAL INDUSTRY 2017

THE DETAILS OF THIS FORM CAN BE E-MAILED TO: gugu@saimm.co.za

☐ I am interested in attending the conference
☐ I am interested in sponsoring the conference
☐ I intend to submit an abstract entitled:

Title: .....

Personal Details: Name .....

Surname .....

Designation .....

Address .....

Tel: ..... Fax: .....

E-mail: .....

SAIMM
THE SOUTHERN AFRICAN INSTITUTE OF MINING AND METALLURGY

For further information contact:
Gugulethu Charlie • Conferencing Co-ordinator • Saimm • P O Box 61127, Marshalltown 2107
Tel: +27 (0) 11 834-1273/7 E-mail: gugu@saimm.co.za • Website: http://www.saimm.co.za

INTERNATIONAL ACTIVITIES

2017

6–7 June 2017 —**Mine Planning Colloquium 2017**
Mintek, Randburg, South Africa
Contact: Camielah Jardine
Tel: +27 11 834-1273/7, Fax: +27 11 838-5923/833-8156
E-mail: camielah@saimm.co.za, Website: http://www.saimm.co.za

7–8 June 2017 —**AIMS - Aachen International Mining Symposia Second International Conference: Mining in Europe**
Aachen, Germany
Contact: Iris Schümmer
Tel: +49-(0) 241-80 95673, Fax: +49-(0) 241-80 92272
E-mail: aims@mre.rwth-aachen.de
Website: http://www.aims.rwth-aachen.de

19–20 June 2017 —**Chrome Colloquium 2017**
What's next for Chrome? A debate on the tough questions
Mintek, Randburg, South Africa
Contact: Camielah Jardine
Tel: +27 11 834-1273/7, Fax: +27 11 838-5923/833-8156
E-mail: camielah@saimm.co.za, Website: http://www.saimm.co.za

25–28 June 2017 — **Emc 2017: European Metallurgical Conference**
Leipzig, Germany
Contact: Jürgen Zuchowski
Tel: +49 5323 9379-0, Fax: +49 5323 9379-37
E-mail: EMC@gdmg.de, Website: http://emc.gdmb.de

27–29 June 2017 —**4th Mineral Project Valuation Colloquium**
Wits Club, The University of the Witwatersrand, Johannesburg
Contact: Gugulethu Charlie
Tel: +27 11 834-1273/7, Fax: +27 11 838-5923/833-8156
E-mail: gugu@saimm.co.za, Website: http://www.saimm.co.za

10–12 July 2017 — **Water 2017 Conference**
Lifeblood of the Mining Industry
Emperors Palace, Hotel Casino Convention Resort, Johannesburg
Contact: Camielah Jardine
Tel: +27 11 834-1273/7, Fax: +27 11 838-5923/833-8156
E-mail: camielah@saimm.co.za, Website: http://www.saimm.co.za

25–26 July 2017 — **Entrepreneurship in Mining Forum**
A Focus on New Business in Mining
De Beers, Johannesburg
Contact: Camielah Jardine
Tel: +27 11 834-1273/7, Fax: +27 11 838-5923/833-8156
E-mail: camielah@saimm.co.za, Website: http://www.saimm.co.za

3–4 August 2017 — **Building a Robust Mineral Industry**
Thriving under prolonged low commodity price environment
Cresta Lodge, Msasa, Harare
Contact: Gugulethu Charlie
Tel: +27 11 834-1273/7, Fax: +27 11 838-5923/833-8156
E-mail: gugu@saimm.co.za, Website: http://www.saimm.co.zaa

7–9 August 2017 —**Rapid Underground Mine & Civil Access Conference 2017**
Emperors Palace, Hotel Casino Convention Resort, Johannesburg
Contact: Camielah Jardine
Tel: +27 11 834-1273/7, Fax: +27 11 838-5923/833-8156
E-mail: camielah@saimm.co.za, Website: http://www.saimm.co.za

15–16 August 2017 —**The SAMREC and SAMVAL Codes**
Advanced Workshop: Can you face your peers?
Emperors Palace, Hotel Casino Convention Resort, Johannesburg
Contact: Gugulethu Charlie
Tel: +27 11 834-1273/7, Fax: +27 11 838-5923/833-8156
E-mail: gugu@saimm.co.za, Website: http://www.saimm.co.za

22–24 August 2017 — **The biennial Southern African Coal Processing Society Conference and Exhibition**
'Coal Processing – the key to profitability'
Graceland Hotel, Casino and Country Club, Secunda
Contact: Gerda Craddock
Tel: +27 11 432-8918, E-mail: gerdac@mineralconcepts.co.za
Website: www.sacoalprep.co.za

30 August–1 September 2017 — **MINESafe Conference 2017**
Striving for Zero Harm—Driving Excellence through Compliance
Emperors Palace, Hotel Casino Convention Resort, Johannesburg
Contact: Camielah Jardine
Tel: +27 11 834-1273/7, Fax: +27 11 838-5923/833-8156
E-mail: camielah@saimm.co.za, Website: http://www.saimm.co.za

11–15 September 2017 — **Uranium 2017 International Conference**
Extraction and Applications of Uranium — Present and Future
Swakopmund Hotel, Swakopmund, Namibia
Contact: Camielah Jardine
Tel: +27 11 834-1273/7, Fax: +27 11 838-5923/833-8156
E-mail: camielah@saimm.co.za, Website: http://www.saimm.co.za

20–21 September 2017 — **Global Mining Standards and Guidelines Group (GMSG)**
Creating community to drive operational excellence
Emperors Palace, Hotel Casino Convention Resort, Johannesburg
Contact: Gugulethu Charlie
Tel: +27 11 834-1273/7, Fax: +27 11 838-5923/833-8156
E-mail: gugu@saimm.co.za, Website: http://www.saimm.co.za

30 September–6 October 2017 — **AfriRock 2017: ISRM International Symposium**—*Rock Mechanics for Africa*
Cape Town Convention Centre, Cape Town
Contact: Camielah Jardine
Tel: +27 11 834-1273/7, Fax: +27 11 838-5923/833-8156
E-mail: camielah@saimm.co.za, Website: http://www.saimm.co.za

17–20 October 2017 — **AMI Precious Metals 2017**
The Precious Metals Development Network (PMDN)
Protea Hotel Ranch Resort, Polokwane
Contact: Camielah Jardine
Tel: +27 11 834-1273/7, Fax: +27 11 838-5923/833-8156
E-mail: camielah@saimm.co.za, Website: http://www.saimm.co.za

18–20 October 2017 — **7th International Platinum Conference**
Platinum—A Changing Industry
Protea Hotel Ranch Resort, Polokwane
Contact: Gugulethu Charlie
Tel: +27 11 834-1273/7, Fax: +27 11 838-5923/833-8156
E-mail: gugu@saimm.co.za, Website: http://www.saimm.co.za

25 October 2017 — **14th Annual Student Colloquium**
Johannesburg
Contact: Gugulethu Charlie
Tel: +27 11 834-1273/7, Fax: +27 11 838-5923/833-8156
E-mail: gugu@saimm.co.za, Website: http://www.saimm.co.za

6–7 November 2017 — **Coal Preparation Society of India 5 International Conference & Exhibition**
'Coal Washing: a sustainable approach towards a greener environment'
Silver Oak Hall, India Habitat Centre, Lodhi Road,
New Delhi-110003
www.cpsi.org.in

Company Affiliates

The following organizations have been admitted to the Institute as Company Affiliates

3M South Africa (Pty) Limited
AECOM SA (Pty) Ltd
AEL Mining Services Limited
Air Liquide (PTY) Ltd
AMEC Foster Wheeler
AMIRA International Africa (Pty) Ltd
ANDRITZ Delkor(pty) Ltd
Anglo Operations Proprietary Limited
Anglogold Ashanti Ltd
Arcus Gibb (Pty) Ltd
Aurecon South Africa (Pty) Ltd
Aveng Engineering
Aveng Mining Shafts and Underground
Axis House Pty Ltd
Bafokeng Rasimone Platinum Mine
Barloworld Equipment -Mining
BASF Holdings SA (Pty) Ltd
BCL Limited (BCL001)
Becker Mining (Pty) Ltd
BedRock Mining Support Pty Ltd
Bell Equipment Limited
BHP Billiton Energy Coal SA Ltd
Blue Cube Systems (Pty) Ltd
Bluhm Burton Engineering Pty Ltd(BLU003)
Bouygues Travaux Publics
CDM Group
CGG Services SA
Chamber of Mines
Concor Opencast Mining
Concor Technicrete
Council for Geoscience Library
CRONIMET Mining Processing SA Pty Ltd
CSIR Natural Resources and the Environment (NRE)
Data Mine SA
Department of Water Affairs and Forestry
Digby Wells and Associates
DRA Mineral Projects (Pty) Ltd
Duraset
Elbroc Mining Products (Pty) Ltd
eThekwini Municipality
Expectra 2004 (Pty) Ltd
Exxaro Coal (Pty) Ltd
Exxaro Resources Limited
Filtaquip (Pty) Ltd
FLSmidth Minerals (Pty) Ltd (FFE001)
Fluor Daniel SA (Pty) Ltd
Franki Africa (Pty) Ltd-JHB
Fraser Alexander Group
Geobrugg Southern Africa (Pty) Ltd
Glencore
Goba (Pty) Ltd
Hall Core Drilling (Pty) Ltd
Hatch (Pty) Ltd
Herrenknecht AG
HPE Hydro Power Equipment (Pty) Ltd
IMS Engineering (Pty) Ltd
Ivanhoe Mines SA
Joy Global Inc.(Africa)
Kudumane Manganese Resources
Leco Africa (Pty) Limited
Longyear South Africa (Pty) Ltd
Lonmin Plc
Lull Storm Trading (Pty)Ltd T/A Wekaba Engineering
Magotteaux (Pty) Ltd
MBE Minerals SA Pty Ltd
MCC Contracts (Pty) Ltd
MD Mineral Technologies SA (Pty) Ltd
MDM Technical Africa (Pty) Ltd
Metalock Engineering RSA (Pty)Ltd
Metorex Limited
Metso Minerals (South Africa) Pty Ltd
MineRP Holding (Pty) Ltd
Mintek
MIP Process Technologies (Pty) Limited
MSA Group (Pty) Ltd
Multotec (Pty) Ltd
Murray and Roberts Cementation
Nalco Africa (Pty) Ltd
Namakwa Sands(Pty) Ltd
Ncamiso Trading (Pty) Ltd
New Concept Mining (Pty) Limited
Northam Platinum Ltd - Zondereinde
PANalytical (Pty) Ltd
Paterson & Cooke Consulting Engineers (Pty) Ltd
Perkinelmer
Polysius A Division Of Thyssenkrupp Industrial Sol
Precious Metals Refiners
Rand Refinery Limited
Redpath Mining (South Africa) (Pty) Ltd
Rocbolt Technologies
Rosond (Pty) Ltd
Royal Bafokeng Platinum
Roytec Global (Pty) Ltd
RungePincockMinarco Limited
Rustenburg Platinum Mines Limited
Salene Mining (Pty) Ltd
Sandvik Mining and Construction Delmas (Pty) Ltd
Sandvik Mining and Construction RSA(Pty) Ltd
SANIRE
SENET (Pty) Ltd
Senmin International (Pty) Ltd
Smec South Africa
SMS group Technical Services South Africa (Pty) Ltd
Sound Mining Solution (Pty) Ltd
SRK Consulting SA (Pty) Ltd
Technology Innovation Agency
Time Mining and Processing (Pty) Ltd
Timrite Pty Ltd
Tomra (Pty) Ltd
Ukwazi Mining Solutions (Pty) Ltd
Umgeni Water
Webber Wentzel
Weir Minerals Africa
Worley Parsons RSA (Pty) Ltd

SAIMM
THE SOUTHERN AFRICAN INSTITUTE OF MINING AND METALLURGY

7–8 August 2017—CONFERENCE | 9 August 2017—TECHNICAL VISIT

EMPERORS PALACE, GAUTENG

RAPID UNDERGROUND MINE and CIVIL ACCESS CONFERENCE 2017

ANNOUNCEMENT & CALL FOR PAPERS/PRESENTATIONS

BACKGROUND

This conference is in response to the industry being under immense pressure to sink shafts and develop tunnels in safer and more efficient ways. The global call for no harm has been taken very seriously. The advance rates and daily production has come under immense pressure to improve and shorten the entire project period to make it financially viable. We can sink shafts and develop tunnels without hurting people, however to repeatedly achieve this while achieving the productivity targets has proven to be a challenge. We need to critically examine all aspects related to the sinking process. The way in which we conduct the entire project, right from mine concept study through to commissioning and handover all needs to be considered. Shaft sinking and tunnelling is not only about the sinking cycle. There are many diverse factors that influence the sinking process including: business drivers in the concept phase, mining methodologies and technology alternatives in the pre-feasibility stages, cost and timing parameters in the feasibility as well as partner selection, technical criteria and management systems during the execution phase. Mechanisation attempts to remove people from the hazards of sinking and to provide a continuous consistent advance rate has made great strides in the past five years.

OBJECTIVES

The objective of this conference is to demonstrate an understanding from mining companies, sinking contractors, EPCM organizations and investors on their perception of the current process. The idea is to look at current best practice, Research and Development that is in process and to raise suggestions on how to improve the process using experiences collectively gained worldwide. At the very least the conference must identify areas of action in order to plan for improvements going forward. Otherwise, deeper ore resources may remain beyond our reach for the foreseeable future (and mining of asteroids may become a reality).

WHO SHOULD ATTEND

The Conference will be of value to:

- All stakeholders involved in the shaft sinking arena for mine access and heavy underground civil projects
- Mine owners, executives and management
- Underground civil construction companies
- Engineering design and consulting companies
- Project management practitioners
- Mining entrepreneurs
- Hydropower experts and other underground civil experts
- Technology suppliers and consumers
- Health, safety and risk management, personnel and officials
- Governmental minerals and energy personnel
- Research and academic personnel
- Rock engineers
- All engineering disciplines
- Consultants
- Contractors
- Financiers

Supported by

South African National Committee on Tunnelling

Sponsored by

AVENG SHAFTS & UNDERGROUND

HERRENKNECHT Tunnelling Systems

MASTER DRILLING

Murray & Roberts

Murray & Roberts Cementation

PALMIERI GROUP

WorleyParsons resources & energy

FOR FURTHER INFORMATION CONTACT:

Head of Conferencing: Camielah Jardine **E-mail:** camielah@saimm.co.za **Tel:** +27 11 834 1273/7 **www.saimm.co.za**

ELBROC
MINING PRODUCTS (PTY) LTD

TH ARCH SUPPORT SYSTEMS

APPLICATIONS

- Tunnel junctions
- Over and under ore passes
- Haulage
- Incline shaft portals
- Active support through bad ground conditions, dykes, faults, friable ground

BENEFITS

- Simple and fast installation
- High load carrying capacity
- Long operational life
- Suitable for tunnels from 4.15m to 5.5m wide
- Upright support beams cater for tunnel heights from 3.1 to 6.5m
- Cost effective
- Dimensional and design flexibility

PROFILE SETS

Ring Set

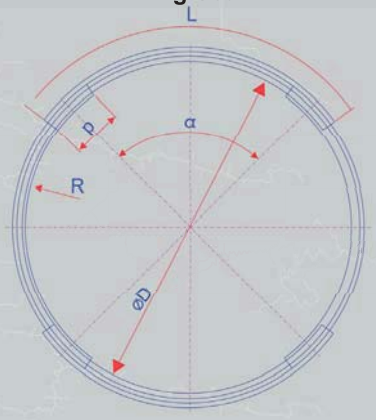

Semi Arch Set

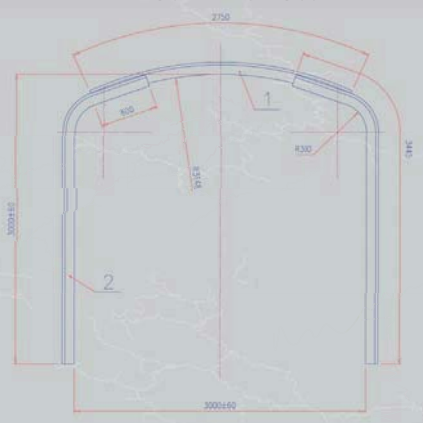

Half Arch Set

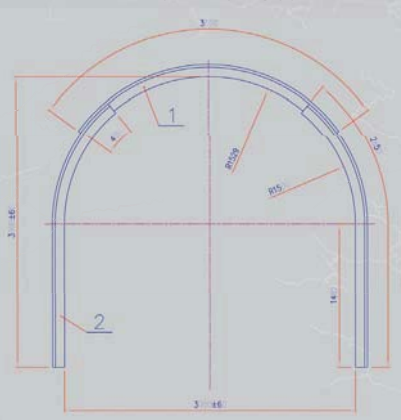

Production capabilities:

- Standard arch lengths from 1.8m to 5.5m
- Minimal curvature R 1000mm, at R 1200mm at R 1600mm

SABS ISO 9001

FOR OUR FULL PRODUCT RANGE
PLEASE VISIT OUR WEBPAGE

a member of the rbh royal bafokeng holdings

Tel: 011 974 8013 • Fax: 011 974 2019 • sales@elbroc.co.za

www.elbroc.co.za

mogs